DISSERTATION

MICROFLUIDIC CULTURE OF HUMAN HEPATOCYTES AND ENDOTHELIAL CELLS

WITH APPLICATIONS IN DRUG TOXICITY SCREENING

Submitted by

Brenton R. Ware

Graduate Degree Program in Bioengineering

In partial fulfillment of the requirements

For the Degree of Doctor of Philosophy

Colorado State University

Fort Collins, Colorado

Spring 2018

Doctoral Committee:

    Advisor: Salman R. Khetani

    Daniel L. Gustafson
    Charles S. Henry
    David C. Twedt

ABSTRACT

MICROFLUDIC CULTURE OF HUMAN HEPATOCYTES AND ENDOTHELIAL CELLS

WITH APPLICATIONS IN DRUG TOXCITY SCREENING

Drug-induced liver injury (DILI) continues to be a major problem for patient health and pharmaceutical expenditures, partially due to inadequacies of current model systems for predicting hepatotoxicity prior to clinical trials. In the drug development pipeline, many platforms are implemented depending on the stage of development, the number of compounds in question, and the specific hypothesis being studied. Primary human hepatocytes (PHHs) are considered the 'gold standard' for *in vitro* screening, as they retain a full complement of drug metabolizing enzymes and transporters. However, PHHs are in limited supply and lack the genetic diversity representative of the human population.

In this dissertation, we explore alternative cell sources to PHHs such as iPSC-derived hepatocytes, mouse hepatocytes, and the hepatocarcinoma cell line HepaRG in an engineered liver platform. We found that each of these cell types showed a high level of hepatic functions when incorporated into a micropatterned co-culture (MPCC) of the hepatocyte type in question with 3T3-J2 murine embryonic fibroblasts. MPCCs of PHHs and 3T3-J2 fibroblasts were then challenged with known hepatotoxins and their non-toxic structural drug analogs before undergoing global gene expression analysis. These analyses revealed that hepatotoxins caused a differential expression of significantly more genes than the non-toxic analogs, and the corresponding pathways could reveal underlying mechanisms of drug toxicity. Next, these *in vitro* models were supplemented with endothelial cells to give a more complete representation of liver physiology.

We found that co-cultures of hepatocytes and endothelial cells rapidly lost functionality, but tri-cultures of hepatocytes, endothelial cells, and 3T3-J2 fibroblasts were stable for multiple weeks. However, endothelia in the body experience shear stress from fluid flow, a phenomenon not mimicked with traditional *in vitro* cultures. Thus, we developed an *in vitro* platform for perfusing cultures with a physiologic level of shear stress. This system, constructed of tissue culture polystyrene with polydimethylsiloxane, was modeled using computational software and compared alongside static controls.

Ultimately, we believe these platforms can be incorporated as the liver compartment into a "body-on-a-chip" platform used to understand multi-organ effects of drugs and diseases that impact the liver including diabetes, hepatitis B/C, and malaria.

ACKNOWLEDGEMENTS

First, I would like to acknowledge and thank my advisor, Dr. Salman Khetani, for everything that he has done for me throughout my time as a doctoral student and his leadership of the Microfabricated Tissue Models Laboratory. The opportunities and insight that he has provided have given me the best possible preparation for my future work and career. His high expectations have encouraged me to continuously improve and pursue excellence in research and in life. He has also been a great source of timeless, useful wisdom such as, "Just find a nice girl in your church. If there aren't any, find a new church."

I also value the help and time of my committee members, Dr. Daniel Gustafson, Dr. Charles Henry, and Dr. David Twedt. Their insights and expertise in drug toxicity, microfabrication, and liver injury have proven to be invaluable in giving my research projects direction and seeing this dissertation through to a successful conclusion.

I have similarly appreciated the friendship and help of my colleagues in the Microfabricated Tissue Models Laboratory, past and present, including Matthew Davidson, Christine Lin, Dustin Berger, Chase Monckton, Grace Brown, Mitch Durham, Wendy Sunada, Kim Ballinger, Yang Yuan, and Sam Allsup. It has been quite beneficial to work alongside these researchers, share in their triumphs and failures, and be challenged to become the best researcher possible. Theodore Christoforidis and Dr. David Eddington of the Biological Microsystems Laboratory were also very helpful with device design, microfabrication, and COMSOL troubleshooting.

Finally, I would like to show my gratitude to my entire family and my two church families. My parents, Brad and Nancy Ware, have been so instrumental in everything I have done

throughout my entire life, and I cannot thank them enough for how they have equipped me to succeed and for all they continue to do for me. My brother LT Brandon Ware (USN), Grandpa Hilgers, Grandmom Ware, Uncle Mark Ware, and Frisco have also given me quite a bit of encouragement and support to complete my studies. So many dear Christian friends at Mountain View Community Church in Fort Collins and Holy Trinity Church in Chicago, including Pastor Oscar and Megan Leiva (Obed, Judah, and Ezra too!), Pastor Jason McConahy, Jon and Jenny McElwain (Josie, Julia, and Janelle too!), Alex Fout, Christian and Hee Park, Kim Martin, David Knight, DeeAnn Turpin, Jennie Van Diemen, and many, many more have been there to celebrate with me in the good times and there to build me up in the not-so-good times. Most of all, I must acknowledge and thank Dr. Anastasia Ware—my beloved bride, my best friend, and my dear sister in Christ—for her companionship, inspiration, and understanding of what goes in to completing a Ph.D. It has been a joy to share so much of life with her, from walking through the rain/snow to roasting marshmallows to our daily prayers together. The road ahead of us is long and winding, but I couldn't (and don't want to!) imagine it without her.

Ultimately, the LORD has set me on this path, provided me with everything, and I owe it all to Him. "I will lift up my eyes to the mountains; from where shall my help come? My help comes from the LORD, who made heaven and earth. He will not allow your foot to slip; He who keeps you will not slumber." (Psalm 121:1-3, NASB).

DEDICATION

This work is dedicated to the memory of my grandparents, Col. Richard M. Ware (USAF, December 12, 1919 – September 2, 2011) and Nancy J. Hilgers (August 7, 1938 – September 30, 2016). I was blessed to get to have them in my life for so many years and trust that I am a better person for even knowing them, yet alone being loved, mentored, and guided by them. Every day, I not only miss my grandparents, but the adventures, holidays, stories, and laughter that we would share from Kansas City, Green Mountain Falls, and the Lake of the Ozarks. Let their energetic spirit, optimism, wisdom, and humor continue to live on since the world is a better place because of it.

TABLE OF CONTENTS

LIST OF TABLES

LIST OF FIGURES

CHAPTER 1 - Introduction[1]

1.1 The Liver

1.1.1 Liver Structure and Function

The human liver is located in the upper right quadrant of the abdomen, is protected by the rib cage, and weighs ~1.5 kg in a 70-kg human. As a wedge-shaped organ, the liver can be primarily divided into the left lobe (~30-40% of the liver mass) and right lobe when looking from the front of the body.[1] From the visceral surface, the quadrate and caudate lobes are also visible. The falciform ligament separates the left lobe from the right, and the hilus separates the quadrate and caudate lobes.[2] On the microscale, hepatocytes (main liver parenchymal cells) interact with extracellular matrix (ECM) proteins, stromal cells (i.e. endothelia, Kupffer macrophages, and stellate cells, see Section 1.1.2), and soluble factors in a precisely defined architecture known as the sinusoid as illustrated in Figure 1.1. A complex network of vasculature is also a key feature of the liver (see Section 1.1.3) due to its role in metabolism.

As the largest and most metabolically active internal organ, the liver is responsible for over 500 functions. These functions include detoxifying drugs and environmental chemicals, neutralizing endogenously-produced substances (i.e. ammonia, bilirubin), synthesizing proteins (i.e. albumin, clotting factors), producing bile, metabolizing glucose and fatty acids, decomposing erythrocytes, and a variety of other processes. The liver has the capacity to regulate its size and growth while being able to regenerate itself quickly upon injury; after a 70% hepatectomy (surgical removal of the liver), the liver will return to a pre-operation within just a few weeks.[3]

---

[1] Portions of this chapter appear in the following:
Ware, B.R., & Khetani, S.R. Engineered liver platforms for different phases of drug development. *Trends in Biotechnology.* 2017. 35(2): 172-183, with permission from Elsevier.
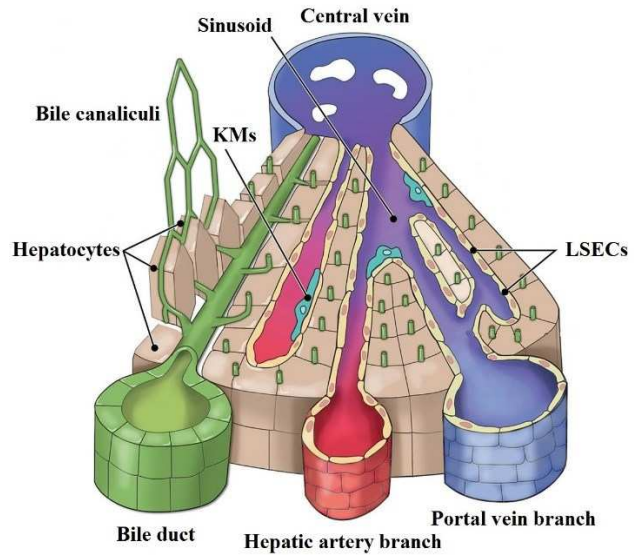
Figure 1.1: Microanatomy of the liver sinusoid. Hepatocytes, liver sinusoidal endothelial cells (LSECs), and Kupffer macrophages (KMs) interact in a precise geometry. Adapted from [4].

1.1.2 Cell Types of the Liver

Hepatocytes, the main parenchymal of the liver, comprise about 80% of the liver's volume and 60% of the total cell population.[5] They are responsible for most of the functioned described above, especially protein synthesis, nutrient metabolism, and xenobiotic processing.

Liver sinusoidal endothelial cells (LSECs) play a major role in liver physiology and disease and are the most abundant non-parenchymal cell (NPC) type of the liver, comprising about 70% of the NPC fraction.[6] As a major portion of the sinusoid, LSECs act as a barrier between flowing blood and hepatocytes. Among the most important functions of LSECS are the filtration of nutrients from the blood[7], secretion of various biochemicals such as cytokines[7], and contributing to regeneration following liver injury[8]. Acetylated low-density lipoproteins (acLDL) are an oxidized, non-native form of LDL that are taken up almost exclusively by LSECs to reduce the amount taken up by macrophages.[6,9] Open fenestrae, a key morphological feature of LSECs, have a diameter of 150-175 nm and allow for the exchange of soluble and particulate material from the blood in the sinusoid to the space of Disse.[10,11]

Kupffer macrophages (KMs) are the resident macrophages in the liver and responsible for the immune response against pathogens in the liver. Due to the liver's connection with the intestine via the portal vein, the liver is exposed to many xenobiotic agents consumed from the external environment. As such, KMs can be activated after exposure to endotoxins from bacteria such as lipopolysaccharide (LPS, a major component of bacterial cell walls). LPS triggers KMs to secrete tumor necrosis factor α (TNF-α), which causes neutrophils to adhere to LSECs.[12] Functional activity of KMs stimulated with LPS include the phagocytosis of bioparticles, expression of cluster of differentiation 68 (CD68), and the secretion of interleukin-6 (IL-6) and TNF-α.[5]

Hepatic stellate cells (HSCs) comprise about 5% of the total cell population of the liver and are normally responsible for storing vitamin A (retinol) and aiding in liver regeneration.[13] Upon injury or diseases such as non-alcoholic steatohepatitis (NASH), HSCs can become activated and differentiate into myofibroblastic cells that secrete proinflammatory cytokines and excessive collagen which may impact drug metabolism and other important liver functions.[14,15]

Cholangiocytes, also known as biliary epithelial cells, line the bile ducts that drain the contents of the bile canaliculi into the gall bladder. Depending on the position within the complex biliary tree, sections of the bile ducts can be lined with 4 up to 40 cholangiocytes.[16] Normally functioning cholangiocytes contain a variety of aquaporins, transporters, and ion exchangers responsible for maintaining homeostasis of the solutes dissolved in hepatic blood.[17] Furthermore, diseased cholangiocytes can cause downstream inhibitions of hepatic functions including biliary inflammation and fibrosis.[17]

The interactions between hepatocytes and the other cell types are summarized in Figure 1.2.
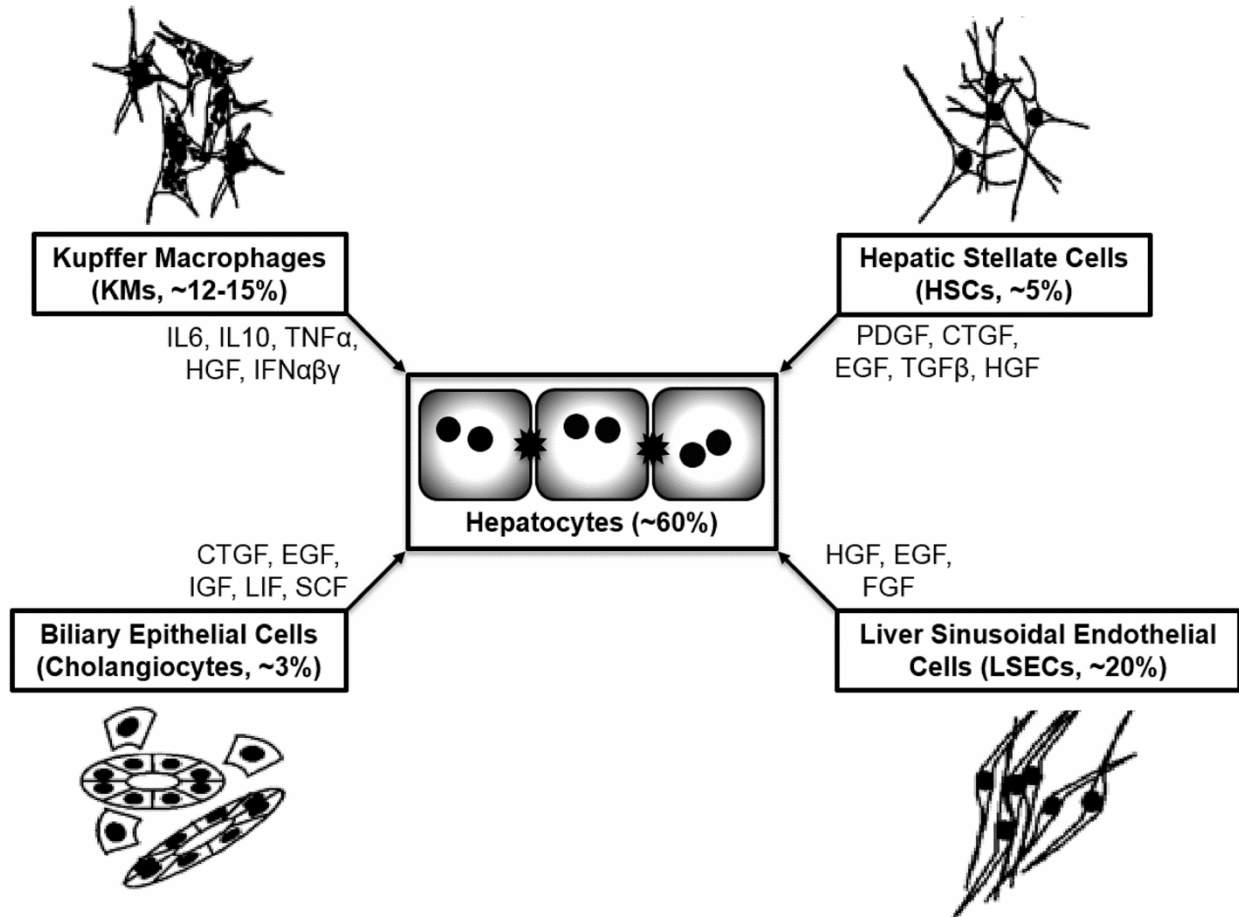
Figure 1.2: Parenchymal and non-parenchymal cell types of the liver. Kupffer macrophages (KMs), hepatic stellate cells (HSCs), liver sinusoidal endothelial cells (LSECs), and biliary epithelial cells are the major non-parenchymal cells (NPCs) in the liver. By secreting the indicated molecules, these NPCs impact on the phenotype of primary human hepatocytes (PHHs). Percentages represent the relative number of each cell type in the human liver. Adapted from [18].

1.1.3 Hepatic Blood Flow

Due to its high metabolic activity, the liver is quite vascularized and requires a large volume (~25% of total cardiac output) of blood perfusion.[19] With a dual blood supply, the hepatic artery delivers well-oxygenated blood (~1/3 of the blood supply) from the cardiovascular system while the portal vein delivers poorly oxygenated, nutrient rich blood (~2/3 of the blood supply) from the intestine.[20] Virtually all nutrients absorbed in the intestines, with the exception of some complex lipids, reach the liver via the portal vein.[1] From this blood supply, a complex network of vessels splits into several orders of branches, where the count tends to increase while the radius of each tends to decrease.[21] Ultimately, these branches split off into the sinusoids (Figure 1.1), which are typically the smallest and most prominent type of vasculature.[21] Blood flow through the sinusoids is often regulated throughout the vascular network through the contraction of smooth muscle cells, LSECs, HSCs, and KMs.[22] This ensures that the hepatocytes are evenly supplied with nutrients via the sinusoidal network.[23] Downstream, the sinusoids converge into larger and larger branches.[21] Lastly, the hepatic blood exits the liver through the hepatic vein for return through the vena cava.

1.1.4 Hepatic Zonation

While the liver is responsible for a vast number of metabolic processes, it is highly specialized in that different spatial zones of the liver maintain a unique set of functions. As illustrated in Figure 1.1, the portal triad (hepatic artery, portal vein, and bile duct) represents the periportal or zone 1 region of the liver. The oxygen- and nutrient-rich blood provided from the hepatic artery and portal vein, respectively, yields a high concentration of insulin and glucagon under ~10% O_2.[24] As blood flows through the sinusoid, the concentrations of insulin, glucagon,

and oxygen decrease due to consumption by hepatocytes and NPCs.[25] This perivenous or zone 3 region of the liver precedes the central vein with the centrilobular or zone 2 region in between.

Functionally, hepatocytes have vastly different processes along the sinusoid. Drug metabolizing enzymes for Phase I and some Phase II processes (i.e. CYP450 and sulfation, Section 1.2.1) show higher expression in the periportal region, while other Phase II enzymes (i.e. glucuronidation) are more highly expressed in the perivenous region (Figure 1.3). Metabolically, the heterogeneity reflects the concentration of oxygen and hormones in the various sections. The higher oxygen tension in the periportal region leads to greater β-oxidation, while glycolysis and lipogenesis are more prevalent in the perivenous region.

NPCs also have zonated phenotypes throughout the liver. First, the composition of the NPC population is dependent on the specific zone of the liver. In LSECs, the distribution of fenestrations on the cellular surface is noticeably zonated. As assessed by scanning electron microscopy, the average fenestration diameter slightly decreases from 110.7 ± 0.2 nm in the periportal zone to 104.8 ± 0.2 nm in the centrilobular zone.[11] Over this span, the density of fenestrations increases from 9 fenestrations/μm^2 to 13 fenestrations/μm^2, which raises the overall porosity from 6% to 8%.[11]
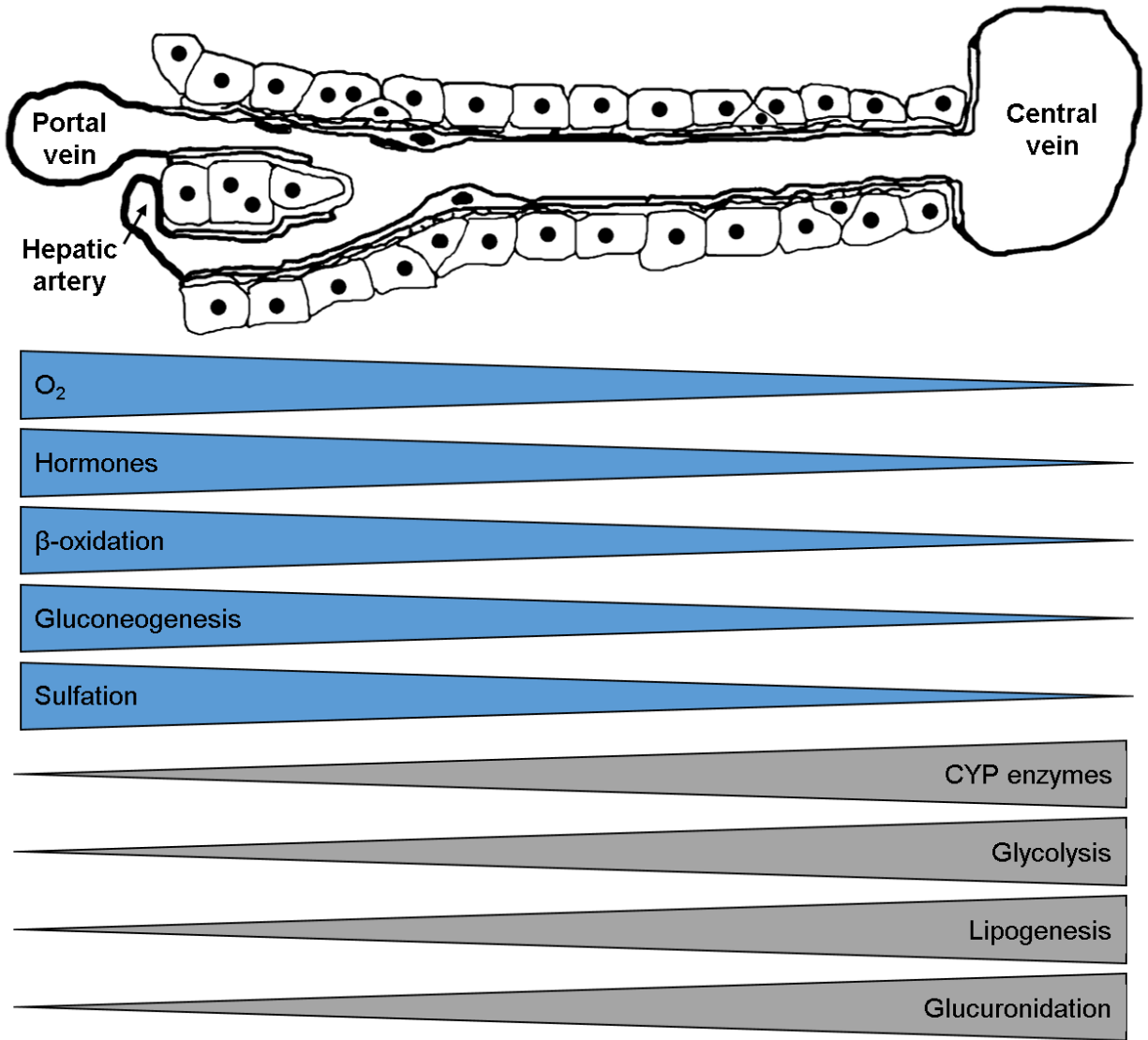
Figure 1.3: Functional heterogeneity along the liver sinusoid. With the sinusoid's dual blood supply from the cardiovascular system (via the hepatic artery) and the intestine (via the portal vein), the levels of oxygen and hormones are relatively high in the periportal zone. As blood flows towards the central vein, nutrients are depleted which leads to the varying levels of functions along the sinusoid. For simplicity, the bile duct is not shown. Adapted from [24], [26], and [27].

1.2 Drug Metabolism

1.2.1 Liver Enzymes and Processes

A major class of drug metabolizing enzymes responsible for the processing and detoxification of drugs and xenobiotic agents are the cytochrome P450 (CYP450) family of enzymes. In a prototypical three-step process of drug metabolism and excretion, CYP450 enzymes are responsible for Phase I metabolism, the redox reactions that reduce the hydrophobicity of previously lipophilic compounds. Most clinically-relevant drugs are metabolized by the isoforms 1A2, 2C9, 2C19, 2D6, 2E1, and 3A4, with 3A4 metabolizing about half of the drugs.[28] However, the metabolites of these Phase I reactions can be reactive and cause cellular damage by a variety of mechanisms.[29] This is followed by conjugation with a highly polar group such as sulfate, glucuronide, or glutathione to the metabolite of the Phase I reactions. Lastly, the Phase II metabolites are excreted into either the bile canaliculi or blood via Phase III transporters. As an example, coumarin is processed via CYP2A6 as illustrated in Figure 1.4. While known as 'metabolic detoxification', this sequence can actually metabolize many xenobiotics into pharmacologically active or toxic by-products.[30]
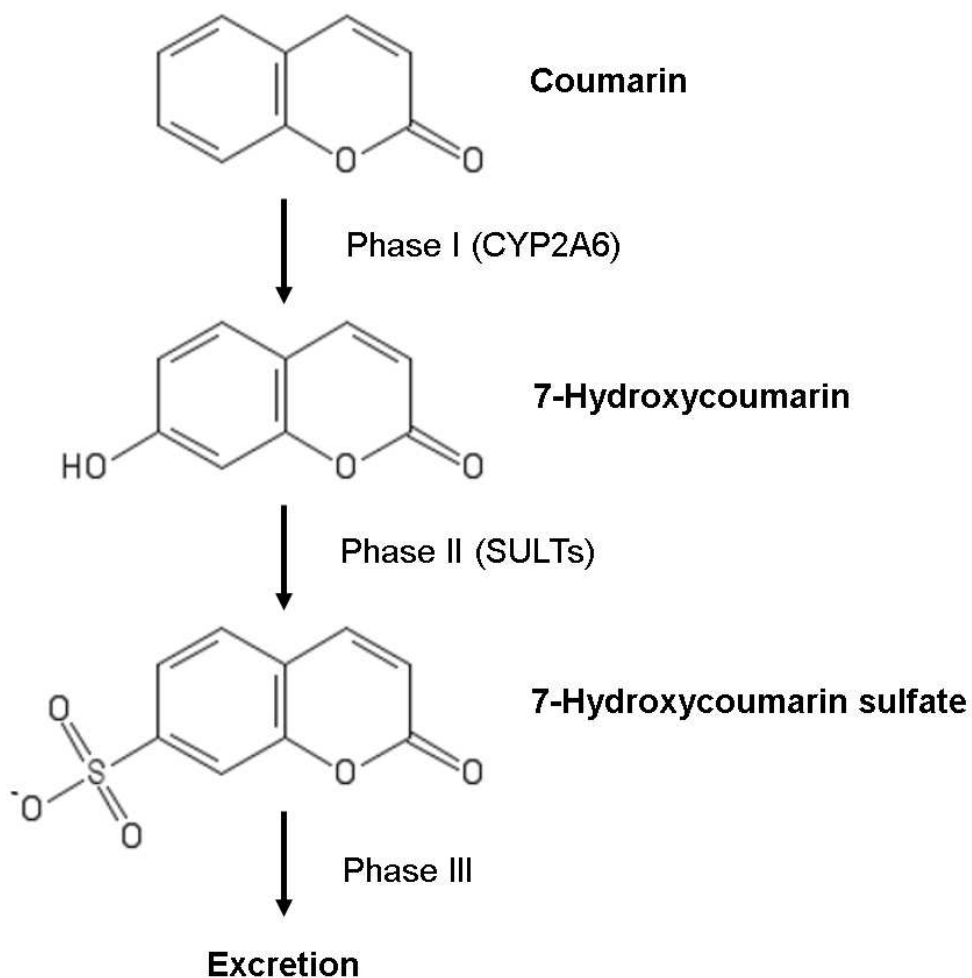
Figure 1.4: Prototypical three-phase process of drug metabolism. Coumarin, normally a hydrophobic molecule, is processed via the CYP2A6 enzyme which adds a hydroxyl group to increase its hydrophilicity. Phase II enzymes such as sulfotransferases (SULTs) further increase the hydrophilic character by adding a large, polar group to the molecule. Finally, the processed compound is excreted via Phase III transporters.

1.2.2 Drug-Induced Liver Injury

Drug-induced liver injury (DILI) is a major problem for patient well-being as it can cause liver necrosis, steatosis, cholestasis, fibrosis, carcinoma, or hepatitis.[31,32] Mechanisms of this injury can include production of toxic metabolites that deplete glutathione and bind macromolecules (i.e. diclofenac), dissipate mitochondrial membrane potential (i.e. troglitazone), accumulate within mitochondria (i.e. amiodarone), and inhibit bile salt export proteins (i.e. clozapine).[33,34] Additionally, DILI continues to be a major cause of pre-launch attrition, restrictions on use, black-box warnings, and post-market withdrawal of pharmaceuticals.[31] As an overall process, drug discovery is an expensive (~$3-5B/drug) and time-consuming (12-15 years) endeavor, partly due to the difficulty in predicting toxicity.[35] In fact, DILI is the cause for ~40% of drug failures in the clinical trial stage of development and has been associated with about 1000 drugs brought to market.[36] Acetaminophen (APAP, the active ingredient in Tylenol®) is today's leading cause (at least 42%) of acute liver failures in the United States.[29]

Current preclinical drug screenings are varied with each having a unique set of advantages and disadvantages. For instance, liver slices maintain *in vivo* architecture but rapidly lose function and cannot be used for large scale screens; microsomes are ideal for high-throughput screening, yet lack the cellular machinery required for toxicity screens. Cell lines derived from hepatocarcinomas provide an abundant cell source, but display irregular morphology and abnormal levels of liver functions.[37] Thus, primary human hepatocytes (PHHs) are now considered the 'gold standard' for *in vitro* toxicology applications despite the lack of robust availability of healthy tissue and limited donor diversity. Many *in vitro* platforms utilized by pharmaceutical companies today such as hepatocyte imaging assay technology (HIAT), while having good specificity (i.e. false positive rates less than 5%), have sensitivities between 30% and 50% for drugs of various classes

and mechanisms of action.[37,38] Some of the drugs not identified as toxic could be due to stromal cell interactions (i.e. clomiphene citrate[39]), incomplete CYP450 activity (i.e. dapsone[40]), inflammation[18], improper dosing, or donor-to-donor variability.

1.3 Platforms Used in the Drug Development Pipeline

1.3.1 Pipeline Overview

Drug development starts when a compound library (~10,000-20,000) is tested in a high-throughput format for activity (i.e. inhibition) against a protein implicated in a disease.[41] If the target protein is unidentified, the compounds are tested to alleviate a diseased phenotype in cells (i.e. phenotypic drug discovery).[42] The lead "hit" compound and its backups then undergo adsorption, distribution, metabolism, excretion, and toxicity (ADME/Tox) characterization *in vitro* and in animals before entering human clinical trials (Figure 1.5). In spite of the large amount of money (~\$3-5B) and time (12-15 years) invested during drug development, ~90% of compounds fail during clinical trials, with one-third of such failures attributed to organ toxicity.[43] The liver is especially susceptible to such toxicity due to its central role in drug metabolism. Drug-induced liver injury (DILI) is a leading cause of drug attrition in preclinical and clinical testing, black-box warnings on marketed drugs, the withdrawal of previously approved drugs, and acute liver failures.[31]
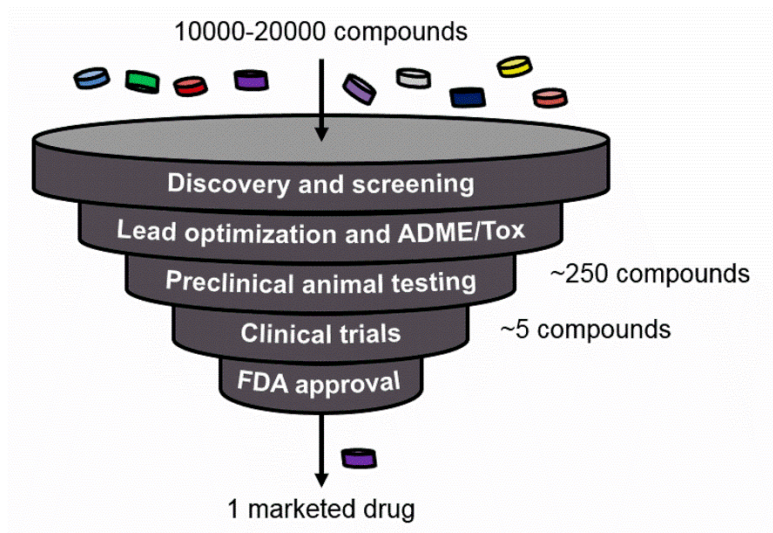
Figure 1.5: The drug development pipeline. Starting with a set of between 10,000 and 20,000 compounds created via combinatorial chemistry, early stages of the pipeline greatly reduce the number of potential compounds for further development. Eventually only one drug gets launched into the marketplace after $3-5B and 12-15 years of going through the pipeline. The discovery/screening, lead optimization and ADME/Tox (absorption, distribution, metabolism, excretion, and toxicity), and preclinical animal testing are the phases where engineered human liver models can make the greatest impact to reduce and, in some cases, replace the usage of animals and prevent harm to patients in clinical trials and in the marketplace.

Animal models are not always good predictors of human-relevant DILI due to significant species-specific differences in drug metabolism pathways.[44] Thus, *in vitro* models of the human liver are important to understand human drug metabolism and toxicity before clinical trials.[5] Such models can also aid in phenotypic drug discovery against liver diseases (i.e. hepatitis B/C viral infections, fatty liver disease, fibrosis, carcinoma).[45] Primary human hepatocytes (PHHs) are ideal for creating human liver models; however, their liver-specific functions rapidly decline in conventional culture formats, which leads to a low (<50%) sensitivity for DILI prediction.[5,38] Therefore, engineers have developed tools that can control the cellular microenvironment towards enabling higher and more stable PHH functions for several weeks.[5] The ability to test drugs chronically on stable PHHs has led to significant improvements in sensitivities for DILI detection and better modeling of liver diseases. The latest efforts towards "organ-on-a-chip" platforms are geared towards understanding how drug metabolism in the liver affects efficacy and/or toxicity in other tissues.[46]

1.3.2 High-Throughput Hepatic Systems

In early drug development, when many compounds need to be tested and the number of compounds is limiting, culture platforms should be high-throughput, cost relatively little, and provide actionable data quickly (within 24-48 hours). In the context of the liver, metabolic stability, major metabolites, and the toxicity of compounds are important parameters to evaluate.[5] To reduce cost, cancerous hepatic cell lines (i.e. THLE-2, HepG2, Hep3B, HepaRG) can provide an initial assessment of drug toxicity; however, for proper metabolism the use of PHHs becomes important because cell lines downregulate levels of drug metabolism enzymes (both mRNA and protein level) in the human liver.[47]

Kwon *et al.* designed a microchip platform for transducing 3D liver cell cultures with genes for drug metabolism studies (Figure 1.6A).[48] The platform features 532 reaction vessels (micropillars and corresponding microwells) on a 75 mm and 25 mm outline. Cells are suspended in a Matrigel™ droplet (~60 nL), which is spotted on a micropillar. The micropillar is then placed into a corresponding microwell containing recombinant adenoviruses. THLE-2 cells were transduced with adenoviruses to manipulate the expression of human drug metabolism enzyme genes. A single microarray was used to create 84 combinations of metabolic gene expressions, which provided information on which enzyme combinations led to drug toxicity in cells. In another example, a 3D Hep3B microarray was coupled with a microarray containing various combinations of recombinant drug metabolism enzymes to evaluate the metabolism-mediated toxicity of drugs.[49] Ultimately, PHHs will better capture complex mechanisms of DILI where the ratios of many enzymes and transporters may be important. Therefore, adapting the aforementioned platforms to PHHs (in addition to cell lines) will be important, while continuing to reduce cell numbers and drug amounts in the droplets, which is desirable for early drug development.

Other platforms can also form 3D spheroids of uniform sizes, as opposed to spheroids of heterogeneous sizes that can become necrotic in their cores if the diameter becomes too large (>200 µm) for adequate oxygen diffusion. Hanging drops of uniform sizes containing HepG2 or PHHs can be cultured in a specialized plate, which causes the formation of spheroids of controlled diameters (253 ± 7.4 µm) within 4 days.[50] These spheroids are then transferred to another multi-well plate for drug screening (Figure 1.6B). Miyamoto *et al.* developed a tapered cell seeding device containing 400 microwells with a top aperture (500 µm × 500 µm) and a bottom aperture (300 mm diameter circle) per microwell to form HepG2 spheroids of uniform diameters.[51] Fukuda

and Nakazawa designed a spheroid microarray that allowed stable immobilization of 100 μm rat hepatocyte spheroids in microwells for probing cytochrome P450 (CYP450) enzyme activities following drug treatment.[52]

Spheroidal cultures are not always compatible with high content screening (HCS), in which multiplexed fluorescent readouts are used to screen for DILI liabilities at the organelle level in individual cells (i.e. mitochondria or reactive oxygen species, ROS). On the other hand, monolayer cultures are well-suited for HCS.[38] For instance, in micropatterned co-cultures (MPCCs) of PHHs and supportive non-parenchymal cells (NPCs), the PHH fluorescent signals can be computationally separated from the NPC signals.[53] In this model, multi-well plates are subjected to soft lithography utilizing polydimethylsiloxane (PDMS) stamps to micropattern collagen islands onto which PHHs selective attach and are subsequently surrounded by NPCs (Figure 1.7A).[54] The diameter/spacing of the PHH domains have been optimized to enable optimal cell–cell interactions between PHHs and NPCs, which leads to higher and more stable (4–6 weeks) liver functions than randomly distributed co-cultures. MPCCs are routinely cultured in a 96-well plate format (Figure 1.7B), but more recently the Bhatia group has adapted MPCCs to a 384-well plate.

MPCCs have been validated using well-annotated compounds for applications in drug development. Wang *et al.* detected a significantly greater number of clinically-relevant drug metabolites in MPCCs than in short-term PHH suspensions.[55] Lin *et al.* showed that MPCCs predicted 73%, 92%, and 96% of the clearance rates for 26 drugs within 2-fold, 3-fold, and 4-fold of their *in vivo* rates, respectively.[56] On the other hand, suspension hepatocytes and conventional monolayers predicted only 30–50% of the clearance rates for tested drugs within 4-fold of their *in vivo* rates. In addition, MPCCs recapitulated drug–drug interactions that can affect drug clearance in patients.[57] In another study, MPCCs were dosed with clinical hepatotoxins for 9 days, which

improved the sensitivity for DILI detection to 66% versus 29% in short-term monocultures[58] MPCCs have also been used to model liver diseases towards utility in phenotypic drug discovery. Specifically, MPCCs can be infected with several pathogens, such as hepatitis B virus[59], hepatitis C virus[60], and malaria[61], and they can be used to screen for glucose-lowering diabetes drugs[62].

The availability of cryopreserved PHHs allows the construction of on-demand cultures for drug screening. However, PHHs are a limited resource for sustainable drug screening using the same donor(s) and are limited in the genetic diversity available to predict inter-individual differences in DILI outcomes, which are relevant in the clinic.[31] On the other hand, induced pluripotent stem cells (iPSCs) can be derived from many patients and are a nearly infinite cell source for drug screening. Protocols to differentiate iPSCs into hepatocyte-like cells (iPSC-HHs) use growth factors inspired from embryology; however, liver functions remain very low (<10%) relative to adult PHHs.[63] Engineering tools can be used to further mature iPSC-HHs.[64] Takayama *et al.* created a nanopillar plate for the spheroidal culture of iPSC-HHs, which helped to further improve liver functions.[65] Berger *et al.* showed that the MPCC technique further matures and stabilizes iPSC-HH functions for 4 weeks.[66] Furthermore, such 'iMPCCs' treated with 37 hepatotoxins for 6 days yielded a sensitivity (65%) that was similar to the sensitivity obtained in PHH-based MPCCs (70%) using the same drug set, while the specificity in both models was 100% using 10 non-hepatotoxic drugs (see Chapter 2). These results suggest that iPSC-HHs in an engineered platform may be suitable for an initial drug toxicity screen; however, mechanistic inquiries into drug responses as in later stages of drug development will require detailed comparisons of the molecular pathways affected by drugs in iPSC-HHs and PHHs.
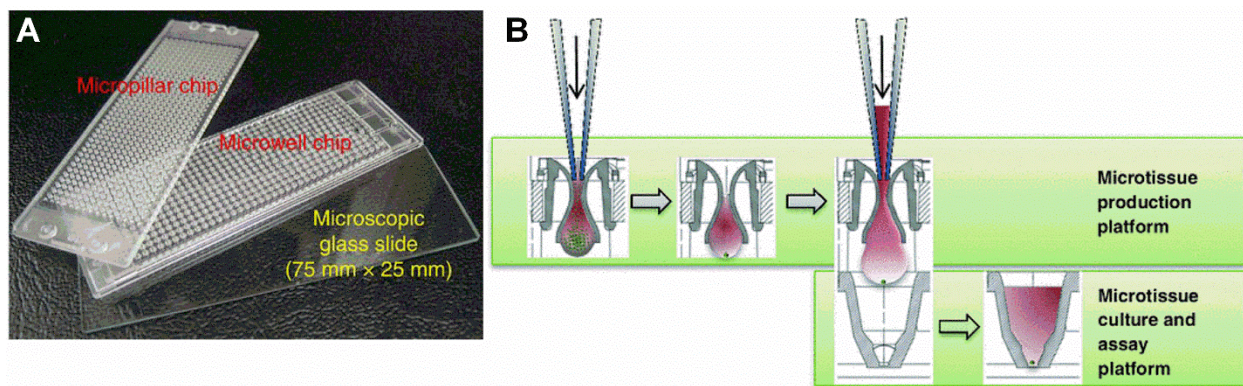
Figure 1.6: High-throughput hepatic systems. (A) A 532-well micropillar and microwell plate combination that can contain as little as 60 nL in each well. Hepatic cells (i.e. THLE-2) suspended in a Matrigel™ droplet are spotted on each micropillar, which are then placed in a microwell containing recombinant adenoviruses. The adenoviruses are engineered to transduce the cells with different combinations of drug metabolism genes towards determining enzymes involved in the observed toxicity of a drug. Adapted from [49] with permission from Nature Publishing Group. **(B)** Hanging-drop method for generating liver spheroids of controlled diameters. Briefly, a cell mixture is seeded into the wells of a specialized 96-well plate that allows the spheroid to form and mature in a hanging drop. The spheroids are then transferred to another culture plate for drug dosing. Adapted from [50] with permission from Springer.
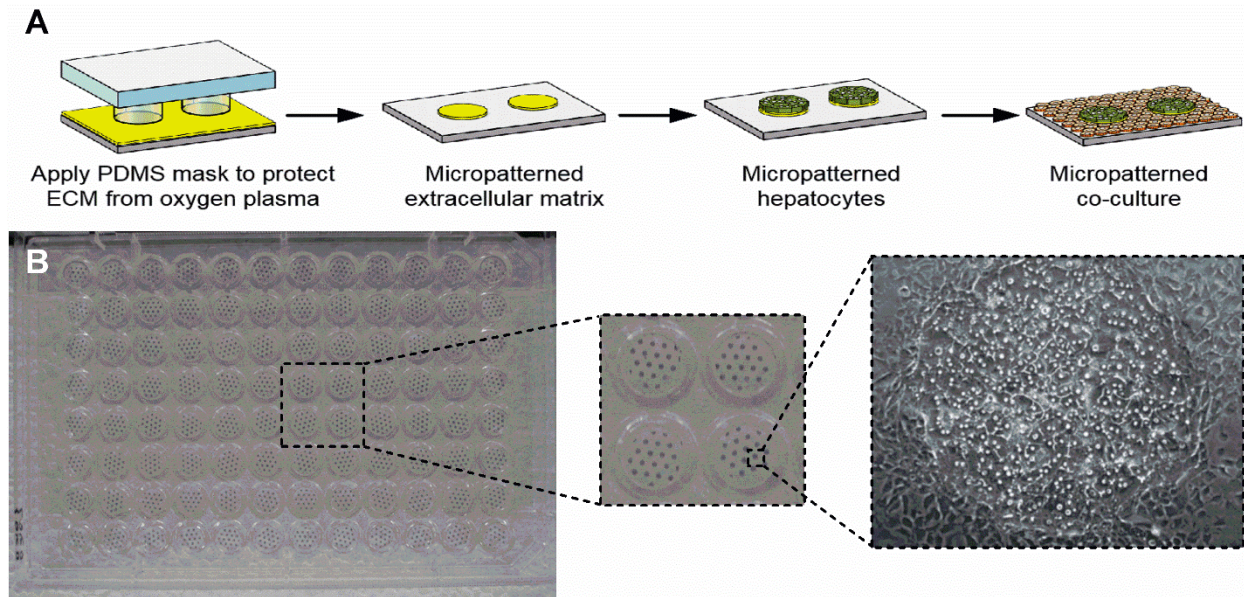
Figure 1.7: Micropatterned co-cultures. **(A)** Tissue culture polystyrene (or glass) can be uniformly coated with extracellular matrix protein (ECM) such as collagen and protected with a polydimethylsiloxane (PDMS) stamp. Exposed areas of ECM are ablated under oxygen plasma, leaving micropatterned ECM islands that match the geometry of the PDMS stamp. Hepatocytes selectively attach to ECM islands, and non-parenchymal cells (NPCs) fill in the surrounding area. **(B)** An industry standard 96-well plate showing uniform hepatocyte islands micropatterned using the process in panel 'A'. The NPCs used in this example are 3T3-J2 murine embryonic fibroblasts surrounding the primary human hepatocyte colonies. Reprinted from [5] with permission from Sage Publications. More recently, MPCCs have been adapted to a 384-well plate format by the Bhatia group at the Massachusetts Institute of Technology.

1.3.3 Engineered Liver Co-Cultures

As a lead candidate compound progresses through drug development, its effects on tissue types need to be investigated at the mechanistic level in a more physiological context where high-throughput and rapid screening are not always required given the significant reduction in the number of compounds for testing relative to early drug development (Figure 1.5). While hepatic cell lines provide cheap and abundant cell sources for high-throughput systems deployed during early drug development, they are not suitable for accurately modeling complex physiological outcomes during lead optimization because they are limited to single donors and downregulate drug metabolism pathways.[47] By contrast, PHHs can mitigate such limitations of cell lines. In addition to PHHs, NPCs resident in the liver are known to either experience toxicity to drugs directly and/or secrete molecules that regulate PHH response.[18] Thus, investigators have incorporated one or more liver NPCs alongside hepatocytes into engineered liver models, as discussed below; however, it is not yet clear how to incorporate cholangiocytes for bile drainage into a separate compartment as *in vivo*, which could determine drug disposition in the bile. Initial designs of devices are often tested with rat liver cells or cell lines, although adaptation to primary human liver cells is progressing rapidly.

1.3.3.1 Static Platforms

The MPCC platform is modular in that the NPC population can be modified without significantly affecting PHH homotypic interactions on the micropatterned domains for the proper formation of bile canaliculi between the hepatocytes. Nguyen *et al.* first allowed MPCCs to stabilize for 1 week and then seeded human liver Kupffer macrophages (KMs) atop the monolayer.[67] Stimulating KMs with bacterial lipopolysaccharide (LPS) led to cytokine-mediated downregulation of hepatic CYP450s, which can affect drug outcomes. Current studies are focused

on creating MPCCs with other liver NPCs, while maintaining the multi-well format for screening several drugs or conditions.

Other groups have created PHH-NPC co-cultures in 3D configurations. Kostadinova *et al.* seeded a mixture of liver NPCs (LSECs, HSCs, and KMs) onto a porous nylon scaffold in a 24-well format followed by seeding of PHHs 1 week later. PHHs displayed CYP450 activities for 3 months, while the NPCs expressed prototypical markers.[68] Drug toxicity studies showed the ability of the co-cultures to predict clinical outcomes. In a scaffold-free example, the hanging drop culture method discussed above was used to create spheroids of PHHs, KMs, and endothelia.[50] Trovafloxacin-induced hepatotoxicity was exacerbated when KMs were activated via LPS.

In contrast to a random orientation of cell types in the aforementioned spheroids, bioprinting can be used to position liver NPCs relative to PHHs to create a compartmentalized architecture that can provide insights into how the relative positions of the cell types changes upon drug treatment. Organovo developed bioprinted co-cultures containing PHHs, HSCs, and LSECs in a 24-well plate format. Ma *et al.* bioprinted iPSC-HHs, endothelial cells, and adipose-derived stem cells in a hexagonal architecture embedded in a hydrogel that mimics the liver lobule.[69]

1.3.3.2 Perfused "Liver-on-a-Chip" Platforms

In comparison to static models, perfusion of cultures permits continuous nutrient exchange, better oxygen delivery, and physiologic shear stress; however, complexities in liquid handling are introduced together with reduced throughput relative to multi-well plates. Miniaturized microfluidic bioreactors can further allow control over the soluble microenvironment of cells at a scale similar to the functional unit of a tissue (Figure 1.8A).[46] The Griffith group engineered a device in which preformed hepatic aggregates adhered to the collagen-coated walls of an array of microchannels were perfused, which led to higher hepatic functions than static controls.[70] This

platform was later adapted to co-cultures between rat hepatocytes and LSECs.[71] Toh *et al.*

designed a microfluidic chip to generate linear gradients of drug concentrations and establish dose–

response curves for drugs incubated on rat hepatocytes.[72] Similar concentration gradients were

established in another biochip designed to mimic the liver sinusoid.[73] The Leclerc group has

designed biochips for characterizing the metabolic profiles of rat hepatocytes[74,75], evaluating drug

metabolism in PHHs[76,77], and investigating drug-induced ROS formation and glutathione (GSH)

depletion in rat hepatocytes[78] and HepG2/C3a cells[79]. Chao *et al.* cultured PHH monolayers in a

microfluidic platform for evaluating drug clearance[80], which was extended by Novik *et al.* to

PHH/NPC co-cultures[81]. The co-cultures under flow were capable of clearing compounds with

better correlation to *in vivo* clearance values than the static controls. More modern spheroidal

cultures feature microfluidic connections that can enable continuous perfusion of medium. Kim

et al. used such a platform for monitoring rat hepatic spheroids over time[82], while Frey *et al.* used

a similar method for evaluating the toxicity of the anticancer drug 5-fluorouracil[83].
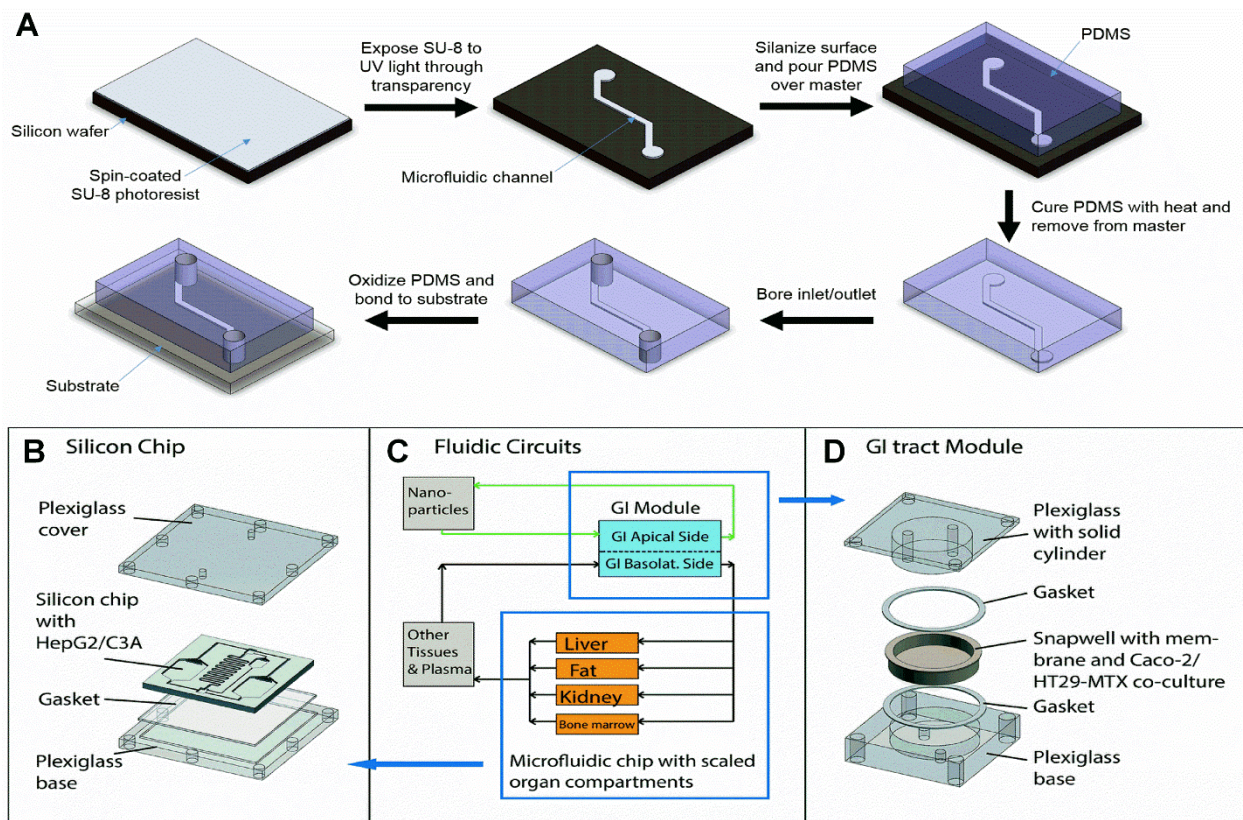
Figure 1.8: "Liver-on-a-chip" platforms. **(A)** "Liver-on-a-chip" platforms are often manufactured with soft lithography techniques, whereby a design is transferred to SU-8 photoresist using ultraviolet (UV) light through a high-resolution mask such as a transparency. Polydimethylsiloxane (PDMS) is then poured over the patterned SU-8 to construct the microfluidic channel. After curing and boring the inlet and outlet ports, the PDMS is oxidized and bonded to the device substrate. **(B)** A "liver-on-a-chip" platform featuring HepG2/C3A cells is established on a silicon chip sandwiched between plexiglass layers. **(C)** Using a physiologically-based pharmacokinetic (PBPK) model, the fluidic circuit is designed to mimic the interactions between the liver and gastrointestinal (GI) compartments. **(D)** The liver on-a-chip platform is connected with a GI platform consisting of a co-culture of Caco-2 and HT29-MTX cells. Reprinted from [84] with permission from the Royal Society of Chemistry.

Several groups have created co-cultures of PHHs and endothelial cells in microfluidic devices, although primary human LSECs are not always used because of limited availability. Bovine aortic endothelial cells were used in a biochip that separates hepatocytes from endothelia with either an extracellular matrix (ECM) protein layer or a microporous membrane.[85] Bovine pulmonary microcapillary endothelial cells were incorporated into a layered model to induce the formation of capillary-like structures.[86] Two groups used EA.hy926 (transformed endothelial cells) in lieu of primary cells in their microfluidic devices, which also contained LX-2 cells (immortalized HSC line), U937 monocytes (cell line from lung lymphoma), and PHHs in a layered sinusoid-like architecture.[87,88] However, the aforementioned readily available cell types cannot fully mimic human liver physiology. To eliminate the endothelial cells altogether, some groups have developed devices that simulate the endothelial fenestrations with artificial barrier slits[72,89,90]; however, such devices are devoid of PHH-LSEC crosstalk which is important in liver diseases.[91]

Microfluidic devices are more difficult to set up and handle relative to multi-well plates. Therefore, to aid ease of usability and allow rapid assessment of drug effects, real-time monitoring of toxicity biomarkers is being incorporated into microfluidic devices. Bavli *et al.* developed a biochip with a computer-controlled microfluidic switchboard that can simultaneously monitor mitochondrial respiration, glucose, and lactate in HepG2/C3A aggregates in real-time.[92] A shift from oxidative mitochondrial respiration to glycolysis was then shown after treatment with two hepatotoxins. Rennert *et al.* established a liver biochip consisting of human umbilical vein endothelial cells and monocyte-derived macrophages in the vascular plane that was separated from the hepatic plane containing HepaRG and LX-2 cells with a membrane mimicking the space of Disse.[93] Luminescence-based sensor spots were integrated in the chip for real-time measurement of oxygen consumption. Vernetti *et al.* created a platform in which PHHs, EA.hy926, U937

monocytes, and LX-2 cells were sequentially layered in a microfluidic device that had fluorescent protein biosensors inside ~20% of the PHHs to detect apoptosis and ROS following drug exposure.[87] Finally, other groups have developed microfluidic devices with incorporated antibody-based biosensors for monitoring transforming growth factor β1 (TGF-β1), an activator of HSCs.[94,95]

Oxygen gradients can modulate hepatic CYP450 expression along the length of the sinusoid (zonation), which can cause zonal patterns of DILI.[96] Allen *et al.* generated oxygen gradients across rat hepatocyte/fibroblast co-cultures by cell-mediated depletion of oxygen dissolved in the culture medium from the inlet to the outlet of a bioreactor.[97] The oxygen gradient led to an *in vivo*-like higher expression of CYP450s and greater acetaminophen toxicity in the hepatocytes subjected to the low-oxygen regions (outlet) as compared to the high-oxygen regions (inlet). Sato *et al.* also developed a biochip for providing a continuous oxygen gradient to cultured mouse hepatocytes.[98] Peng *et al.* designed a 16-well device with channels underneath the cell culture chamber to introduce oxygen-scavenging chemicals and induce hypoxic conditions.[99]

1.3.4 "Organ-on-a-Chip" Platforms

Drug metabolism in the liver can affect the efficacy and/or toxicity of drugs in other organ systems. Thus, "organ-on-a-chip" platforms with microfluidic perfusion are being developed to investigate the interactions between tissue types following drug exposure.[46] The Shuler lab designed an early "organ-on-a-chip" model in which cell lines were used to model lung, liver, and fat compartments that were linked with microfluidic flow to investigate drug biodistribution.[100] Use of cell lines is common in current "organ-on-a-chip" designs to show proof-of-concept prior to transitioning to primary cells, which can be more difficult to source and culture in complex devices.

25

The liver and the intestine are connected *in vivo* by the portal circulation and the common bile duct. Often drugs and their metabolites can undergo enterohepatic recirculation between the liver and the intestine, and this can increase exposure of both organs. Esch *et al.* constructed a liver/intestine chip to investigate nanoparticle toxicity (Figure 1.8B–D).[84] The liver compartment was modeled with HepG2/C3A cells cultured in a silicon chip between plexiglass layers, while the intestine was represented with a co-culture of Caco-2 (colon carcinoma) and HT29-MTX (mucus-secreting colon epithelia) cells. When only the liver compartment was exposed to nanoparticles, the HepG2/C3A cells released more aspartate aminotransferase (cellular injury marker) than the vehicle-only control. This phenomenon was exacerbated when the liver and intestine compartments were connected via microfluidic channels. Bricks *et al.* coupled polycarbonate cell culture inserts and microfluidic biochips to create a platform in which the liver compartment and intestinal compartments were mimicked by HepG2/C3A and Caco-2 cells, respectively.[101] The transport of phenacetin through the intestinal barrier and its metabolism into acetaminophen by the liver compartment were demonstrated.

In addition to the intestine, interactions of the liver with other organs are also important for evaluating drug effects. Chouca-Snouber *et al.* created a microfluidic biochip that combined HepG2/C3A or HepaRG liver and MDCK (Madin–Darby canine kidney) cell lines.[102] Ifosfamide was metabolized by HepaRG cells, but not by HepG2/C3A cells, into a metabolite that was toxic to MDCK cells. Materne *et al.* created a biochip consisting of liver spheroids with HepaRG and primary HSCs, and differentiated NT2 cell neurospheres.[103] After 2 weeks of dosing with 2,5-hexanedione (neurotoxin), the co-cultures were more sensitive than the single-tissue cultures in the biochip. Similar techniques have been used with liver–tumor interactions for studying

endothelial permeability.[104] Other groups have used biochips to study liver–skin interactions in troglitazone-induced toxicity[105] and topical substance exposure[106].

Physiologically-based pharmacokinetic (PBPK) modeling is a powerful application for "organs-on-a-chip" devices because it can provide insights into the key clinical parameters of a drug (i.e. maximum plasma concentration and half-life). Kimura *et al.* developed a liver–lung–intestine model for PBPK analysis. While the cell lines HepG2, A549, and Caco-2 were used, they were still able to model the distribution of three anticancer drugs.[107] Similarly, Sung *et al.* modeled liver–tumor–marrow interactions using a microfluidic chip with cell lines, and derived a PK model for the distribution of 5-fluorouracil.[108] Their results showed that, compared to static cultures, the microfluidic device was able to more accurately reproduce liver metabolism of the cancer prodrug tegafur to 5-fluorouracil, which was toxic to the tumor model.

Finally, a few groups have created four-organ chips. Maschmeyer *et al.* combined intestine, skin, liver, and kidney modules onto a chip and assessed the functionality of the cells over 28 days.[109] Oleaga *et al.* combined cardiac, muscle, neuronal, and liver modules and evaluated the toxicities of doxorubicin, atorvastatin, valproic acid, acetaminophen, and *N*-acetyl-*m*-aminophenol.[110] With increased research funding from federal agencies (i.e. National Institutes of Health and Defense Advanced Research Projects Agency), the development of multi-organ chips with greater automation and better physiological relevance (i.e. using primary cells) will continue to grow.

1.4 *In Vitro* Assays for Hepatic Functions

1.4.1 Hepatic Morphology

As assessed by phase contrast microscopy, the morphology of hepatocyte cultures can be evaluated over time. Three major features are present in differentiated hepatocytes, namely a

polygonal shape, multi-nucleation, and the presence of functional bile canaliculi. A polygonal shape is representative of most epithelial cells, while multi-nucleation signifies a cell that has undergone nuclear division without cytokinesis. Functional bile canaliculi form between adjacent hepatocytes for the export of bile and can be stained with the fluorescent dye 5 (and 6)-carboxy-2',7'-dichlorofluorescein (CDF).

1.4.2 Albumin

Albumin is a major plasma protein responsible for maintaining osmotic pressure in the blood. Culture supernatants containing secreted albumin can undergo analysis via a competitive ELISA. Briefly, an assay plate is coated with albumin so all wells are coated identically. Collected supernatants are added to the assay plate along with an anti-albumin antibody tagged with horseradish peroxidase (HRP). The albumin coated on the wells and the albumin in the samples will "compete" for the antibody. 3,3',5,5'-tetramethylbenzidine (TMB), the substrate for HRP, is added to each well and acts as an electron donor for the conversion of HRP to water. This reaction causes the solution to develop a blue color before the addition of 0.5 N HCl stops the reaction and changes the color to yellow. The resulting assay plates, similar to Figure 1.9, are read at 450 nm for the primary signal and at 650 nm for the background signal.
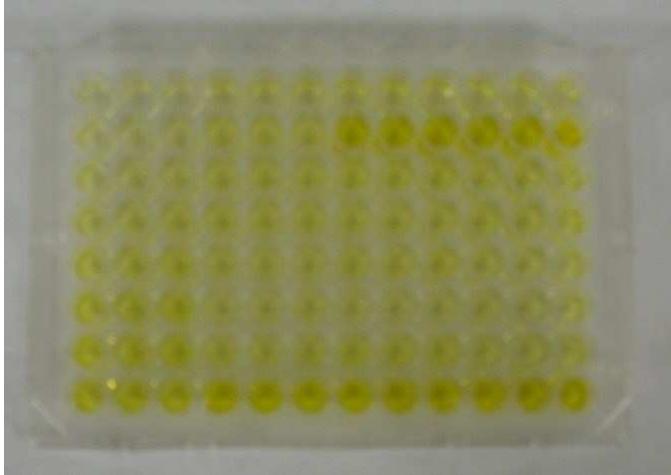
Figure 1.9: Sample albumin assay plate. Following a competitive albumin ELISA with 3,3',5,5'-tetramethylbenzidine and HCl quenching, the resultant assay wells have a yellow color that can be measured at 450 nm with 650 nm background subtraction. Since this is a competitive assay, the color intensity is inversely proportional to the amount of albumin present. The left three columns are standards of known albumin concentrations.

1.4.3 Urea

Upon amino acid catabolism, ammonia is produced from the deamination of amino acids; the ammonia is subsequently detoxified by hepatocytes into urea. When media supernatants are mixed with diacetyl monoxime and acid under heat, urea reacts with the diacetyl group to form a pink chromogen. The assay plates, similar to the one shown in Figure 1.10, are read at 540 nm for the major signal and at 650 nm for the background signal.
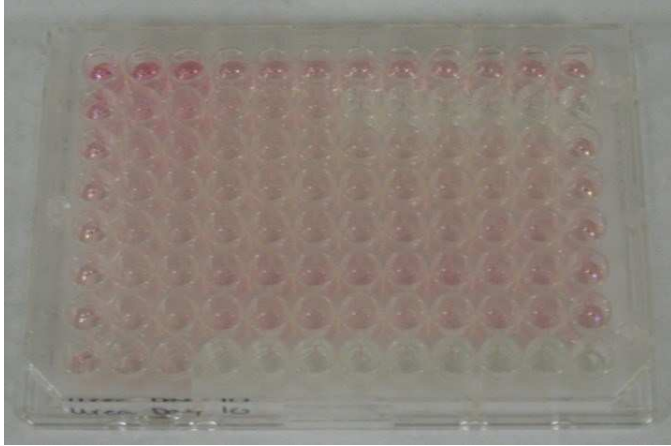
Figure 1.10: Sample urea assay plate. Upon the combination of urea, diacetyl monoxine, and acid under heat, a pink chromogen is produced in an intensity directly proportional to the urea concentration. Standards of known concentration are included as a comparison.

1.4.4 Cytochrome P450 Enzymes

The activities of specific CYP450 isoforms can be evaluated with *in situ* optical readouts. A popular method for doing this is with the P450-Glo™ kit from Promega (Madison, WI), whereby cultures are incubated with an isoform-specific substrate and a luminescent product is generated. In the case of CYP3A4, the luciferin-IPA substrate is applied to cultures, and the CYP3A4 enzyme cleaves the isopropyl alcohol (IPA) group off the luciferin group. Afterwards, a luciferase detection reagent is added after the reaction is completed, which produces a quantifiable luminescent signal.

Alternatively, cultures can be incubated with isozyme-specific substrates listed in Table 1.1, and the resulting metabolites in supernatants can be assessed via liquid chromatography-mass spectrometry. For instance, phenacetin undergoes a CYP1A2-mediated *O*-dealkylation reaction, which can then be quantified by the amount of acetaminophen generated.

Table 1.1: FDA-approved CYP450 substrates and corresponding metabolites

CYP450 Isoform	Substrate	Metabolite
CYP1A2	Phenacetin	Acetaminophen
CYP2B6	Bupropion	Hydroxybupropion
CYP2C8	Paclitaxel	6α-Hydroxypaclitaxel
CYP2C9	Tolbutamide	4-Hydroxytolbutamide
CYP2C19	*S*-mephenytoin	4-Hydroxy-*S*-mephenytoin
CYP2D6	Dextromethorphan	Dextrorphan
CYP2E1	Chlorzoxazone	6-Hydroxychlorzoxazone
CYP3A4	Testosterone	6β-Hydroxytestosterone

Note. Table adapted from [5].

1.4.5 Other Liver-Specific Functions

In addition to the aforementioned markers, cultures can be probed for other biochemicals secreted by hepatocytes depending on the hypothesis in question. For instance, the amount of glucose metabolized can inquire about the effects of exogeneous insulin provided to hepatic cultures.[111] Other markers include fibrinogen (glycoprotein that enzymatically converts thrombin to fibrin upon vascular injury), transferrin (glycoprotein that regulate the level of free iron in biological fluids), and alanine aminotransferase (enzyme for catalyzing the transfer of an amino group from L-alanine to α-ketoglutarate), all proteins that are synthesized in the liver.[5,63,68]

1.4.6 Non-Hepatocyte-Specific Biomarkers

Biochemical markers that are not specific to hepatocytes can be evaluated for the overall health of cultures. For instance, levels of the energy-carrying molecule ATP and antioxidant glutathione (GSH) have been compared in drug-treated cultures against solvent-only controls.[58] Both of these markers can be measured via the luminescent assays CellTiter-Glo® and GSH-Glo™, respectively, from Promega. However, unlike biochemicals secreted into culture medium supernatants, cells must be lysed for these assays to be effective; this necessitates a set of cell cultures for each time point needed. Similar markers include lactate dehydrogenase, aspartate dehydrogenase, and 3-(4,5-dimethylthiazol-2-yl)-2,5-diphenyltetrazolium bromide. Biochemical signals would have contributions from all cell types present in cultures, not solely hepatocytes.

1.5 Research Objectives

1.5.1 Use iPSC-Derived Hepatocytes for Toxicity Studies

As we have previously demonstrated a high level of liver specific-functions from iPSC-derived hepatocytes in the MPCC format, we wanted to run a screen of 47 drugs from different classes and mechanisms of action to compare the predictive power of these so-called iMPCCs to

conventional cultures of iPSC-derived hepatocytes and MPCCs from PHHs. Furthermore, we wanted to compare the responses of structural drug analogs and the bioactivation pathways of acetaminophen.

1.5.2 Culture Mouse Hepatocytes In Vitro

With the large number of genetically diverse mouse strains available, we wanted to demonstrate long-term cultures of mouse hepatocytes using co-culture strategies. We then sought to show a toxicity profile and bioactivation pathways of acetaminophen in mouse hepatocytes that were comparable to those in human hepatocytes.

1.5.3 Use HepaRG Cells for Toxicity Studies

Instead of using expensive, limited primary cells, we wanted to incorporate the hepatocarcinoma cell line HepaRG into an engineered platform and characterize the platform for the expression of hepatic and biliary markers. Lastly, we wanted to compare the binary toxicity predictions using the same 47 drugs tested in iMPCCs.

1.5.4 Run Toxicogenomic Analyses

To probe the mechanisms of drug toxicity, we focused on the global gene expression of cultures treated with the Type II diabetes drugs troglitazone and rosiglitazone over 1, 7, and 14 days. As opposed to high drug doses necessary to elicit a measurable response with traditional markers, we chose pharmacologically-relevant doses to alter the gene expression signature without causing overt toxicity. Lastly, we extended the study to three other structural drug analog pairs to validate the trends observed with troglitazone and rosiglitazone.

1.5.5 Co-Culture Hepatocytes and Endothelia

As endothelial cells represent most of the non-parenchymal cells in the liver, we wanted to determine an optimal culture between hepatocytes and endothelial cells. Furthermore, we chose

to verify that the cultures were not only maintaining a high level of hepatospecific functions, but were also maintaining endothelial markers. Lastly, we wanted to demonstrate the utility of endothelia-containing cultures in screening drugs known to cause toxicity to endothelia.

1.5.6 Establish a Microfluidic Hepatocyte-Fibroblast Co-Culture Model

As opposed to static culture platforms, we chose to design a perfused, long-term liver culture for evaluating the effects of shear stress on hepatic cultures and then validate the shear stress on hepatic cultures in that design using computational software. We then desired to test the design to compare perfused cultures with static cultures.

CHAPTER 2 - iPSC-Derived Hepatocytes in Drug Toxicity Testing[2]

Primary human hepatocytes (PHHs) are a limited resource for drug screening, their quality for *in vitro* use can vary considerably across different lots, and a lack of available donor diversity restricts our understanding of how human genetics affect drug-induced liver injury (DILI). Induced pluripotent stem cell-derived human hepatocyte-like cells (iPSC-HHs) could provide a complementary tool to PHHs for high-throughput drug screening, and ultimately enable personalized medicine. Here, we hypothesized that previously developed iPSC-HH-based micropatterned co-cultures (iMPCCs) with murine embryonic fibroblasts could be amenable to long-term drug toxicity assessment. iMPCCs, created in industry-standard 96-well plates, were treated for 6 days with a set of 47 drugs, and multiple functional endpoints (albumin, urea, ATP) were evaluated in dosed cultures against vehicle-only controls to enable binary toxicity decisions. We found that iMPCCs correctly classified 24 of 37 hepatotoxic drugs (65% sensitivity), while all 10 non-toxic drugs tested were classified as such in iMPCCs (100% specificity). On the other hand, conventional confluent cultures of iPSC-HHs failed to detect several liver toxins that were picked up in iMPCCs. Results for DILI detection in iMPCCs were remarkably similar to published data in PHH-MPCCs (65% versus 70% sensitivity) that were dosed with the same drugs. Furthermore, iMPCCs detected the relative hepatotoxicity of structural drug analogs and recapitulated known mechanisms of acetaminophen toxicity *in vitro*. Thus, iMPCCs could provide a robust tool to screen for DILI potential of large compound libraries in early stages of drug development using an abundant supply of commercially available iPSC-HHs.

2.1 Introduction and Background

Induced pluripotent stem cells (iPSCs) were first generated from adult dermal fibroblasts with the ectopic expression of four genes (Oct3/4, Sox2, c-Myc, and Klf4).[112–114] Most current techniques for differentiating iPSCs into iPSC-derived human hepatocyte-like cells (iPSC-HHs) involve a series of soluble factors designed to replicate those seen during embryonic development (i.e. FGF2, HGF, and OsM), and several groups have been successful in generating iPSC-HHs.[63,115–124] Such iPSC-HHs could provide a nearly unlimited supply of cells for building sustainable, high-throughput culture models for drug screening.[125] Furthermore, the genetic diversity seen in the human population can be more accurately modeled using multiple donors of iPSC-HHs, which can give greater insights into how genetic variations can impact idiosyncratic toxicity.[64] However, it is widely accepted that iPSC-HHs generated using temporal delivery of growth factors and ECMs alone have very low and declining functions (i.e. CYP450 activities) relative to adult PHHs.[63,116] Recent appraisals of drug toxicities in iPSC-HH cultures have been restricted to highly toxic compounds with acute dosings. Even then, several overtly liver toxic compounds in the clinic were not identified correctly in such cultures[65,126], potentially due to the very low activities of drug metabolism enzymes. Comparisons of DILI predictive power between functionally stable iPSC-HH and PHH cultures using the same drugs with diverse mechanisms of action should help spur the use of iPSC-HHs in drug toxicity assessments.

Co-culture with liver- and non-liver-derived stromal cells from multiple species has long been known to stabilize the phenotype of primary hepatocytes from human and animal livers *in vitro*[127,128]; organizing primary hepatocytes into the MPCC platform onto collagen-coated domains with empirically optimized dimensions and surrounding them with 3T3-J2 murine embryonic fibroblasts further improved hepatic functionality and longevity.[54] MPCCs induce long-term liver

functions in multiple species of primary hepatocytes and have been shown to predict clinical drug outcomes with significantly higher sensitivities than conventional culture models.[54,55,58] We recently optimized the MPCC technique for use with commercially available iPSC-HHs (iCell® Hepatocytes from Cellular Dynamics International), demonstrating substantial improvements in iPSC-HH functions for at least 4 weeks *in vitro* when benchmarked against multiple PHH donors and in contrast to a declining liver phenotype in conventional iPSC-HH monolayers.[66] In particular, iPSC-HHs in these so-called iPSC-HH-based micropatterned co-cultures (iMPCCs) contain an *in vivo*-like hepatocyte morphology and polarity, secrete albumin and urea, display activities of major CYP450 and Phase II enzymes, show drug-mediated CYP450 induction, and downregulate fetal markers.

In this study, we used a set of 47 drugs to assess the sensitivity and specificity of iMPCCs for DILI prediction and compared our results with both conventional iPSC-HH monolayers created from the same iPSC-HH donor as well as previously published results in PHH-MPCCs using an identical drug set.[58] We also demonstrated proof-of-concept in detecting donor-dependent differences in drug toxicity by using two separate donors of commercial iPSC-HHs. Furthermore, we explored the potential of iMPCCs for detecting the differential toxicity of structural drug analogs and to probe mechanisms of drug toxicity, two applications that are well-suited for the drug development pipeline. In the future, iMPCCs could be useful for a first tier drug toxicity screen prior to further studies in limited PHHs. As additional iPSC-HH lines with genetically diverse backgrounds become commercially available, we anticipate that iMPCCs could be useful to elucidate mechanisms underlying inter-individual susceptibilities to drug toxicity.

2.2 Materials and Methods

2.2.1 Processing of Induced Pluripotent Stem Cell-Derived Hepatocyte-Like Cells

iPSC-HHs were provided by Cellular Dynamics International (CDI; Madison, WI) and are available commercially as iCell Hepatocytes. Per information provided by CDI, iPSC-HH donor 1 is a Caucasian female whose iPSCs were originally reprogrammed from dermal fibroblasts, while iPSC-HH donor 2 is a Caucasian male whose iPSCs were originally reprogrammed from peripheral blood mononuclear cells. The iPSC-HHs from donor 1 were obtained fresh in flasks, whereas iPSC-HHs from donor 2 were cryopreserved in vials. Upon arrival, fresh iPSC-HHs were processed according to manufacturer-supplied protocols. In brief, iPSC-HH cell aggregates were retrieved from the cell shipment flask and pelleted via centrifugation ($100 \times g$ for 1 min). The pellet was rinsed with divalent cation-free Hank's Balanced Saline Solution (Hyclone, South Logan, UT) and further centrifuged at $100 \times g$ for 1 min. Pelleted cell aggregates were dissociated with 0.5% (m/v) trypsin-EDTA (Life Technologies, Grand Island, NY) for 7 min with intermittent swirling, neutralized with a 1:1 solution of Roswell Park Memorial Institute 1640 medium (RPMI; Life Technologies) and fetal bovine serum (Life Technologies), and pelleted via centrifugation ($100 \times g$ for 5 min) to remove the trypsin solution. De-aggregated iPSC-HHs were re-suspended in KryoThaw (SciKon Innovations, Research Triangle Park, NC) and again centrifuged to remove dead cells and excess debris ($100 \times g$ for 10 min). Finally, single iPSC-HHs were diluted in CDI's recommended plating medium (RPMI with 1 µM dexamethasone, 2% (v/v) B27 (Life Technologies), 1% (v/v) penicillin-streptomycin (Corning Life Sciences, Tewksbury, MA), and 20 ng/mL oncostatin-M (R&D Systems, Minneapolis, MN). Cryopreserved vials of iPSC-HHs from donor 2 were processed according to manufacturer protocols.

2.2.2 Fibroblast Culture

Murine embryonic 3T3-J2 fibroblasts were a gift from Howard Green of Harvard Medical School.[129] Cells were cultured at 37°C, 10% CO_2 in Dulbecco's modified Eagle's medium (Corning Life Sciences) with high glucose, 10% (v/v) bovine calf serum (Life Technologies), and 1% (v/v) penicillin-streptomycin. Fibroblasts were passaged up to 12 times prior to use in iMPCCs.

2.2.3 Establishment of iPSC-HH Cultures

Tissue culture polystyrene 96-well plates (Corning Life Sciences) were coated for 2 hours with 25 µg/mL rat tail collagen-I (Corning Life Sciences) and rinsed twice with sterile water. Following CDI's protocols, processed iPSC-HHs were diluted to a density of 8×10^5 cells/mL and seeded in collagen-coated plates (50 µL/well) to create conventional confluent monolayers (iCCs). Maintenance medium was replaced after the first 24 hours and every other day thereafter.

To create iMPCCs, tissue culture polystyrene 96-well plates were collagen coated as described above, and subjected to polydimethylsiloxane mask-based soft lithography to micropattern circular collagenous islands (500 µm diameter with 1200 µm center-to-center spacing).[66] iPSC-HHs were seeded at a density of 6.67×10^5 cells/mL into collagen micropatterned wells (50 µL/well). After allowing 4-5 hours for cellular attachment and spreading onto collagen-coated islands, wells were washed 3× in RPMI base medium to remove unattached cells, leaving ~4500 iPSC-HHs per well in 96-well format (~14 islands/well). The iPSC-HHs that attached to collagen domains were positive for both albumin and glycogen as previously shown.[66] 3T3-J2 fibroblasts were subsequently seeded at a density of 3×10^5 cells/mL (50 µL/well) and allowed to fill the remaining area surrounding the iPSC-HH islands. Micropatterned pure iPSC-

HH cultures (iMPHs), which did not receive 3T3-J2 fibroblasts, were used as density-matched controls. Culture medium was changed every other day as previously described.[66]

2.2.4 Hepatic Morphological, Functionality, and Health Assessments

The morphology of iPSC-HHs was monitored using an EVOS®FL cell imaging system (Life Technologies) with standard 4×, 10×, and 20× phase contrast objectives. Culture supernatants were assayed for albumin levels using a competitive enzyme-linked immunosorbent assay (MP Biomedicals, Santa Ana, CA) with horseradish peroxidase detection and 3,3',5,5'-tetramethylbenzidine (Rockland, Boyertown, PA) as the substrate.[54] Urea production was measured via a colorimetric endpoint analysis with diacetyl monoxime, acid, and heat (Stanbio Labs, Boerne, TX). CYP3A4 activity in iPSC-HH cultures was measured using the luminescence-based luciferin-IPA assay from Promega (Madison, WI) per manufacturer's instructions. ATP levels in cell lysates were quantified by CellTiter-Glo (Promega); levels in iMPCCs were subtracted from fibroblast-only controls to assess iPSC-HH-only contributions. Albumin, urea, and ATP assays were conducted on the same wells. Absorbance and luminescence for the aforementioned assays were measured using a BioTek (Winooski, VT) Synergy H1 tri-mode plate reader.

2.2.5 Drug Dosing Studies

After ~1 week of stabilization, cultures were dosed three times in serum-free culture medium (i.e. little to no binding of drug to protein) every other day at $25 \times C_{max}$ and $100 \times C_{max}$ (total human plasma concentration, Table 2.1). The DMSO concentration that iPSC-HH cultures were exposed to was kept at 0.1% (v/v) relative to culture medium for all compounds except that 0.2% (v/v) was used for five compounds (acetazolamide, cyclophosphamide, hydroxyurea, mefenamic acid, and quinine), while 1.0% (v/v) was used for three compounds (phenacetin, phenylbutazone,

and pyrazinamide) due to solubility issues. Compounds and dose ranges were selected from a previous study[38] to include true positive (TP, compounds that were correctly identified as toxic in primary hepatocyte imaging assay technology [HIAT]), true negative (TN, compounds that were correctly identified as non-toxic in HIAT), and false negative (FN, compounds that were incorrectly identified as non-toxic in HIAT) compounds. All compounds were purchased from either Sigma-Aldrich (St. Louis, MO) or Cayman Chemical (Ann Arbor, MI). Vehicle-only controls were maintained at each DMSO concentration listed above.

For some studies, the glutathione (GSH) depleting agent L-buthionine (S,R)-sulfoximine (BSO; Sigma-Aldrich) was co-incubated at a dose of 200 µM with acetaminophen (APAP) following the same treatment schedule described above (i.e. three repeat dosings over 6 days). Additional cultures were co-incubated with APAP and 10 µM of the broad CYP450 inhibitor 1-aminobenzotriazole (ABT; Sigma-Aldrich). Controls with only BSO or ABT (i.e. no APAP) were included for baseline toxicity measurement.

2.2.6 Data Analysis

Data processing and visualization were performed using Microsoft Excel and GraphPad Prism (La Jolla, CA), respectively. For each assay, data were normalized to the appropriate vehicle-only control, and mean and standard deviation values were calculated three technical replicates for each of the drug doses administered. TC_{50} values (concentration that decreased the measured endpoints by 50%) for each assay were interpolated using linear curve fitting between the dose at which the assay signal was greater than 50% of control values and the dose at which the assay signal was below 50% of control values. A compound that yielded a TC_{50} value $\leq 100 \times C_{max}$ for any one of the three assays was classified as 'toxic', while a compound that had TC_{50} values $>100 \times C_{max}$ (i.e. could not be interpolated within the dose range tested) for all three

assays was classified as 'non-toxic'. Sensitivity was defined as the fraction of correctively predicted positive toxins to all positive toxins in the clinic ([TP]/[TP + FN]). Specificity was defined as the fraction of correctly predicted negatives (i.e. non-hepatotoxic) to all negatives in the clinic ([TN]/[TN + FP]). TP = true positives, FN = false negatives, TN = true negatives, and FP = false positives. All findings were confirmed in at least two independent experiments from iPSC-HH derived from donor 1, while iPSC-HHs from donor 2 were incubated with a subset of drugs.

2.3 Results

2.3.1 Functional Stability of the iMPCC Platform

Khetani and Bhatia have previously developed a MPCC platform in which primary hepatocytes are organized onto collagen-coated islands of empirically optimized dimensions and subsequently surrounded by 3T3-J2 murine embryonic fibroblasts,[54] now known to induce robust functions in hepatocytes from multiple species.[130] We have recently adapted and optimized the MPCC technique for culture with iPSC-HHs, commercially available as iCell® Hepatocytes by Cellular Dynamics International (CDI; Madison, WI). Liver functions (albumin secretion, urea synthesis, CYP3A4 activity) in these so-called iMPCCs (500 μm diameter with 1200 μm center-to-center spacing) were found to be significantly higher and stable for 4 weeks as compared with a declining phenotype in density-matched micropatterned pure iPSC-HH (iMPH) monolayers (Figure 2.1A-C). Furthermore, iPSC-HHs in iMPCCs displayed prototypical polygonal hepatic shape, distinct nuclei/nucleoli, and presence of bile canaliculi between cells. On the other hand, iPSC-HHs looked 'de-differentiated' (i.e. spread out) in pure monolayers without fibroblasts after a week in culture (Figure 2.1D-E). The stability of iMPCCs allowed us to carry out the repeat drug treatment protocol as described in subsequent sections.

In addition to the aforementioned dataset, liver gene expression and functions (including major CYP450 enzymes and Phase II conjugation) in iMPCCs have been more extensively characterized earlier[66], and were shown to be significantly higher and more stable for at least 4 weeks when compared to declining functions in commonly employed conventional confluent monolayers. In brief, analysis of iMPCC whole genome microarrays by CellNet[131], a network biology platform used to evaluate the fidelity of engineered cells by measuring the establishment of tissue-specific gene regulatory networks, classified iMPCCs as exclusively liver, with liver-specific gene regulatory network scores that fell within the range of scores obtained for two freshly isolated PHH donors. Albumin secretion by iMPCCs was within the range of donor diversity observed in PHH-MPCCs, while urea production was ~30-50% of PHH-MPCCs. CYP450 activity levels in iMPCCs ranged from ~5% (CYP2C19) to ~70% (CYP1A2) of PHH-MPCCs. We showed up to ~90% of CYP3A4 activity in iMPCCs relative to conventional 24 hour-old PHH cultures and ~40-55% relative to functionally stable PHH-MPCCs from multiple donors. Finally, the albumin to alpha-fetoprotein protein ratio in iMPCCs increased from 7.2 on day 11 to 12.2 on day 21 of culture, thereby demonstrating improving maturity of iPSC-HHs over time.
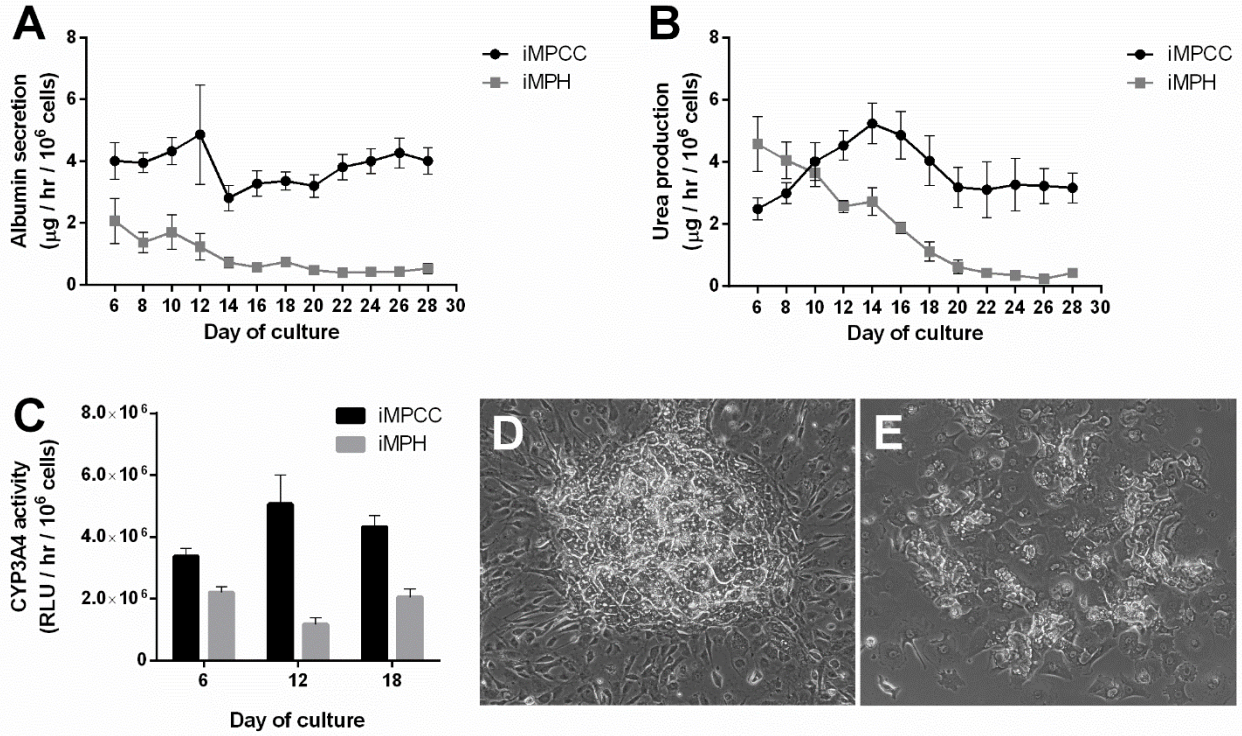
Figure 2.1: Characterization of the iPSC-HH-based micropatterned co-culture (iMPCC) model. **(A)** Albumin secretion, **(B)** urea production, and **(C)** CYP3A4 activity of iMPCCs and micropatterned iPSC-HHs without 3T3-J2 fibroblasts (iMPHs) over 4 weeks in culture. All error bars represent standard deviations (n = 3). **(D)** iMPCC and **(E)** iMPH island morphology after 14 days in culture.

2.3.2 Compound Selection, Culture Dosing, and Criteria for Toxicity Decisions

We selected 47 compounds from a previously published study in which conventional sandwich-cultured PHHs were dosed with compounds for 24 hours followed by analysis via hepatocyte imaging assay technology (HIAT) to assess organelle dysfunctions (i.e. mitochondrial membrane potential, reactive oxygen species).[38] Thirteen of these compounds were reported as DILI positive (TPs), meaning that hepatotoxicity was observed for these drugs in HIAT at a concentration at or below $100 \times C_{max}$ (maximum plasma concentration reported for humans). Ten drugs did not elicit hepatotoxicity in HIAT at a test concentration of $100 \times C_{max}$ and are also considered safe in humans (TNs). Another 24 DILI compounds were not identified as toxic utilizing HIAT, but are known to cause clinical DILI (FNs). In addition, PHH-MPCCs have been previously dosed over 5-9 days with these same compounds and binary decisions on toxicity potential have been published.[58] Here, we sought to compare drug responses in iMPCCs relative to PHH-based models used in these previously published studies.

Preliminary investigations using nine compounds (acetaminophen, amiodarone, aspirin, dextromethorphan, diclofenac, propranolol, rosiglitazone, troglitazone, and warfarin) revealed that the sensitivity in iMPCCs to be the highest while maintaining 100% specificity after 6 days of dosing (three drug treatments administered every other day) based on the TC_{50} criteria described below. Albumin, urea, and ATP levels were assessed in iMPCCs using the same wells. While albumin and urea are liver-specific markers and are not secreted by the 3T3-J2 fibroblasts used here, ATP is present in both cell types and thus fibroblast-only control cultures were carried out alongside iMPCCs to determine effects of drugs on iPSC-HHs in particular. Since intracellular GSH was previously found to be less sensitive for binary DILI prediction in PHH-MPCCs[58], it was not tested in iMPCCs here. That being said, GSH levels can prove to be useful in a more

investigative scenario where drug bioactivation is suspected to be the mechanism of toxicity. Sample drug dose responses in iMPCCs for hepatotoxins and non-liver toxins are shown in Figure 2.2.

The DMSO concentration that iPSC-HH cultures were exposed to was kept at 0.1% (v/v) relative to culture medium for 39 of 47 compounds tested, while 0.2% (v/v) was used for five compounds, and 1.0% (v/v) was used for three compounds due to solubility issues (Table 2.1). Increasing levels of DMSO in culture medium, as expected from previously published data[132], did indeed cause a reduction in CYP3A4 activity in the cultures (~8% reduction at 0.1% (v/v) DMSO concentration, ~25% at 0.2% (v/v), and ~40% at 1.0% (v/v)). However, appropriate control cultures at each DMSO concentration were used to normalize data from drug-dosed cultures to enable binary decisions as described below. A compound was declared 'toxic' if the TC_{50}, the drug concentration that reduces endpoint functional activity to 50% of vehicle-only controls, was at or below $100 \times C_{max}$ for at least one of the multiplexed assays on iMPCCs. If the TC_{50} value was $>100 \times C_{max}$ for all three multiplexed assays (i.e. could not be interpolated from the dose range tested), the compound was considered 'non-toxic'. Table 2.1 provides the C_{max} values, formula weights, known clinical DILI classifications, and toxic/non-toxic decisions in iMPCCs relative to published information using PHH-MPCCs and the HIAT assay. If applicable, the DILI severity score from the Liver Toxicity Knowledge Base (LTKB), provided by the United States Food and Drug Administration, appears in the respective column of Table 2.1. C_{max} values for these compounds varied widely across the entire set, from 0.004 µM for betahistine 2HCl to 793.9 µM for hydroxyurea.
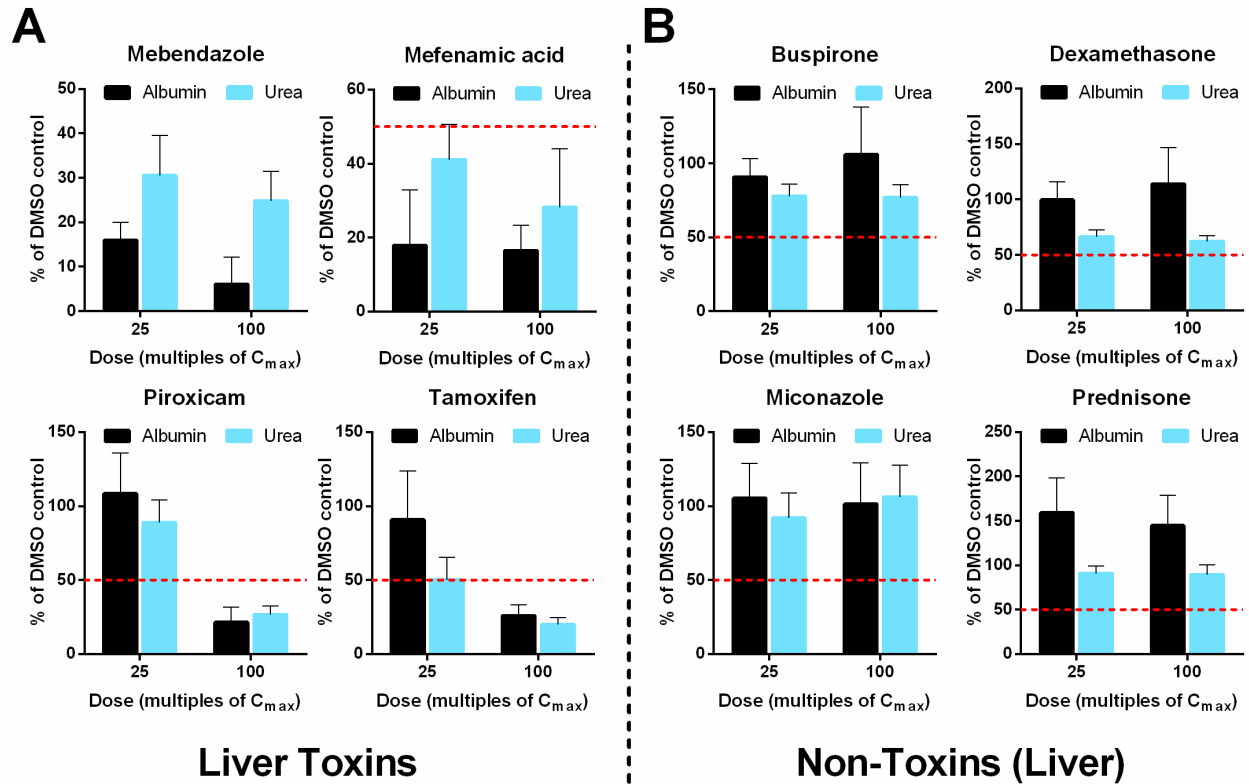
Figure 2.2: Dose-dependent downregulation of albumin and urea secretion in iMPCCs following drug dosing. (A) iMPCCs were dosed for 6 days (fresh drug added to culture medium every 2 days) with prototypical hepatotoxins. Albumin and urea secretion were assessed in culture supernatants. **(B)** Same as in panel 'A' but non-toxic drugs with respect to the liver were tested on iMPCCs. All data were normalized to DMSO-only control cultures. Error bars represent standard deviations (n = 3).

Table 2.1: Compounds tested and binary decisions of toxicity in different models

Compound name	C$_{max}$ (μM)	FW (g/mol)	DMSO (vol%)	DILI Severity	DILI Category	DILI Clinical	HIAT	PHH-MPCCs	iMPCCs
TPs in HIAT									
Acetaminophen	151.170	138.91	0.2	N/A	P2	+	+	+	+
Amiodarone	0.806	681.80	0.1	8	P2	+	+	+	+
Benzbromarone	4.361	424.10	0.1	-2	P1	+	+	+	+
Clozapine	0.951	326.83	0.1	2	P2	+	+	+	+
Diclofenac	8.023	318.10	0.1	7	P2	+	+	+	+
Flurbiprofen	57.356	244.27	0.1	3	P2	+	+	+	+
Mebendzole	0.126	295.30	0.1	3	P2	+	+	+	+
Mefenamic acid	26.959	241.30	0.2	N/A	P2	+	+	+	+
Phenacetin	13.401	179.22	1.0	N/A	P2	+	+	+	+
Phenylbutazone	486.772	308.37	1.0	N/A	P2	+	+	+	+
Quinine	9.254	391.47	0.2	N/A	P2	+	+	+	+
Trazodone HCl	5.065	408.32	0.1	N/A	P2	+	+	+	+
Troglitazone	6.387	441.50	0.1	-2	P1	+	+	+	+
TNs in HIAT									
Aspirin	5.526	180.16	0.1	N/A	O2	–	–	–	–
Buspirone	0.005	421.96	0.1	3	N1	–	–	–	–
Dexamethasone	0.224	392.47	0.1	3	N1	–	–	–	–
Dextromethorphan HBr	0.028	370.30	0.1	N/A	N1	–	–	–	–
Fluoxetine	0.049	345.79	0.1	3	N2	–	–	–	–
Miconazole	0.024	479.10	0.1	N/A	N1	–	–	–	–
Prednisone	0.068	358.43	0.1	N/A	N2	–	–	–	–
Propranolol	0.201	295.81	0.1	3	N1	–	–	–	–
Rosiglitazone	1.120	357.43	0.1	N/A	N2	–	–	–	–
Warfarin	4.868	308.34	0.1	5	N2	–	–	–	–
FNs in HIAT									
Acetazolamide	135.142	222.25	0.2	N/A	P2	+	–	+	–
Betahistine 2HCl	0.004	209.12	0.1	6	P2	+	–	–	–
Captopril	4.284	217.29	0.1	7	P2	+	–	–	–
Chloramphenicol palmitate	19.991	561.54	0.1	N/A	P2	+	–	–	–
Ciprofloxacin HCl	11.476	331.34	0.1	7	P2	+	–	+	+
Clomiphene citrate	0.022	598.10	0.1	N/A	P2	+	–	–	–
Clomipramine	0.191	351.30	0.1	N/A	P2	+	–	+	+
Cyclophosphamide	265.359	279.10	0.2	5	P2	+	–	+	+
Cyproterone acetate	0.656	416.94	0.1	N/A	O1	+	–	+	+
Danazol	0.074	337.50	0.1	8	P1	+	–	–	–
Dapsone	6.007	248.30	0.1	N/A	P1	+	–	+	–
Estrone	0.022	270.37	0.1	N/A	P2	+	–	–	–
Hydroxyurea	793.925	76.05	0.2	8	P2	+	–	+	+
Imipramine HCl	0.087	316.87	0.1	3	P2	+	–	+	+
Isoniazid	76.609	137.14	0.1	8	P1	+	–	+	+
Maleic acid	1.000	160.04	0.1	N/A	O1	+	–	+	–
Methimazole	1.868	114.17	0.1	8	P2	+	–	–	–
Nifedipine	0.271	346.30	0.1	3	P2	+	–	–	–
Norgestrel	0.009	312.45	0.1	N/A	P2	+	–	–	–
Nortriptyline HCl	0.122	299.84	0.1	8	P2	+	–	+	+
Piroxicam	5.135	331.37	0.1	3	P2	+	–	–	+

Compound name	C_{max} (µM)	FW (g/mol)	DMSO (vol%)	DILI Severity	DILI Category	Clinical	HIAT	PHH-MPCCs	iMPCCs
Progesterone	0.193	314.46	0.1	N/A	P2	+	–	–	–
Pyrazinamide	407.174	123.11	1.0	3	P2	+	–	+	+
Tamoxifen	0.162	371.53	0.1	6	P2	+	–	+	+

Notes. Compounds were selected from the study by Xu *et al.*[38] where HIAT was applied to ECM-sandwich cultures of PHHs dosed for 24 hours with various drugs. DILI severity scores from the LTKB (Liver Toxicity Knowledge Base) of the U.S. Food and Drug Administration[133]: "N/A" indicates not applicable/no information in the database, negative numbers indicate the drug was withdrawn from the market, and higher positive numbers indicate a greater DILI concern. DILI categorization: P1, DILI type 1, dose-dependent (toxic); P2, DILI type 2, idiosyncratic (toxic); N1, not known to cause liver injury (non-toxic); N2, sporadic cases (<10) of liver injury reported but generally considered by doctors as a safe drug to use for humans (non-toxic); O1, hepatotoxic in animals, untested in humans (toxic); O2, elevated liver enzymes observed in humans but does not lead to frank liver toxicity (non-toxic). Clinical classification per Xu *et al.*[38]: considered a liver toxin (+) or a non-liver toxin (–). Model predictions: All models were dosed up to $100 \times C_{max}$ for each compound and classified as liver toxins or non-toxins based on specific algorithms as described in methods. The HIAT-sandwich classifications are from Xu *et al.*[38], the PHH-MPCC classifications are from Khetani *et al.*[58], while the iMPCC (using iPSC-HHs) classifications represent the data collected in this study.

2.3.3 DILI True Positive Compounds

C_{max} values for the 13 TP compounds used in this study varied from 0.126 µM for mebendazole to 486.8 µM for phenylbutazone. Figure 2.3A provides the interpolated TC_{50} values for these compounds as calculated by albumin and urea, two critical functions of the liver which have been recently shown to be as sensitive for DILI detection in PHHs *in vitro* as more conventional endpoints such as ATP and GSH.[58] Furthermore, albumin and urea can be monitored in cell culture supernatants over time without the need to lyse the cultures. We found that iMPCCs, similar to PHH-MPCCs and the HIAT assay, correctly detected all 13 TP compounds as 'toxic' based on the TC_{50} algorithm described above. Urea production by iMPCCs was reduced by at least 50% following administration of all 13 compounds, while albumin secretion was reduced by at least 50% following administration of 12 of the 13 compounds (flurbiprofen being the exception). ATP (data not shown) was reduced by at least 50% by 10 of 13 compounds (except flurbiprofen, mebendazole, and troglitazone). Thus, as with PHH-MPCCs, ATP data in iMPCCs proved to be less sensitive than albumin and urea secretion for DILI detection.
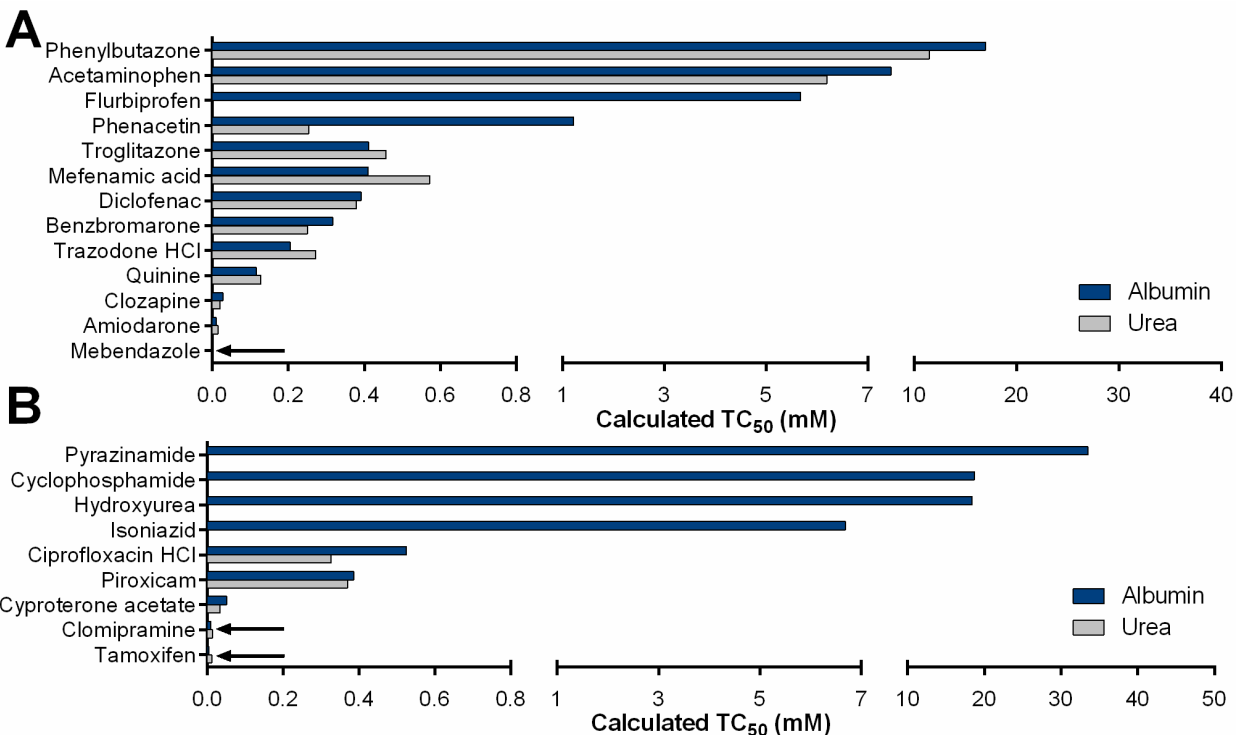
Figure 2.3: Rank ordering of hepatotoxins in iMPCCs. **(A)** Albumin and urea secretion TC_{50} values of HIAT TP compounds[38] (see Table 2.1) that were picked up correctly in iMPCCs. TC_{50} is defined as the interpolated drug concentration that reduces the endpoint to 50% of DMSO-only controls. Arrows indicate a measurable but very low TC_{50} (i.e. very toxic compound) that could be interpolated from the dose range tested for each compound ($\leq 100 \times C_{max}$), while missing bars indicate a TC_{50} that could not be interpolated ($> 100 \times C_{max}$). **(B)** Rank ordering as in panel 'A', but for HIAT FN compounds detected correctly in the iMPCC model.

2.3.4 DILI True Negative Compounds

C_{max} values of the TN compounds tended to be lower than those for the TP compounds and ranged from 0.005 µM for buspirone to 5.526 µM for aspirin. None of the 10 TN compounds tested showed a 50% or greater reduction in albumin, urea, or ATP in iMPCCs. Hence, all were correctly identified as 'non-toxins' in all three models that were compared (iMPCCs, PHH-MPCCs, and HIAT). Therefore, the specificity of the iMPCC assay was not lower than the aforementioned PHH-based models.

2.3.5 DILI False Negative Compounds

C_{max} values for the 24 FN compounds ranged from 0.004 µM for betahistine 2HCl to 793.9 µM for hydroxyurea. Eleven of the 24 FN compounds caused at least a 50% reduction in at least one or more of the markers (albumin, urea, or ATP) evaluated in iMPCCs. TC_{50} values from the iMPCC albumin and urea data are presented graphically in Figure 2.3B. Ciprofloxacin HCl and piroxicam caused reductions in all three parameters while clomipramine, cyproterone acetate, and tamoxifen caused reductions in albumin and urea. Hydroxyurea was the only compound that led to reductions in both albumin and ATP, but not urea likely due to its interference with the urea assay. Albumin was the only marker reduced by at least 50% following dosing of iMPCCs with cyclophosphamide, isoniazid, and pyrazinamide. Urea was the only marker reduced by at least 50% following dosing of iMPCCs with imipramine HCl and nortriptyline HCl.

2.3.6 Comparison of Drug Toxicity in iMPCCs with Other Models

For the drugs that were correctly identified as 'toxic' in both iMPCCs and in PHH-MPCCs in a previous study[58], we compared TC_{50} values for albumin secretion in both models (Table 2.2). Twelve of these 21 compounds led to albumin TC_{50} values higher in iMPCCs relative to PHH-MPCCs, while nine compounds had albumin TC_{50} values higher in PHH-MPCCs relative to

iMPCCs. Albumin secretions in PHH-MPCCs (but not in iMPCCs) was not reduced by at least 50% in response to cyproterone acetate, isoniazid, and phenacetin within the dose range tested (i.e. no TC_{50} for albumin could be interpolated). However, PHH-MPCCs were able to correctly identify three 'toxic' FN drugs that were missed in iMPCCs: acetazolamide, dapsone, and maleic acid (Table 2.1). The aforementioned differences between iMPCCs and PHH-MPCCs in drug toxicity outcomes could potentially be due to donor-dependent phenomena. Indeed, when we dosed PHH-MPCCs created from another donor with acetazolamide, dapsone, and maleic acid, we found that only dapsone was called 'toxic' based on the aforementioned algorithm, while the other two compounds were called 'non-toxic' (Table 2.3). Interestingly, piroxicam was picked up in iMPCCs containing donor 1 iPSC-HHs, but not in PHH-MPCCs, which further suggests donor-dependent differences.

Next, we selected 13 drugs (TP or FN) that were picked up as toxins in iMPCCs to test on conventional confluent iPSC-HH cultures (iCCs, created per protocols from CDI) from the same donor cells. Five of these 13 compounds failed to show toxicity in iCCs (~38% reduction in sensitivity, Table 2.4). For instance, phenacetin was picked up in the HIAT assay using PHHs[38], PHH-MPCCs[58], and iMPCCs here, but not using the iCC model.

Table 2.2: Comparison of albumin TC$_{50}$ values in PHH-MPCCs and iMPCCs

| Compound name | Albumin TC$_{50}$ (µM) | |
	PHH-MPCCs	iMPCCs
TPs in HIAT		
Acetaminophen	8804.1	9772.1
Amiodarone	8.5	9.7
Benzbromarone	31.3	316.5
Clozapine	39.6	27.8
Diclofenac	141.9	391.5
Flurbiprofen	2406.8	5683.4
Mebendzole	11.6	1.9
Mefenamic acid	1291.9	410.3
Phenacetin	N/A	1213.3
Phenylbutazone	6414.4	16968.9
Quinine	251.6	115.7
Trazodone HCl	64.8	205.5
Troglitazone	339.9	456.7
FNs in HIAT		
Ciprofloxacin HCl	160.0	525.3
Clomipramine	9.4	9.4
Cyclophosphamide	1449.4	18670.7
Cyproterone acetate	N/A	51.0
Hydroxyurea	28616.2	18398.4
Isoniazid	N/A	6681.1
Pyrazinamide	20420.3	33457.5
Tamoxifen	3.2	4.2

Note. "N/A" indicates that a TC$_{50}$ value (the linearly interpolated concentration at which activity decreases by 50% of DMSO-only controls) was above 100×C$_{max}$ and therefore could not be calculated based on the dose range tested.

Table 2.3: Comparison of PHH-MPCCs and iMPCCs

Compound name	PHH-MPCC functions (% of DMSO-only control)			iMPCC functions (% of DMSO-only control)		
	Albumin	Urea	ATP	Albumin	Urea	ATP
Acetazolamide	96.1	84.7	127.8	59.2	86.0	103.0
Dapsone	66.3	**46.9**	93.3	134.1	87.2	127.6
Maleic acid	87.6	65.4	89.9	78.0	83.0	93.2

Notes. Data is presented as percentages of functions in drug-treated cultures relative to DMSO-only control cultures. Bolded value dips below 50%. The PHH donor used here (HUM4011 from Triangle Research Labs, male, Caucasian, age 26, BMI 18, no history of smoking, alcohol, or drug use) was different than used in the prior study.[58]

Table 2.4: Hepatotoxins tested in iPSC-HH confluent monolayers (iCCs) and iMPCCs

Compound name	Liver toxin (+) or non-toxin (−)		
	Clinical	iCC	iMPCCs
Benzbromarone	+	+	+
Ciprofloxacin HCl	+	+	+
Clozapine	+	+	+
Cyclophosphamide	+	+	+
Cyproterone acetate	+	−	+
Diclofenac	+	+	+
Flurbiprofen	+	+	+
Hydroxyurea	+	+	+
Isoniazid	+	−	+
Phenacetin	+	−	+
Piroxicam	+	+	+
Pyrazinamide	+	−	+
Tamoxifen	+	−	+

Note. Bolded compounds are those where there are different calls in the models.

2.3.7 Overall Sensitivity and Specificity at TC$_{50}$

We define model sensitivity as the portion of clinical hepatotoxins correctly identified as 'toxic' *in vitro* ([TP]/[TP + FN]), while the specificity as the portion of non-liver toxic compounds correctly identified as 'non-toxic' *in vitro* ([TN]/[TN + FP]). As detailed in Table 2.5, iMPCCs and PHH-MPCCs had sensitivities of 65% and 70%, respectively, for the 37 hepatotoxic compounds tested. Both models correctly identified all 10 non-liver toxins and thus had a specificity of 100%.

Table 2.5: Confusion matrix for binary decisions in PHH-MPCCs and iMPCCs

	Model-predicted DILI in MPCCs		
Actual DILI	Positive	Negative	Total
Positive	PHH: 26	PHH: 11	37
	iPSC-HH: 24	iPSC-HH: 13	
Negative	PHH: 0	PHH: 10	10
	iPSC-HH: 0	iPSC-HH: 10	
Total	PHH: 26	PHH: 21	47
	iPSC-HH: 24	iPSC-HH: 23	

Note. Sensitivity: 70% and 65% for PHH-MPCCs and iMPCCs, respectively. Specificity: 100% for both models.

2.3.8 Comparison of TC₅₀ Values Across iPSC-HH Donors in iMPCCs

iPSC-HHs from a second donor were incorporated into the iMPCC platform (see Section 2.2.3) and the cultures were dosed for 6 days with all 24 drugs correctly classified as 'liver toxins' with the first iPSC-HH donor and five non-toxic control drugs. The albumin and urea TC_{50} values for the two donors are shown in Table 2.6. While there are differences in the TC_{50} values across the two donors as expected, both donors correctly classified 22 of the 24 liver toxins and all five non-toxins. The second donor was not able to correctly two of the 24 drugs as liver toxins, namely phenacetin and piroxicam.

Table 2.6: Comparison of TC$_{50}$ values between iPSC-HH donors cultured in iMPCCs

Compound name	Donor 1 TC$_{50}$ (µM)		Donor 2 TC$_{50}$ (µM)	
	Albumin	Urea	Albumin	Urea
TPs in HIAT				
Acetaminophen	9772.1	6195.9	4990.1	2773.8
Amiodarone	9.7	15.1	15.6	12.7
Benzbromarone	316.5	249.8	N/A	78.9
Clozapine	27.8	20.9	111.2	13.7
Diclofenac	391.5	378.3	3239.9	142.2
Flurbiprofen	5683.4	N/A	2222.0	N/A
Mebendzole	1.9	2.3	3.1	1.9
Mefenamic acid	410.3	572.2	567.0	518.3
Phenacetin	1213.3	253.3	N/A	N/A
Phenylbutazone	16968.9	11497.6	51639.0	15866.9
Quinine	115.7	127.9	216.5	311.8
Trazodone HCl	205.5	272.4	N/A	97.5
Troglitazone	411.4	456.7	486.3	262.5
TNs in HIAT				
Aspirin	N/A	N/A	N/A	N/A
Buspirone	N/A	N/A	N/A	N/A
Dexamethasone	N/A	N/A	N/A	N/A
Miconazole	N/A	N/A	N/A	N/A
Prednisone	N/A	N/A	N/A	N/A
FNs in HIAT				
Ciprofloxacin HCl	525.3	326.3	275.2	289.1
Clomipramine	9.4	13.8	2.9	3.1
Cyclophosphamide	18670.7	N/A	10165.7	11818.3
Cyproterone acetate	51.0	33.1	12.7	16.5
Hydroxyurea	18398.4	N/A	10679.9	N/A
Imipramine HCl	N/A	5.9	1.1	1.1
Isoniazid	6681.1	N/A	N/A	2672.1
Nortriptyline HCl	N/A	7.7	3.9	4.0
Piroxicam	387.0	370.0	N/A	N/A
Pyrazinamide	33457.5	N/A	N/A	19344.8
Tamoxifen	4.2	11.7	4.5	3.7

Notes. "N/A" indicates that a TC$_{50}$ value (the interpolated concentration at which cell function decreases by 50% of respective DMSO-only controls) was above 100×C$_{max}$ for a given endpoint and therefore could not be calculated from the dose range used. Bolded compounds are those for which neither of the two endpoints could be used to interpolate a TC$_{50}$ value for donor 2.

2.3.9 Structural Drug Analogs and Bioactivation of Acetaminophen

When treated with structural drug analogs, the iMPCC platform was able to distinguish differences in toxicity between known hepatotoxins and their less toxic analogs. Figure 2.4A shows albumin secretion in iMPCCs treated with increasing doses of tolcapone (hepatotoxic) or entacapone for up to 96 hours. Only tolcapone led to a severe decline in iMPCC albumin secretion with time and dose, whereas albumin secretion remained relatively steady when iMPCCs were treated with entacapone. A similar trend was observed with the analogs troglitazone (hepatotoxic) and rosiglitazone (Figure 2.4B).

To probe drug activation, iMPCCs were co-incubated with APAP and compounds that are known to impact the metabolic pathways of APAP. When iMPCCs were treated with both the GSH depleting agent L-buthionine (S,R)-sulfoximine or BSO, and multiple doses of APAP, they experienced a significantly greater decline in albumin secretion than when treated with APAP alone (Figure 2.5A). On the other hand, treating iMPCCs with both the broad CYP450 inhibitor 1-aminobenzotriazole (ABT), and APAP led to a reduction in toxicity (i.e. increase in albumin output) than when treated with APAP alone (Figure 2.5B). Neither BSO nor ABT alone led to downregulation of albumin secretion in iMPCCs (data not shown). The aforementioned results suggest that APAP toxicity in iMPCCs occurs through CYP450-mediated formation of a reactive metabolite that is subsequently detoxified via GSH, as observed both *in vitro* in primary hepatocytes[130] and *in vivo* in rodents.[134]
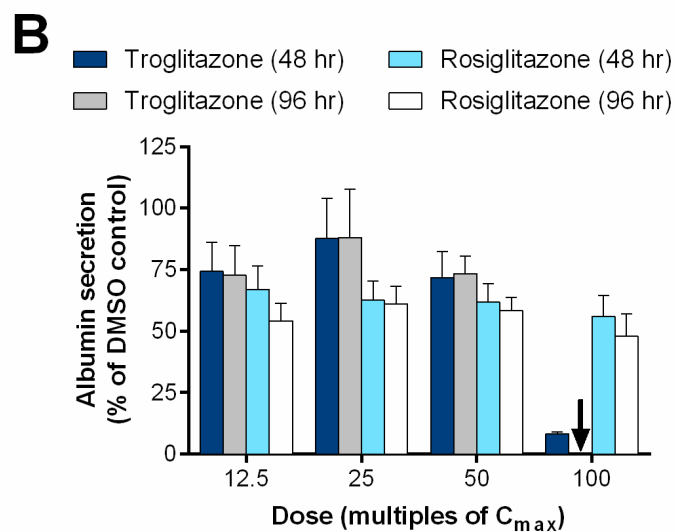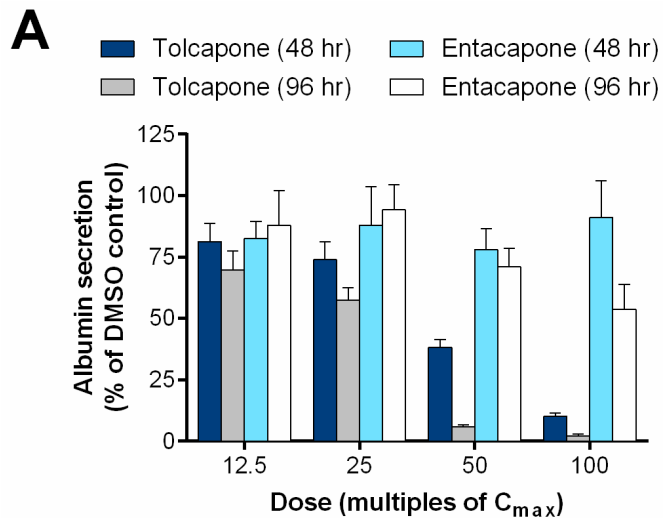
Figure 2.4: Differential toxicity of structural drug analogs in the iMPCC model. **(A)** Time- and dose-dependent albumin secretion in iMPCCs treated for up to 96 hours (fresh drug added to culture medium every 48 hours) with tolcapone (hepatotoxic) and entacapone (non-toxic with respect to the liver). **(B)** Same as in panel 'A' except troglitazone (hepatotoxic) and rosiglitazone (non-toxic with respect to the liver) were utilized. The arrow indicates undetectable albumin secretion in cultures dosed with troglitazone for 96 hours. All data were normalized to DMSO-only controls. Error bars represent standard deviations (n = 3).
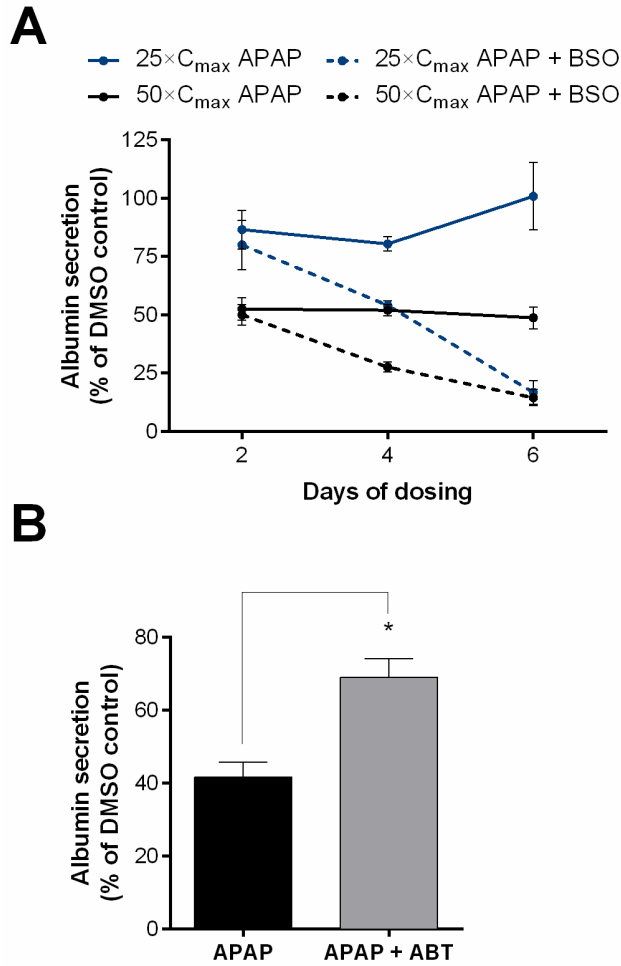
Figure 2.5: Bioactivation of acetaminophen in the iMPCC model. **(A)** Time- and dose-dependent albumin secretion in iMPCCs dosed with acetaminophen (APAP) with or without the GSH depleting agent L-buthionine (S,R)-sulfoximine (BSO) at 200 µM. **(B)** Albumin secretion after 4 days of treatment (fresh drug added to culture medium every 2 days) with $100 \times C_{max}$ APAP with or without the broad CYP450 inhibitor 1-aminobenzotriazole (ABT) at 10 µM. BSO and ABT alone (without APAP) did not lead to downregulation of albumin secretion in iMPCCs (data not shown). All data were normalized to DMSO-only controls. Error bars represent standard deviations (n = 3). *$p < 0.05$ (Student's t test, GraphPad Prism software).

2.4 Discussion

In contrast with a limited supply of PHHs, iPSC-HHs could provide a nearly unlimited supply of cells for screening compound libraries in early drug discovery where structure-activity relationships can aid in the design of safer and more efficacious drugs. These cells could also enable a better understanding of inter-individual susceptibility to drugs, including mechanisms underlying idiosyncratic drug toxicity.[125] We have recently shown that when housed in an MPCC format with murine embryonic fibroblasts (iMPCCs), iPSC-HHs from multiple donors display significantly greater levels and stability of major hepatic functions (i.e. CYP450 activities) for ~4 weeks as opposed to a declining phenotype in conventional iPSC-HH monolayers.[66] Here, we showed that the predictive power for DILI assessment in iMPCCs was remarkably similar (65-70% sensitivity, 100% specificity) to their PHH-MPCC counterparts (Table 2.1). Furthermore, we also demonstrated iMPCC utility in assessing donor-dependent differences in drug toxicity outcomes, detecting differential toxicity of structural drug analogs, and probing bioactivation mechanisms underlying DILI using APAP.

We chose 47 drugs from different classes that have previously been tested in sandwich-cultured PHHs using HIAT and PHH-MPCCs.[38,58] Given the variable drug concentrations observed in human blood, partially attributed to polymorphisms in hepatic drug metabolism enzymes and transporter proteins, drug doses up to $100 \times C_{max}$ were selected as justified previously.[38] Nonetheless, our dose selection here enabled quantitative comparisons between iPSC-HH responses and those observed with PHHs in the aforementioned studies. As with PHH-MPCCs, liver dysfunction in iMPCCs was assessed via albumin and urea secretions in supernatants, while overall viability was assessed using ATP in cell lysates. The 3T3-J2 fibroblasts did not secrete albumin and urea, while ATP levels in iMPCCs were ~2-fold higher

than in fibroblast-only controls. Select compounds were used to first optimize the timing of dosing (three drug doses over 6 days) such that sensitivity was improved without compromising high specificity. A drug was called 'toxic' if a TC_{50} value could be interpolated for any of the three endpoints within the dose range tested, while the drug was called 'non-toxic' if none of the endpoints yielded an interpolated TC_{50} value.

All 13 TP compounds were correctly identified in iMPCCs. Urea production was the most sensitive endpoint (13 of 13 compounds), followed by albumin (12 of 13) and ATP (9 of 13). Furthermore, none of the 10 TN compounds caused a reduction of 50% or more in any endpoint. Thus, non-destructive measurement of albumin and urea in medium can suffice for an initial dose- and time-dependent assessment of drug toxicity in both iMPCCs and PHH-MPCCs.[58] Other parameters such as GSH or high content imaging of organelle dysfunctions can subsequently be used for a detailed, mechanistic exploration of hepatotoxicity. The 100% sensitivity for TP compounds and 100% specificity for TN compounds observed in iMPCCs were consistent with studies using PHH cultures.[38,58]

From the 24 FN compounds, 11 were detected as toxic in iMPCCs. For these compounds, albumin secretion was the most sensitive endpoint (9 of 11 compounds), followed by urea (7 of 11), and ATP (3 of 11). Two compounds (ciprofloxacin and piroxicam) caused a $\geq 50\%$ reduction in all three markers, while four others (clomipramine, cyproterone acetate, hydroxyurea, and tamoxifen) caused a reduction in two markers. Hydroxyurea was the only compound to be identified as toxic with ATP and albumin; however, this compound interfered with the urea assay. When the 13 compounds correctly identified as toxic in iMPCCs were also tested in conventional confluent iPSC-HH monolayers from the same donor, five (cyproterone acetate, phenacetin, isoniazid, pyrazinamide, and tamoxifen) failed to show toxicity, leading to a ~38% reduction in

sensitivity. Thus, the iMPCC platform improved the sensitivity for drug toxicity detection in iPSC-HHs over conventional monolayers.

Drugs tested here cause hepatic injury through diverse mechanisms such as toxic metabolites that deplete glutathione and bind macromolecules (i.e. acetaminophen), dissipate mitochondrial membrane potential (i.e. troglitazone), accumulate within mitochondria (i.e. amiodarone), induce steatosis (i.e. amiodarone), and inhibit transporters (i.e. clozapine).[33,34] Here, we showed glutathione depletion and bioactivation as potential mechanisms underlying acetaminophen toxicity in iMPCCs, which is consistent with *in vitro* studies using primary hepatocytes[130] and acetaminophen's known mode of action *in vivo*.[134] Furthermore, consistent with other studies in cell lines and PHHs[38,135,136], we found that some idiosyncratic toxins (i.e. troglitazone and isoniazid) could be properly classified using cellular stress markers in iMPCCs, potentially because such hepatic stress is a first step in the cascade of mechanisms that cause overt liver injury in specific patients (as opposed to adaption and recovery in others) with one or more co-varying factors such as genetics, disease, and environmental stimuli.

The sensitivity for drug toxicity detection in iMPCCs was 65% versus 70% in PHH-MPCCs and ~35% with HIAT. Three compounds (acetazolamide, dapsone, and maleic acid) were correctly identified as toxic by PHH-MPCCs, but not iMPCCs. However, dosing of PHH-MPCCs from another donor using these compounds correctly classified only dapsone. Furthermore, piroxicam was detected correctly as toxic in iMPCCs, but not in PHH-MPCCs. We also tested 29 drugs in iMPCCs created using cryopreserved iPSC-HHs from a second donor to demonstrate proof-of-concept of on-demand and multi-donor screening. While there were differences in the TC_{50} values of the endpoints, the binary calls for 27 of 29 drugs were consistent across the two donors. The two exceptions were phenacetin and piroxicam, which were not detected as toxins in

the second donor even though liver functions in iMPCCs were within the range expected. Thus, the aforementioned donor-dependent differences illustrate the need to test several donors in a prospective drug screening campaign. With rapid advances in iPSC technology, multiple donors of iPSC-HHs that reflect some of the genetic diversity seen in humans are likely to become available commercially and thus could be used to better understand inter-individual susceptibilities to drug toxicity.

Even though iMPCCs improved the sensitivity of drug toxicity detection over conventional cultures of both iPSC-HHs and PHHs, they did not pick up ~35% of the liver toxins tested. Such FNs could be due to interaction of hepatocytes with liver stroma (i.e. endothelia and Kupffer macrophages) and/or the adaptive immune system, extra-hepatic events, and genetic polymorphisms across different donors.[34,137] Nonetheless, we have designed iMPCCs to be modular in that interactions between different donors of iPSC-HHs and donor-matched stromal cells can be studied without significant changes to iPSC-HH homotypic interactions on the micropatterned ECM domains.

Limited *in situ* cell observation by conventional microscopy and nutrient transport limitations makes high-throughput screening in 3D iPSC-HH cultures non-trivial.[65,138–140] Flowing medium can mitigate the nutrient transport limitations; however, inclusion of a flow circuit for each well generally introduces complexities in liquid handling and larger media volumes with increasing quantities of novel compounds.[141] Thus, static 2D hepatic monolayers are widely favored in industrial settings[142], not only for the aforementioned reasons, but when engineered with controlled homotypic and heterotypic interactions, monolayers provide for some of the highest functional levels, longevity, and predictive power of clinical outcomes reported to date.[54,55,58,143] While MPCCs enable a more *in vivo*-like hepatic morphology as opposed to

flattened out (de-differentiated) hepatocytes, it is a monolayer platform amenable to high content imaging[53], which has proven useful for understanding effects of drugs on key organelles implicated in DILI.[38,144] That being said, a new generation of micro-dispensers and micro-pumps are being designed to enable high-throughput and automated microfluidics for "human-on-a-chip" platforms.[141] Thus, inclusion of iMPCCs into a microfluidic device to understand the effects of organ-organ crosstalk on drug toxicity outcomes is a worthwhile endeavor we are pursuing.

In conclusion, iMPCCs have sensitivity and specificity for drug toxicity detection comparable to PHH-MPCCs and significantly higher than conventional confluent cultures of both iPSC-HHs and PHHs. The iMPCCs were also able to distinguish between known hepatotoxins and less toxic drug analogs, and demonstrate known *in vivo* mechanisms underlying APAP toxicity. None of the published platforms for iPSC-HH maturation,[63,116] including iMPCCs, fully mature iPSC-HHs toward adult PHHs. However, with advances in commercial scale differentiation and manufacturing protocols and engineered culture models such as iMPCCs, the use of more functionally mature iPSC-HHs in predictive drug screening is now feasible. More broadly, we anticipate that iMPCCs, created from multiple donors, could prove useful for modeling mechanisms underlying patient-specific DILI and other diseases.

CHAPTER 3 - Culture of Primary Mouse Hepatocytes[3]

Rats are often utilized for the *in vivo* drug testing required by regulatory agencies such as the United States Food and Drug Administration; however, the limited strains of rats employed during drug development are only ~50% predictive of human drug-induced liver injury (DILI). In contrast, many inbred strains of mice are available to researchers and have been shown to be useful for identifying gene variants that may underlie susceptibility of specific patients to toxicity caused by certain drug classes. *In vitro* liver cultures are useful for screening a large number of compounds during early drug development towards refining and reducing the usage of animals for costly and time-consuming *in vivo* testing. However, as we show here, primary mouse hepatocytes cultured in an extracellular matrix protein gel sandwich rapidly decline in prototypical morphology and phenotypic functions. Thus, we adapted and optimized a previously developed micropatterned co-culture (MPCC) platform for the culture of primary mouse hepatocytes. Hepatocytes were cultured onto collagen-coated domains of empirically optimized dimensions and surrounded by 3T3-J2 murine embryonic fibroblasts. The mMPCCs created using freshly isolated mouse hepatocytes from C57Bl/6J, NOD/ShiLtJ, and CD-1 strains displayed high levels of albumin secretion, urea synthesis, and cytochrome P450 (CYP2D, 3A) enzyme activities for ~1 month. Similar longevity of functions was observed with cryopreserved mouse hepatocytes in mMPCCs. Furthermore, mMPCCs showed time- and dose-dependent hepatotoxicity induced by acetaminophen, a prototypical drug used to demonstrate mMPCC utility for drug screening.

---

[3] Portions of this chapter are to appear in the following:
Ware, B.R., Brown, G.E., Soldatow, V.Y., LeCluyse, E.L., & Khetani, S.R. Long-term engineered cultures of primary mouse hepatocytes for genotype-phenotype studies. (in preparation for *Toxicological Sciences*)

Finally, inducing CYP3A activity via dexamethasone exacerbated acetaminophen-induced hepatotoxicity in mMPCCs as observed in previously reported *in vivo* studies. In conclusion, mMPCCs created from multiple mouse strains sustain high levels of hepatic functions for ~1 month and have utility in drug screening and for fundamental biological investigations.

3.1 Introduction and Background

Drug-induced liver injury (DILI) is a leading cause of pharmaceutical attrition and acute liver failures.[31] To mitigate the risk of DILI and other organ toxicities, regulatory agencies require live animal studies (one rodent and one non-rodent species) before the initiation of human clinical drug trials. However, the rat, which is often the rodent species of choice for drug testing, is only ~50% predictive of human DILI,[44,58] often due to significant species-specific differences in drug metabolism pathways.[145] Furthermore, the lack of genetic diversity in rat strains employed routinely in the pharmaceutical industry does not allow detailed investigations into the genetic basis of idiosyncratic (unpredictable) DILI that occurs only in select patients. In contrast, many well-characterized strains of mice are available, including classical inbred lines and genetically-modified mice. More recently, the 'Collaborative Cross', a multiparental recombinant inbred panel, has been introduced to model the complexity of the human genome towards elucidating the interactions between allele combinations and the environment underlying human diseases.[146] For the substrate-specificity of some enzymes (i.e. CYP1A, CYP3A), mice more closely resemble humans than even monkeys.[147] Therefore, when coupled with human-relevant assays to account for any species-specific differences in the metabolism of particular drugs,[18] mice represent a promising model for the preclinical safety screening of pharmaceuticals and could supplement toxicity data from other species.

Owing to their high cost, slow turnaround, and the need for larger quantities of novel compounds, *in vivo* animal studies are less suitable for compound selection during the early stages of drug development. In contrast, *in vitro* cultures can be used within a faster and cheaper context with a large number of compounds for structure-activity relationship-based optimizations geared towards selecting the most promising compounds (i.e. those with an optimal balance of predicted efficacy and safety) for *in vivo* testing. In the case of the liver, isolated primary hepatocytes are ideal for drug screening since they are relatively simple to use in high-throughput culture formats and contain the full complement of enzymes, transporters, and cofactors necessary for the investigation of drug metabolism and toxicity.[142] However, primary mouse hepatocytes rapidly lose phenotypic functions in culture models that rely only on extracellular matrix (ECM) protein manipulations.[148] For instance, mouse hepatocytes cultured on adsorbed collagen have undetectable expression levels of hepatocyte nuclear factor 4α and albumin after 5 days.[149] While a collagen gel sandwich improved gene expression of mouse hepatocytes in the aforementioned study, their morphology degraded after 24 hours in culture, and improvements at the functional level were not determined. Even more advanced matrices for cell seeding, such as poly[*N-p*-vinylbenzyl-4-*O*-β-D-galactopyranosyl-D-gluconamide] with E-cadherin-Fc[150] and polyacrylamide gels of *in vivo*-like stiffness[151], were not able to rescue the mouse hepatocyte phenotype. Thus, short-term cultures of functionally declining mouse hepatocytes are not suitable for chronic drug treatment towards mimicking exposure scenarios in live animals and in the clinic.

Co-culture of primary hepatocytes with non-parenchymal cells (NPCs) can induce hepatic functions for longer durations (weeks) than ECM-only models.[127] While hepatocyte-NPC co-cultures have shown promise for rat and human hepatocytes, their utility for stabilizing mouse hepatocytes is relatively unexplored. Previously, Khetani and Bhatia developed a micropatterned

73

co-culture (MPCC) platform where primary hepatocytes were first cultured onto collagen-coated domains of empirically optimized dimensions and then surrounded by 3T3-J2 murine embryonic fibroblasts.[54] MPCCs created using primary human[56] and rat[152] hepatocytes maintain hepatic morphology and polarity, secrete albumin and urea, and display high CYP450 and Phase II enzyme activities for ~4 weeks; however, MPCC utility for long-term mouse hepatocyte culture has not been shown. Therefore, here we sought to determine morphological features and phenotypic functions of primary mouse hepatocytes from different strains cultured within MPCCs for several weeks. We then utilized acetaminophen as a model drug to explore the potential of so-called mMPCCs for detecting time- and dose-dependent drug-induced hepatotoxicity and probing bioactivation mechanisms underlying such responses, two applications that are useful for drug development.

3.2 Materials and Methods

3.2.1 Isolation and Processing of Hepatocytes

Primary mouse hepatocytes from various strains (C57Bl/6J, NOD/ShiLtJ, and CD-1) were isolated at the Hamner Institutes for Health Sciences (Research Triangle Park, NC) and shipped fresh to Colorado State University (Fort Collins, CO). Briefly, the animals were anesthetized with isolfluorane, and the liver was perfused with a two-step collagenase method.[148] A catheter was inserted through the heart into the superior vena cava, and the liver was perfused first with a divalent cation-free DMEM-based buffer with EGTA at 37°C for 4 minutes, and then with Earle's Balanced Salt Solution containing collagenase and protease (Vitacyte, Indianapolis, IN) for 6-8 minutes. The liver was then excised and dissociated in William's E medium supplemented with 10% FBS, 100 U/mL penicillin, 100 μg/mL streptomycin, 15 mM HEPES, 0.1 μM dexamethasone, 4 μg/mL insulin, and 4 mM GlutaMAX™. Hepatocytes were next filtered

through a 105 μm nylon mesh, washed once by low speed centrifugation, purified by Percoll® (GE Healthcare Life Sciences, Pittsburgh, PA) gradient centrifugation, and transferred to a T-25 tissue culture flask placed on an orbital shaker (50 rpm) in an incubator (37°C, 5% CO_2) for 30 minutes. Cells were then washed by low speed centrifugation and stored in cold storage medium (HypoThermosol®-FRS, BioLife Solutions, Bothell, WA) for shipment. Some of the mouse hepatocytes were cryopreserved using a process modified from a published protocol.[153] Briefly, hepatocytes were suspended in CryoStor medium (BioLife Solutions) supplemented with FBS and fructose before being dispensed in 2 mL cryovials (USA Scientific, Ocala, FL). These cryovials were then placed into a liquid nitrogen step-down freezer before being stored in a liquid nitrogen vapor-phase dewar below -150°C. Following receipt of fresh hepatocytes at Colorado State University, cells were centrifuged at 600 rpm for 8 minutes, and the supernatant was discarded and replaced with fresh medium. Cryopreserved vials were thawed at 37°C for 90-120 seconds followed by dilution with 50 mL of pre-warmed culture medium. The cell suspension was centrifuged and resuspended in fresh medium as described above. Cell viability was assessed using the trypan blue exclusion method, and was found to be >90% for freshly isolated hepatocytes and >80% for cryopreserved hepatocytes.

3.2.2 Establishment of Hepatocyte Cultures

Micropatterned co-cultures (MPCCs) were created as previously described[66] and illustrated in Figure 3.1. Briefly, adsorbed rat tail collagen-I (Corning Life Sciences, Tewksbury, MA) was lithographically patterned in each well of a 24-well plate to create 500 μm diameter circular domains spaced 1200 μm apart, center-to-center. Mouse hepatocytes selectively attached to the collagen domains leaving ~25,000 attached hepatocytes on ~90 collagen-coated islands within each well of a 24-well plate. 3T3-J2 murine embryonic fibroblasts were seeded 18 to 24 hours

later at ~90,000 cells per well to create mouse MPCCs (mMPCCs). Micropatterned pure hepatocyte cultures (mMPHs), which did not receive murine fibroblasts, were used as density-matched controls. Hepatocyte culture medium containing high glucose DMEM (Corning Life Sciences) base was replaced on mMPCCs and mMPHs every 2 days (300 µL/well for 24-well plate). Other components of the culture medium have been described previously.[154]

For conventional cultures, processed mouse hepatocytes were diluted to a final density of 1×10^6 cells/mL, seeded in collagen-coated plates (500 µL/well), and allowed to attach for 4 hours. To complete an ECM sandwich model, Matrigel™ was added to the culture medium at 250 µg/mL, which caused a gelled overlay to form on the adherent hepatocytes. Culture medium was replaced after the first 24 hours of seeding and every other day thereafter.
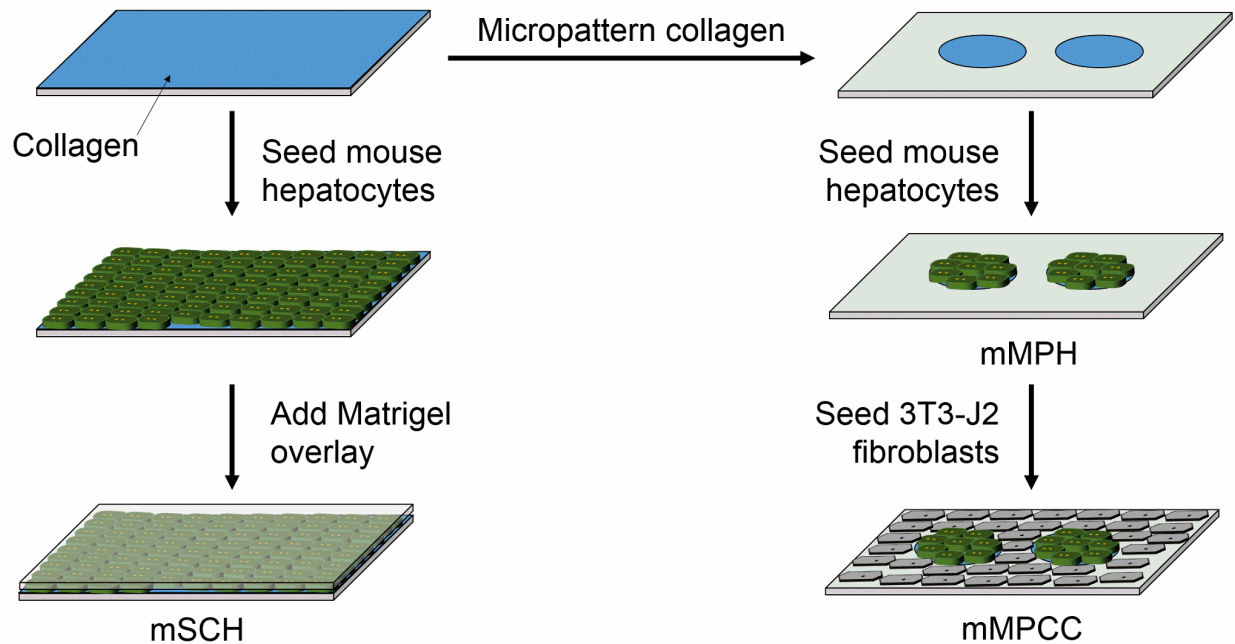
Figure 3.1: Comparison of culture models. After tissue culture polystyrene is uniformly coated with rat tail collagen, three different culture models can be established. Mouse sandwich-cultured hepatocytes (mSCH) adhere to the adsorbed collagen and are then sandwiched with a Matrigel™ overlay. Micropatterned pure hepatocytes (mMPHs) are prepared by using soft lithography to micropattern the collagen into domains/islands of a defined geometry and seeding mouse hepatocytes to fill the collagen islands. Micropatterned co-cultures (mMPCCs) begin as mMPHs, and 3T3-J2 murine embryonic fibroblasts are seeded the following day.[66]

3.2.3 Morphological and Functional Assessments

The morphology of cultures was monitored using an EVOS®FL cell imaging system with standard 4×, 10×, and 20× phase contrast objectives (Thermo Fisher Scientific, Waltham, MA). Culture supernatants were assayed for albumin levels using a competitive enzyme-linked immunosorbent assay (ELISA, MP Biomedicals, Santa Ana, CA) with horseradish peroxidase detection and 3,3',5,5'-tetramethylbenzidine (TMB, Rockland Immunochemicals, Boyertown, PA) as the substrate.[54] Urea concentration in culture supernatants was assayed using a colorimetric endpoint assay utilizing diacetyl monoxime with acid and heat (Stanbio Labs, Boerne, TX).[54] CYP2D and CYP3A enzyme activities were measured by first incubating the cultures with substrates (luciferin-ME EGE for CYP2D and luciferin-IPA for CYP3A from Promega Life Sciences, Madison, WI) for 1 hour at 37°C and then detecting the luminescence of produced metabolite (luciferin) according to manufacturer's protocols. Absorbance and luminescence for the aforementioned assays were measured using a BioTek (Winooski, VT) Synergy H1 multi-mode plate reader.

3.2.4 Acetaminophen Exposure Studies

After allowing mMPCCs to stabilize for ~1.5 weeks, cultures were treated with acetaminophen (APAP) in serum-free culture medium. APAP concentrations were chosen up to 30 mM and were administered three times over six days with every medium change. For some studies, the CYP450 inducer dexamethasone (DEX; Sigma-Aldrich, St. Louis, MO), was co-incubated at 10 μM with APAP (5 mM) in serum-free culture medium following the same treatment schedule described above. Control cultures were treated with DEX and APAP alone.

All findings were confirmed in independent experiments from at least two different donors of the same mouse strain. Data processing was performed using Microsoft Excel, and GraphPad Prism (La Jolla, CA) was used for displaying results. For each assay, mean and standard deviation values were calculated using three technical replicates and normalized to the number of hepatocytes seeded in each well. For the drug exposure studies, functions in all treated cultures were compared to functions in drug-free controls, and functional data are reported as percentages of that control.

3.3 Results

3.3.1 Characterization of Pure Hepatocyte Cultures

Upon seeding into collagen-coated wells and overlaying with Matrigel™ (Figure 3.1), mouse sandwich-cultured hepatocytes or mSCH (C57Bl/6J strain, herein referred to as C57) showed standard hepatic morphology with a polygonal shape, multi-nucleation, and distinct nuclei/nucleoli (Figure 3.2A). However, hepatocytes in mSCHs became de-differentiated (i.e. spread out) after 1 and 2 weeks of culture (Figure 3.2B-C). When C57 hepatocytes were seeded onto micropatterned collagen islands without co-culture with fibroblasts (mouse micropatterned pure hepatocytes or mMPH, Figure 3.1), a similar morphological decline was observed as with mSCHs (Figure 3.2D-F). Furthermore, hepatic functions (albumin, urea, CYP2D/3A activities) in both mSCH and mMPH formats rapidly declined to nearly undetectable levels after a few days in culture (Figure 3.2G-H).
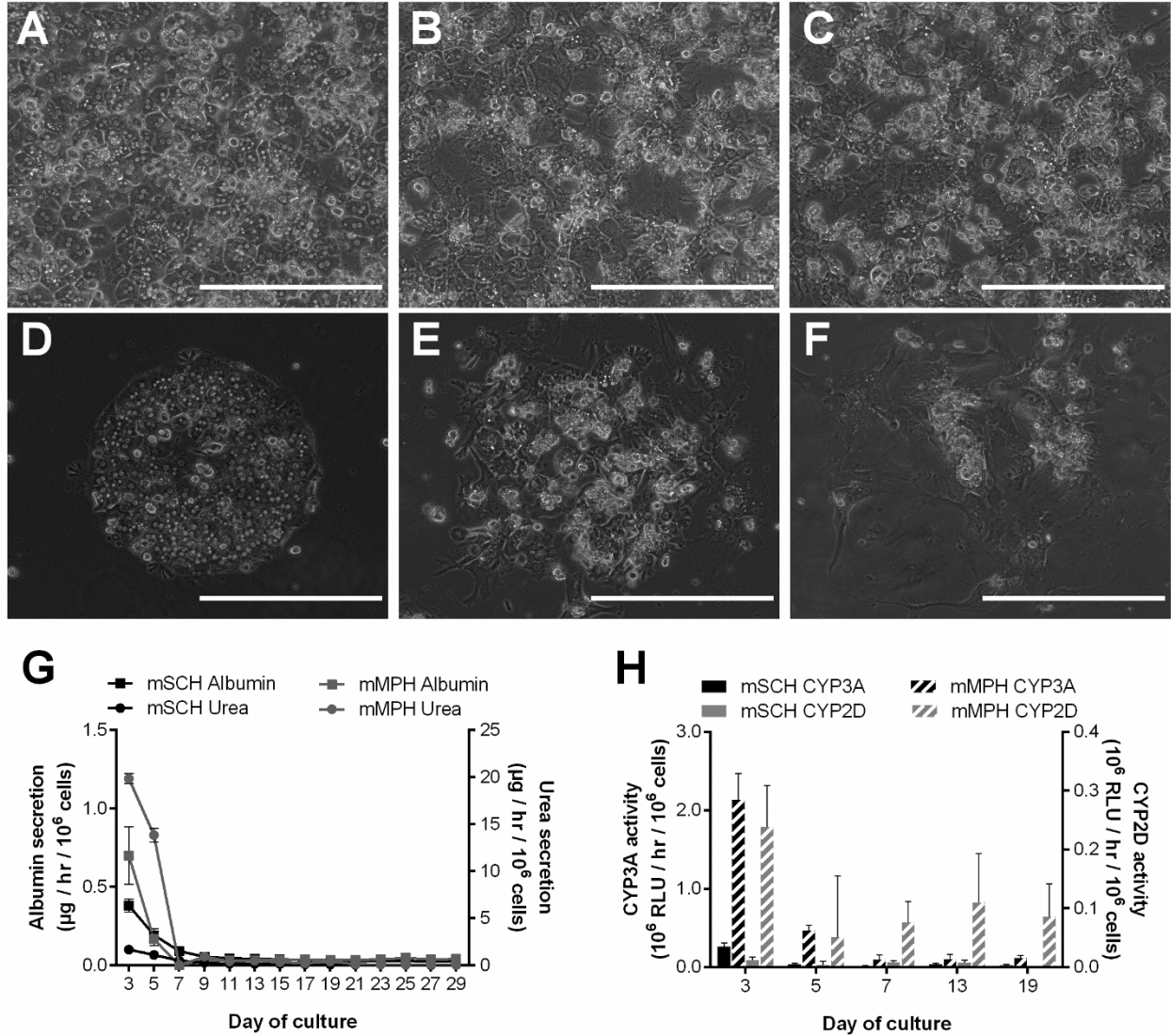
Figure 3.2: Pure cultures of mouse hepatocytes. Freshly isolated mouse hepatocytes (C57Bl/6J strain) were seeded onto adsorbed collagen and then sandwiched with a Matrigel™ overlay (mouse sandwich-cultured hepatocytes or mSCHs). Prototypical hepatocyte morphology in mSCHs after **(A)** 1 day of seeding degraded after **(B)** 1 week and **(C)** 2 weeks of culture. Similarly, micropatterned pure cultures (mMPH) devoid of fibroblasts showed a normal morphology of mouse hepatocytes after **(D)** 1 day of culture that became de-differentiated (i.e. spread out) after **(E)** 1 week and **(F)** 2 weeks of culture. All scale bars = 400 µm. At the functional level, both mSCHs and mMPHs showed a rapid decline of **(G)** albumin and urea secretion levels and **(H)** CYP450 activities. Error bars represent standard deviations (n = 3).

3.3.2 Optimizing the MPCC Platform for Mouse Hepatocytes of Multiple Strains

The MPCC platform, in which hepatocytes are micropatterned onto collagen-coated domains of empirically optimized dimensions using soft lithographic tools and subsequently co-cultured with 3T3-J2 murine embryonic fibroblasts (Figure 3.1), was first developed to enhance and stabilize functions in primary human hepatocytes for several weeks *in vitro*.[54] Since then, this platform has been shown to enhance and stabilize functions of primary rat hepatocytes[152] and induced pluripotent stem cell-derived human hepatocytes.[66] Here, we adapted and optimized the MPCC platform for primary mouse hepatocytes by varying the collagen domain diameter and center-to-center spacing to change the surface area occupied by the mouse hepatocytes in each well (Figure 3.3A). We observed higher liver functions when less surface area in each well was occupied by the hepatocytes (Figure 3.3B).

Next, we characterized hepatic morphology in C57 mMPCCs for ~1 month *in vitro*. The hepatocytes showed prototypical morphology (polygonal shape, distinct nuclei/nucleoli) on the day of seeding (Figure 3.4A). Hepatocyte islands retained their shape in mMPCCs over at least 3 weeks of culture (Figure 3.4B-C). These trends were also observed when hepatocytes from the NOD/ShiLtJ strain (herein referred to as NOD) (Figure 3.5A-C) and the CD-1 strain (Figure 3.6A-C) were used in mMPCCs. Hepatocytes in mMPCCs formed visible bile canaliculi, which were also found to be functional as assessed by the active excretion of fluorescent 5 (and 6)-carboxy-2',7'-dichlorofluorescein (CDF) into the bile canaliculi between adjacent hepatocytes[155] (Figure 3.7). However, over time the 3T3-J2 fibroblasts integrated within the confluent hepatocyte colonies, which caused the hepatocyte morphology/shape to not be as clearly demarcated as has been observed with rat[152] and human[56] hepatocytes within MPCCs. Even though hepatocyte morphology was not well demarcated within the islands over time, phenotypic functions (albumin,

81

urea, CYP2D and CYP3A activities) were retained for ~1 month in C57 mMPCCs (Figure 3.4D-E), NOD mMPCCs (Figure 3.5D-E), and CD-1 mMPCCs (Figure 3.6D-E). While hepatocytes from all three strains had similar urea secretions in mMPCCs, the albumin production in NOD hepatocytes was about one-fifth of the C57 and CD-1 hepatocytes. In contrast, mMPCCs created using the same batch of mouse hepatocytes had significantly higher functions on a per cell basis than those observed in sandwich cultures (Figure 3.2G-H vs. Figure 3.4D-E). In particular, urea secretion levels were 15-fold, 30-fold, and 156-fold higher in mMPCCs than in mSCHs after 3, 7, and 13 days in culture, respectively. Albumin secretion levels were 19-fold, 108-fold, and 333-fold higher in mMPCCs than in mSCHs after 3, 7, and 13 days in culture, respectively. CYP2D activities were 50-fold and 96-fold higher in mMPCCs than in mSCHs after 3 and 13 days in culture, respectively. Finally, CYP3A activities were 9-fold and 64-fold higher in mMPCCs than in mSCHs after 3 and 13 days in culture, respectively.
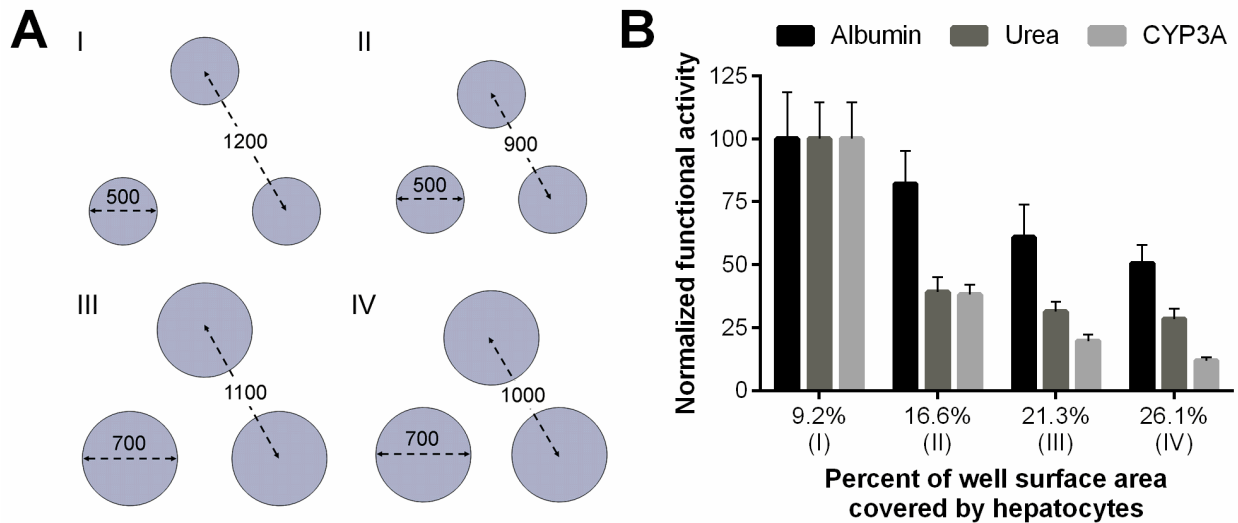
Figure 3.3: Optimization of the micropatterned co-culture platform. **(A)** Various micropatterned geometries (i.e. confluent clusters) allowed mouse hepatocytes to cover 9.2% (500 μm island diameter with 1200 μm center-to-center spacing), 16.6% (500 μm diameter, 900 μm center-to-center), 21.3% (700 μm diameter, 1100 μm center-to-center), or 26.1% (700 μm diameter, 1000 μm center-to-center) of the available surface area in each well of an industry standard 24-well plate, and then the hepatocytes were surrounded by 3T3-J2 murine embryonic fibroblasts to created micropatterned co-cultures (mMPCCs). All dimensions shown are in microns. **(B)** Albumin secretion, urea production, and CYP3A activity in mMPCCs from a representative time point (day 15) are shown, although similar trends were observed over multiple weeks. All data were normalized to the 9.2% geometry (500 μm diameter, 1200 μm center-to-center). Error bars represent standard deviations (n = 3).
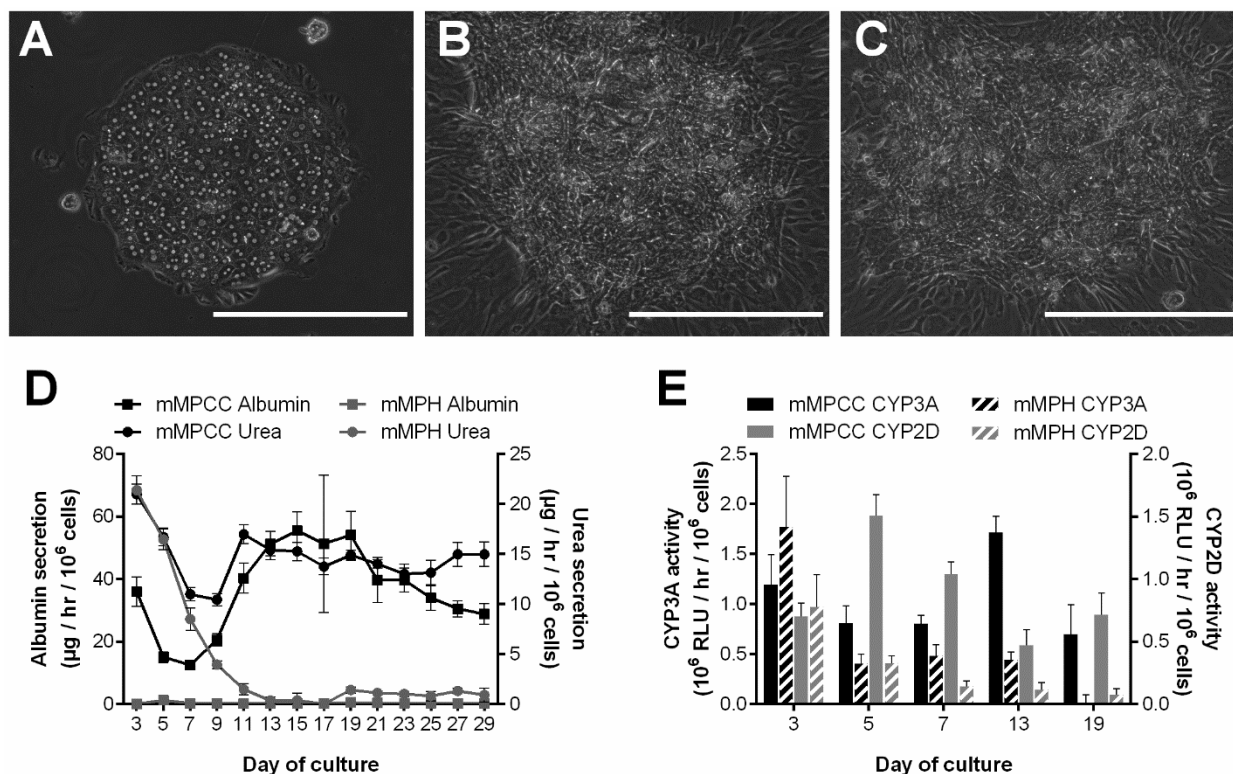
Figure 3.4: Morphology and liver functions of freshly isolated C57Bl/6J mouse hepatocytes in micropatterned cultures over time. **(A)** Freshly isolated C57 mouse hepatocytes can be micropatterned onto collagen-coated circular domains and display prototypical morphology under phase contrast on the day of seeding and prior to co-culture with 3T3-J2 fibroblasts. In micropatterned co-cultures (mMPCCs) containing the fibroblasts, hepatocytes retain their morphological features after **(B)** 1 week and **(C)** 2 weeks in culture. All scale bars = 400 µm. **(D)** Time series of albumin and urea secretions in C57 mMPCCs. **(E)** Time series of CYP2D and CYP3A enzyme activities in mMPCCs. Error bars represent standard deviations (n = 3).
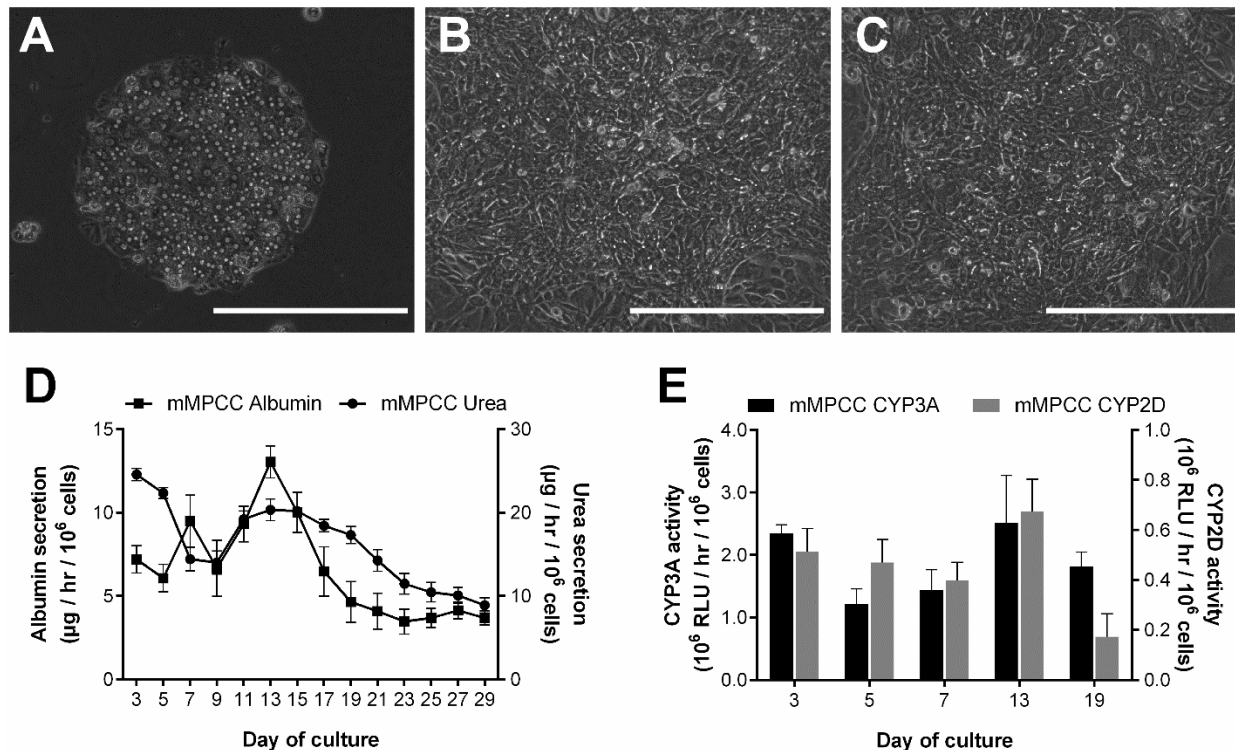
Figure 3.5: Morphology and liver functions of NOD/ShiLtJ mouse hepatocytes in micropatterned cultures over time. **(A)** Freshly isolated NOD mouse hepatocytes can be micropatterned onto collagen-coated circular domains and display prototypical morphology under phase contrast on the day of seeding and prior to co-culture with 3T3-J2 fibroblasts. In micropatterned co-cultures (mMPCCs) containing the fibroblasts, hepatocytes retain their morphological features after **(B)** 1 week and **(C)** 2 weeks in culture. All scale bars = 400 μm. **(D)** Time series of albumin and urea secretions in NOD mMPCCs. **(E)** Time series of CYP2D and CYP3A enzyme activities in mMPCCs. Error bars represent standard deviations (n = 3).
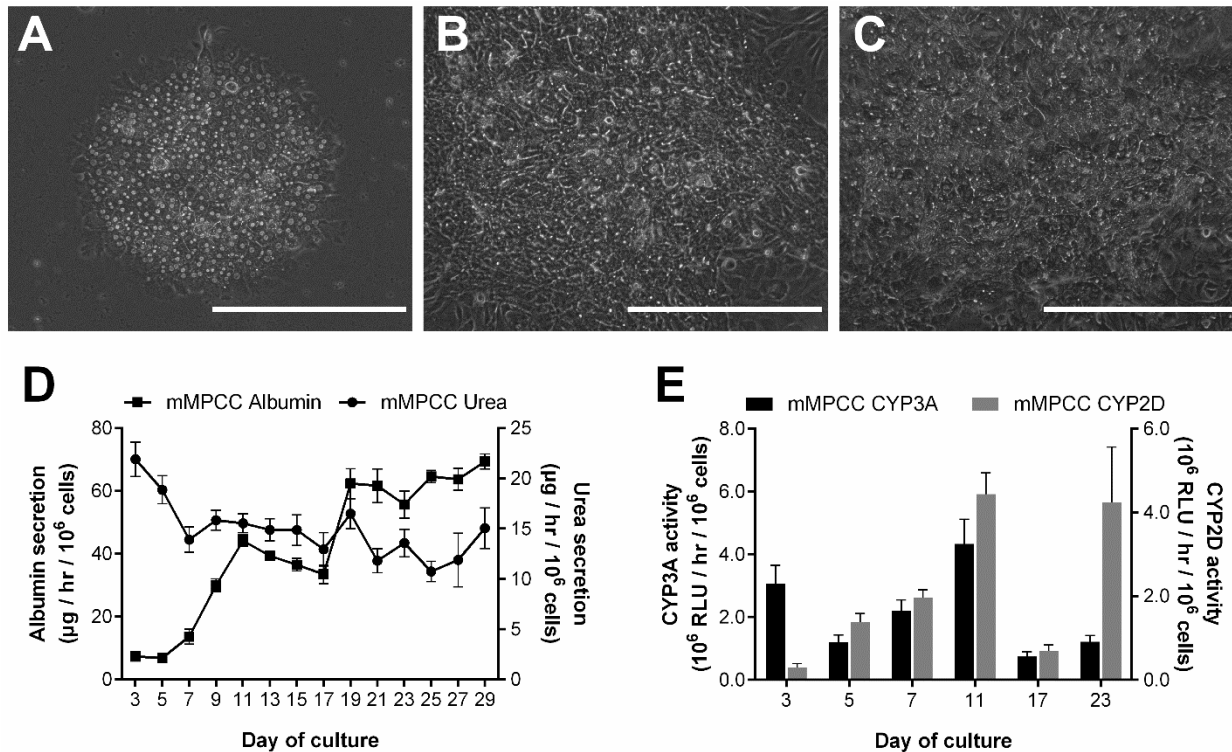
Figure 3.6: Morphology and liver functions of CD-1 mouse hepatocytes in micropatterned cultures over time. (A) Freshly isolated CD-1 mouse hepatocytes can be micropatterned onto collagen-coated circular domains and display prototypical morphology under phase contrast on the day of seeding and prior to co-culture with 3T3-J2 fibroblasts. In micropatterned co-cultures (mMPCCs) containing the fibroblasts, hepatocytes retain their morphological features after **(B)** 1 week and **(C)** 2 weeks in culture. All scale bars = 400 μm. **(D)** Time series of albumin and urea secretions in CD-1 mMPCCs. **(E)** Time series of CYP2D and CYP3A enzyme activities in mMPCCs. Error bars represent standard deviations (n = 3).
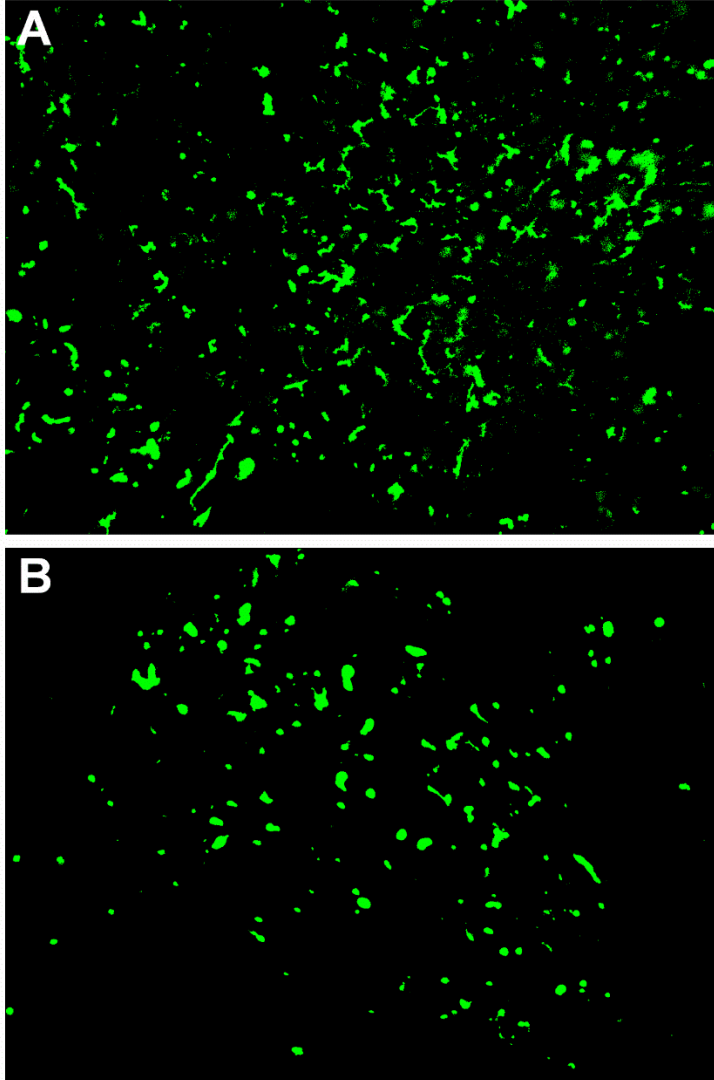
Figure 3.7: Staining for functional bile canaliculi. After 3 weeks in culture, mMPCCs of **(A)** C57Bl/6J mouse hepatocytes and **(B)** NOD/ShiLtJ mouse hepatocytes were washed three times with phenol red-free media, incubated with 2 µg/mL 5-(and 6)-carboxy-2',7'-dichlorofluorescein diacetate (CDF; Molecular Probes, Eugene, OR) for 10 minutes at 37°C, and washed three more times before imaging with fluorescence microscopy (470 nm excitation, 510 nm emission).

3.3.3 Compatibility of Cryopreserved Hepatocytes in mMPCCs

To compare results from cryopreserved hepatocytes with those from fresh cells from the same mouse, we incorporated cryopreserved C57 hepatocytes into mMPCCs and characterized their morphology and functions. Micropatterned cryopreserved hepatocytes showed morphology similar to their fresh counterparts on the day of seeding (Figure 3.8A); however, as with fresh hepatocytes, cryopreserved hepatocytes showed severely degraded morphology after 1 week in culture in mMPHs (not shown), whereas morphology was better retained in mMPCCs over time (Figure 3.8B-C). Albumin secretion in cryopreserved mMPCCs was ~40-50% of secretions in fresh mMPCCs from the same C57 animals, whereas urea secretion and CYP450 activities measured were relatively similar in magnitude in both fresh and cryopreserved mMPCCs (Figure 3.8D-E vs. Figure 3.4D-E). However, urea secretion displayed better stability over time in fresh mMPCCs as compared to cryopreserved mMPCCs. Nonetheless, these results suggest that cryopreserved hepatocytes are compatible with mMPCCs and display high functions for ~4 weeks.
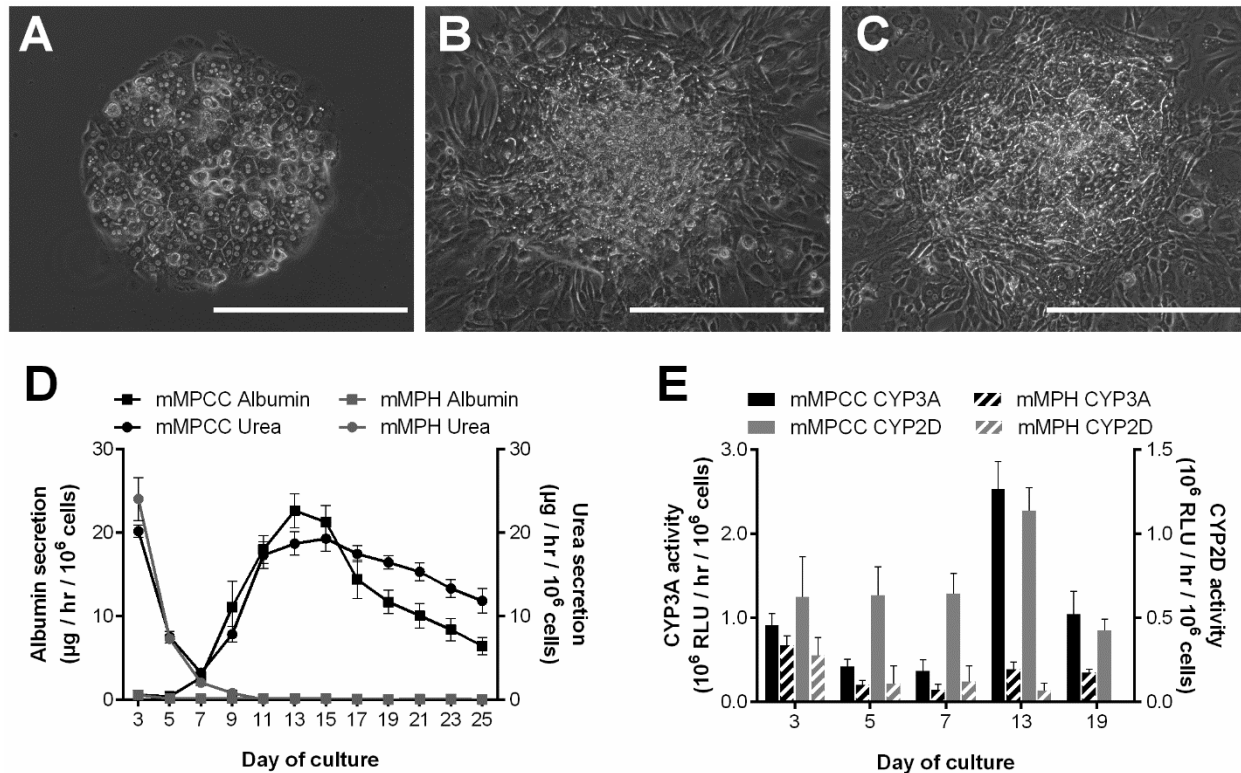
Figure 3.8: Morphology and liver functions of cryopreserved C57Bl/6J mouse hepatocytes in micropatterned cultures over time. **(A)** Cryopreserved C57 mouse hepatocytes can be micropatterned onto collagen-coated circular domains and display prototypical morphology under phase contrast on the day of seeding and prior to co-culture with 3T3-J2 fibroblasts. In micropatterned co-cultures (mMPCCs) containing the fibroblasts, hepatocytes retain their morphological features after **(B)** 1 week and **(C)** 2 weeks in culture. All scale bars = 400 μm. **(D)** Time series of albumin and urea secretions in C57 mMPCCs. **(E)** Time series of CYP2D and CYP3A enzyme activities in mMPCCs. Error bars represent standard deviations (n = 3).

3.3.4 Acetaminophen Toxicity Screening in mMPCCs

To demonstrate the utility of mMPCCs for assessing time- and dose-dependent drug-induced hepatotoxicity, we selected acetaminophen (APAP) because it has a similar metabolism in mouse and human livers (Figure 3.9A).[156,157] We used albumin and urea secretions as markers of hepatotoxicity since these markers have been shown to be as sensitive and specific as ATP for the detection of hepatotoxicity of drugs from multiple classes.[58] Furthermore, albumin and urea can be measured non-destructively in culture supernatants to appraise longitudinal responses in the same cells, and these markers are secreted by hepatocytes but not fibroblasts unlike other injury markers such as lactate dehydrogenase. Figure 3.9B-C shows the time- and dose-dependent albumin and urea secretions of C57 mMPCCs treated with APAP, while Table 3.1 quantifies the IC$_{50}$ value (interpolated APAP concentration that reduces an endpoint signal by 50%) for albumin and urea secretions. Overall, IC$_{50}$ values were similar across both functional endpoints and decreased from ~13 mM APAP following 2 days of treatment to ~6 mM APAP following 6 days of treatment. To demonstrate mMPCC utility for probing bioactivation mechanisms underlying drug toxicity, C57 mMPCCs were co-incubated with APAP (5 mM) and dexamethasone, a known inducer of CYP450 activity. In particular, when treated with a mixture of 10 µM dexamethasone and 5 mM APAP, mMPCCs experienced a significantly greater decline in albumin and urea secretions than when treated with APAP or dexamethasone alone (Figure 3.9D-E).

90
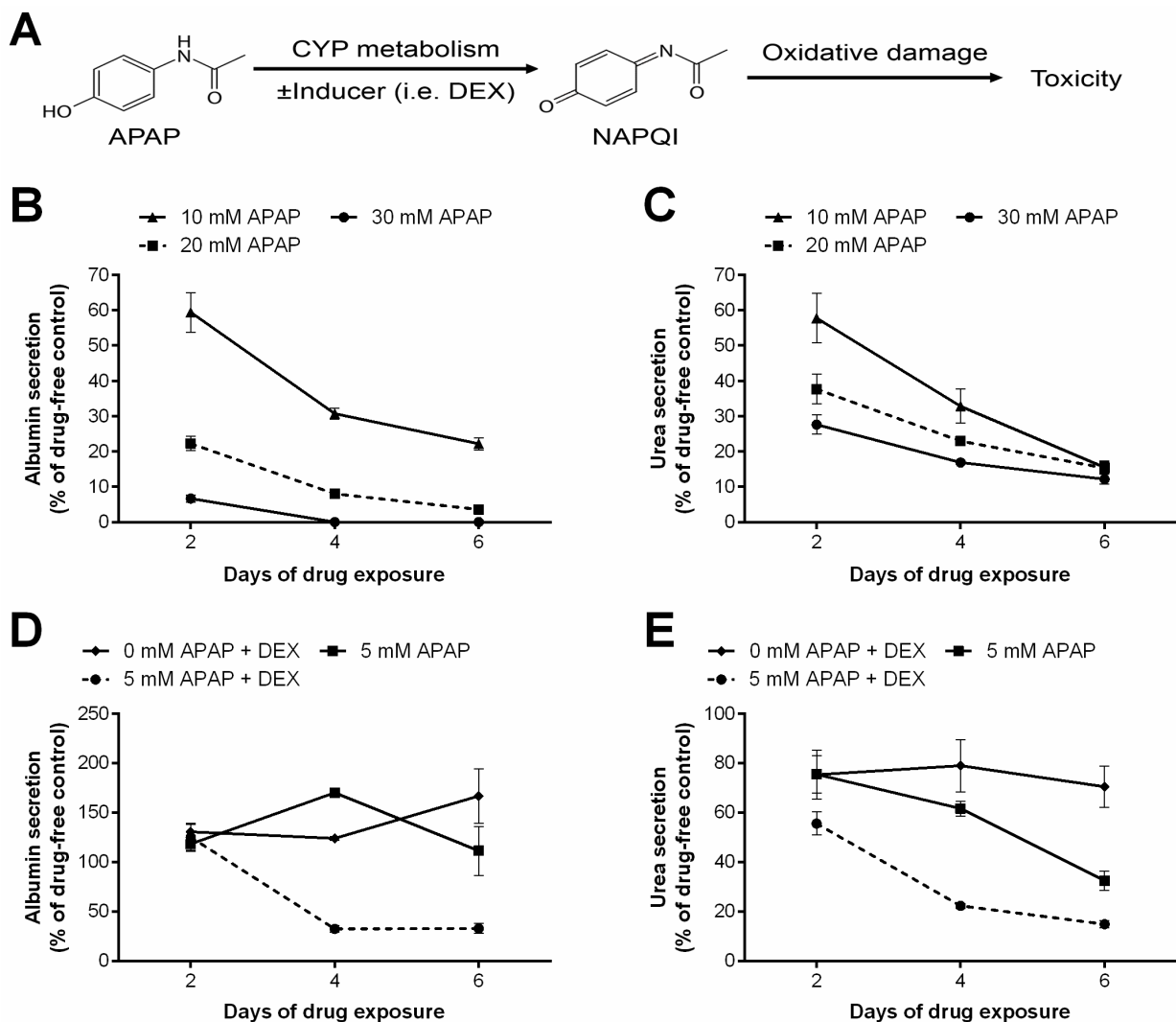
Figure 3.9: Acetaminophen toxicity in C57Bl/6J mouse hepatocytes. **(A)** Acetaminophen (APAP) is metabolized by CYP450 enzymes to the reactive intermediate N-acetyl-p-benzoquinone imine (NAPQI), which causes toxicity via oxidative damage. CYP450 activity is induced with dexamethasone (DEX), which exacerbates NAPQI formation and leads to further oxidative damage. C57 mouse hepatocytes were incorporated into the mMPCC model, allowed to stabilize, and treated with 0 mM, 10 mM, 20 mM, or 30 mM APAP in serum-free culture medium. **(B)** Albumin secretion and **(C)** urea production were quantified after 2, 4, and 6 days of APAP exposure. Additional mMPCCs were treated with 5 mM APAP with or without DEX at 10 µM. **(D)** Albumin secretions and **(E)** urea productions were quantified after 2, 4, and 6 days of compound exposure. Effects of DEX alone on biochemical outputs are also shown. All data from compound treated cultures were normalized to data in drug-free control cultures. Error bars represent standard deviations (n = 3).

Table 3.1: Time-dependent IC$_{50}$ values for APAP-treated C57 mMPCCs

Days of drug exposure	Albumin IC$_{50}$ (mM)	Urea IC$_{50}$ (mM)
2	12.53	13.87
4	7.21	7.44
6	6.43	5.91

3.4 Discussion

Accurate prediction of drug effects in humans from preclinical animal studies that are required by regulatory agencies is critically important during drug development. Species-specific differences have been shown to impact drug metabolism, drug targets, and pathophysiology; these will continue to be criteria for selecting an 'appropriate' animal model.[5] Several CYP450 enzymes across mouse, rat, rabbit, dog, micropig, and monkey models show wide differences between humans, and no species as clearly superior across all CYP450 isozymes.[147] Despite these differences, the large panel of inbred mouse strains (e.g. Collaborative Cross) available is useful for identifying gene variants that may underlie susceptibility of patients to toxicity due to certain drug classes. *In vitro* cultures are useful for conducting structure-activity relationship optimizations on a large number of compounds during early drug development towards refining and reducing animal usage for costly and time-consuming *in vivo* testing. However, in the case of the liver, primary mouse hepatocytes on adsorbed collagen rapidly decline in functions, which restricts their utility for chronic drug treatment. Thus, we adapted and optimized the previously developed MPCC platform for primary mouse hepatocytes from multiple strains, and demonstrated for the first time their long-term culture for several weeks. We then utilized a model compound, acetaminophen, to show the utility of mMPCCs for monitoring time- and dose-dependent drug-induced hepatotoxicity and determining the role of bioactivation in such outcomes.

The ECM gel sandwich slows down the decline of liver gene expression in mouse hepatocytes as compared to cultures on adsorbed collagen; however, functional assessments have been lacking.[149] Therefore, we created ECM sandwich cultures (adsorbed collagen with Matrigel™ overlay) of primary mouse hepatocytes (C57Bl/6J strain) and evaluated morphological

features and phenotypic functions that included albumin secretion, urea synthesis, and CYP450 (2D, 3A) activities. Sandwich cultures displayed severely degraded hepatic morphology, and functions declined rapidly within the first week of culture. For instance, CYP3A activity declined to 6% and albumin secretion declined to 23% of day 3 levels by the first week of culture. Therefore, an ECM sandwich is not able to rescue mouse hepatocytes. In contrast, mMPCCs created from the same hepatocyte strain/batch displayed phenotypic functions for ~1 month at levels ~9-fold to 50-fold higher on a per cell basis than sandwich cultures after 3 days. In addition to the C57Bl/6J strain, we also created mMPCCs using primary mouse hepatocytes from the NOD/ShiLtJ and CD-1 strains since these three strains are used commonly. We found that even though hepatocytes were initially confluent on the collagen-coated islands, over time the fibroblasts integrated within the hepatocyte colonies across all three strains, which caused the hepatocyte morphology/shape to not be as clearly demarcated as observed with primary rat[152] and human[56] hepatocytes within MPCCs. Homologous junctions between the fibroblasts and hepatocytes from the same species may cause such integration of the two cell types in the same island. While such integration did not entirely disrupt the formation of functional bile canaliculi between adjacent hepatocytes as assessed via CDF excretion,[155] the extent of bile canaliculi formation in mMPCCs was lower than observed in rat and human MPCCs. Nonetheless, use of the same supportive cell type in MPCCs created using hepatocytes from different species allows comparisons of the morphological/functional changes and provides a consistent NPC background for drug studies designed to select an appropriate animal species for *in vivo* testing. Even though they are devoid of major liver functions, 3T3-J2 fibroblasts are known to express molecules present in the liver, such as decorin and T-cadherin, that can induce hepatic functions.[158] 3T3-J2 fibroblasts are also advantageous in their ease of propagation, contact-inhibited growth in culture,

and lack of detectable liver functions.[54,127,152,158]   Interestingly, the architecture (i.e. island diameter/spacing) that was found to induce the highest functional levels in mMPCCs was the same optimal architecture (500 μm diameter, 1200 μm center-to-center spacing) determined for MPCCs containing primary human hepatocytes[54] or iPSC-derived human hepatocytes[66].   Such a consistency in architectural dependence suggests that similar mechanisms underlie homotypic interactions in all three sources of hepatocytes and their heterotypic interactions with 3T3-J2 fibroblasts.   Even though hepatocyte morphology was not well demarcated within the islands, functions were retained for ~1 month in mMPCCs created from all three strains.   However, NOD mMPCCs secreted lower levels of albumin (~4-fold to 5-fold) than C57 and CD-1 mMPCCs.   On the other hand, mMPCCs from all three strains secreted similar urea levels over time. It is not clear whether the aforementioned functional similarities and differences across mMPCCs created from different strains are due to culture artifacts or inherent physiological differences.   Measurements of these functions would be required in live animals under identical housing and nutritional conditions to appraise the degree of correlation between *in vitro* and *in vivo* levels.   Nonetheless, high function of mouse hepatocytes from all three strains in mMPCCs constitutes a significant advance over conventional approaches.

The use of cryopreserved hepatocytes allows for more convenient creation of cultures and the use of the same batch/lot of hepatocytes over many experiments than fresh cells.   Thus, we evaluated morphological/phenotypic changes in mMPCCs created using fresh and cryopreserved C57 hepatocytes from the same animals.   While hepatic morphology over time was similar, albumin secretion in cryopreserved mMPCCs was ~40-50% of secretions in fresh mMPCCs.   On the other hand, urea secretion and CYP450 activities measured were relatively similar over time in both fresh and cryopreserved mMPCCs.   While further optimizations in the cryopreservation

protocol may enable better similarities in functional outputs across fresh and cryopreserved mMPCCs, our results show that cryopreserved mouse hepatocytes are compatible within mMPCCs and can retain functions for ~1 month.

In order to demonstrate mMPCC utility in drug toxicity screening, we chose APAP because of its relevance to modern medicine and the parallel pathways of metabolism between humans and mice. *In vivo*, CYP2E/CYP3A in both humans and mice produces the toxic metabolite, *N*-acetyl-*p*-benzoquinone imine (NAPQI), from APAP.[159,160] Here, we monitored albumin and urea secretions in drug-treated mMPCCs because albumin and urea are as sensitive/specific as ATP for the detection of DILI *in vitro*[58,161], and albumin/urea can be measured non-destructively in culture supernatants to evaluate longitudinal outcomes in the same cells. APAP caused time- and dose-dependent toxicity over 6 days of exposure in C57 mMPCCs. In particular, the IC_{50} values for both albumin and urea secretions were similar and decreased from ~13 mM APAP following 2 days of dosing to ~6 mM APAP following 6 days of treatment. The longevity of the mMPCC platform enables repeat/chronic drug dosing which is not always possible with declining monolayer or sandwich cultures. Additionally, since mMPCCs do not require an ECM gel overlay, drug binding with the proteins in the gel is minimized and thus cultures are exposed to the actual concentration used. To demonstrate the utility of mMPCCs for elucidating mechanisms of drug toxicity, we probed the role of bioactivation in APAP-induced hepatotoxicity. In rodents, treatment with known CYP450 inducers results in increased APAP hepatotoxicity.[162] Here, we mimicked this effect in C57 mMPCCs by treatment with dexamethasone, a known inducer of CYP3A in multiple species.[130,162,163] While dexamethasone (10 μM) itself was not toxic, its inclusion with APAP (5 mM) exacerbated decreases in albumin and urea secretion as compared to

APAP alone (e.g. urea levels in DEX+APAP-treated mMPCCs were ~36% of APAP-treated mMPCCs after 4 days of exposure).

Three-dimensional cultures would enable a full understanding of the interactions between hepatocytes, non-parenchymal cells, and flowing nutrients. However, such a model would require a complex flow circuit that uses greater quantities of media and novel compounds for initial toxicity screens. Thus, two-dimensional hepatic cultures are widely favored in industrial settings[142], not only for the relative simplicity of culture and limited media, but monolayers with controlled homotypic and heterotypic interactions have been shown to have some of the highest functional levels, longevity, and accurate prediction of clinical outcomes reported to date.[54,55,58,143,161] Enabling a more *in vivo*-like hepatic morphology as opposed to spread out (de-differentiated) hepatocytes, mMPCCs are a monolayer platform permitting high content imaging[53], a significant tool for elucidating the effects of various drugs on key organelles implicated in drug toxicity.[38,144]

In conclusion, we demonstrate for the first time that the MPCC platform maintains the longevity and functionality of primary mouse hepatocytes from multiple strains for ~4 weeks, which is essential for evaluating chronic drug toxicity as well as mechanisms underlying such toxicity. We anticipate that mMPCCs created from multiple strains, including transgenic mice, can be useful in the future to understand the role of genetics in drug-induced hepatotoxicity as well for fundamental biological investigations.

CHAPTER 4 - Toxicity Screens in HepaRG Cultures[4]

Isolated primary human hepatocytes (PHHs) are the 'gold standard' cell source for *in vitro* models used in preclinical drug screening. However, significant shortages of available tissue and the variable quality among lots make PHHs an expensive resource for high-throughput screening required in the early stages of drug development. Cell lines such as HepaRG offer the potential of an inexpensive, robust screening platform. Still, conventional culture models display low levels of liver-specific functions and poor drug toxicity predictions. Here, we hypothesized that HepaRG cells, when incorporated into a previously developed micropatterned co-culture (MPCC) with murine embryonic fibroblasts, could be amenable to long-term culture for drug toxicity assessment. HepaRG-MPCCs, created in industry-standard plates, displayed high levels of hepatic specific functions (i.e. albumin, CYP450 activities) for over 4 weeks in culture. HepaRG-MPCCs were then treated for 6 days with a set of 47 drugs, and multiple functional endpoints (albumin, ATP) were evaluated in dosed cultures against vehicle-only controls to enable binary toxicity decisions. We found that HepaRG-MPCCs correctly classified 20 of 37 hepatotoxic drugs (54% sensitivity), while all 10 non-toxic drugs tested were correctly classified (100% specificity). On the other hand, conventional confluent cultures of HepaRG cells failed to detect several liver toxins that were picked up in HepaRG-MPCCs. These results for drug toxicity prediction in HepaRG-MPCCs were superior to those in published studies. In conclusion, HepaRG cells incorporated into MPCCs can provide a robust tool for the long-term screening of the toxic potential of compounds in large libraries early in drug development.

---

[4] Portions of this chapter are to appear in the following:
Ware, B.R., Ballinger, K.R., & Khetani, S.R. Enhancing hepatic functions of the HepaRG cell line via micropatterned co-culture with supportive stromal fibroblasts. (in preparation for *Toxicological Sciences*)

4.1 Introduction and Background

Drug-induced liver injury (DILI) continues to be a leading cause of acute liver failures, the prelaunch attrition of pharmaceuticals, and the withdrawal of previously approved drugs.[5] While regulatory agencies require animal testing prior to the start of human clinical trials, species-specific differences in drug metabolism necessitate the use of human-relevant models in preclinical screenings for safety and efficacy, and popular models include liver slices, microsomes, and primary human hepatocytes (PHHs). Liver slices suffer from a rapid loss in viability and cannot be incorporated into high-throughput screening platforms; microsomes do not display adequate levels of drug metabolizing enzymes and thus cannot be used to evaluate toxicity; PHHs, while considered the 'gold standard' for *in vitro* toxicity screens because they maintain phenotypic functions for multiple weeks, are in limited supply and have significant lot-to-lot variability. This in turn raises the cost of PHHs which severely hinders them from being a viable cell source for the high-throughput screening of large compound libraries early in the drug development pipeline.[164]

Hepatocarcinoma cell lines can offer a nearly unlimited supply of inexpensive, robust cells amenable to high-throughput drug screening. One popular line is HepaRG, which was first isolated from the liver tumor of a patient also afflicted with hepatitis C viral infection.[165] This bi-potential cell line can differentiate down the hepatic and biliary lineages *in vitro*, and has been shown to be more differentiated and functional than HepG2 and other cell lines.[166] Previous studies have evaluated cytochrome P450 (CYP450) activity[167], sinusoidal and canalicular membrane transporters at the transcriptional and functional levels[168,169], and drug clearance rates[170,171] in HepaRG cultures. Despite their potential for *in vitro* drug screening, it is widely accepted that HepaRG cells have a limited set of hepatic functions and reduced CYP450 activity compared to PHHs when cultured in conventional (i.e. ECM sandwich) formats.[172] Gerets *et al.*

showed that, while drug clearance rates were similar between HepaRG and PHHs, the sensitivity of drug toxicity predictions in conventional HepaRG cultures (16%) was significantly lower than PHH cultures (44%).[37] Other studies using conventional HepaRG cultures have shown 67% and 71% sensitivity with 73% and 100% specificity for drug toxicity predictions, although these inquiries were generally focused on overtly toxic drugs and did not include a comparison to PHHs.[173,174] More in-depth inquiries have studied the cytotoxicity of amiodarone and its metabolites[175], and aflatoxin B1 with or without the CYP3A4 inhibitor ketoconazole[176] on conventional HepaRG cultures. Advanced culturing techniques such as the 3D spheroid have shown improvements in CYP450 enzyme induction and binary toxicity predictions relative to traditional monolayer cultures, although these are not amenable to high content screening.[170,177,178]

The hepatic phenotype of PHHs, primary animal hepatocytes, and iPSC-derived human hepatocytes has been shown to be stabilized *in vitro* via co-culture with stromal cells from multiple sources.[66,127,128] Hepatic function and culture longevity were further improved when incorporated into a micropatterned co-culture (MPCC), whereby PHHs were arranged onto collagen domains of empirically optimized dimensions and surrounded by 3T3-J2 murine embryonic fibroblasts.[54] These fibroblasts have been shown to induce the highest functions when compared to other 3T3 clones[158], liver macrophages[67], liver sinusoidal endothelial cells[179], and hepatic stellate cells[13]. As a non-liver cell source, 3T3-J2 fibroblasts can stabilize the hepatic phenotype of PHHs independently of liver stromal cells, thereby allowing long-term studies exclusively on hepatocytes. Furthermore, higher throughput biological inquiries and drug toxicity screens are possible since the MPCC platform can be scaled to an industry-standard 384-well plate[164], and high content imaging studies can be performed since the model is a 2D monolayer[53]. MPCCs of PHHs and 3T3-J2 fibroblasts have been successfully implemented in several drug development

applications including drug clearance prediction[56,180], drug hepatotoxicity[58], enzyme induction[54], drug metabolite identification[55], and drug-mediated modulation of glucose metabolism[62].

In this study, we hypothesized that HepaRG cells incorporated into the MPCC format could provide improved hepatic functions for multiple weeks of culture. Towards that end, we incorporated HepaRG cells into the MPCC format, characterized the expression of hepatic versus biliary markers, evaluated hepatic functions of the cultures, and demonstrated induction of cytochrome P450 (CYP450) enzymes. We then demonstrated proof-of-concept for drug toxicity testing by screening a library of 47 drugs of various classes and mechanisms of action that have been previously tested in PHHs.[58] With future improvements to the platform, we envision HepaRG cells in MPCCs as a robust first-tier toxicity screen for the early stages of drug development where high-throughput and low cost are essential criteria for testing platforms.[164]

4.2 Materials and Methods

4.2.1 Processing of HepaRG Cells

Cryopreserved differentiated HepaRG cells (HPR116) were a gift from Biopredic International (Saint Grégoire, France), thawed in a 37°C water bath, and suspended in seeding media (William's E base (Sigma-Aldrich, St. Louis, MO) with 1.5% (v/v) HEPES buffer (Corning Life Sciences, Tewksbury, MA), 1% (v/v) ITS+ Premix (Corning Life Sciences), 1% (v/v) penicillin/streptomycin (Corning Life Sciences), 100 nM dexamethasone (Sigma-Aldrich), and 7 ng/mL glucagon (Sigma-Aldrich)). Cells were centrifuged at 360×g for 2 minutes, resuspended in fresh seeding media, and counted.

4.2.2 Fibroblast Culture

Murine embryonic 3T3-J2 fibroblasts were a gift from Howard Green of Harvard Medical School.[129] Cells were cultured at 37°C, 10% CO_2 in Dulbecco's Modified Eagle's Medium

(DMEM; Corning Life Sciences) with high glucose, 10% (v/v) bovine calf serum (Life Technologies, Carlsbad, CA), and 1% (v/v) penicillin-streptomycin. Fibroblasts were passaged up to 12 times prior to use in co-cultures with HepaRG cells.

4.2.3 Establishment of HepaRG/3T3-J2 Micropatterned Co-Cultures (HepaRG-MPCCs)

Industry-standard tissue culture polystyrene 24-well plates (Corning Life Sciences) were coated for 2 hours with 25 µg/mL rat tail collagen-I (Corning Life Sciences) and rinsed twice with sterile water. After drying, these plates were subjected to polydimethylsiloxane (PDMS) mask-based soft lithography to micropattern circular collagen islands (500 µm diameter, 1200 µm center-to-center spacing) as previously described.[54,66] Cryopreserved HepaRG cells were processed as described above and seeded at a density of 6.67×10^5 cells/mL into collagen micropatterned wells (300 µL/well). After allowing 2-3 hours for cellular attachment and spreading onto collagen-coated islands, wells were washed $3\times$ in DMEM base medium to remove unattached cells, leaving $\sim 3 \times 10^4$ cells per well in 24-well format ($\sim$90 islands/well). 3T3-J2 fibroblasts were seeded 12-18 hours later at a density of 3×10^5 cells/mL (300 µL/well) and allowed to fill the remaining area surrounding the HepaRG islands. Cultures for drug dosing studies were all seeded in standard 96-well plates, with each well requiring 1/6 the volume of a 24-well plate well. Culture supernatants were changed with fresh, serum-containing medium every other day.

4.2.4 Establishment of HepaRG Confluent Conventional (HepaRG-CCs)

24-well plates were coated for 2 hours with 25 µg/mL rat tail collagen-I, rinsed twice with sterile water, and allowed to dry. Processed HepaRG cells were seeded at a density of 1×10^6 cells/mL into collagen coated wells (500 µL/well). After allowing 2-3 hours for cellular attachment and spreading onto collagen, wells were replaced with 500 µL/well fresh, serum-

containing medium. Culture supernatants were changed with fresh, serum-containing medium every other day.

4.2.5 Hepatic Morphological, Functionality, and Health Assessments

The morphology of HepaRG-MPCCs was monitored using an EVOS®FL cell imaging system (Life Technologies) with standard 4×, 10×, and 20× phase contrast objectives. Albumin secretions were assessed with an enzyme-linked immunosorbent assay (ELISA) with horseradish peroxidase detection and 3,3',5,5'-tetramethylbenzidine as the substrate.[54] Urea production was measured via a colorimetric endpoint analysis with diacetyl monoxime, acid, and heat (Stanbio Labs, Boerne, TX). CYP3A4 and CYP2C9 activities were quantified using the luciferin-IPA (3 µM, 1 hour) and luciferin-H (100 µM, 3 hours) luminescent assays, respectively, from Promega Life Sciences (Madison, WI) according to manufacturer-supplied protocols. CYP2A6 activity was measured by incubating cultures for 1 hour with 50 µM coumarin (Sigma-Aldrich) and evaluating the production of the fluorescent metabolite 7-hydroxycoumarin via fluorescence output (355 nm excitation, 460 nm emission). CYP1A2 activity was quantified by incubating cultures for 3 hours with 5 µM 7-ethoxyresorufin (Sigma-Aldrich) and measuring the fluorescent metabolite resorufin (550 nm excitation, 585 nm emission) generated via the CYP1A2-mediated *O*-dealkylation of 7-ethoxyresorufin.

4.2.6 Immunofluorescent Staining

Cultures were fixed with 4% paraformaldehyde (Alfa Aesar, Wand Hill, MA), permeabilized with 0.1% triton X-100 (Amresco, Solon, OH) for 10 minutes, and rinsed with 1× phosphate buffered saline (PBS; Corning Life Sciences). Cultures were then incubated for 30 minutes at 37ºC with a blocking buffer consisting of 5% goat serum (Pierce Thermo Scientific, Rockford, IL) in PBS. Rabbit anti-human albumin and mouse anti-human cytokeratin 19 (CK19)

primary antibodies (Rockland Immunochemicals, Limerick, PA, and GeneTex, Irvine, CA, respectively) were diluted in blocking buffer (1:100) and incubated on the cultures for 1 hour at 37ºC. 4',6-diamidino-2-phenylindole (DAPI; MP Biomedicals, Solon, OH) was added to the cultures at 300 nM for the final 15 minutes of incubation. Cultures were then imaged using red fluorescent protein (RFP; 531 nm excitation, 593 nm emission), green fluorescent protein (GFP; 470 nm excitation, 510 nm emission), and DAPI (357 nm excitation, 447 nm emission) light cubes with the EVOS®FL cell imaging system.

4.2.7 Enzyme Induction Analysis

CYP450 induction studies were carried out by treating cultures in serum-free culture medium with rifampin (25 µM, Sigma-Aldrich), omeprazole (50 µM, Sigma-Aldrich), or 0.1% (v/v) dimethyl sulfoxide (DMSO; Corning Life Sciences) for 4 days. Following the incubation, cultures were evaluated for CYP3A4 and CYP2C9 activities using the luminescent assays described above.

4.2.8 Drug Dosing Studies

After ~1 week of stabilization, cultures were dosed in serum-free culture medium (i.e. limited binding of drug to serum proteins) for 6 days (3 doses that corresponded to standard media changes) at $25 \times C_{max}$ or $100 \times C_{max}$ (the maximum concentration in human plasma, Table 4.1) following the protocols previously utilized.[161,181] The DMSO concentration that MPCCs were exposed to was kept at 0.1% (v/v) relative to culture medium except for five compounds that used 0.2% (v/v) and three compounds that used 1.0% (v/v) due to limited DMSO solubility (Table 4.1). All compounds were purchased from either Sigma-Aldrich or Cayman Chemical (Ann Arbor, MI). Following the drug treatment, cultures were evaluated for ATP activity using the CellTiter-Glo kit (Promega); levels in HepaRG-MPCCs were subtracted from fibroblast-only controls to assess

HepaRG-specific contributions. Vehicle-only controls were maintained at each DMSO concentration to serve as a baseline for comparison.

4.2.9 Data Analysis

Data processing and visualization were performed using Microsoft Excel and GraphPad Prism (La Jolla, CA). Functional data was normalized to the number of HepaRG cells seeded into each well. For each toxicity assay, data were normalized to the appropriate vehicle-only control, and mean and standard deviation values were calculated using three technical replicates for each of the drug doses administered. TC_{50} values (concentration that decreased the measured endpoints by 50%) for each assay were interpolated using linear curve fitting between the dose at which the assay signal was greater than 50% of control values and the dose at which the assay signal was less than or equal to 50% of control values. A compound that yielded a TC_{50} value less than or equal to $100 \times C_{max}$ for albumin and/or ATP assays was classified as "toxic", while a compound that had TC_{50} values greater than $100 \times C_{max}$ (i.e. could not be interpolated within the dose range tested) for both assays was classified as "non-toxic". Sensitivity was defined as the portion of correctly predicted positive toxins to all positive toxins in the clinic ([TP] / [TP + FN]). Specificity was defined as the portion of correctly predicted negatives (i.e. non-liver-toxins) to all negatives in the clinic ([TN] / [TN + FP]). TP = true positives, FN = false negatives, TN = true negatives, FP = false positives.

4.3 Results

4.3.1 Establishment of HepaRG-MPCCs and HepaRG-CCs

HepaRG cells could be cultured in both the HepaRG-MPCC and HepaRG-CC formats as illustrated in Figure 4.1A. When cultured with culture medium containing 2% (v/v) DMSO, HepaRG-MPCCs were successfully micropatterned onto collagen islands (Figure 4.1B). After

seeding 3T3-J2 fibroblasts and 1-2 weeks of culture, HepaRG cells were retained on the collagen islands and maintained prototypical hepatic morphology (i.e. polygonal shape, multi-nucleation) (Figure 4.1C-D). HepaRG cells seeded in the HepaRG-CC format filled in the collagen-coated surface the day after seeding (Figure 4.1E). Following 1 week and 2 weeks of culture, HepaRG cells tended to contract and fill up less of the available surface area (Figure 4.1F-G). When using DMSO-free culture medium, HepaRG cells could also fill in the collagen islands (Figure 4.2A) that are retained through 1 week and 2 weeks of culture (Figure 4.2B-C). In the HepaRG-CC format without using DMSO in culture medium, HepaRG cells filled in the available surface area upon seeding (Figure 4.2D). Cultures maintained coverage of the surface area after 1 week (Figure 4.2E) and 2 weeks (Figure 4.2F) of culture, as opposed to using 2% (v/v) DMSO in the culture medium.
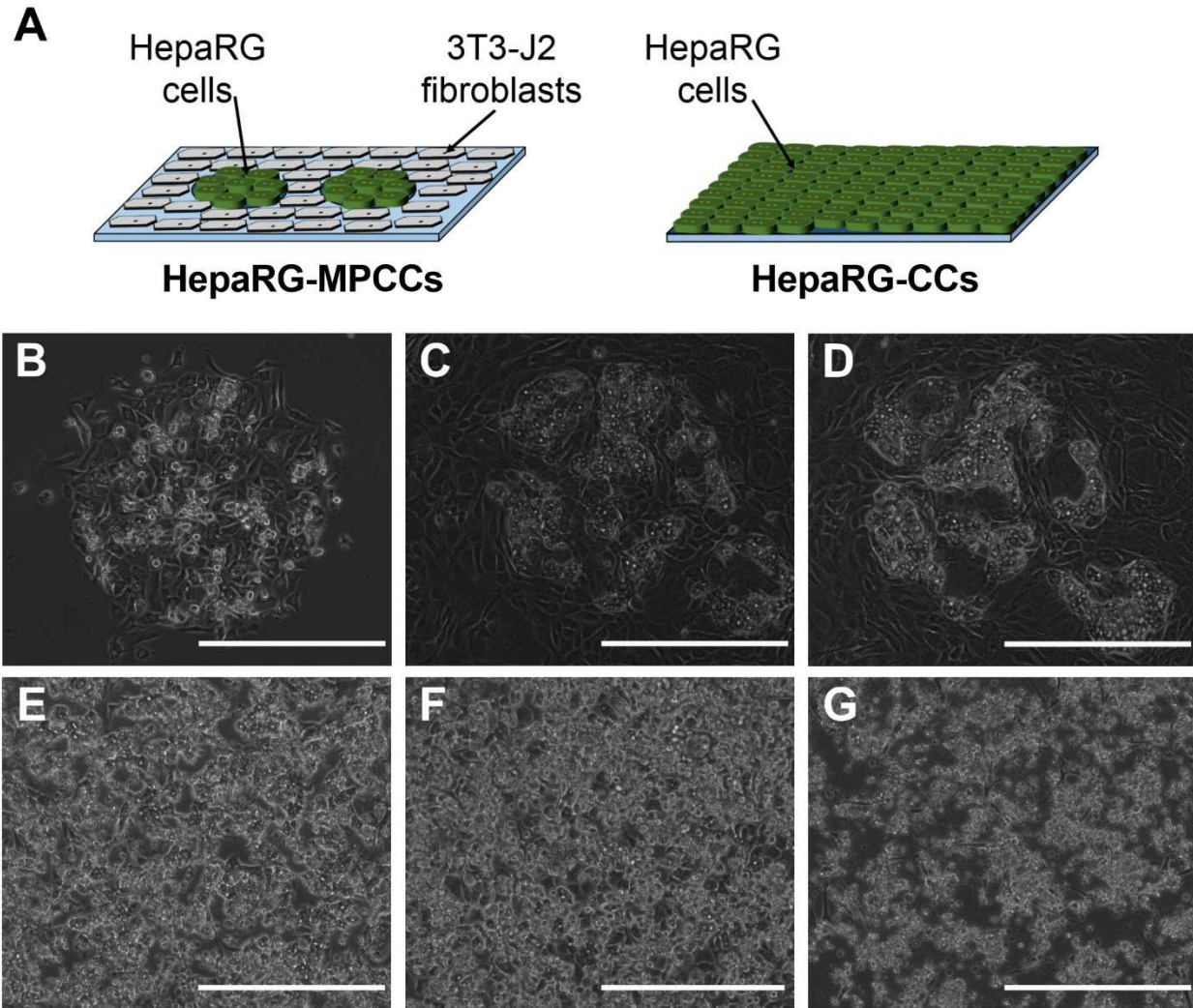
Figure 4.1: Morphology of HepaRG cells in culture over time with DMSO-containing medium. **(A)** Illustration of the differences between HepaRG-MPCCs with 3T3-J2 fibroblasts and HepaRG-CCs. **(B)** As assessed by phase contrast morphology, HepaRG cells patterned onto collagen islands using 2% (v/v) DMSO-containing culture medium. Following seeding of 3T3-J2 fibroblasts, hepatic morphology was maintained in HepaRG-MPCCs after both **(C)** 1 week and **(D)** 2 weeks in culture. HepaRG-CCs were also assessed for morphology after **(E)** 1 day, **(F)** 1 week, and **(G)** 2 weeks in culture. All scale bars = 400 μm.
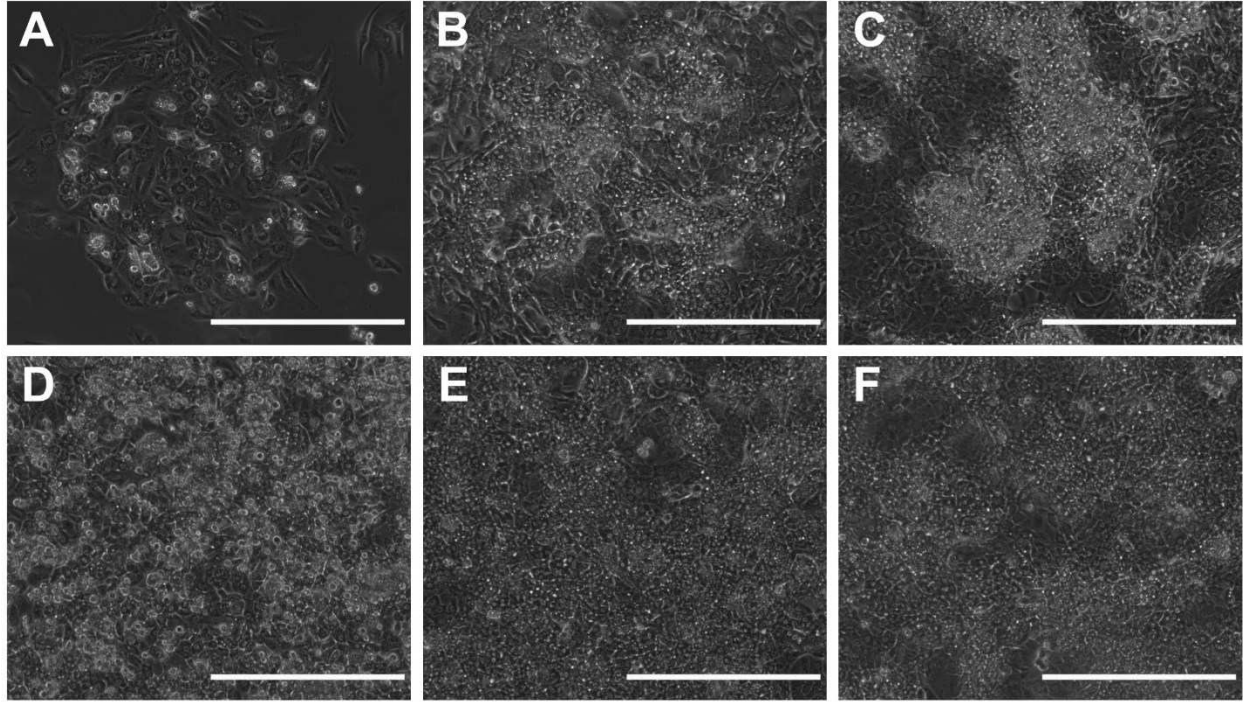
Figure 4.2: Morphology of HepaRG cells in culture over time with DMSO-free medium. (A) As assessed by phase contrast microscopy, HepaRG cells selectively patterned onto collagen islands with DMSO-free culture medium. Following seeding of 3T3-J2 fibroblasts to complete HepaRG-MPCCs, islands were maintained after **(B)** 1 week and **(C)** 2 weeks in culture. HepaRG-CCs were also assessed for morphology after **(D)** 1 day, **(E)** 1 week, and **(F)** 2 weeks in culture. All scale bars = 400 µm.

4.3.2 Functional Stability of the HepaRG-MPCC Platform

Culture supernatants were collected and assayed for albumin and urea secretions for 4 weeks of *in vitro* culture. HepaRG-MPCCs cultured without DMSO tended to increase albumin secretion over time and reached steady-state albumin secretions of ~10 µg/hr/10^6 cells (Figure 4.3A), which is within the donor diversity observed in PHHs.[56] By contrast, HepaRG-CCs without DMSO maintained albumin levels of ~0.5 µg/hr/10^6 cells (Figure 4.3B). Both HepaRG-MPCCs and HepaRG-CCs cultured with 2% (v/v) DMSO had virtually undetectable levels of albumin. Similar trends were observed with urea secretions in that HepaRG-MPCCs without DMSO cultures maintained much higher urea secretions (~1.5-2 µg/hr/10^6 cells, Figure 4.3C) than HepaRG-CCs (~0.1-0.2 µg/hr/10^6 cells, Figure 4.3D), although these levels are less than 10% of the levels observed in PHHs.[56] Addition of 2% (v/v) DMSO to culture medium caused a noticeable reduction in urea secretions to less than 50% of DMSO-free cultures.

Evaluating the activities of CYP450 enzymes revealed similar trends as albumin and urea data. CYP3A4 activity was more stable in HepaRG-MPCCs compared to HepaRG-CCs over 4 weeks in culture (Figure 4.4A). Interestingly, HepaRG-MPCCs with 2% (v/v) DMSO in culture medium showed higher levels of CYP3A4 activity than cultures without DMSO, which contrasts with previous literature.[132] On the other hand, CYP2C9, CYP2A6, and CYP1A2 activity maintained stable activities of ~0.3-0.4 10^6 RLU/hr/10^6 cells, ~4-6 µM 7-hydroxycoumarin/hr/10^6 cells, and ~0.3-0.4 µM resorufin/hr/10^6 cells, respectively, in HepaRG-MPCCs (Figure 4.4B-D). These three isoforms generally showed higher activity when cultured in DMSO-free culture medium compared to medium with 2% (v/v) DMSO. HepaRG-CCs had CYP2C9, CYP2A6, and CYP1A2 activity less than 10% of their HepaRG-MPCC counterparts regardless of the inclusion of DMSO in culture medium.
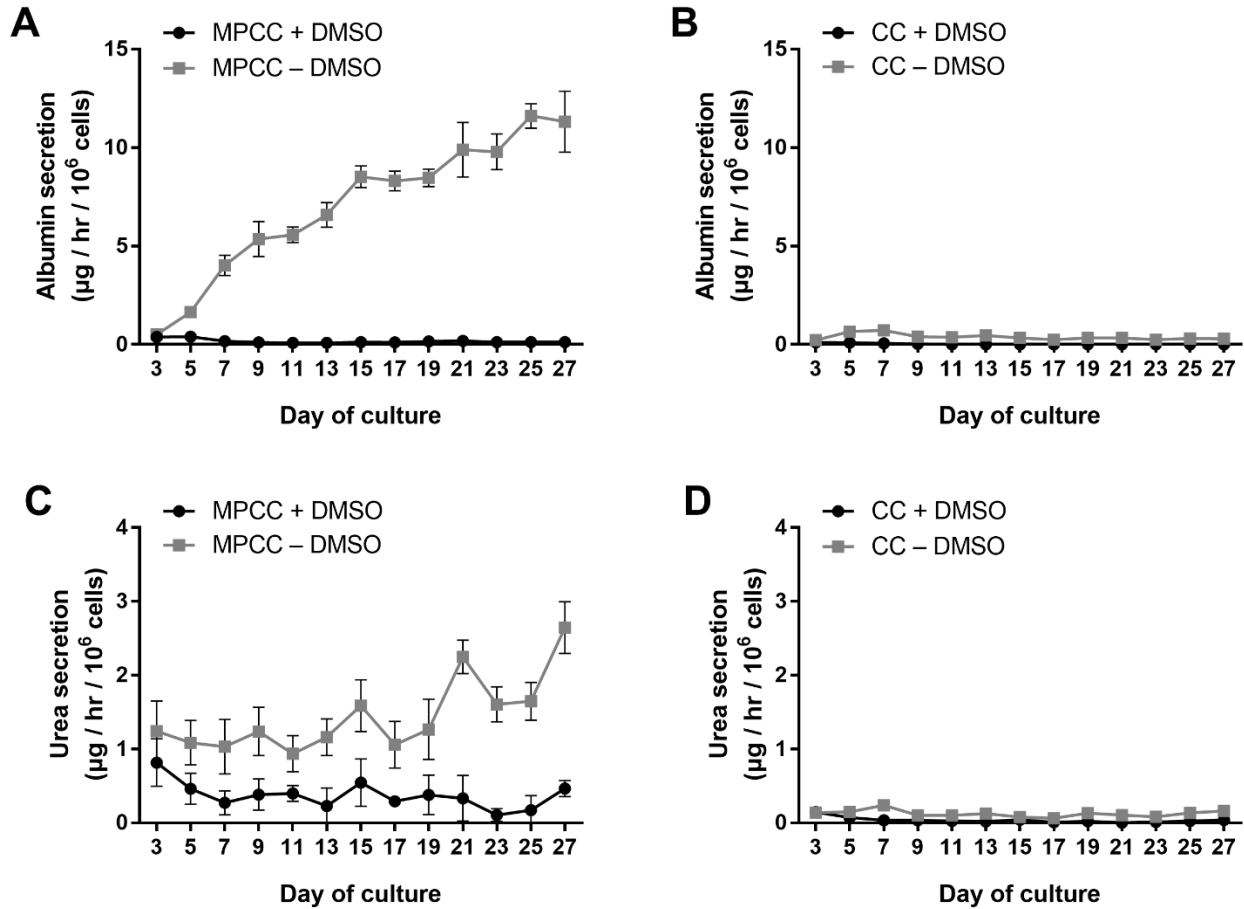
Figure 4.3: Hepatospecific functions in HepaRG cultures. **(A)** Albumin secretion and **(B)** urea secretion were quantified for 4 weeks in culture for both HepaRG-MPCCs and HepaRG-CCs with or without 2% (v/v) DMSO in cell culture medium. All error bars represent standard deviations (n = 3).
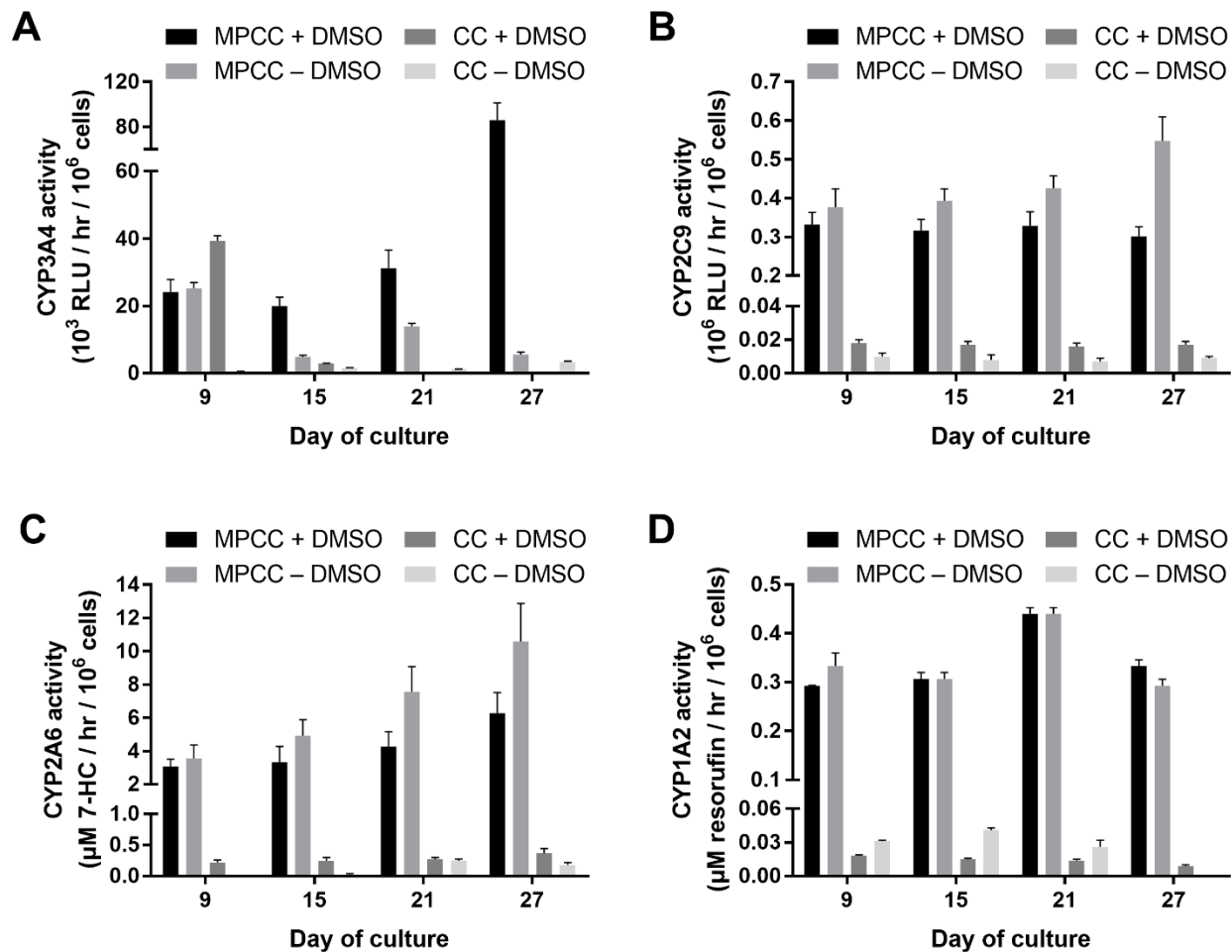
Figure 4.4: CYP450 enzyme activities of HepaRG cultures. As assessed by various luminescent and fluorescent substrates (see Section 4.2.5), HepaRG-MPCCs and HepaRG-CCs with or without 2% (v/v) DMSO in cell culture medium were quantified for **(A)** CYP3A4, **(B)** CYP2C9, **(C)** CYP2A6, and **(D)** CYP1A2 activities. All error bars represent standard deviations (n = 3).

4.3.3 Differentiation Towards Hepatic and Biliary Lineages

As HepaRG cells are known to be bi-potential (capable of differentiating into either the hepatic or biliary lineages), we conducted immunofluorescent staining on HepaRG cells in both HepaRG-MPCCs and HepaRG-CCs. In HepaRG-MPCCs, the expression of albumin (hepatospecific marker) was highly concentrated in the HepaRG island (Figure 4.5). On the other hand, albumin expression in HepaRG-CCs was more diffuse and not as concentrated around the cellular nuclei. The expression of cytokeratin 19 (CK19; biliary-specific marker) tended to co-localize with the expression of albumin in both model systems.
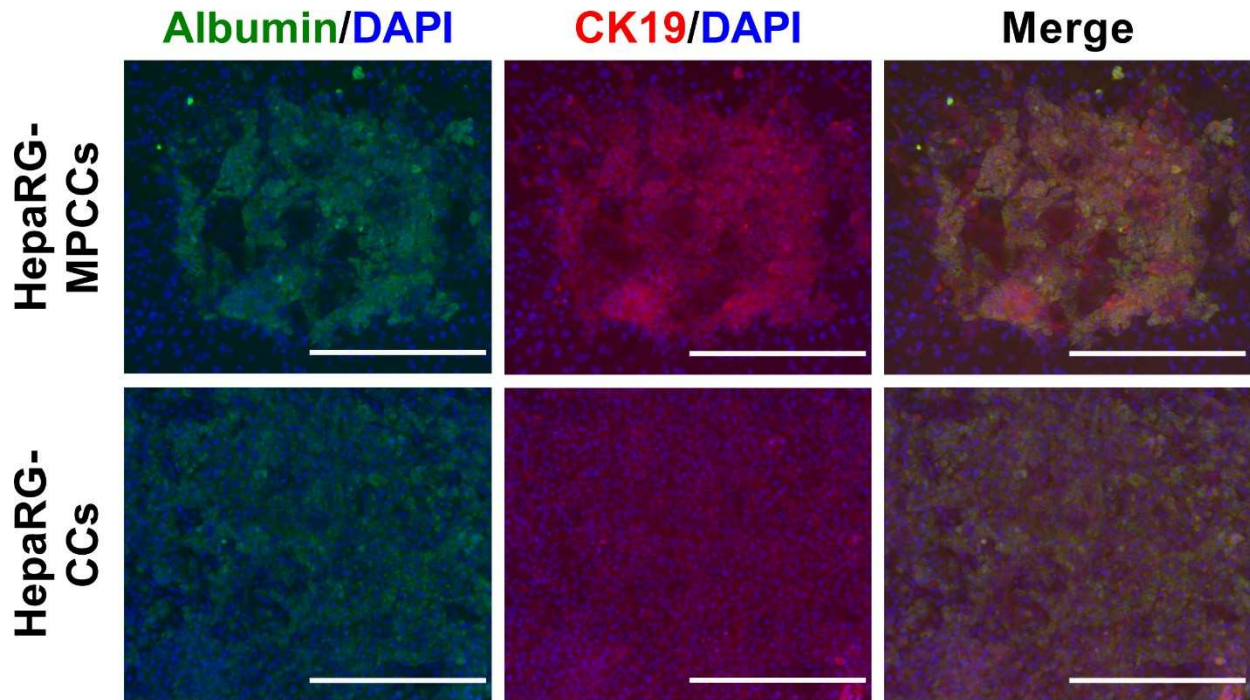
Figure 4.5: Immunostaining of HepaRG cultures. After a week in culture, HepaRG-MPCCs showed a high level of the hepatospecific marker albumin (green) that was concentrated to the island of HepaRG cells. HepaRG-CCs tended to show a lower level of albumin expression that was not as evident in the cellular cytoplasm. The biliary-specific marker cytokeratin 19 (CK19; red) tended to co-localize with albumin in both culture models as evidenced in the merged images. All scale bars = 400 μm.

4.3.4 Enzyme Induction Studies

As a demonstration of the utility for screening drug-drug interactions with HepaRG-MPCCs, we screened the prototypical inducers rifampin and omeprazole to compare CYP450 activity with respect to a DMSO control. In HepaRG-MPCCs, CYP3A4 activity was induced ~9-fold and ~6-fold after 4 days of treatment with rifampin and omeprazole, respectively (Figure 4.6A). Rifampin induced CYP3A4 activity in HepaRG-CCs to a similar level as HepaRG-MPCCs; however, CYP3A4 activity in HepaRG-CCs was not induced by omeprazole. On the other hand, omeprazole caused a ~2-fold and ~4-fold induction of CYP1A2 activity in HepaRG-MPCCs and HepaRG-CCs, respectively (Figure 4.6B). Rifampin did not induce CYP1A2 activity in either model.
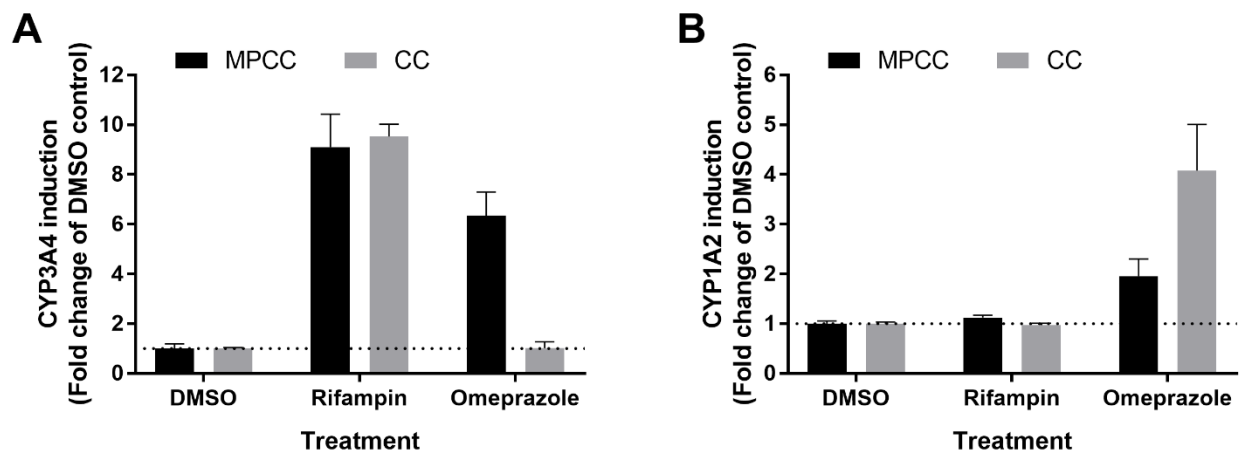
Figure 4.6: Enzyme induction in HepaRG cultures. As assessed by the appropriate luminescent or fluorescent substrates (see Section 4.2.5), the fold change induction of **(A)** CYP3A4 and **(B)** CYP1A2 was quantified upon treatment with 25 µM rifampin or 50 µM omeprazole for 4 days. Data are plotted as a fold change relative to DMSO-only controls. All error bars represent standard deviations (n = 3).

4.3.5 Compound Selection, Culture Dosing, and Criteria for Toxicity Decisions

To provide a robust comparison of toxicity prediction in HepaRG-MPCCs and PHHs cultured in various formats, we selected 47 compounds utilized in previous studies.[38,58] These compounds have been screened in conventional sandwich-cultured PHHs for 24 hours and assessed with hepatocyte imaging assay technology (HIAT) or in PHH-MPCCs dosed over 5-9 days. Thirteen of these compounds were reported as true positives (TPs), meaning that hepatotoxicity was observed both clinically and in HIAT at a concentration at or below $100 \times C_{max}$ (maximum plasma concentration reported for humans). Ten drugs did not elicit hepatotoxicity in HIAT at a concentration of up to $100 \times C_{max}$ and are also considered safe in humans (true negatives or TNs). Another twenty-four DILI compounds were not identified as toxic utilizing HIAT, but are known to cause human hepatotoxicity (false negatives or FNs). PHH-MPCCs were treated with these drugs over 5-9 days and binary decisions on toxicity potential have been published.[58] Here, we sought to compare drug responses in HepaRG-MPCCs relative to PHH-based models used in these previously published studies.

Based on our previous studies[161,181], we chose to dose HepaRG-MPCCs for 6 days (three drug treatments administered with standard media changes every other day). Albumin and ATP levels were assessed in HepaRG-MPCCs using the same wells. While albumin is a liver-specific marker not secreted by 3T3-J2 fibroblasts, ATP is present in both cell types and thus fibroblast-only control cultures were carried out alongside HepaRG-MPCCs to determine effects of drugs specifically on HepaRG cells. Sample drug dose responses in HepaRG-MPCCs for hepatotoxins and non-liver-toxins are shown in Figure 4.7.

Increasing levels of DMSO in culture medium is known to downregulate the CYP450 activity of multiple isoforms, which could alter the metabolism and toxicity profile of various

drugs.[132] Thus, the DMSO concentration that HepaRG cultures were exposed to was kept at 0.1%

(v/v) relative to culture medium for 39 of 47 compounds tested, while 0.2% (v/v) was used for 5

compounds, and 1.0% (v/v) was used for 3 compounds due to limited solubility in DMSO (Table

4.1). Control cultures at each DMSO concentration were used to normalize data properly from

drug-treated cultures and enable the binary decisions as described below. As outlined in our

previous studies[161,181], a compound was declared "toxic" if the TC_{50} – the drug concentration that

reduces endpoint functional activity to 50% of vehicle-only controls – was at or below $100 \times C_{max}$

for at least one of the multiplexed assays on HepaRG-MPCCs. If the TC_{50} value was greater than

$100 \times C_{max}$ for both albumin and ATP (i.e. could not be interpolated from dose range tested), the

compound was considered "non-toxic". Table 4.1 provides the C_{max} values, formula weights,

known clinical DILI classifications, and toxic/non-toxic decisions in HepaRG-MPCCs relative to

published information using PHH-MPCCs and the HIAT assay. If applicable, the DILI severity

score from the Liver Toxicity Knowledge Base (LTKB) from the FDA appears in the proper

column of Table 4.1. C_{max} values for these compounds varied widely across the entire set, from

0.004 μM for betahistine 2HCl to 793.9 μM for hydroxyurea.
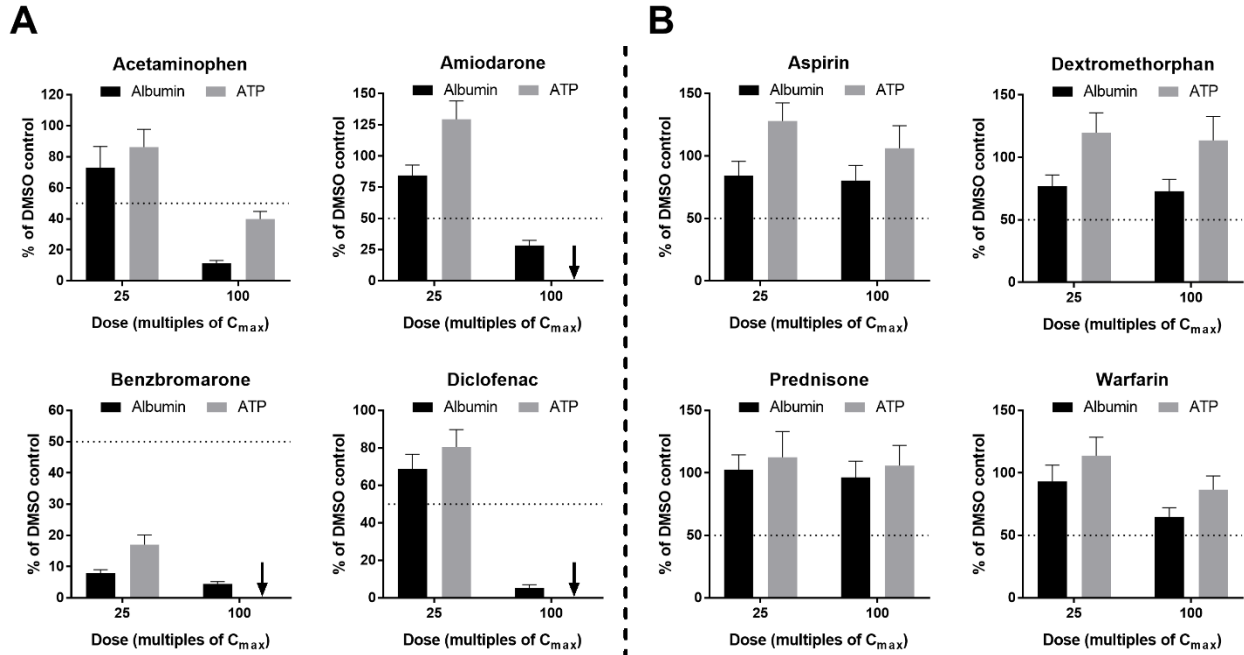
Figure 4.7: Dose-dependent downregulation of albumin secretions and ATP activity in HepaRG-MPCCs following drug dosing. (A) Following 6 days of treatment with prototypical hepatotoxins (three drug doses applied every other day with standard media changes), albumin secretions and ATP activity in HepaRG-MPCCs showed a severe downregulation compared to DMSO-only controls. **(B)** Non-toxic drugs with respect to the liver did not show such downregulation following the same drug treatment schedule described in panel 'A'. All data were normalized to DMSO-only controls, and arrows indicate undetectable ATP levels. Error bars represent standard deviations (n = 3).

Table 4.1: Compounds tested and binary decisions of toxicity in different models

Compound name	C_{max} (µM)	FW (g/mol)	DMSO (vol%)	DILI Severity	DILI Category	DILI Clinical	HIAT	PHH-MPCCs	HepaRG-MPCCs
TPs in HIAT									
Acetaminophen	151.170	138.91	0.2	N/A	P2	+	+	+	+
Amiodarone	0.806	681.80	0.1	8	P2	+	+	+	+
Benzbromarone	4.361	424.10	0.1	-2	P1	+	+	+	+
Clozapine	0.951	326.83	0.1	2	P2	+	+	+	+
Diclofenac	8.023	318.10	0.1	7	P2	+	+	+	+
Flurbiprofen	57.356	244.27	0.1	3	P2	+	+	+	+
Mebendzole	0.126	295.30	0.1	3	P2	+	+	+	+
Mefenamic acid	26.959	241.30	0.2	N/A	P2	+	+	+	+
Phenacetin	13.401	179.22	1.0	N/A	P2	+	+	+	+
Phenylbutazone	486.772	308.37	1.0	N/A	P2	+	+	+	+
Quinine	9.254	391.47	0.2	N/A	P2	+	+	+	+
Trazodone HCl	5.065	408.32	0.1	N/A	P2	+	+	+	+
Troglitazone	6.387	441.50	0.1	-2	P1	+	+	+	+
TNs in HIAT									
Aspirin	5.526	180.16	0.1	N/A	O2	–	–	–	–
Buspirone	0.005	421.96	0.1	3	N1	–	–	–	–
Dexamethasone	0.224	392.47	0.1	3	N1	–	–	–	–
Dextromethorphan HBr	0.028	370.30	0.1	N/A	N1	–	–	–	–
Fluoxetine	0.049	345.79	0.1	3	N2	–	–	–	–
Miconazole	0.024	479.10	0.1	N/A	N1	–	–	–	–
Prednisone	0.068	358.43	0.1	N/A	N2	–	–	–	–
Propranolol	0.201	295.81	0.1	3	N1	–	–	–	–
Rosiglitazone	1.120	357.43	0.1	N/A	N2	–	–	–	–
Warfarin	4.868	308.34	0.1	5	N2	–	–	–	–
FNs in HIAT									
Acetazolamide	135.142	222.25	0.2	N/A	P2	+	–	+	–
Betahistine 2HCl	0.004	209.12	0.1	6	P2	+	–	–	–
Captopril	4.284	217.29	0.1	7	P2	+	–	–	+
Chloramphenicol palmitate	19.991	561.54	0.1	N/A	P2	+	–	–	–
Ciprofloxacin HCl	11.476	331.34	0.1	7	P2	+	–	+	+
Clomiphene citrate	0.022	598.10	0.1	N/A	P2	+	–	–	–
Clomipramine	0.191	351.30	0.1	N/A	P2	+	–	+	+
Cyclophosphamide	265.359	279.10	0.2	5	P2	+	–	+	+
Cyproterone acetate	0.656	416.94	0.1	N/A	O1	+	–	+	+
Danazol	0.074	337.50	0.1	8	P1	+	–	–	–
Dapsone	6.007	248.30	0.1	N/A	P1	+	–	+	–
Estrone	0.022	270.37	0.1	N/A	P2	+	–	–	–
Hydroxyurea	793.925	76.05	0.2	8	P2	+	–	+	+
Imipramine HCl	0.087	316.87	0.1	3	P2	+	–	+	–
Isoniazid	76.609	137.14	0.1	8	P1	+	–	+	–
Maleic acid	1.000	160.04	0.1	N/A	O1	+	–	+	–
Methimazole	1.868	114.17	0.1	8	P2	+	–	–	–
Nifedipine	0.271	346.30	0.1	3	P2	+	–	–	–
Norgestrel	0.009	312.45	0.1	N/A	P2	+	–	–	–
Nortriptyline HCl	0.122	299.84	0.1	8	P2	+	–	+	–
Piroxicam	5.135	331.37	0.1	3	P2	+	–	–	+

| | | | | DILI | | | Model predictions | | |
Compound name	C_{max} (μM)	FW (g/mol)	DMSO (vol%)	Severity	Category	Clinical	HIAT	PHH-MPCCs	HepaRG-MPCCs
Progesterone	0.193	314.46	0.1	N/A	P2	+	−	−	−
Pyrazinamide	407.174	123.11	1.0	3	P2	+	−	+	−
Tamoxifen	0.162	371.53	0.1	6	P2	+	−	+	−

Notes. Compounds were selected from the study by Xu *et al.*[38] where HIAT was applied to ECM-sandwich cultures of PHHs dosed for 24 hours with various drugs. DILI severity scores from the LTKB (Liver Toxicity Knowledge Base) of the U.S. Food and Drug Administration[133]: "N/A" indicates not applicable/no information in the database, negative numbers indicate the drug was withdrawn from the market, and higher positive numbers indicate a greater DILI concern. DILI categorization: P1, DILI type 1, dose-dependent (toxic); P2, DILI type 2, idiosyncratic (toxic); N1, not known to cause liver injury (non-toxic); N2, sporadic cases (<10) of liver injury reported but generally considered by doctors as a safe drug to use for humans (non-toxic); O1, hepatotoxic in animals, untested in humans (toxic); O2, elevated liver enzymes observed in humans but does not lead to frank liver toxicity (non-toxic). Clinical classification per Xu *et al.*[38]: considered a liver toxin (+) or a non-liver toxin (−). Model predictions: All models were dosed up to $100 \times C_{max}$ for each compound and classified as liver toxins or non-toxins based on specific algorithms as described in methods. The HIAT-sandwich classifications are from Xu *et al.*[38], the PHH-MPCC classifications are from Khetani *et al.*[58], while the HepaRG-MPCC classifications represent the data collected in this study.

4.3.6 DILI TP Compounds

C_{max} values for the 13 TP compounds used here varied from 0.126 µM for mebendazole to 486.8 µM for phenylbutazone. For all 13 of these compounds, albumin secretions were reduced by at least 50% relative to DMSO-only controls, which thus gave accurate "toxic" predictions for these drugs and matches results from PHH-MPCCs. ATP levels were reduced by at least 50% upon treatment with 10 of these 13 drugs (mebendazole, phenacetin, and trazodone HCl being the exceptions). TC_{50} values are presented graphically in Figure 4.8A. In general, the TC_{50} value for each compound was lower (i.e. more sensitive) with albumin compared to ATP, although most were within 2-fold of each other. Thus, as observed in PHH-MPCCs, ATP data is less sensitive than albumin secretions for DILI detection.[58]
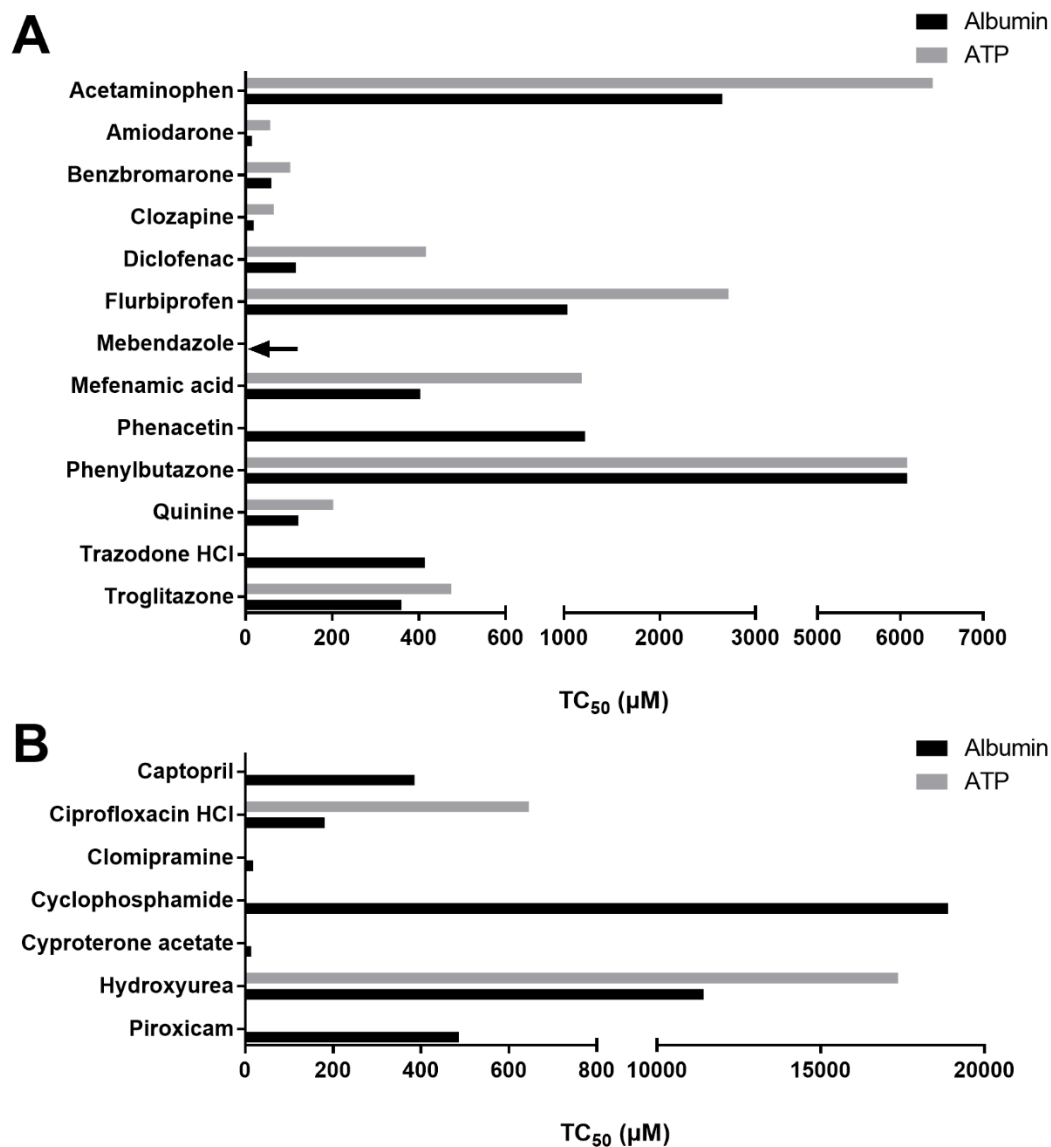
Figure 4.8: TC$_{50}$ values of hepatotoxins in HepaRG-MPCCs. (A) TC$_{50}$ values, the interpolated drug concentration that reduces the endpoint biochemical signal to 50% of DMSO-only controls, as measured by albumin secretions and ATP activity for HIAT TP compounds. The arrow indicates a measurable but very low TC$_{50}$ (i.e. very toxic compound) that could be interpolated at a dose $\leq 100 \times C_{max}$, while missing bars indicate a TC$_{50}$ above $100 \times C_{max}$. **(B)** TC$_{50}$ values as in panel 'A', but for HIAT FN compounds correctly classified in the HepaRG-MPCC model.

122

4.3.7 DILI TN Compounds

In general, C_{max} values for the ten TN compounds tended to be lower than those for the TP compounds and ranged from 0.005 μM for buspirone to 5.526 μM for aspirin. None of the TN compounds tested caused at least a 50% reduction in either albumin secretions or ATP activity in HepaRG-MPCCs treated with up to $100 \times C_{max}$ of the drug being tested. Thus, all were correctly identified as 'non-toxins' in HepaRG-MPCCs, PHH-MPCCs, and HIAT.

4.3.8 DILI FN Compounds

C_{max} values for the 24 FN compounds ranged from 0.004 μM for betahistine 2HCl to 793.9 μM for hydroxyurea. Seven of the 24 FN compounds caused at least a 50% reduction in albumin secretions from HepaRG-MPCCs relative to DMSO-only controls at a dose of $100 \times C_{max}$. Of these seven, ciprofloxacin HCl and hydroxyurea also caused ATP levels to be reduced by at least 50%. Captopril, clomipramine, cyclophosphamide, cyproterone acetate, and piroxicam only downregulated albumin secretions. TC_{50} values from the HepaRG-MPCC albumin and ATP data are presented graphically in Figure 4.8B.

4.3.9 Overall Sensitivity and Specificity Based on TC_{50} Criteria

In our system, we define model sensitivity as the portion of clinical hepatotoxins correctly identified as "toxic" *in vitro* ([TP] / [TP + FN]), while the specificity as the portion of non-liver-toxic compounds correctly identified as "non-toxic" *in vitro* ([TN] / [TN + FP]). As detailed in Table 4.2, HepaRG-MPCCs and PHH-MPCCs had sensitivities of 54% and 70%, respectively, for the 37 hepatotoxic compounds tested. Both models correctly identified all 10 non-toxins and thus had a specificity of 100%.

Table 4.2: Confusion matrix for binary decisions in PHH-MPCCs and HepaRG-MPCCs

	Model-predicted DILI in MPCCs		
Actual DILI	Positive	Negative	Total
Positive	PHH: 26	PHH: 11	37
	HepaRG: 20	HepaRG: 17	
Negative	PHH: 0	PHH: 10	10
	HepaRG: 0	HepaRG: 10	
Total	PHH: 26	PHH: 21	47
	HepaRG: 20	HepaRG: 27	

Note. Sensitivity: 70% and 54% for PHH-MPCCs and HepaRG-MPCCs, respectively. Specificity: 100% for both models.

4.3.10 Comparison of Toxicity Prediction in HepaRG-MPCCs and HepaRG-CCs

For the drugs that were correctly identified as "toxic" in HepaRG-MPCCs (both TP and FN), we compared binary calls in HepaRG-CCs. Three of these compounds (captopril, clomipramine, and cyproterone acetate) failed to show toxicity in HepaRG-CCs (Table 4.3). Interestingly, these three compounds were correctly identified in PHH-MPCCs[58] and HepaRG-MPCCs here, but not in the HIAT assay using PHHs[38] or HepaRG-CCs.

Table 4.3: Comparison of toxicity predictions in HepaRG-MPCCs and HepaRG-CCs

Compound name	Clinical DILI	Model prediction	
		HepaRG-CCs	HepaRG-MPCCs
Acetaminophen	+	+	+
Amiodarone	+	+	+
Benzbromarone	+	+	+
Captopril	+	−	+
Ciprofloxacin HCl	+	+	+
Clomipramine	+	−	+
Clozapine	+	+	+
Cyclophosphamide	+	+	+
Cyproterone acetate	+	−	+
Diclofenac	+	+	+
Flurbiprofen	+	+	+
Hydroxyurea	+	+	+
Mebendazole	+	+	+
Mefenamic acid	+	+	+
Phenacetin	+	+	+
Phenylbutazone	+	+	+
Piroxicam	+	+	+
Quinine	+	+	+
Trazodone HCl	+	+	+
Troglitazone	+	+	+
Aspirin	−	−	−
Prednisone	−	−	−

Note. Boldfaced compounds indicate different binary calls between HepaRG-MPCCs and HepaRG-CCs.

4.4 Discussion

As opposed to a limited, expensive supply of PHHs, hepatocarcinoma cell lines offer the advantages of being inexpensive and amenable to high-throughput screening when large compound libraries would need to be screened for overt toxicity. While it is generally accepted that HepaRG cells are more differentiated and mature than other cell lines[166], they tend to show low levels of hepatic functions and poor drug toxicity predictions.[37,172] In contrast with the declining phenotype of conventional monolayer cultures of primary human hepatocytes (PHHs), micropatterned co-cultures (MPCCs) of PHHs with 3T3-J2 fibroblasts have been shown to stabilize the hepatic phenotype *in vitro*.[54] These 3T3-J2 fibroblasts have been shown to induce hepatic functions to a higher level than other 3T3 clones [158], hepatic stellate cells[13], Kupffer macrophages[67], and liver sinusoidal endothelial cells[179]. This suggests that the 3T3-J2 fibroblasts are involved in key processes necessary for stabilizing hepatocyte functionality *ex vivo*. While this so-called "co-culture effect" has not yet been fully explained, we speculate that the 3T3-J2 fibroblasts express various molecules found in the liver, such as decorin[158], vascular endothelial growth factor D[158], and T-cadherin[182], which have all been implicated in the ability of these fibroblasts to induce functions in hepatocytes from multiple species.[5] Thus, we hypothesized here that HepaRG cells could be incorporated into the MPCC format and subsequently display higher levels of hepatic functions and yield better drug toxicity predictions than HepaRG cells cultured in conventional formats.

With their bi-potential character, HepaRG cells can be evaluated for both hepatic and biliary functions. Many reports have characterized the hepatospecific activities and toxicity of HepaRG cells.[37,167,173,174,177] Other studies have reported biliary-specific functions such as cholestasis, disruption of bile salt export pump proteins, and toxicity of bile acids.[183–186] However,

most of these studies were carried out for at most 24 hours, which does not provide an accurate description of the long-term effects drugs might have on hepatocytes *in vivo*. We have found that, when incorporated into either the HepaRG-MPCC or HepaRG-CC format, HepaRG cells retain both their hepatic and biliary character as evidenced by the expression of albumin and cytokeratin 19 (CK19), respectively. However, the low levels of hepatospecific functions (i.e. albumin secretions, CYP450 activities) in HepaRG-CCs suggest that the biliary character of the HepaRG cells is insufficient to sustain the hepatic phenotype. As previously demonstrated with PHHs, primary animal hepatocytes, and iPSC-derived hepatocytes[5], we show here that 3T3-J2 fibroblasts can support the hepatic phenotype for multiple weeks *in vitro*.

While many protocols for differentiating HepaRG cells down the hepatic lineage require up to 2% (v/v) DMSO[175,187], we chose to use a DMSO-free medium formulation because it yielded a higher, more stable level of albumin secretions and CYP450 (2C9, 2A6, 1A2) activity than cultures with a DMSO-containing medium and because the HepaRG cells used here were pre-differentiated. Furthermore, an increasing level of DMSO has been shown to downregulate drug metabolism activity[132], which could provide an inaccurate toxicity profile. Interestingly, while albumin levels fit within the donor diversity of PHHs, the low levels of urea secretions by HepaRG-MPCCs could be indicative of an incomplete set of nitrogen metabolism pathways. Even so, functional levels of HepaRG-CCs were ~10% of HepaRG-MPCCs suggesting that the MPCC platform is improving hepatic functions more than in pure cultures. Furthermore, the induction of CYP3A4 via omeprazole was displayed in HepaRG-MPCCs, but not HepaRG-CCs, as has previously been shown in PHHs.[54,188]

To demonstrate the utility of HepaRG-MPCCs in the early stages of drug development, we chose to screen a compound library of 47 compounds that have been previously tested in sandwich-

cultured PHHs using HIAT[38] and PHH-MPCCs[58]. We selected drug doses up to $100 \times C_{max}$ to parallel those earlier studies, because the liver has variable drug concentrations, and because drug concentrations in blood can vary from individual to individual due to polymorphisms in drug metabolizing enzymes and transporters. Drugs tested here represent many different classes and mechanisms of action, and can cause hepatic injury by generating toxic metabolites that deplete glutathione and bind macromolecules (i.e. acetaminophen), dissipating mitochondrial membrane potential (i.e. troglitazone), accumulating within mitochondria (i.e. amiodarone), inducing steatosis (i.e. amiodarone), and inhibiting transporters (i.e. clozapine).[33,34] Furthermore, consistent with other studies in PHHs, other cell lines, and induced pluripotent stem cell-derived human hepatocyte-like cells (iPSC-HHs)[38,58,135,136,161], we found that some idiosyncratic toxins (i.e. troglitazone) could be properly classified using cellular stress markers in HepaRG-MPCCs, possibly because such hepatic stress is an early step in the cascade of processes that cause overt liver injury in some patients with one or more co-varying factors such as genetics, disease, and concurrent medications (in contrast with adaptation and recovery in others).

The sensitivity for drug toxicity detection in HepaRG-MPCCs was 54% versus 70% in PHH-MPCCs and ~35% with HIAT. Eight compounds (acetazolamide, dapsone, imipramine HCl, isoniazid, maleic acid, nortriptyline HCl, pyrazinamide, tamoxifen) were correctly identified as toxic by PHH-MPCCs, but not HepaRG-MPCCs. However, captopril was detected correctly as toxic in HepaRG-MPCCs, but not in PHH-MPCCs. All 13 TP compounds were correctly identified as hepatotoxins. Albumin secretions correctly classified all 13 compounds, while ATP activity failed to identify mebendazole, phenacetin, and trazodone HCl as toxins. From the 24 FN compounds, seven were detected as toxic in HepaRG-MPCCs. Albumin secretion was the more sensitive endpoint (all seven compounds) compared to ATP (only ciprofloxacin HCl and

hydroxyurea). Furthermore, the TC_{50} for all hepatotoxins correctly identified was lower when calculated with albumin secretions compared with ATP activity. This observation concurs with prior studies that have found albumin secretions (liver-specific marker) to be more sensitive than ATP (general viability marker) for detecting drug-induced liver injury *in vitro*.[58,161] Moreover, as albumin can be measured via analysis of culture supernatants, a time series of drug toxicity responses can be collected with a single set of cultures. When the 20 compounds that were correctly identified as toxic in HepaRG-MPCCs were also tested in HepaRG-CCs, three (captopril, clomipramine, cyproterone acetate) failed to show toxicity, leading to a 15% reduction in sensitivity. Thus, the HepaRG-MPCC platform improved the sensitivity for drug toxicity detection in HepaRG cells over conventional monolayers.

Even though HepaRG-MPCCs improved the sensitivity of drug toxicity detection over conventional cultures of PHHs, they failed to pick up ~45% of the liver toxins tested. Such false negatives could be a result of interactions between hepatocytes and liver stroma (i.e. endothelia, Kupffer macrophages) or the adaptive immune system, the cancerous background of HepaRG cells, extra-hepatic events, and genetic polymorphisms observed in the human population.[34,137] Nonetheless, HepaRG-MPCCs and the MPCC platform in general are modular in that interactions between hepatocytes from multiple sources and stromal cells of interest can be studied without significant changes to the homotypic interactions between HepaRG cells on the micropatterned collagen islands.

The cell source for *in vitro* platforms to detect drug toxicity will continue to be a major criterion, and we believe there is not a single cell source ideal for all stages of the drug development pipeline.[164] PHHs continue to be the 'gold standard' for *in vitro* screening as they maintain a full repertoire of drug metabolizing enzymes and transporters. PHH-MPCCs yielded a 70% sensitivity

when screened with the same 47 compounds used here.[58] Recently, we have demonstrated the utility of iPSC-HHs in the MPCC format for drug screening, and showed sensitivity in between that of PHH-MPCCs and HepaRG-MPCCs.[161] While this cell source can address the donor-donor diversity concerns not possible with PHHs or HepaRG cells, the process for generating iPSC-HHs has not been fully optimized and standardized across laboratories. Thus, HepaRG cells will likely remain a viable cell source in the early stages of drug development, where culture platforms need to have high throughput, low costs, and rapid turnaround times. Despite the lower sensitivity compared to PHH-MPCCs, HepaRG-MPCCs show an improved sensitivity with undiminished specificity compared with conventional monolayers as demonstrated both here and in previous literature.[37,173]

High-throughput screening necessary early in the drug development pipeline is hindered by 3D culture due to limited *in situ* cell observation via conventional microscopy and nutrient transport limitations. Even so, spheroid cultures of HepaRG cells have shown superior toxicity predictions to monolayer cultures[170], and spheroid co-cultures of HepaRG cells and hepatic stellate cells have been treated with methotrexate, thioacetamide, and allyl alcohol to introduce fibrosis[189,190]. Continuous medium exchange via flow can mitigate the nutrient transport limitations seen with 3D cultures; however, flow circuits in each well generally introduce difficulties in liquid handling.[141] Thus, monolayers in a static format are widely favored in industrial settings[142], not only for these reasons, but when engineered with controlled homotypic and heterotypic interactions, monolayers yield some of the highest functional levels, longevity, and accurate prediction of clinical outcomes reported to date[54,55,58,143]. MPCCs combine such homotypic and heterotypic interactions in a monolayer platform amenable to high content

imaging[53], which has proven useful for understanding effects of drugs on key organelles implicated in DILI.[38,144]

In conclusion, HepaRG cells in the MPCC platform display high levels of hepatic functions for 4 weeks *in vitro*. This longevity enabled long-term drug toxicity screening which yielded sensitivity and specificity superior to conventional confluent monolayers of HepaRG cells. As additional hepatic stromal cell types (i.e. Kupffer macrophages, stellate cells) are co-cultured with HepaRG cells, we anticipate that HepaRG-MPCCs could be used to better understand hepatic diseases (i.e. hepatitis B/C) and improve toxicity predictions *in vitro*.

CHAPTER 5 - Toxicogenomic Analyses[5]

Global gene expression profiling is useful for elucidating a drug's mechanism of action (MOA) on the liver; however, such profiling in rats is not very sensitive for predicting human drug-induced liver injury, while de-differentiated monolayers of primary human hepatocytes (PHHs) do not permit chronic drug treatment. In contrast, micropatterned co-cultures (MPCCs) containing PHH colonies and 3T3-J2 fibroblasts maintain a stable liver phenotype for 4-6 weeks. Here, we used MPCCs to test the hypothesis that global gene expression patterns in stable PHHs can be used to distinguish clinical hepatotoxic drugs from their non-liver-toxic analogs and understand the MOA prior to the onset of overt hepatotoxicity. We found that MPCCs treated with the clinical hepatotoxic/non-liver-toxic pair troglitazone/rosiglitazone at each drug's reported and non-toxic C_{max} (maximum concentration in human plasma) for 1, 7, and 14 days displayed a total of 12, 269, and 628 differentially expressed genes, respectively, relative to the vehicle-treated control. Troglitazone modulated >75% of transcripts across pathways such as fatty acid and drug metabolism, oxidative stress, inflammatory response, and complement/coagulation cascades. Escalating rosiglitazone's dose to that of troglitazone's C_{max} increased modulated transcripts relative to the lower dose; however, over half the identified transcripts were still exclusively modulated by troglitazone. Lastly, other hepatotoxins (nefazodone, ibufenac, and tolcapone) also induced a greater number of differentially expressed genes in MPCCs than their non-liver-toxic analogs (buspirone, ibuprofen, and entacapone) following 7 days of treatment. In conclusion,

MPCCs allow evaluation of time- and dose-dependent gene expression patterns in PHHs treated chronically with analog drugs.

5.1 Introduction and Background

Prediction of drug-induced liver injury (DILI) in humans is critically important during preclinical drug testing since DILI remains a leading cause of drug attrition in the marketplace.[31] However, animals are less than 50% predictive of human DILI[44], potentially due to significant species-specific differences in drug metabolism pathways.[145] Therefore, several *in vitro* models of the human liver have been developed for investigating DILI.[191] While cancerous and immortalized cell lines as well as precision-cut liver slices are available for incorporating into various culture platforms, primary human hepatocytes (PHHs) are considered to be the 'gold standard' for *in vitro* drug screening since they are relatively simple to use in medium-to-high throughput culture formats and contain the full complement of enzymes/co-factors required for drug metabolism.[142]

In contrast to pure PHH monolayers that display a rapid decline in phenotypic functions[191], co-culture of PHHs with both liver- and non-liver-derived non-parenchymal cells (NPCs) can transiently stabilize major liver functions.[127] Further exercising precise control over homotypic interactions between PHHs and their heterotypic interactions with 3T3-J2 murine embryonic fibroblasts can enhance the PHH phenotype and stabilize it for 4-6 weeks as compared to low levels of functions and a premature functional decline in randomly-distributed co-cultures of the same two cell types.[54] This so-called 'micropatterned co-culture' (MPCC) platform has also been shown to induce high levels of cytochrome P450 (CYP450) and Phase II conjugation enzyme activities for 4+ weeks in cryopreserved PHHs from multiple donors, which enables on-demand drug screening.[56] Such long-term functional stability of MPCCs allows for repeat treatment with

drugs, which has proven useful for improving the sensitivity of DILI detection over acute treatment in conventional PHH monolayers.[58] In particular, when treated with 54 clinical hepatotoxins and 10 non-liver-toxins for up to 9 days, human MPCCs were found to have ~78% sensitivity and 90% specificity when measuring ATP and glutathione levels in cell lysates, and albumin secretion and urea synthesis in culture supernatants. Such sensitivity in MPCCs for DILI detection was a ~2-fold improvement over the treatment of collagen/Matrigel™ sandwiched PHH cultures with the same set of drugs for 24 hours.[38] However, the use of a limited number of functional endpoints in the aforementioned studies did not provide detailed mechanistic insights into diverse pathways of the liver that are affected by the hepatotoxins relative to their non-toxic structural analogs. However, the doses tested in both MPCCs and sandwich-cultured PHHs ranged from $1 \times C_{max}$ to $100 \times C_{max}$ for each drug, where C_{max} is the reported maximal drug concentration in human plasma. Xu *et al.* justified the use of doses up to $100 \times C_{max}$ due to inter-individual differences in drug concentrations.[38] However, while a dose range up to $100 \times C_{max}$ has proven effective for binning compounds into toxic and non-toxic categories for an early drug screen, it remains unclear whether such concentrations are achieved for the tested compounds within the livers of patients in the clinic. Therefore, it is desirable to dose drugs closer to their anticipated/predicted C_{max} values in order to better model clinical scenarios.

Thiazolidinediones are a relatively new class of drugs designed to treat Type II diabetes mellitus by reducing free fatty acids in plasma, improving glucose transportation in muscle, and reducing insulin levels through ligating the peroxisome proliferator-activated receptor gamma (PPARγ).[192] The structural analogs troglitazone, rosiglitazone, and pioglitazone all belong to the thiazolidinedione class of drugs and have different relative hepatotoxicity, with troglitazone being the most toxic.[193] While the mechanism of toxicity is not fully elucidated, it is theorized that

troglitazone causes formation of toxic metabolites, mitochondrial dysfunction, oxidative stress, and inhibition of bile salt transporters.[194]

In contrast to a limited number of functional endpoints, global gene expression profiling has proven useful to identify the mechanism of action of hepatotoxins.[195] One goal of such a toxicogenomic (TGx) analysis is to identify genes that are candidate biomarkers of adverse effects of drugs, which could be modulated prior to the onset of overt cellular toxicity, as is the case for the majority of patients who are treated with approved drugs and do not experience severe DILI. However, TGx studies in rats have suffered from a lack of sensitivity for predicting human DILI[36,196], while such studies in conventional PHH cultures have been restricted to short-term (days) treatment with high drug doses due to a decline in PHH gene expression levels and functions.[197–199] Such short-term treatment of PHH cultures with hepatotoxic/non-liver-toxic drug analogs may not fully capture the diverse pathways that are differentially affected when PHHs are treated repeatedly over several weeks. We set out to test this hypothesis by using MPCCs. In particular, MPCCs were treated for 24 hours, 7 days, and 14 days with dimethyl sulfoxide (DMSO), troglitazone (hepatotoxin), or rosiglitazone, the non-liver-toxic structural analog of troglitazone, at the drugs' respective C_{max}, the maximum drug concentration reported in human plasma. Functions (WST-1, albumin secretion, urea synthesis, and CYP3A4 activity) and global gene expression profiles (via Affymetrix whole genome human microarrays) in MPCCs were assessed at each time-point to determine the effects of each drug relative to the DMSO control. Next, we evaluated global gene expression profiles in MPCCs treated for 7 days with troglitazone and rosiglitazone at the same concentration to determine drug-specific versus concentration-specific effects. Finally, MPCCs were treated for 7 days with three additional pairs of clinical hepatotoxins and non-liver-toxins (nefazodone/buspirone, ibufenac/ibuprofen, and

tolcapone/entacapone) and gene expression changes were compared to those obtained in MPCCs treated with troglitazone/rosiglitazone.

5.2 Materials and Methods

5.2.1 Fibroblast Culture

3T3-J2 murine embryonic fibroblasts were maintained in high glucose Dulbecco's modified Eagle's medium (DMEM; Corning Life Sciences, Tewksbury, MA) with 10% (v/v) bovine serum (Thermo Fisher Scientific, Waltham, MA) and 1% (v/v) penicillin-streptomycin (Corning Life Sciences) solution. The fibroblasts were passaged no more than 12 times prior to use in co-cultures with hepatocytes as described below.

5.2.2 Establishment of Micropatterned Co-Cultures (MPCCs)

Cryopreserved primary human hepatocytes (PHHs) were purchased from vendors permitted to sell products derived from human organs procured in the United States by federally designated organ procurement organizations (BioreclamationIVT, Baltimore, MD, and Triangle Research Labs, Durham, NC). The PHH donors used in this study included JNB (19-year-old Caucasian female with a history of lupus who died of intracranial hemorrhage secondary to stroke) from BioreclamationIVT, and HUM4043 (6-month-old Caucasian female who died of anoxia/blunt injury) and HUM4055A (54-year-old Caucasian female who died of stroke) from Triangle Research Labs. PHHs were thawed, counted, and assessed for viability per the manufacturers' instructions. MPCCs were created as previously described.[56] Briefly, adsorbed rat tail collagen-I (Corning Life Sciences) was lithographically patterned in each well of a 24-well plate to create 500 μm diameter circular domains spaced 1200 μm apart, center-to-center. PHHs selectively attached to the collagen domains leaving ~25,000 attached PHHs on ~90 collagen-coated islands within each well of a 24-well plate. 3T3-J2 murine embryonic fibroblasts were

seeded 18 to 24 hours later at ~90,000 cells per well in a 24-well plate to create MPCCs. Hepatocyte culture medium containing a high glucose DMEM (Corning Life Sciences) base was replaced on MPCCs every 2 days (300 µL/well for a 24-well plate). Other components of the culture medium have been described previously.[154] The morphology of MPCCs was monitored using an EVOS®FL cell imaging system (Thermo Fisher Scientific) with phase contrast objectives.

5.2.3 Drug Dosing

Troglitazone, rosiglitazone, ibufenac, ibuprofen, tolcapone, and entacapone were purchased from Cayman Chemical (Ann Arbor, MI), while nefazodone and buspirone were obtained from Sigma-Aldrich (St. Louis, MO). All drugs were dissolved in 100% dimethyl sulfoxide (DMSO; Corning Life Sciences). The reported C_{max} values for the drugs were obtained from published studies.[38,200] After allowing the MPCCs to functionally stabilize for ~1 week, the cultures were treated in serum-free hepatocyte culture medium for 24 hours, 7 days, or 14 days with DMSO at 0.1% (v/v), troglitazone at its reported C_{max} (2.82 µg/mL), or rosiglitazone at its C_{max} (0.373 µg/mL). Additional MPCCs were treated for 7 days with rosiglitazone at troglitazone's C_{max} (2.82 µg/mL), nefazodone at its reported C_{max} (434.55 ng/mL), buspirone at its C_{max} (2.11 ng/mL), ibufenac at its C_{max} (19.23 µg/mL), ibuprofen at its C_{max} (31.87 µg/mL), tolcapone at its C_{max} (4.51 µg/mL), or entacapone at its C_{max} (1.91 µg/mL). Fresh drug was administered with media changes every other day for the duration of the study. The DMSO concentration that MPCCs were exposed to was kept at 0.1% (v/v) relative to the culture medium for all conditions tested since increasing levels of DMSO in culture medium is known to cause a downregulation of CYP3A4 in PHHs,[132] which may alter the toxicity profiles of drugs.

5.2.4 Biochemical Assays

Urea concentration in collected cell culture supernatants was assayed using a colorimetric endpoint assay utilizing diacetyl monoxime with acid and heat (Stanbio Labs, Boerne, TX).[54] CYP3A4 enzyme activity was measured by first incubating cultures with substrate (luciferin-IPA from Promega Life Sciences, Madison, WI) for 1 hour at 37°C and then detecting the luminescence of produced metabolite (luciferin) on a Synergy H1 multi-mode reader (Biotek, Winooski, VT) according to manufacturer's protocols. Cell viability was assessed with the WST-1 kit from Roche Life Science (Indianapolis, IN). CYP3A4, urea, and WST-1 assays were conducted on the same wells.

5.2.5 Gene Expression Assays

Total RNA was isolated and purified using the RNeasy mini kit (Qiagen, Valencia, CA) and genomic DNA was digested using DNase-I (New England Biolabs, Ipswich, MA). RNA samples were then sent to the Whitehead Institute (Cambridge, MA) or the University of Illinois at Chicago Core Genomics Facility where they were inspected for quality, hybridized to Affymetrix GeneChip™ Human Genome U133 Plus 2.0 microarrays, and quantified using previously published protocols.[54] Control RNA samples from pure 3T3-J2 cultures treated for 7 days with either DMSO or troglitazone (2.82 µg/mL) were also hybridized to the U133 Plus 2.0 human microarrays in order to determine which transcripts were called 'present' due to the mouse RNA and would thus constitute noise in the analysis. All Affymetrix microarray data utilized in this study have been submitted to the Gene Expression Omnibus (GEO accession: GSE85180).

For qPCR, ~10 µL of purified RNA was reverse transcribed into complementary DNA (cDNA) using the high capacity cDNA reverse transcription kit (Thermo Fisher Scientific). Then, 250 ng of cDNA was added to each qPCR reaction along with pre-designed Solaris™ (GE

Healthcare Dharmacon, Lafayette, CO) human-specific primer/probe sets according to manufacturer's protocols. The primer/probe sets were selected to be human-specific without cross-reactivity to 3T3-J2 mouse DNA and included: stearoyl-CoA desaturase (*SCD*), acyl-CoA synthetase medium chain family member 3 (*ACSM3*), elongation of very long chain fatty acids 2 (*ELOVL2*), cluster of differentiation 36 (*CD36*), mannose binding lectin 2 (*MBL2*), FBJ murine osteosarcoma viral oncogene homolog (*FOS*), chromosome 10 open reading frame 10 (*C10orf10*), and high mobility group 20B (*HMG20B*). Some of these transcripts showed greater than 2-fold upregulation (*SCD*, *ACSM3*, *ELOVL2*, *CD36*, and *MBL2*) or less than 2-fold change (*FOS*, *C10orf10*, and *HMG20B*) in troglitazone-treated MPCCs relative to DMSO controls from the Affymetrix microarray data and were thus used a validation set in another donor of PHHs (HUM4043). Hepatic gene expression was normalized to the housekeeping gene, glyceraldehyde 3-phosphate dehydrogenase (*GAPDH*). qPCR was performed on a MasterCycler RealPlex-2 (Eppendorf, Hamburg, Germany).

5.2.6 Data Analysis

Raw intensity values on the Affymetrix microarrays were normalized, modeled, and compared using the DNA Chip (dChip) Analyzer software.[201] Data from all chips were normalized to MPCCs treated with DMSO for 7 days (invariant set normalization). Probe sets marked as 'present' on the 3T3-J2-only control chip were omitted from further analysis. Differentially expressed genes upon treatment of MPCCs with troglitazone or rosiglitazone at each time-point were defined as those transcripts with a |fold change| > 2.0 and |difference in expression| > 100 in drug-treated MPCCs relative to DMSO-only controls. For the other drug pairs for which another PHH donor was used in MPCCs, a |fold change| > 1.5 and |difference in expression| > 50 were used as filtering criteria to ensure a sufficient number of differentially expressed genes for analysis

140

as compared to the aforementioned selection criteria for troglitazone and rosiglitazone. Then, the Database for Annotation, Visualization, and Integrated Discovery (DAVID) was used to identify Kyoto Encyclopedia of Genes and Genomes (KEGG) pathways and Gene Ontology (GO) processes from the differentially expressed gene sets.[202] Data from biochemical and qPCR assays were analyzed and graphed using Microsoft Excel and GraphPad Prism (La Jolla, CA).

5.3 Results

5.3.1 Treatment of MPCCs for up to 2 Weeks with Troglitazone or Rosiglitazone

5.3.1.1 PHH Morphology and Functions

Overall viability in MPCCs (JNB donor), as assessed by the cleavage of WST-1 to formazan by cellular mitochondrial dehydrogenases (not specific to hepatocytes), was not significantly altered over 2 weeks of treatment with troglitazone or rosiglitazone at their respective C_{max} values as compared to treatment with 0.1% (v/v) DMSO (Figure 5.1A). Furthermore, hepato-specific urea (Figure 5.1B) secretion was also not significantly affected in drug treated MPCCs relative to MPCCs treated with DMSO over 2 weeks. On the other hand, both rosiglitazone and troglitazone induced CYP3A4 activity in MPCCs by ~2.5-fold and ~9-fold of DMSO controls, respectively, following 1 week of treatment (Figure 5.1C). Following 2 weeks of treatment, the fold induction had increased to ~17.5-fold and ~50-fold for rosiglitazone and troglitazone, respectively. Between 1 and 2 weeks of treatment, MPCCs created with the JNB donor displayed a downregulation of the aforementioned markers even in DMSO-treated controls, which is likely due to the use of a serum-free culture medium that prevents proper fibroblast growth that is necessary to support the phenotype of susceptible PHH donors. However, we used a serum-free drug incubation medium to be consistent with the *in vitro* drug treatment protocols routinely employed with hepatocyte culture[38,58] towards assessing a drug's effects on cells in the absence of

141

drug binding to bovine proteins at 10% (v/v) that do not mimic the protein concentration in human plasma. Lastly, the morphology of PHHs within MPCCs was not significantly affected upon drug treatment for 1 week (Figure 5.1D-F) as compared to DMSO-treated controls. In particular, PHHs retained prototypical polygonal shape, contained distinct nuclei/nucleoli, and formed visible bile canaliculi under phase contrast microscopy across all treatments. We also confirmed in another PHH donor (HUM4055A) that neither hepatic function, as assessed by albumin secretion (Figure 5.2A), nor morphology (Figure 5.2B) were affected in MPCCs treated with either troglitazone or rosiglitazone at their respective C_{max} for up to 2 weeks. Therefore, at their respective C_{max} doses, neither rosiglitazone nor troglitazone had adverse effects on PHH phenotype but were still able to induce CYP3A4, which suggests that the cells were able to respond appropriately to the drugs.
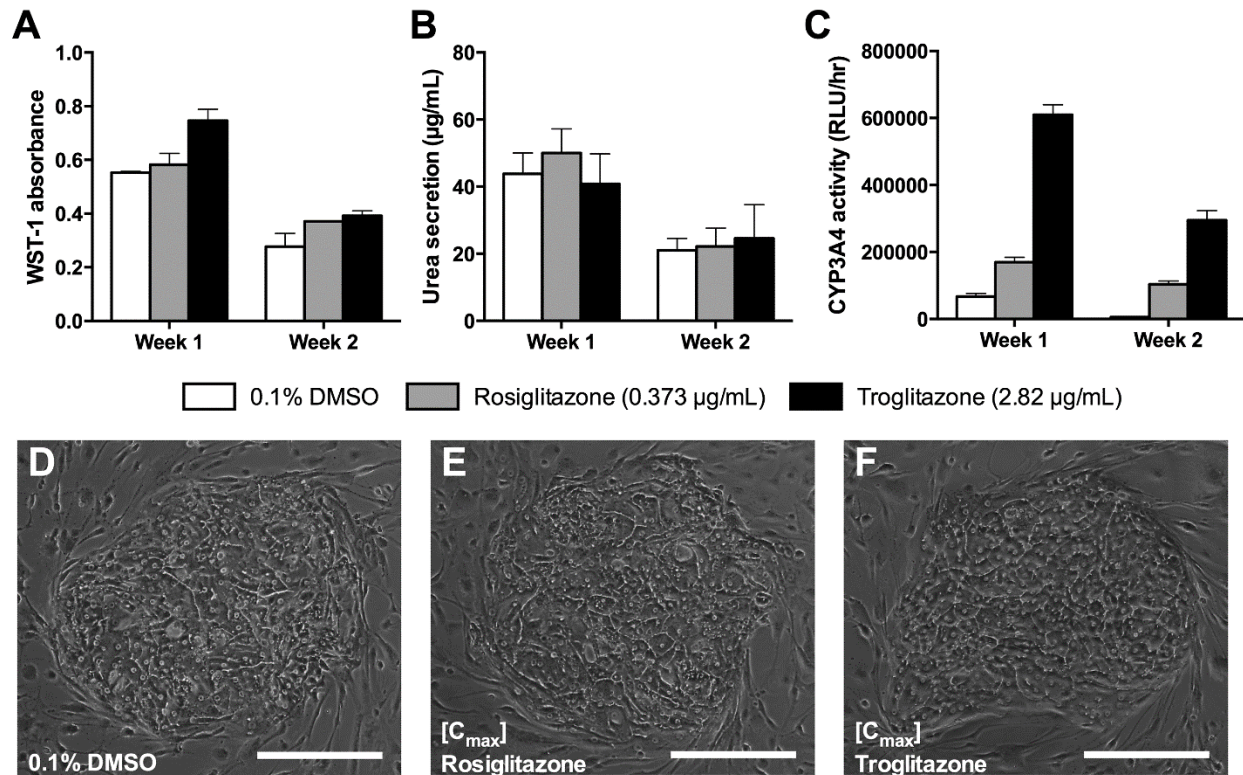
Figure 5.1: Overall viability and hepatic functions in MPCCs treated with troglitazone or rosiglitazone at their respective C$_{max}$ levels for up to 14 days. Overall culture viability as assessed with **(A)** WST-1 and **(B)** hepatic urea secretion were not significantly affected in MPCCs (JNB donor) treated for up to 2 weeks with 2.82 µg/mL troglitazone or 0.373 µg/mL rosiglitazone relative to MPCCs treated with 0.1% (v/v) DMSO. On the other hand, **(C)** CYP3A4 activity was induced by both rosiglitazone and troglitazone. All error bars represent standard deviations (n = 3). Hepatic morphology in cultures treated with **(D)** 0.1% (v/v) DMSO, **(E)** rosiglitazone at 0.373 µg/mL, or **(F)** troglitazone at 2.82 µg/mL showed no significant differences after 7 days of treatment. All scale bars = 250 µm.
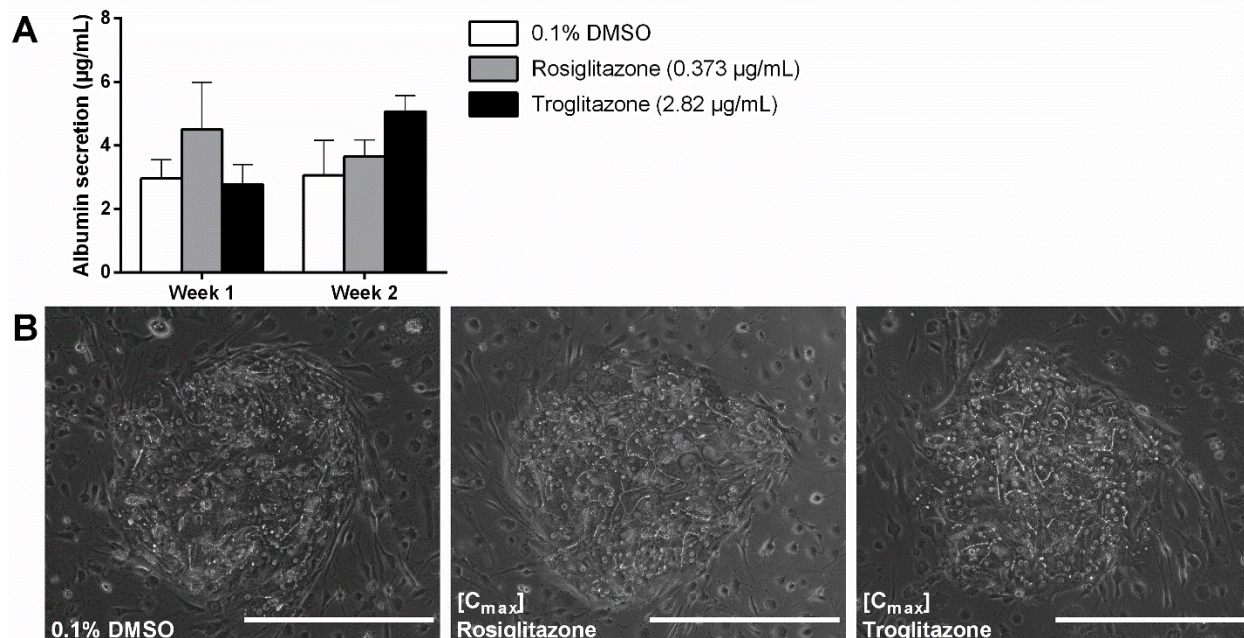
Figure 5.2: Albumin secretions in MPCCs treated with troglitazone or rosiglitazone for up to 14 days. (A) Hepatic albumin secretions (HUM4055A donor) were not significantly affected in MPCCs treated for up to 2 weeks with troglitazone (2.82 µg/mL) or rosiglitazone (0.373 µg/mL) relative to MPCCs treated with 0.1% (v/v) DMSO. All error bars represent standard deviations (n = 3). **(B)** Hepatic morphology was not significantly affected in cultures treated for 14 days as described in panel 'A'. All scale bars = 400 µm.

5.3.1.2 Time-Dependent Gene Expression Analysis

RNA from pure 3T3-J2s treated with 0.1% (v/v) DMSO for 7 days was used to determine *murine* transcripts that were called 'present' on a human Affymetrix GeneChip and thus excluded from further analysis (~18% of the total MPCC transcripts). Next, we identified 'differentially expressed genes' as those transcripts with a |fold change| > 2.0 and |difference in expression| > 100 in drug-treated MPCCs relative to DMSO-only controls. All of differentially expressed genes in pure 3T3-J2 cultures after 7 days of treatment with troglitazone at its C_{max} (2.82 µg/mL) relative to DMSO-treated 3T3-J2 cultures did not overlap with the differentially expressed genes in troglitazone-treated MPCCs relative to DMSO-treated MPCCs. Thus, the gene expression analysis described below in MPCCs is largely hepatospecific.

After 24 hours of treatment, troglitazone at its C_{max} (2.82 µg/mL) exclusively upregulated the expression of 9 genes and downregulated the expression of 1 gene, while rosiglitazone at its C_{max} (0.373 µg/mL) exclusively upregulated the expression of 1 gene as compared to DMSO-treated controls at 24 hours (Figure 5.3A). Fatty acid binding protein 4 (*FABP4*) was the only transcript upregulated by both troglitazone and rosiglitazone after 24 hours of treatment. After 7 days of treatment, troglitazone exclusively upregulated the expression of 118 genes and downregulated the expression of 143 genes, while rosiglitazone exclusively upregulated the expression of 2 genes total as compared to DMSO-treated controls (Figure 5.3B). Additionally, troglitazone and rosiglitazone both upregulated the expression of 4 genes (phosphoglycerate dehydrogenase [*PHGDH*], fatty acid binding protein 4 [*FABP4*], mannose-binding lectin 2 [*MBL2*], and cluster of differentiation 36 [*CD36*]), and downregulated the expression of 2 genes (hepcidin antimicrobial peptide [*HAMP*] and cysteine-rich C-terminal 1 [*CRCT1*]). Troglitazone induced higher fold changes for all transcripts affected by both drugs (Table 5.1). Lastly, following

14 days of treatment, troglitazone exclusively upregulated the expression of 256 genes and downregulated the expression of 227 genes, while rosiglitazone exclusively upregulated the expression of 13 genes and downregulated the expression of 5 genes as compared to DMSO-treated controls (Figure 5.3C). Moreover, both troglitazone and rosiglitazone upregulated the expression of 106 genes and downregulated the expression of 21 genes. Troglitazone induced a higher fold change for 93% of the overlapping transcripts at day 14 of treatment (Table 5.2).

The aforementioned differentially expressed genes were classified further based on their corresponding Kyoto Encyclopedia of Genes and Genomes (KEGG) pathways, which are a collection of pathways for molecular interactions and reaction networks. After 24 hours of treatment, troglitazone modulated the expression of genes classified in the drug metabolism, linoleic acid metabolism, and retinol metabolism KEGG pathways (Figure 5.4A-B, Table 5.3). Several of these genes corresponded to CYP450 isoforms (2B6, 3A4, 3A7, or 3A43). After 7 days of treatment, troglitazone modulated the expression of genes associated with the primary bile acid biosynthesis, steroid hormone biosynthesis, drug metabolism, linoleic acid metabolism, retinol metabolism, and PPAR (peroxisome proliferator-activated receptor) signaling KEGG pathways (Figure 5.4A-B, Table 5.4). Most of these genes coded for CYP450 enzymes and transporter proteins. Two genes (cluster of differentiation 36 [*CD36*] and fatty acid binding protein 4 [*FABP4*]) were identified in the PPAR signaling KEGG pathway with both troglitazone and rosiglitazone. Lastly, after 14 days of treatment, troglitazone continued to modulate the expression of genes from all the KEGG pathways identified at 7 days of treatment as well as additional pathways for glycolysis/gluconeogenesis, arachidonic acid metabolism, and amino acid metabolism (Figure 5.4A-B, Table 5.5). The differentially expressed genes in MPCCs treated with troglitazone or rosiglitazone at their respective C_{max} concentrations were also classified by the

146

Gene Ontology (GO) processes, which are annotations of genes and gene products (Figure 5.4C-D). Some of the transcripts were clustered in the 'innate immune response', 'inflammatory response', and 'response to wounding' GO processes. Typically, troglitazone modulated a greater number of transcripts in the GO processes as compared to the number of transcripts modulated by both drugs.
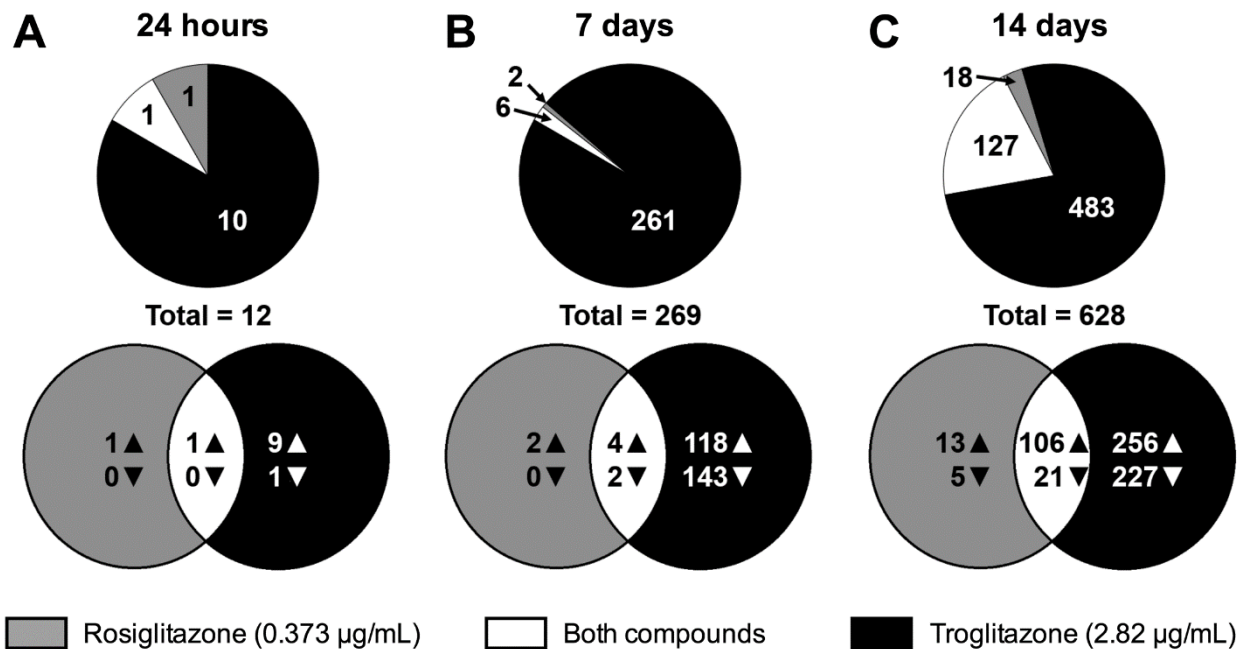
Figure 5.3: Time-dependent global gene expression changes in MPCCs treated with troglitazone or rosiglitazone at their respective C$_{max}$ levels for up to 14 days. The number of genes upregulated or downregulated (|fold change| > 2.0 and |difference in expression| > 100) in MPCCs (JNB donor) by troglitazone (2.82 µg/mL) or rosiglitazone (0.373 µg/mL) or both drugs relative to DMSO after treatment for **(A)** 24 hours, **(B)** 7 days, and **(C)** 14 days.
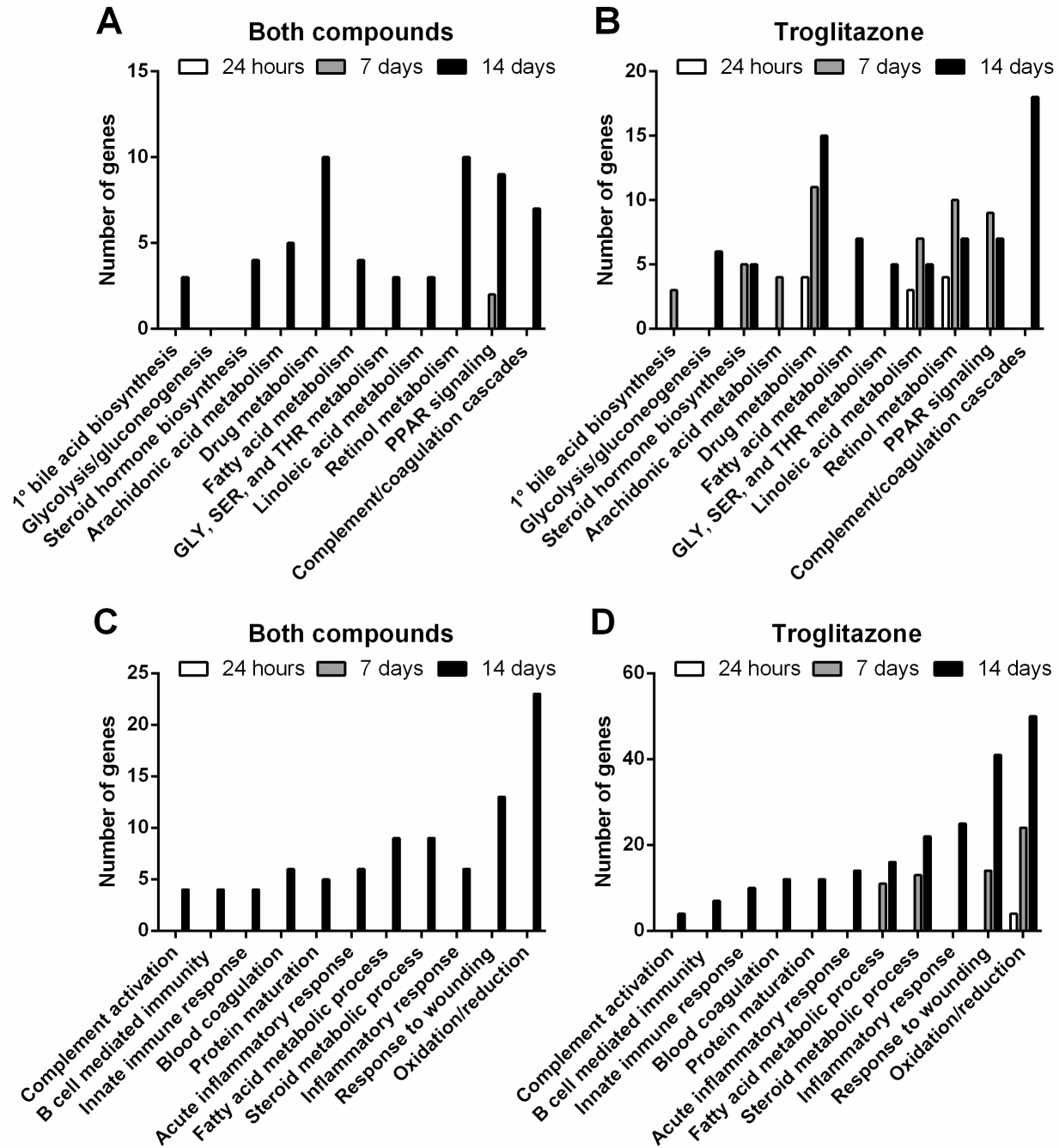
Figure 5.4: Pathway and gene ontology (GO) process analysis for differentially expressed genes in MPCCs treated with troglitazone or rosiglitazone at their respective C_{max} levels for up to 14 days. **(A)** The number of differentially expressed genes across KEGG pathways that are modulated in MPCCs (JNB donor) over time by both troglitazone (2.82 μg/mL) and rosiglitazone (0.373 μg/mL) relative to DMSO. **(B)** Similar pathway analysis as in panel 'A' except data in MPCCs treated with only troglitazone is shown. **(C)** The number of differentially expressed genes across GO processes that are modulated in MPCCs over time by both troglitazone and rosiglitazone relative to DMSO. **(D)** Similar process analysis as in panel 'C' except data in MPCCs treated with only troglitazone is shown.

Table 5.1: Gene expression fold changes in MPCCs (JNB donor) treated for 7 days with troglitazone or rosiglitazone at their respective C$_{max}$ levels relative to DMSO-treated controls

Dchip probe set	Gene symbol	Gene name	EntrezGene	Fold change 0.373 µg/mL rosiglitazone	Fold change 2.82 µg/mL troglitazone
209555_s_at	CD36	CD36 molecule	948	2.58	3.70
220620_at	CRCT1	Cysteine-rich C-terminal 1	54544	-2.58	-21.30
203980_at	FABP4	Fatty acid binding protein 4, adipocyte	2167	2.70	3.16
220491_at	HAMP	Hepcidin antimicrobial peptide	57817	-2.50	-47.33
207256_at	MBL2	Mannose-binding lectin (protein C) 2, soluble (opsonic defect)	4153	2.30	5.59
201397_at	PHGDH	Phosphoglycerate dehydrogenase	26227	2.98	5.54

Note. The transcripts shown were differentially expressed by *both* drugs.

Table 5.2: Gene expression fold changes in MPCCs (JNB donor) treated for 14 days with troglitazone or rosiglitazone at their respective C$_{max}$ levels relative to DMSO-treated controls

Dchip probe set	Gene symbol	Gene name	EntrezGene	Fold change 0.373 µg/mL rosiglitazone	Fold change 2.82 µg/mL troglitazone
209994_s_at	ABCB1	ATP-binding cassette, sub-family B (MDR/TAP), member 1	5243, 5244	2.36	5.07
207819_s_at	ABCB4	ATP-binding cassette, sub-family B (MDR/TAP), member 4	5244	5.24	15.10
221928_at	ACACB	Acetyl-coenzyme A carboxylase beta	32	2.67	4.34
43427_at	ACACB	Acetyl-coenzyme A carboxylase beta	32	2.41	3.94
49452_at	ACACB	Acetyl-coenzyme A carboxylase beta	32	2.36	3.92
238160_at	ACOT12	Acyl-CoA thioesterase 12	134526	2.66	4.11
205364_at	ACOX2	Acyl-coenzyme A oxidase 2, branched chain	8309	3.77	7.05
207820_at	ADH1A	Alcohol dehydrogenase 1A (class I), alpha polypeptide	124	3.96	5.46
206262_at	ADH1C	Alcohol dehydrogenase 1C (class I), gamma polypeptide	126	3.54	7.09
206840_at	AFM	Afamin	173	3.48	5.53
210326_at	AGXT	Alanine-glyoxylate aminotransferase	189	3.59	6.53
210327_s_at	AGXT	Alanine-glyoxylate aminotransferase	189	3.43	5.99
210517_s_at	AKAP12	A kinase (PRKA) anchor protein 12	9590	-2.27	-4.65
227529_s_at	AKAP12	A kinase (PRKA) anchor protein 12	9590	-2.59	-5.19
227530_at	AKAP12	A kinase (PRKA) anchor protein 12	9590	-2.16	-3.69
218487_at	ALAD	Aminolevulinate, delta-, dehydratase	210	2.20	3.65
220148_at	ALDH8A1	Aldehyde dehydrogenase 8 family, member A1	64577	2.80	4.88
205141_at	ANG	Angiogenin, ribonuclease, RNase A family, 5	283	2.58	3.60
203747_at	AQP3	Aquaporin 3 (Gill blood group)	360	-2.58	-3.98
39249_at	AQP3	Aquaporin 3 (Gill blood group)	360	-2.16	-3.45
205363_at	BBOX1	Butyrobetaine (gamma), 2-oxoglutarate dioxygenase (gamma-butyrobetaine hydroxylase) 1	8424	2.23	2.41

Dchip probe set	Gene symbol	Gene name	EntrezGene	Fold change 0.373 µg/mL rosiglitazone	Fold change 2.82 µg/mL troglitazone
210538_s_at	BIRC3	Baculoviral IAP repeat-containing 3	330	-2.70	-10.49
237765_at	C14orf68	Chromosome 14 open reading frame 68	283600	4.18	9.42
230677_at	C14orf73	Chromosome 14 open reading frame 73	91828	2.44	4.12
202953_at	C1QB	Complement component 1, q subcomponent, B chain	713	3.76	3.70
205500_at	C5	Complement component 5	727	2.46	3.88
235377_at	C6orf142	Chromosome 6 open reading frame 142	90523	2.57	2.64
206305_s_at	C8A	Complement component 8, alpha polypeptide	731	2.69	3.70
210728_s_at	CALCA	Calcitonin-related polypeptide alpha	796	-2.83	-14.02
203645_s_at	CD163	CD163 molecule	9332	-2.79	-7.84
215049_x_at	CD163	CD163 molecule	9332	-2.72	-7.62
209555_s_at	CD36	CD36 molecule	948	4.03	4.79
204661_at	CD52	CD52 molecule	1043	11.82	8.81
34210_at	CD52	CD52 molecule	1043	7.37	7.41
229468_at	CDK3	Cyclin-dependent kinase 3	1018	3.60	3.38
206910_x_at	CFHR2	Complement factor H-related 2	3080	2.58	4.78
226350_at	CHML	Choroideremia-like (Rab escort protein 2)	1122	-2.84	-6.38
205489_at	CRYM	Crystallin, mu	1428	2.37	3.52
204971_at	CSTA	Cystatin A (stefin A)	1475	2.44	3.64
1494_f_at	CYP2A6	Cytochrome P450, family 2, subfamily A, polypeptide 6	1548	4.63	22.90
207244_x_at	CYP2A6	Cytochrome P450, family 2, subfamily A, polypeptide 6	1548, 1549	3.98	17.21
211295_x_at	CYP2A6	Cytochrome P450, family 2, subfamily A, polypeptide 6	1548	3.38	15.19
214320_x_at	CYP2A6	Cytochrome P450, family 2, subfamily A, polypeptide 6	1548	5.56	25.64
207718_x_at	CYP2A7	Cytochrome P450, family 2, subfamily A, polypeptide 7	1549	3.46	16.63
206754_s_at	CYP2B6	Cytochrome P450, family 2, subfamily B, polypeptide 6	1555, 1556	3.92	23.50
206755_at	CYP2B6	Cytochrome P450, family 2, subfamily B, polypeptide 6	1555	7.19	48.98
208147_s_at	CYP2C8	Cytochrome P450, family 2, subfamily C, polypeptide 8	1558	11.57	38.59
1553977_a_at	CYP39A1	Cytochrome P450, family 39, subfamily A, polypeptide 1	51302	3.19	6.87
220432_s_at	CYP39A1	Cytochrome P450, family 39, subfamily A, polypeptide 1	51302	3.29	6.59

152

Dchip probe set	Gene symbol	Gene name	EntrezGene	Fold change 0.373 µg/mL rosiglitazone	Fold change 2.82 µg/mL troglitazone
205998_x_at	CYP3A4	Cytochrome P450, family 3, subfamily A, polypeptide 4	1576	3.62	29.10
205999_x_at	CYP3A4	Cytochrome P450, family 3, subfamily A, polypeptide 4	1576	2.71	10.15
208367_x_at	CYP3A4	Cytochrome P450, family 3, subfamily A, polypeptide 4	1576	3.25	13.45
205939_at	CYP3A7	Cytochrome P450, family 3, subfamily A, polypeptide 7	1551	3.09	18.13
211843_x_at	CYP3A7	Cytochrome P450, family 3, subfamily A, polypeptide 7	1551	2.96	14.34
207407_x_at	CYP4A11	Cytochrome P450, family 4, subfamily A, polypeptide 11	1579	2.68	4.80
217319_x_at	CYP4A22	Cytochrome P450, family 4, subfamily A, polypeptide 22	284541	3.19	5.83
206514_s_at	CYP4F2	Cytochrome P450, family 4, subfamily F, polypeptide 2	4051, 8529	2.51	3.71
210452_x_at	CYP4F2	Cytochrome P450, family 4, subfamily F, polypeptide 2	8529	2.57	4.87
207406_at	CYP7A1	Cytochrome P450, family 7, subfamily A, polypeptide 1	1581	2.50	10.55
202894_at	EPHB4	EPH receptor B4	2050	2.89	3.96
205892_s_at	FABP1	Fatty acid binding protein 1, liver	2168	2.21	2.44
203980_at	FABP4	Fatty acid binding protein 4, adipocyte	2167	4.38	4.88
238018_at	FAM150B	Family with sequence similarity 150, member B	285016	-3.38	-4.71
209696_at	FBP1	Fructose-1,6-bisphosphatase 1	2203	2.30	3.80
203638_s_at	FGFR2	Fibroblast growth factor receptor 2	2263	9.27	16.44
223979_x_at	FTCD	Formiminotransferase cyclodeaminase	10841	2.35	3.21
213524_s_at	G0S2	G0/G1 switch 2	50486	2.51	4.53
204965_at	GC	Group-specific component (vitamin D binding protein)	2638	3.24	5.32
238518_x_at	GLYCTK	Glycerate kinase	132158	2.99	4.42
225420_at	GPAM	Glycerol-3-phosphate acyltransferase, mitochondrial	57678	5.34	28.02
225424_at	GPAM	Glycerol-3-phosphate acyltransferase, mitochondrial	57678	4.91	22.68
204607_at	HMGCS2	3-hydroxy-3-methylglutaryl-coenzyme A synthase 2 (mitochondrial)	3158	2.64	6.07
31835_at	HRG	Histidine-rich glycoprotein	3273	3.93	10.71
230431_at	Hs.131775.0			-4.02	-4.39
241114_s_at	Hs.146125.1			3.84	6.13

Dchip probe set	Gene symbol	Gene name	EntrezGene	Fold change 0.373 µg/mL rosiglitazone	Fold change 2.82 µg/mL troglitazone
242273_at	Hs.175569.0			-2.72	-2.46
237530_at	Hs.284450.0			2.96	4.13
239744_at	Hs.31444.0			3.57	2.52
230082_at	Hs.49576.0			-2.41	-3.78
205404_at	HSD11B1		3290	2.84	3.98
37512_at	HSD17B6	Hydroxysteroid (17-beta) dehydrogenase 6 homolog (mouse)	8630	2.62	4.82
210095_s_at	IGFBP3	Insulin-like growth factor binding protein 3	3486	2.33	3.76
224469_s_at	INF2	Inverted formin, FH2 and WH2 domain containing	64423	-2.24	-4.31
204987_at	ITIH2	Inter-alpha (globulin) inhibitor H2	3698	2.39	4.33
206541_at	KLKB1	Kallikrein B, plasma (Fletcher factor) 1	3818	2.66	6.17
220437_at	LOC55908	Hepatocellular carcinoma-associated gene TD26	55908	2.56	4.90
209978_s_at	LPA	Lipoprotein, Lp(a)	4018, 5340	2.75	4.92
228648_at	LRG1	Leucine-rich alpha-2-glycoprotein 1	116844	2.74	3.18
207256_at	MBL2	Mannose-binding lectin (protein C) 2, soluble (opsonic defect)	4153	8.53	7.01
218865_at	MOSC1	MOCO sulphurase C-terminal domain containing 1	64757	2.39	2.62
205614_x_at	MST1	Macrophage stimulating 1 (hepatocyte growth factor-like)	4485	2.21	2.64
219796_s_at	MUPCDH	Mucin-like protocadherin	53841	2.62	2.91
207621_s_at	PEMT	Phosphatidylethanolamine N-methyltransferase	10400	3.43	4.17
201397_at	PHGDH	Phosphoglycerate dehydrogenase	26227	2.92	6.27
222078_at	PKLR	Pyruvate kinase, liver and RBC	5313	2.38	4.36
209977_at	PLG	Plasminogen	5340	2.53	4.31
228469_at	PPID	Peptidylprolyl isomerase D	5481	2.39	3.94
222662_at	PPP1R3B	Protein phosphatase 1, regulatory (inhibitor) subunit 3B	79660	2.54	5.73
243669_s_at	PRAP1	Proline-rich acidic protein 1	118471	2.24	3.68
243614_s_at	PRODH2	Proline dehydrogenase (oxidase) 2	58510	5.70	18.94
228930_at	SCARNA15	Small Cajal body-specific RNA 15	677778	-2.54	-3.08
200831_s_at	SCD	Stearoyl-CoA desaturase (delta-9-desaturase)	6319	3.12	6.55

154

Dchip probe set	Gene symbol	Gene name	EntrezGene	Fold change 0.373 µg/mL rosiglitazone	Fold change 2.82 µg/mL troglitazone
200832_s_at	SCD	Stearoyl-CoA desaturase (delta-9-desaturase)	6319	2.45	4.03
211162_x_at	SCD	Stearoyl-CoA desaturase (delta-9-desaturase)	6319	2.63	4.93
211708_s_at	SCD	Stearoyl-CoA desaturase (delta-9-desaturase)	6319	2.66	5.05
223839_s_at	SCD	Stearoyl-CoA desaturase (delta-9-desaturase)	6319	2.36	4.32
205576_at	SERPIND1	Serpin peptidase inhibitor, clade D (heparin cofactor), member 1	3053	2.35	4.09
207298_at	SLC17A3	Solute carrier family 17 (sodium phosphate), member 3	10786	2.37	2.94
239345_at	SLC19A3	Solute carrier family 19, member 3	80704	3.33	5.26
220554_at	SLC22A7	Solute carrier family 22 (organic anion transporter), member 7	10864	3.54	5.64
221662_s_at	SLC22A7	Solute carrier family 22 (organic anion transporter), member 7	10864	2.81	4.69
231398_at	SLC22A7	Solute carrier family 22 (organic anion transporter), member 7	10864	4.17	7.05
223732_at	SLC23A1	Solute carrier family 23 (nucleobase transporters), member 1	9963	2.55	4.14
220435_at	SLC30A10	Solute carrier family 30, member 10	55532	2.24	2.39

Notes. The transcripts shown were differentially expressed by *both* drugs. Shaded rows indicate genes more highly upregulated/downregulated with 0.373 µg/mL rosiglitazone than with 2.82 µg/mL troglitazone.

Table 5.3: Genes identified in KEGG pathways that were modulated in MPCCs (JNB donor) treated for 24 hours with troglitazone or rosiglitazone at their respective C_{max} levels relative to DMSO-treated controls

KEGG pathway	Genes identified with *both* 2.82 µg/mL troglitazone and 0.373 µg/mL rosiglitazone	Genes identified with *only* 2.82 µg/mL troglitazone
Drug metabolism	—	CYP2B6, CYP3A4, CYP3A7, CYP3A43
Linoleic acid metabolism	—	CYP3A4, CYP3A7, CYP3A43
Retinol metabolism	—	CYP2B6, CYP3A4, CYP3A7, CYP3A43

Note. Abbreviation: CYP - cytochrome P450.

Table 5.4: Genes identified in KEGG pathways that were modulated in MPCCs (JNB donor) treated for 7 days with troglitazone or rosiglitazone at their respective C_{max} levels relative to DMSO-treated controls

KEGG pathway	Genes identified with *both* 2.82 µg/mL troglitazone and 0.373 µg/mL rosiglitazone	Genes identified with *only* 2.82 µg/mL troglitazone
1° bile acid biosynthesis	—	AKR1D1, CYP39A1, SLC27A5
Steroid hormone biosynthesis	—	AKR1D1, CYP3A4, CYP3A7, CYP3A43, UGT2B17, ZNF498
Drug metabolism	—	CYP2B6, CYP2C8, CYP2C9, CYP2C19, CYP3A4, CYP3A7, CYP3A43, DPYD, FMO3, UGT2B17, ZNF498
Linoleic acid metabolism	—	CYP2C8, CYP2C9, CYP2C19, CYP3A4, CYP3A7, CYP3A43, ZNF498
Retinol metabolism	—	CYP2B6, CYP2C8, CYP2C9, CYP2C19, CYP3A4, CYP3A7, CYP3A43, RDH16, UGT2B17, ZNF498
PPAR signaling	CD36, FABP4	ACSL1, ACSL4, ANGPTL4, CD36, ME1, PCK1, SCD, SLC27A2, SLC27A5

Notes. Some genes appear in both columns because different probes for the same gene were identified. Abbreviations: ACSL - acyl-CoA synthetase long-chain, AKR - aldo-keto reductase, ANGPTL - angiopoietin-like, CD - cluster of differentiation, CYP - cytochrome P450, DPYD - dihydropyrimidine dehydrogenase, FABP - fatty acid binding protein, FMO - flavin-containing monooxygenase, ME - malic enzyme, PCK - phosphoenolpyruvate carboxykinase, RDH - retinol dehydrogenase, SCD - stearoyl-CoA desaturase, SLC - solute carrier, UGT - glucuronosyltransferase, ZNF - zinc finger protein.

Table 5.5: Genes identified in KEGG pathways that were modulated in MPCCs (JNB donor) treated for 14 days with troglitazone or rosiglitazone at their respective C_max levels relative to DMSO-treated controls

KEGG pathway	Genes identified with *both* 2.82 µg/mL troglitazone and 0.373 µg/mL rosiglitazone	Genes identified with *only* 2.82 µg/mL troglitazone
1° bile acid biosynthesis	ACOX2, CYP7A1, CYP39A1	—
Glycolysis/gluconeogenesis	—	ADH1B, ALDH2, ALDH7A1, ALDOA, ALDOB, PKLR
Steroid hormone biosynthesis	CYP3A4, CYP3A7, CYP7A1, HSD11B1	CYP3A5, CYP3A43, HSD17B7, HSD3B1, ZNF498
Arachidonic acid metabolism	CYP2B6, CYP2C8, CYP4A11, CYP4A22, CYP4F2	—
Drug metabolism	ADH1A, ADH1C, CYP2A6, CYP2A7, CYP2B6, CYP2C8, CYP3A4, CYP3A7, UPB1, XDH	ADH1B, CYP2C9, CYP2C19, CYP3A5, CYP3A43, DPYD, DPYS, FMO3, FMO4, GSTA3, GUSB, MAOB, UPB1, UPP1, ZNF498
Fatty acid metabolism	ADH1A, ADH1C, CYP4A11, CYP4A22	ACADM, ACOX1, ACSL1, ADH1B, ALDH2, ALDH7A1, HADH
GLY, SER, and THR metabolism	AGXT, GLYCTK, PHGDH	AGXT, DMGDH, MAOB, PIPOX, PSAT1
Linoleic acid metabolism	CYP2C8, CYP3A4, CYP3A7	CYP2C9, CYP2C19, CYP3A5, CYP3A43, ZNF498
Retinol metabolism	ADH1A, ADH1C, CYP2A6, CYP2A7, CYP2B6, CYP2C8, CYP3A4, CYP3A7, CYP4A11, CYP4A22	ADH1B, CYP2C9, CYP2C19, CYP3A5, CYP3A43, RDH16, ZNF498
PPAR signaling	ACOX2, CD36, CYP4A11, CYP4A22, CYP7A1, FABP1, FABP4, HMGCS2, SCD	ACADM, ACOX1, ACSL1, CD36, FABP3, SLC27A2, SLC27A5
Complement/coagulation cascades	C1QB, C5, C8A, KLKB1, MBL2, PLG, SERPIND1	C1R, C1S, C2, C3, C8B, CD55, CFH, CFI, F2, F5, F7, F10, F12, F13B, KNG1, SERPINA5, SERPINF2, TFPI

Notes. Some genes appear in both columns because different probes for the same gene were identified. Abbreviations: ACADM - acyl-CoA dehydrogenase, ACOX - acyl-CoA oxidase, ACSL - acyl-CoA synthetase long-chain, ADH - alcohol dehydrogenase, AGXT - alanine-glyoxylate aminotransferase, ALDH - aldehyde dehydrogenase, ALDO - aldolase, C - complement, CD - cluster of differentiation, CYP - cytochrome P450, DMGDH - dimethylglycine dehydrogenase, DPYD - dihydropyrimidine dehydrogenase, DPYS - dihydropyrimidinase, F - coagulation factor, FABP - fatty acid binding protein, FMO - flavin-containing monooxygenase, GLYCTK - glycerate kinase, GSTA - glutathione S-transferase alpha, HADH - hyroxyacyl-CoA dehydrogenase, HMGCS - 3-hyroxy-3-methylglutaryl-CoA synthase, HSD - hydroxysteroid dehydrogenase, KLKB - kallikrein B, KNG - kininogen, MAOB - monoamine oxidase B, MBL - mannose-binding lectin, PHGDH - phosphoglycerate dehydrogenase, PIPOX - pipecolic acid oxidase, PKLR - pyruvate kinase (liver and red blood cell), PLG - plasminogen, PSAT - phosphoserine aminotransferase, RDH - retinol dehydrogenase, SCD - stearoyl-CoA desaturase, SERPIN - serpin peptidase inhibitor, SLC - solute carrier, TFPI - tissue factor pathway inhibitor,

UPB - ureidopropionase beta, UPP - uridine phosphorylase, XDH - xanthine dehydrogenase, ZNF - zinc finger protein.

5.3.1.3 Gene Expression Analysis at Equal Drug Doses

The aforementioned gene expression changes could be either due to the higher (by ~7.5-fold) C_{max} of troglitazone as compared to the C_{max} of rosiglitazone and/or due to the inherent (dose-independent) effects of troglitazone. Therefore, we treated MPCCs for 7 days with troglitazone or rosiglitazone at the same dose, the C_{max} of troglitazone (2.82 µg/mL). Comparing rosiglitazone at 0.373 µg/mL (Figure 5.3B) and at 2.82 µg/mL (Figure 5.5), there was a considerable increase in the transcripts that were modulated by rosiglitazone at the higher dose. Specifically, the higher dose of rosiglitazone exclusively upregulated the expression of 10 genes and downregulated the expression of 3 genes, while troglitazone exclusively upregulated the expression of 93 genes and downregulated the expression of 22 genes as compared to DMSO-treated controls at 7 days. Of the genes differentially expressed by both troglitazone and rosiglitazone, 68 were upregulated and 20 were downregulated. Of these overlapping transcripts, 76% had higher fold changes with troglitazone than with rosiglitazone (Table 5.6).

KEGG pathways identified with the genes differentially expressed by troglitazone and the higher dose of rosiglitazone have roles in drug metabolism and metabolic processes (Figure 5.6A, Table 5.7). As opposed to treatment with the respective C_{max} of each drug, using an equal dose caused more KEGG pathways to be identified with both troglitazone and rosiglitazone, specifically ones for steroid hormone biosynthesis, drug metabolism, linoleic acid metabolism, retinol metabolism, PPAR signaling, and complement/coagulation cascades. Genes associated with these KEGG pathways code for many CYP450 enzymes and transporters, among other proteins. In addition, troglitazone modulated the expression of more genes from the drug metabolism, retinol metabolism, and complement/coagulation cascades pathways. These genes included CYP450

enzymes (*CYP2A6*, *CYP2C9*, and *CYP2C19*) and complement/coagulation factors (*C3* and *C8A*). Rosiglitazone at an equal dose as troglitazone exclusively modulated acyl-coenzyme A oxidase 2 (*ACOX2*), *CYP4A22*, and 3-hydroxy-3-methylglutaryl-CoA synthase, member 2 (*HMGCS2*), all genes that are associated with the PPAR signaling pathway. Interestingly, while identified with troglitazone in the first study (Figure 5.4A-B), the primary bile acid biosynthesis KEGG pathway was not identified with the equal doses. The three genes that were initially identified from this pathway (aldo-keto reductase family 1, member D1 [*AKR1D1*], *CYP39A1*, and solute carrier family 27, member A5 [*SLC27A5*]) were divided into being identified with troglitazone exclusively (*SLC27A5*) and identified with both troglitazone and the higher dose of rosiglitazone (*AKR1D1* and *CYP39A1*). The differentially expressed genes in MPCCs treated with the same concentration of troglitazone or rosiglitazone were also classified into GO processes (Figure 5.6B). Troglitazone modulated a greater number of genes than rosiglitazone in the 'fatty acid metabolic', 'steroid metabolic', 'response to wounding', and 'oxidation/reduction' GO processes.
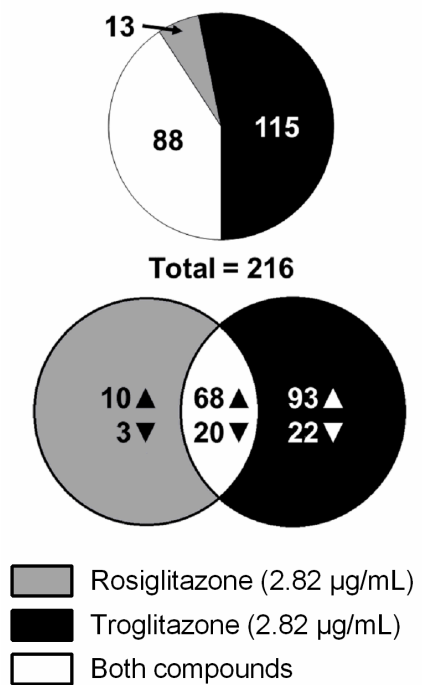
Figure 5.5: Global gene expression changes in MPCCs treated with troglitazone or rosiglitazone at the same concentration for 7 days. The number of genes upregulated or downregulated (|fold change| > 2.0 and |difference in expression| > 100) in MPCCs (JNB donor) by troglitazone (2.82 µg/mL) or rosiglitazone (2.82 µg/mL) or both drugs relative to DMSO after treatment for 7 days.
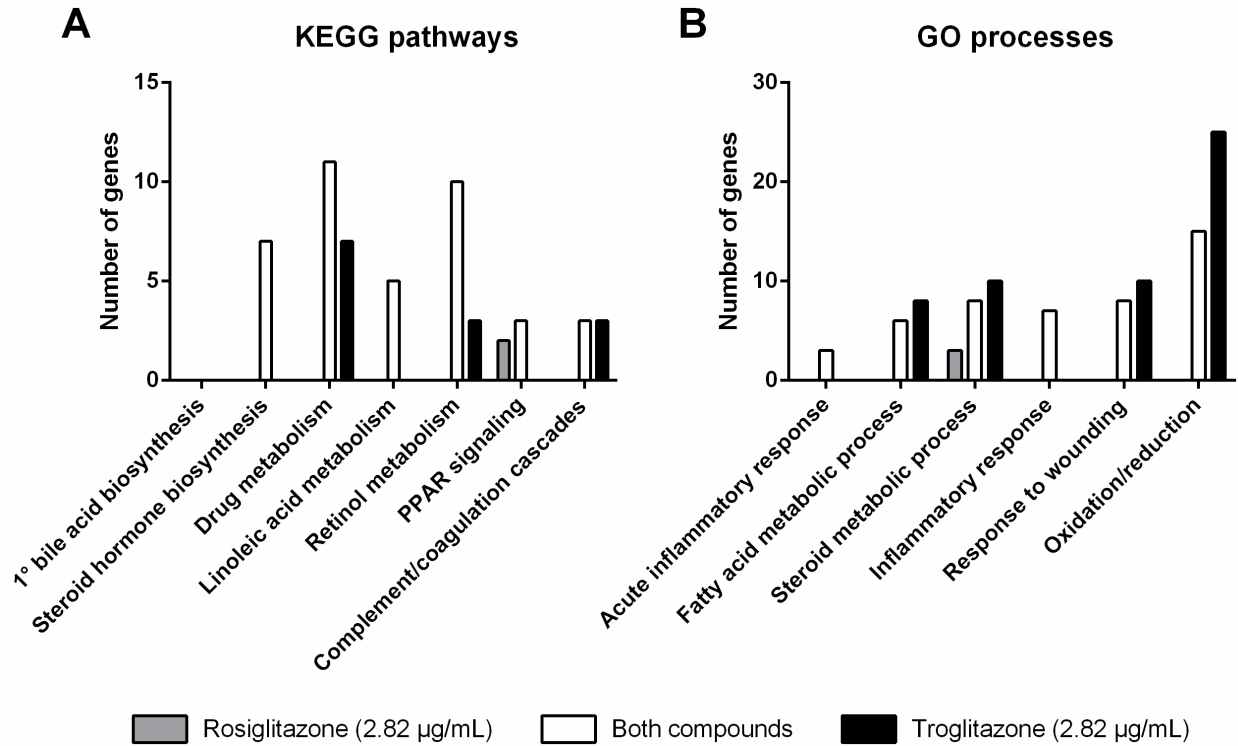
Figure 5.6: Pathway and gene ontology (GO) process analysis for differentially expressed genes in MPCCs treated with troglitazone or rosiglitazone at the same concentration for 7 days. The number of differentially expressed genes across **(A)** KEGG pathways and **(B)** GO processes in MPCCs (JNB donor) by troglitazone (2.82 µg/mL) or rosiglitazone (2.82 µg/mL) or both drugs relative to DMSO after treatment for 7 days.

Table 5.6: Gene expression fold changes in MPCCs (JNB donor) treated for 7 days with troglitazone or rosiglitazone at the same concentration level relative to DMSO-treated controls.

Dchip probe set	Gene symbol	Gene name	EntrezGene	Fold change 2.82 µg/mL rosiglitazone	Fold change 2.82 µg/mL troglitazone
229819_at	A1BG	Alpha-1-B glycoprotein	1	2.38	2.37
209994_s_at	ABCB1	ATP-binding cassette, sub-family B (MDR/TAP), member 1	5243, 5244	2.68	2.53
207819_s_at	ABCB4	ATP-binding cassette, sub-family B (MDR/TAP), member 4	5244	4.69	4.00
207275_s_at	ACSL1	Acyl-CoA synthetase long-chain family member 1	2180	2.36	2.34
210377_at	ACSM3	Acyl-CoA synthetase medium-chain family member 3	6296	3.13	3.15
210326_at	AGXT	Alanine-glyoxylate aminotransferase	189	2.64	3.32
210327_s_at	AGXT	Alanine-glyoxylate aminotransferase	189	2.77	3.69
210517_s_at	AKAP12	A kinase (PRKA) anchor protein 12	9590	-3.37	-4.85
227530_at	AKAP12	A kinase (PRKA) anchor protein 12	9590	-3.32	-4.17
207102_at	AKR1D1	Aldo-keto reductase family 1, member D1 (delta 4-3-ketosteroid-5-beta-reductase)	6718	3.85	4.40
229596_at	AMDHD1	Amidohydrolase domain containing 1	144193	2.36	3.69
206029_at	ANKRD1	Ankyrin repeat domain 1 (cardiac muscle)	27063	-3.14	-3.78
209369_at	ANXA3	Annexin A3	306	-3.45	-4.41
214910_s_at	APOM	Apolipoprotein M	55937	2.42	2.27
205239_at	AREG	Amphiregulin	374	-3.69	-3.08
204999_s_at	ATF5	Activating transcription factor 5	22809	3.42	2.78
210538_s_at	BIRC3	Baculoviral IAP repeat-containing 3	330	-2.80	-2.24
235275_at	BMP8B	Bone morphogenetic protein 8b	656	-2.49	-2.73
235377_at	C6orf142	Chromosome 6 open reading frame 142	90523	3.22	2.64
206979_at	C8B	Complement component 8, beta polypeptide	732	3.12	2.59
207354_at	CCL16	Chemokine (C-C motif) ligand 16	6360	2.24	2.94
201743_at	CD14	CD14 molecule	929	3.44	4.75
203645_s_at	CD163	CD163 molecule	9332	-3.24	-3.49

Dchip probe set	Gene symbol	Gene name	EntrezGene	Fold change 2.82 µg/mL rosiglitazone	Fold change 2.82 µg/mL troglitazone
215049_x_at	CD163	CD163 molecule	9332	-3.60	-3.62
206517_at	CDH16	Cadherin 16, KSP-cadherin	1014	3.61	2.80
220620_at	CRCT1	Cysteine-rich C-terminal 1	54544	-6.78	-13.31
208327_at	CYP2A13	Cytochrome P450, family 2, subfamily A, polypeptide 13	1553	2.17	2.64
1494_f_at	CYP2A6	Cytochrome P450, family 2, subfamily A, polypeptide 6	1548	2.24	2.61
207718_x_at	CYP2A7	Cytochrome P450, family 2, subfamily A, polypeptide 7	1549	2.36	2.85
206754_s_at	CYP2B6	Cytochrome P450, family 2, subfamily B, polypeptide 6	1555, 1556	2.70	4.74
206755_at	CYP2B6	Cytochrome P450, family 2, subfamily B, polypeptide 6	1555	3.04	5.39
208147_s_at	CYP2C8	Cytochrome P450, family 2, subfamily C, polypeptide 8	1558	4.23	4.46
1553977_a_at	CYP39A1	Cytochrome P450, family 39, subfamily A, polypeptide 1	51302	2.49	2.55
220432_s_at	CYP39A1	Cytochrome P450, family 39, subfamily A, polypeptide 1	51302	2.79	3.14
205998_x_at	CYP3A4	Cytochrome P450, family 3, subfamily A, polypeptide 4	1576	6.19	8.36
205999_x_at	CYP3A4	Cytochrome P450, family 3, subfamily A, polypeptide 4	1576	3.27	3.60
208367_x_at	CYP3A4	Cytochrome P450, family 3, subfamily A, polypeptide 4	1576	3.90	4.38
211440_x_at	CYP3A43	Cytochrome P450, family 3, subfamily A, polypeptide 43	64816	3.23	4.73
205939_at	CYP3A7	Cytochrome P450, family 3, subfamily A, polypeptide 7	1551	6.48	7.87
211843_x_at	CYP3A7	Cytochrome P450, family 3, subfamily A, polypeptide 7	1551	5.76	7.05
203980_at	FABP4	Fatty acid binding protein 4, adipocyte	2167	3.37	2.32
203638_s_at	FGFR2	Fibroblast growth factor receptor 2	2263	10.03	7.24
213524_s_at	G0S2	G0/G1 switch 2	50486	2.23	2.47
214240_at	GAL	Galanin prepropeptide	51083	-2.73	-6.23
1564706_s_at	GLS2	Glutaminase 2 (liver, mitochondrial)	27165	2.46	2.92
205531_s_at	GLS2	Glutaminase 2 (liver, mitochondrial)	27165	2.19	2.94
238518_x_at	GLYCTK	Glycerate kinase	132158	2.44	2.77
225420_at	GPAM	Glycerol-3-phosphate acyltransferase, mitochondrial	57678	4.48	6.94
225424_at	GPAM	Glycerol-3-phosphate acyltransferase, mitochondrial	57678	4.35	5.71

Dchip probe set	Gene symbol	Gene name	EntrezGene	Fold change 2.82 µg/mL rosiglitazone	Fold change 2.82 µg/mL troglitazone
204418_x_at	GSTM2	Glutathione S-transferase mu 2	2946	2.09	2.64
207502_at	GUCA2B	Guanylate cyclase activator 2B (uroguanylin)	2981	-2.29	-2.60
220491_at	HAMP	Hepcidin antimicrobial peptide	57817	-8.36	-8.92
243562_at	Hs.117112.0			2.46	3.36
238752_at	Hs.122155.0			2.86	4.33
205404_at	HSD11B0	Hydroxysteroid (11-beta) dehydrogenase 1	3290	2.54	2.69
207826_s_at	ID3	Inhibitor of DNA binding 3, dominant negative helix-loop-helix protein	3399	-3.73	-3.62
201625_s_at	INSIG1	Insulin induced gene 1	3638	2.29	3.39
204698_at	ISG20	Interferon stimulated exonuclease gene 20kDa	3669	-2.65	-2.83
33304_at	ISG20	Interferon stimulated exonuclease gene 20kDa	3669	-2.55	-2.76
207409_at	LECT2	Leukocyte cell-derived chemotaxin 2	3950	2.18	2.83
207256_at	MBL2	Mannose-binding lectin (protein C) 2, soluble (opsonic defect)	4153	4.98	7.22
223723_at	MFI2	Antigen p97 (melanoma associated) identified by monoclonal antibodies 133.2 and 96.5	4241	-2.33	-2.16
225316_at	MFSD2	Major facilitator superfamily domain containing 2	84879	2.38	3.01
207621_s_at	PEMT	Phosphatidylethanolamine N-methyltransferase	10400	2.76	2.55
201397_at	PHGDH	Phosphoglycerate dehydrogenase	26227	4.02	2.52
226147_s_at	PIGR	Polymeric immunoglobulin receptor	5284	4.60	6.83
228469_at	PPID	Peptidylprolyl isomerase D	5481	2.37	2.61
222662_at	PPP1R3B	Protein phosphatase 1, regulatory (inhibitor) subunit 3B	79660	2.55	3.75
243614_s_at	PRODH2	Proline dehydrogenase (oxidase) 2	58510	2.81	2.96
206753_at	RDH16	Retinol dehydrogenase 16 (all-trans)	8608	6.16	7.99
200831_s_at	SCD	Stearoyl-CoA desaturase (delta-9-desaturase)	6319	5.56	4.31
200832_s_at	SCD	Stearoyl-CoA desaturase (delta-9-desaturase)	6319	2.98	2.78
223839_s_at	SCD	Stearoyl-CoA desaturase (delta-9-desaturase)	6319	3.49	3.05

Dchip probe set	Gene symbol	Gene name	EntrezGene	Fold change 2.82 µg/mL rosiglitazone	Fold change 2.82 µg/mL troglitazone
209443_at	SERPINA5	Serpin peptidase inhibitor, clade A (alpha-1 antiproteinase, antitrypsin), member 5	5104	2.52	3.23
206325_at	SERPINA6	Serpin peptidase inhibitor, clade A (alpha-1 antiproteinase, antitrypsin), member 6	866	2.85	3.94
33323_r_at	SFN	Stratifin	2810	-3.09	-5.95
205768_s_at	SLC27A2	Solute carrier family 27 (fatty acid transporter), member 2	11001	2.32	2.99
205769_at	SLC27A2	Solute carrier family 27 (fatty acid transporter), member 2	11001	2.30	3.17
206292_s_at	SULT2A1	Sulfotransferase family, cytosolic, 2A, dehydroepiandrosterone (DHEA)-preferring, member 1	6822	2.72	3.50
1553583_a_at	THRSP	Thyroid hormone responsive (SPOT14 homolog, rat)	7069	4.09	3.91
229476_s_at	THRSP	Thyroid hormone responsive (SPOT14 homolog, rat)	7069	18.49	20.98
229477_at	THRSP	Thyroid hormone responsive (SPOT14 homolog, rat)	7069	17.30	18.60
209387_s_at	TM4SF1	Transmembrane 4 L six family member 1	4071	-2.46	-3.71
215034_s_at	TM4SF1	Transmembrane 4 L six family member 1	4071	-4.00	-4.06
243483_at	TRPM8	Transient receptor potential cation channel, subfamily M, member 8	79054	2.50	2.71
237350_at	TTC36	Tetratricopeptide repeat domain 36	143941	5.28	5.81
207245_at	UGT2B17UP	Glucuronosyltransferase 2 family, polypeptide B17	7367	3.43	8.08
231704_at	ZNF498	Zinc finger protein 498	221785	4.44	5.05

Note. The transcripts shown were differentially expressed by *both* drugs.

Table 5.7: Genes identified in KEGG pathways that were modulated in MPCCs (JNB donor) treated for 7 days with troglitazone or rosiglitazone at the *same* concentration level relative to DMSO-treated controls

KEGG pathway	Genes identified with *only* 2.82 µg/mL rosiglitazone	Genes identified with *both* 2.82 µg/mL troglitazone and 2.82 µg/mL rosiglitazone	Genes identified with *only* 2.82 µg/mL troglitazone
1° bile acid biosynthesis	—	—	—
Steroid hormone biosynthesis	—	AKR1D1, CYP3A4, CYP3A7, CYP3A43, HSD11B1, UGT2B17, ZNF498	—
Drug metabolism	—	CYP2A6, CYP2A7, CYP2A13, CYP2B6, CYP2C8, CYP3A4, CYP3A7, CYP3A43, GSTM2, UGT2B17, ZNF498	CYP2A6, CYP2C9, CYP2C19, DPYD, DPYS, FMO3, GSTM1
Linoleic acid metabolism	—	CYP2C8, CYP3A4, CYP3A7, CYP3A43, ZNF498	—
Retinol metabolism	—	CYP2A6, CYP2A7, CYP2B6, CYP2C8, CYP3A4, CYP3A7, CYP3A43, RDH16, UGT2B17, ZNF498	CYP2A6, CYP2C9, CYP2C19
PPAR signaling pathway	ACOX2, CYP4A22, HMGCS2	C8B, MBL2, SERPINA5	—
Complement/coagulation cascades	—	C8B, MBL2, SERPINA5	C3, C8A, SERPIND1

Notes. Abbreviations: ACOX - acyl-CoA oxidase, AKR - aldo-keto reductase, ALDH - aldehyde dehydrogenase, ARG - arginase, ASL - argininosuccinate lyase, C - complement, CYP - cytochrome P450, DPYD - dihydropyrimidine dehydrogenase, DPYS - dihydropyrimidinase, FMO - flavin-containing monooxygenase, GLYCTK - glycerate kinase, GSTM - glutathione S-transferase mu, HMGCS - 3-hyroxy-3-methylglutaryl-CoA synthase, MBL - mannose-binding lectin, ODC - ornithine decarboxylase, RDH - retinol dehydrogenase, SERPIN - serpin peptidase inhibitor, UGT - glucuronosyltransferase, ZNF - zinc finger protein.

5.3.1.4 Consistency of Microarray Results Across Independent Experiments

MPCCs created using the same PHH donor (JNB) across two independent experiments were treated with troglitazone (2.82 µg/mL) and 0.1% (v/v) DMSO for 7 days and the gene expression signatures were obtained via Affymetrix microarrays. Both experiments yielded similar numbers of differentially expressed genes by troglitazone relative to DMSO in key KEGG pathways such as primary bile acid biosynthesis, steroid hormone biosynthesis, arachidonic acid metabolism, drug metabolism, linoleic acid metabolism, retinol metabolism, and PPAR signaling (Figure 5.7A). Furthermore, the absolute fold changes of the genes identified in these KEGG pathways showed a strong correlation across the two experiments (Figure 5.7B).
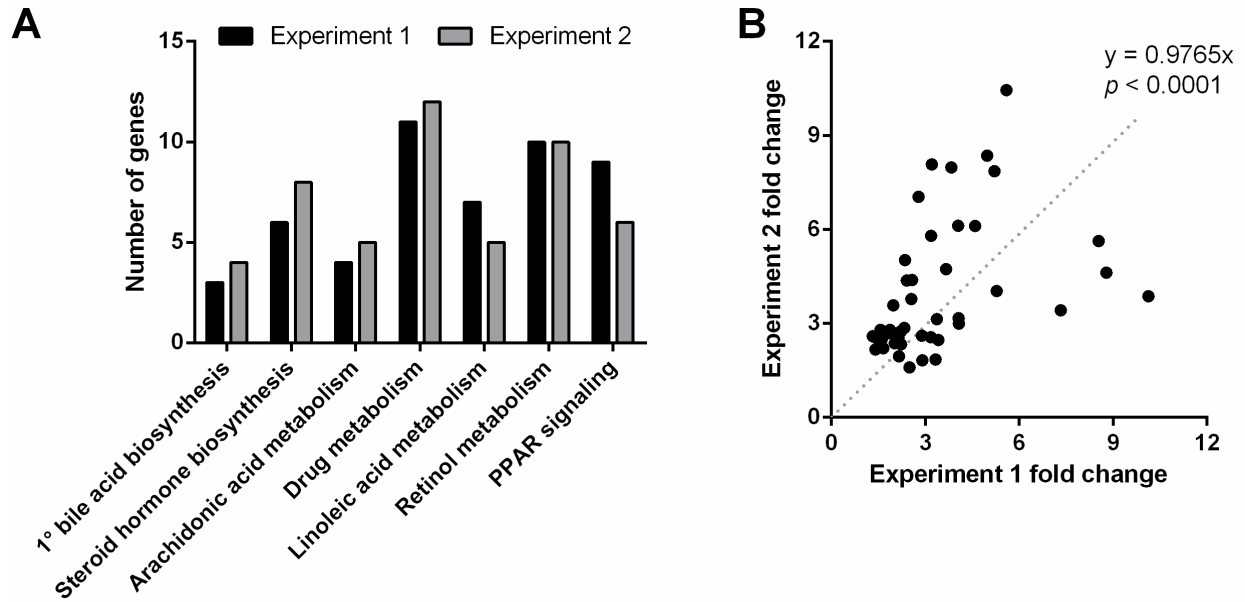
Figure 5.7: Consistency of microarray results across independent experiments. **(A)** The number of differentially expressed genes in KEGG pathways that are modulated in MPCCs (JNB donor) treated for 7 days with troglitazone (2.82 µg/mL) relative to a DMSO control are plotted across two independent experiments using the same primary human hepatocyte donor (JNB). **(B)** Fold gene expression changes for all transcripts included in the KEGG pathways are plotted between the two independent experiments.

5.3.1.5 qPCR Validation in Another PHH Donor

Select transcripts with a high level of upregulation in MPCCs (JNB donor) treated with troglitazone for 7 days as compared to DMSO-treated controls were also validated via qPCR using another cryopreserved PHH donor (HUM4043). These genes included stearoyl-CoA desaturase (*SCD*), acyl-CoA synthetase medium chain family member 3 (*ACSM3*), elongation of very long chain fatty acids 2 (*ELOVL2*), cluster of differentiation 36 (*CD36*), and mannose binding lectin 2 (*MBL2*). Expression of these genes in the second PHH donor using qPCR correlated well with the first PHH donor using microarray analysis (Figure 5.8). Furthermore, genes that were not flagged as differentially expressed in the microarray analysis were also selected for qPCR validation. In particular, the qPCR analysis showed that FBJ murine osteosarcoma viral oncogene homolog (*FOS*), chromosome 10 open reading frame 10 (*C10orf10*), and high mobility group 20B (*HMG20B*) were not modulated greater than 2-fold in troglitazone-treated MPCCs relative to DMSO-treated controls, respectively.
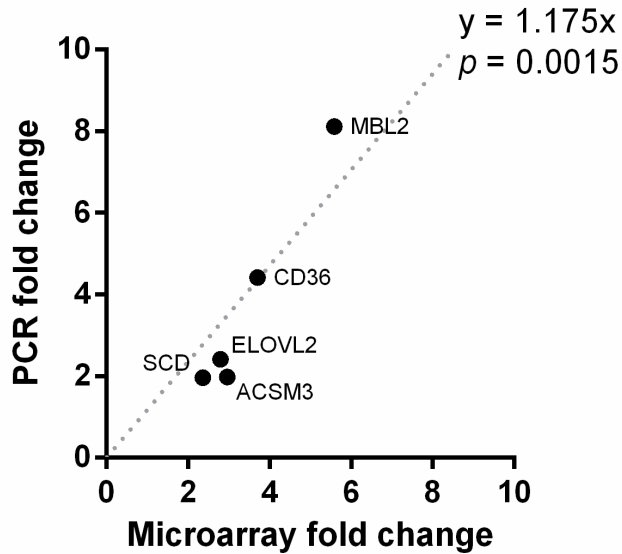
Figure 5.8: Quantitative polymerase chain reaction (qPCR) validation of microarray results. Select transcripts with a high level of upregulation identified via microarray analysis in troglitazone-treated MPCCs (7 days of treatment) were also validated via qPCR using a second PHH donor, HUM4043 (Triangle Research Labs). Genes studied were *SCD* (stearoyl-CoA desaturase), *ACSM3* (acyl-CoA synthetase medium chain family member 3), *ELOVL2* (elongation of very long chain fatty acids 2), *CD36* (cluster of differentiation 36), and *MBL2* (mannose binding lectin 2). Fold gene expression changes in qPCR validation are plotted against the microarray data obtained from the first PHH donor, JNB (BioreclamationIVT). Additional genes (*FOS* [FBJ murine osteosarcoma viral oncogene homolog], *C10orf10* [chromosome 10 open reading frame 10], and *HMG20B* [high mobility group 20B]) were used as negative controls and had a |fold change| < 2.0 in both the microarray analysis and qPCR validation.

171

5.3.2 Treatment of MPCCs for 1 Week with Three Other Pairs of Structural Analog Drugs

MPCCs created using the HUM4055A PHH donor (since the JNB PHH donor used for treatment with troglitazone or rosiglitazone was no longer available from BioreclamationIVT) were treated for 1 week with three other pairs of hepatotoxic and non-liver-toxic structural analog drugs at their respective C_{max} values, namely nefazodone (434.55 ng/mL) and buspirone (2.11 ng/mL), ibufenac (19.23 µg/mL) and ibuprofen (31.87 µg/mL), and tolcapone (4.51 µg/mL) and entacapone (1.91 µg/mL). None of these drugs at these doses caused downregulation of either albumin or urea secretion in MPCCs relative to DMSO-treated controls (Figure 5.9). Furthermore, the morphology of PHHs within MPCCs was not significantly affected by treatment with the aforementioned drug pairs for 1 week (Figure 5.10). Use of the same filtering criteria for identifying differentially expressed genes as that used for studies with troglitazone and rosiglitazone led to only 17-24 transcripts (versus 269 transcripts with troglitazone and rosiglitazone) across the three pairs of drugs relative to DMSO-treated controls (Figure 5.11) after 7 days of treatment, which is likely due to donor-dependent differences across the two experiments. Nonetheless, the hepatotoxin in each pair upregulated the expression of a greater number of genes than the non-liver-toxic analog.

Next, we used a |fold change| > 1.5 and |difference in expression| > 50 to identify differentially expressed genes in drug-treated MPCCs relative to DMSO-only controls. Nefazodone at its C_{max} (434.55 ng/mL) exclusively upregulated the expression of 55 genes and downregulated the expression of 33 genes, while buspirone at its C_{max} (2.11 ng/mL) exclusively upregulated the expression of 13 genes and downregulated the expression of 14 genes as compared to DMSO-treated controls at 7 days of treatment (Figure 5.12A). Both nefazodone and buspirone upregulated the expression of 11 genes and downregulated the expression of 23 genes. Ibufenac

at its C_{max} (19.23 µg/mL) exclusively upregulated the expression of 79 genes and downregulated the expression of 92 genes, while ibuprofen at its C_{max} (31.87 µg/mL) exclusively upregulated the expression of 12 genes and downregulated the expression of 5 genes as compared to DMSO-treated controls at 7 days (Figure 5.12B). Both ibufenac and ibuprofen upregulated the expression of 11 genes and downregulated the expression of 26 genes. Tolcapone at its C_{max} (4.51 µg/mL) exclusively upregulated the expression of 57 genes and downregulated the expression of 31 genes, while entacapone at its C_{max} (1.91 µg/mL) exclusively upregulated the expression of 9 genes and downregulated the expression of 9 genes as compared to DMSO-treated controls at 7 days (Figure 5.12C). Both tolcapone and entacapone upregulated the expression of 33 genes and downregulated the expression of 9 genes. Therefore, even with a less conservative filtering criteria, the hepatotoxin in each pair upregulated the expression of a greater number of genes than the non-liver-toxic analog.

The aforementioned differentially expressed genes were classified further into KEGG pathways and GO processes. Nefazodone exclusively modulated the expression of genes classified in the leukocyte transendothelial migration, cell adhesion molecules, retinol metabolism, and pathways in cancer KEGG pathways (Figure 5.13A, Table 5.8). Ibufenac exclusively modulated the expression of genes classified in the steroid hormone biosynthesis, fatty acid metabolism and biosynthesis, retinol metabolism, tyrosine metabolism, and PPAR signaling pathways (Figure 5.13B, Table 5.9). Tolcapone exclusively modulated the expression of genes classified in the ECM-receptor interaction and proteoglycans in cancer pathways, while both tolcapone and entacapone modulated the expression of genes classified in the leukocyte transendothelial migration and cell adhesion molecules pathways (Figure 5.13C, Table 5.10). Classifying the differentially expressed genes into GO processes also revealed that the hepatotoxic drug in each

pair led to a greater number of processes to be modulated than the non-liver-toxic structural analog. In particular, nefazodone exclusively modulated the expression of genes classified in the innate immune response, cell motility, and cellular response to chemical stimulus processes. Ibufenac exclusively modulated the expression of genes classified in the steroid metabolic, fatty acid metabolic, lipid metabolic, oxidation-reduction, and response to chemical stimulus/organic substance processes. Finally, tolcapone exclusively modulated the expression of genes classified in the cell-cell signaling and response to chemical stimulus/organic substance processes. Therefore, as observed with troglitazone and rosiglitazone, each hepatotoxin in the three other pairs of structural analog drugs led to a greater number of differentially expressed transcripts, KEGG pathways, and GO processes than the corresponding non-liver-toxic structural analog.
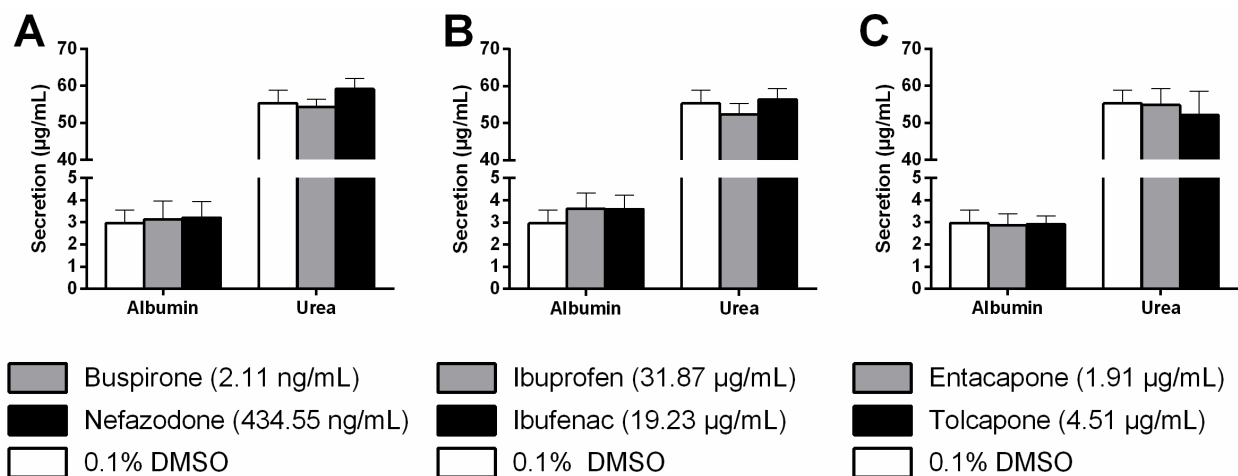
Figure 5.9: Albumin and urea secretions in MPCCs treated with additional clinical hepatotoxic/non-liver-toxic drug pairs at their respective C$_{max}$ levels for 7 days. Neither albumin secretions nor urea secretions were significantly affected in MPCCs (HUM4055A donor) treated for 7 days with **(A)** nefazodone/buspirone, **(B)** ibufenac/ibuprofen, or **(C)** tolcapone/entacapone relative to DMSO-only controls. All error bars represent standard deviations (n = 3).
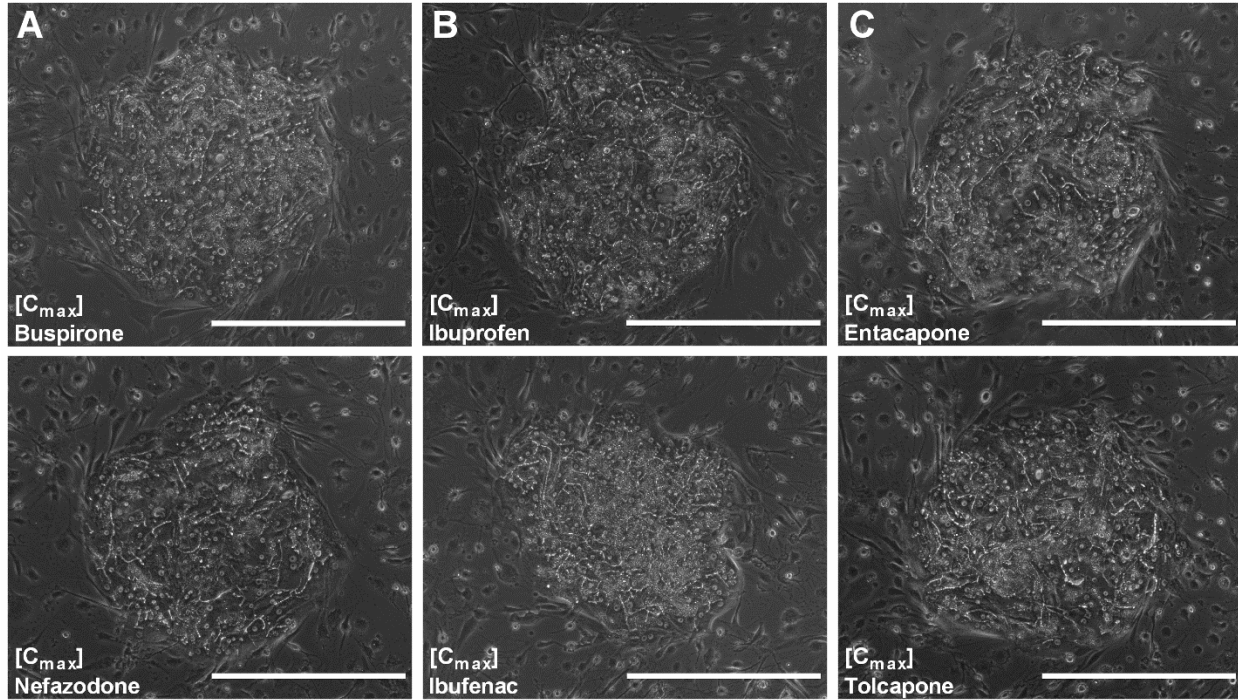
Figure 5.10: Hepatic morphology in MPCCs treated with additional clinical hepatotoxic/non-liver-toxic drug pairs at their respective C_{max} levels for 7 days. Hepatic morphology in MPCCs (HUM4055A donor) treated for 7 days with **(A)** nefazodone/buspirone, **(B)** ibufenac/ibuprofen, or **(C)** tolcapone/entacapone was not significantly affected relative to the DMSO-controls (see panel 'B' in Figure 5.2). All scale bars = 400 µm.
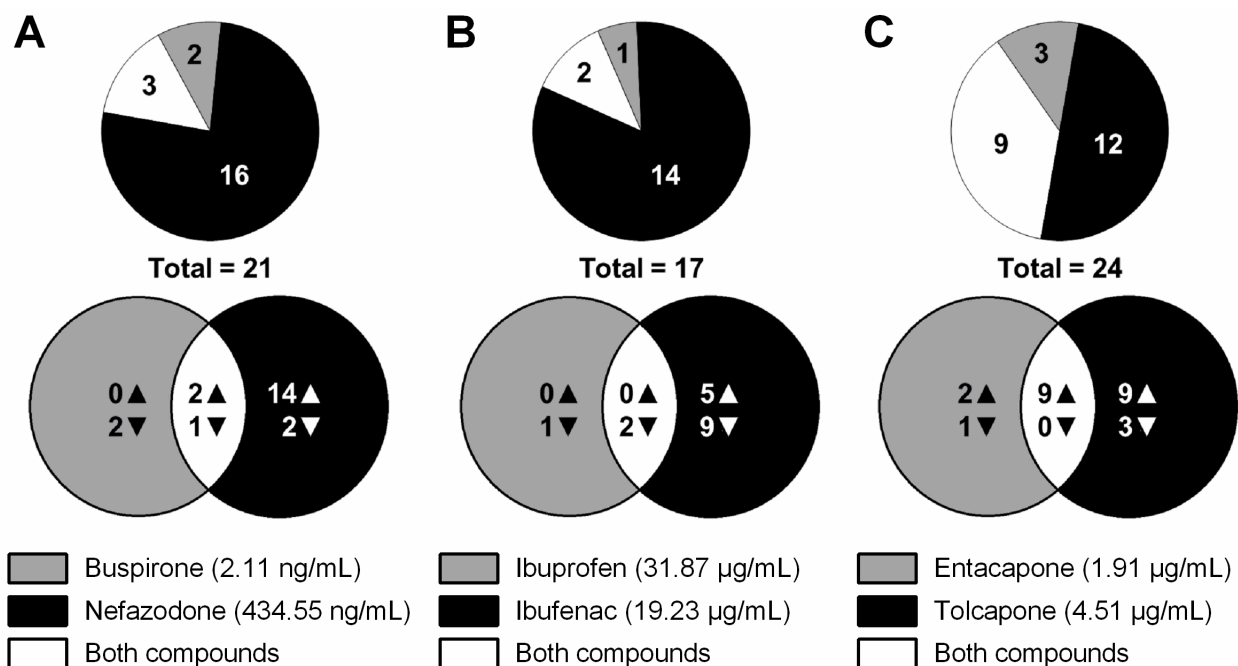
Figure 5.11: Global gene expression changes (determined using conservative filtering criteria) in MPCCs treated with additional clinical hepatotoxic/non-liver-toxic drug pairs at their respective C_{max} levels for 7 days. **(A)** The number of genes upregulated or downregulated ($|$fold change$| > 2.0$ and $|$difference in expression$| > 100$) in MPCCs (HUM4055A donor) by nefazodone (434.55 ng/mL) or buspirone (2.11 ng/mL) or both these drugs relative to DMSO after treatment for 7 days. **(B)** Similar analysis as in panel 'A' except MPCCs were treated with ibufenac (19.23 µg/mL) or ibuprofen (31.87 µg/mL). **(C)** Similar analysis as in panel 'A' except MPCCs were treated with tolcapone (4.51 µg/mL) or entacapone (1.91 µg/mL).

177
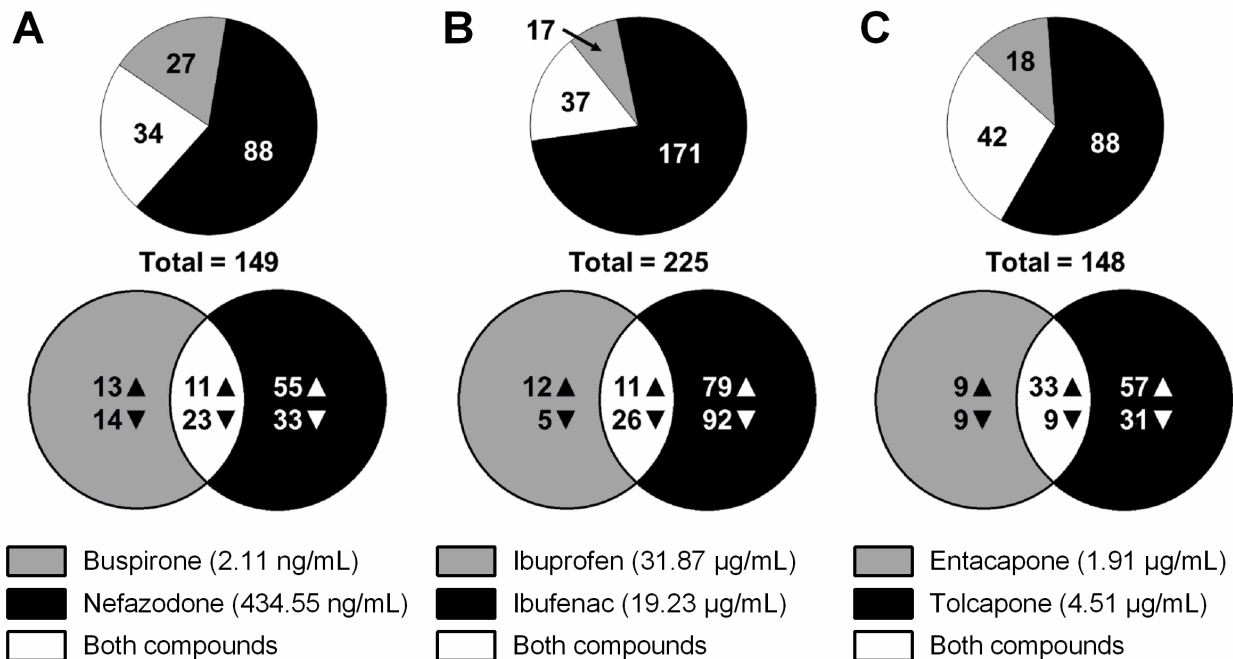
Figure 5.12: Global gene expression changes in MPCCs treated with additional clinical hepatotoxic/non-liver-toxic drug pairs at their respective C$_{max}$ levels for 7 days. **(A)** The number of genes upregulated or downregulated (|fold change| > 1.5 and |difference in expression| > 50) in MPCCs (HUM4055A donor) by nefazodone (434.55 ng/mL) or buspirone (2.11 ng/mL) or both these drugs relative to DMSO after treatment for 7 days. **(B)** Similar analysis as in panel 'A' except MPCCs were treated with ibufenac (19.23 µg/mL) or ibuprofen (31.87 µg/mL). **(C)** Similar analysis as in panel 'A' except MPCCs were treated with tolcapone (4.51 µg/mL) or entacapone (1.91 µg/mL).

178
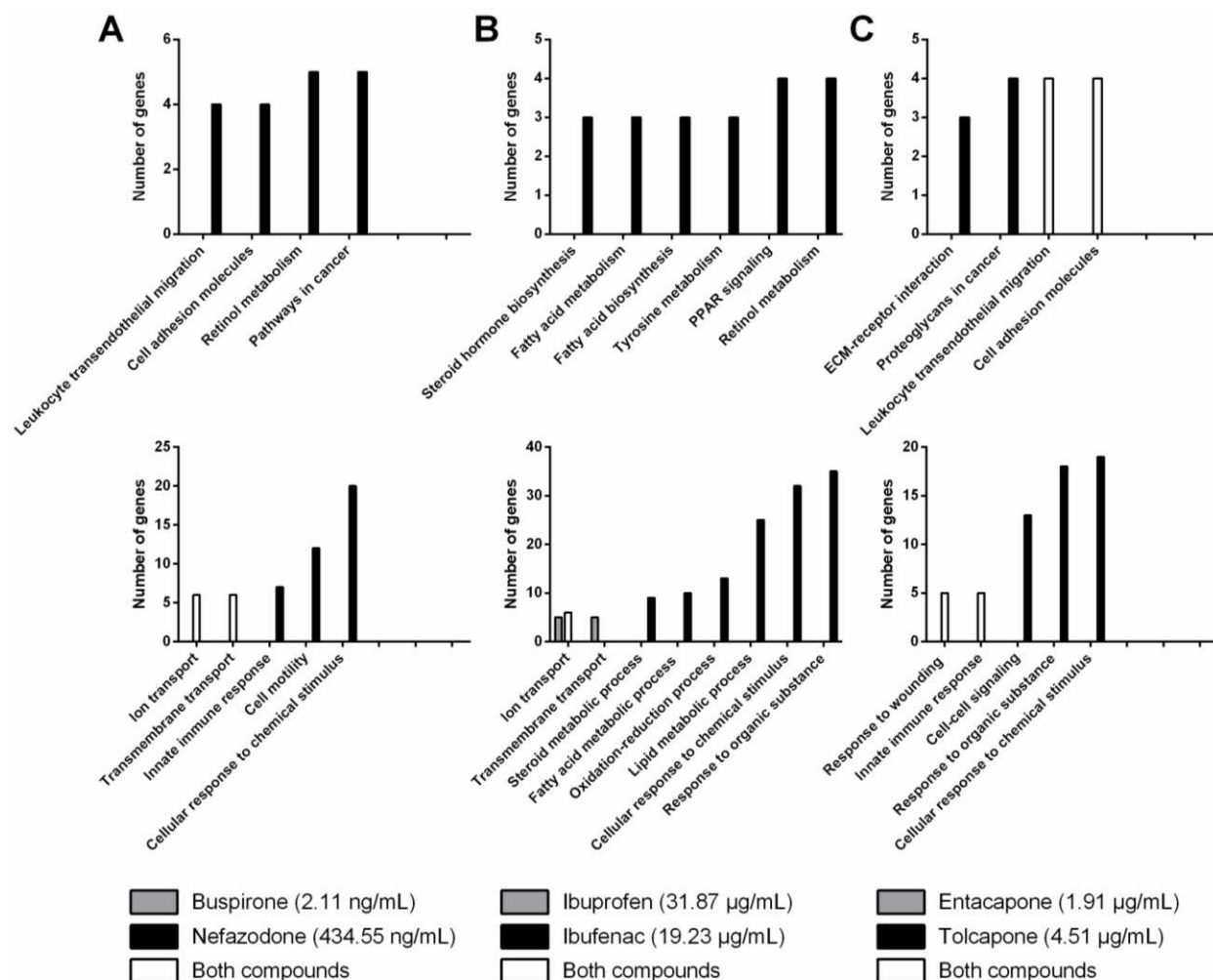
Figure 5.13: Pathway and gene ontology (GO) process analysis for differentially expressed genes in MPCCs treated with additional clinical hepatotoxic/non-liver-toxic drug pairs at their respective C_{max} levels for 7 days. (A) The number of differentially expressed genes across KEGG pathways (top) or GO processes (bottom) that are modulated in MPCCs (HUM4055A donor) by nefazodone (434.55 ng/mL) or buspirone (2.11 ng/mL) or both these drugs relative to DMSO after treatment for 7 days. **(B)** Similar analysis as in panel 'A' except MPCCs were treated with ibufenac (19.23 µg/mL) or ibuprofen (31.87 µg/mL). **(C)** Similar analysis as in panel 'A' except MPCCs were treated with tolcapone (4.51 µg/mL) or entacapone (1.91 µg/mL).

Table 5.8: Genes identified in KEGG pathways that were modulated in MPCCs (HUM4055A donor) treated for 7 days with nefazodone or buspirone at their respective C_{max} levels relative to DMSO-treated controls

KEGG pathway	Genes identified with *both* 434.55 ng/mL nefazodone and 2.11 ng/mL buspirone	Genes identified with *only* 434.55 ng/mL nefazodone
Leukocyte transendothelial migration	—	CDH5, CLDN5, CXCR4, PECAM1
Cell adhesion molecules	—	CDH5, CLDN5, ICAM2, PECAM1
Retinol metabolism	—	CYP2B6, CYP3A4, CYP3A7, CYP4A22, ZNF498
Pathways in cancer	—	CEBPA, CXCR4, FGFR2, GNG11, PGF

Note. Abbreviations: CEBPA - CCAAT/enhancer binding protein alpha, CDH - cadherin, CLDN - claudin, CXCR - chemokine (C-X-C motif) receptor, CYP - cytochrome P450, FGFR - fibroblast growth factor receptor, GNG - guanine nucleotide binding protein, ICAM - intercellular adhesion molecule, PECAM - platelet-endothelial cell adhesion molecule, PGF - placental growth factor, ZNF - zinc finger protein.

Table 5.9: Genes identified in KEGG pathways that were modulated in MPCCs (HUM4055A donor) treated for 7 days with ibufenac or ibuprofen at their respective C$_{max}$ levels relative to DMSO-treated controls

KEGG pathway	Genes identified with *both* 19.23 µg/mL ibufenac and 31.87 µg/mL ibuprofen	Genes identified with *only* 19.23 µg/mL ibufenac
Steroid hormone biosynthesis	—	CYP3A7, UGT2B15, ZNF498
Fatty acid metabolism	—	ACSL3, ACSL5, SCD
Fatty acid biosynthesis	—	ACACB, ACSL3, ACSL5
Tyrosine metabolism	—	DDC, HGD, TAT
PPAR signaling	—	ACSL3, ACSL5, GK, SCD
Retinol metabolism	—	CYP2B6, CYP3A7, UGT2B15, ZNF498

Note. Abbreviations: ACACB - acetyl-CoA carboxylase beta, ACSL - acyl-CoA synthetase long-chain, CYP - cytochrome P450, DDC - dopa decarboxylase, GK - glycerol kinase, HGD - homogentisate 1,2-dioxygenase, SCD - stearoyl-CoA desaturase, TAT - tyrosine aminotranserase, UGT - UDP glucuronosyltransferase, ZNF - zinc finger protein.

Table 5.10: Genes identified in KEGG pathways that were modulated in MPCCs (HUM4055A donor) treated for 7 days with tolcapone or entacapone at their respective C$_{max}$ levels relative to DMSO-treated controls

KEGG pathway	Genes identified with *both* 4.51 µg/mL tolcapone and 1.91 µg/mL entacapone	Genes identified with *only* 4.51 µg/mL tolcapone
ECM-receptor interaction	AGRN, COL4A1, HSPG2	—
Proteoglycans in cancer	HSPG2, IQGAP1, TIMP3, TLR2	—
Leukocyte transendothelial migration	—	CDH5, CLDN5, CXCR4, PECAM1
Cell adhesion molecules	—	CDH2, CLDN5, ICAM2, PECAM1

Note. Abbreviations: AGRN - agrin, CDH - cadherin, CLDN - claudin, COL - collagen, CXCR - chemokine (C-X-C motif) receptor, HSPG - heparin sulfate proteoglycan, ICAM - intercellular adhesion molecule, IQGAP - IQ motif containing GTPase activating protein, PECAM - platelet-endothelial cell adhesion molecule, TIMP - TIMP metallopeptidase inhibitor, TLR - toll-like receptor.

5.4 Discussion

We demonstrate using a toxicogenomics approach that exposing functional PHHs within MPCCs to pharmacologically-relevant (i.e. relative C_{max} levels) drug doses for up to 14 days can be used to better elucidate a drug's mode of action and distinguish the gene expression signature induced by clinical hepatotoxins from their non-liver-toxic analogs. We selected troglitazone (hepatotoxin) and rosiglitazone (non-liver toxin), two thiazolidinediones with known differences in hepatotoxicity to determine time- and dose-dependent effects on global gene expression patterns in MPCCs.[192] Dosing MPCCs with these drugs at their respective C_{max} values for up to 14 days did not cause loss of cell viability as assessed by mitochondrial dehydrogenase activity nor downregulation of hepatic urea secretion, a sensitive marker for hepatotoxicity detection.[58] In contrast, both drugs caused an expected induction of CYP3A4 activity.[203] Furthermore, we used the hepatotoxin/non-liver toxin pairs nefazodone/buspirone, ibufenac/ibuprofen, and tolcapone/entacapone to further validate MPCC utility for such analysis.

Dosing in a serum-free culture medium caused an expected decline in baseline MPCC functions over time in select PHH donors, potentially due to insufficient fibroblast growth for optimally supporting the phenotype of 'sensitive' PHH donors. Nonetheless, functions and gene expression levels were detected at sufficiently high levels in serum-free conditions to enable 14 days of drug treatment. Indeed, consistent with the short-term treatment of PHHs[204], troglitazone and rosiglitazone induced CYP3A4 activity in MPCCs even after 14 days of incubation. More broadly, treating MPCCs with drugs in a serum-free medium allows improved clinical prediction for drug clearance,[56,180] metabolite identification,[55] and hepatotoxicity[58] relative to PHH monolayers. Ideally, use of human plasma with PHH culture could help elucidate the effects of drug-protein binding on cellular outcomes since both troglitazone and rosiglitazone can heavily

bind to plasma proteins. However, it is not trivial to obtain human plasma batches of consistent composition/qualities for *in vitro* studies. Furthermore, how major PHH functions are affected by incubation with human plasma needs to be investigated before drug studies.

While a serum-free medium is widely used to investigate the intrinsic effects of drugs on cells[37,180], it does not mimic drug binding to human plasma proteins and how such binding may influence the unbound intracellular drug concentration that affects cellular processes.[205] The presence of uptake/efflux transporters in PHHs can lead to further changes in intracellular drug concentrations.[206] The use of undiluted human plasma on polarized PHHs can mitigate such a limitation; however, the effects of human plasma batches of different compositions and quality on the levels/longevity of PHH functions over weeks needs to be investigated. Nonetheless, our use of the C_{max} for each drug approximates the relative differences in potencies across analogs, which can be extended to the predicted efficacious concentrations at the portal triad of the liver sinusoid for preclinical compounds.

One of the possible drawbacks of the MPCC model is the contribution of genetic material from multiple species, namely the 3T3-J2 murine embryonic fibroblasts. In this study, we used human-specific microarray chips and excluded from the analysis any genes that were present in the 3T3-J2 fibroblasts. Future inquiries may find that genes present in both PHHs and 3T3-J2 fibroblasts complicate the toxicogenomic analysis and will need to be addressed with more sophisticated algorithms. One potential solution is to implement a "selective trypsinization protocol," whereby MPCCs are briefly treated with 0.05% trypsin-EDTA to detach 3T3-J2 fibroblasts while leaving PHH islands intact; however, the effectiveness of this method depends on the state of the hepatocytes being treated. Fluorescence-activated cell sorting was also not used since the time required can potentially modulate gene expression. Instead, we excluded from

analysis those transcripts that were called 'present' when pure 3T3-J2 murine RNA was hybridized to the human microarray (~18% of the total MPCC transcripts). Furthermore, the differentially expressed genes from a human microarray in pure 3T3-J2 cultures treated with troglitazone for 1 week as compared to cultures treated with DMSO did not overlap with differentially expressed genes in MPCCs treated under identical conditions. Ultimately, RNA sequencing can help exclude those sequences that map to the mouse genome and also reveal novel drug-modulated transcripts. However, microarrays are currently a more cost-effective solution with straightforward bioinformatics analysis for obtaining an assessment of the drug's effects on known transcripts. Stromal contamination is not unique to this system, as this would be seen in any study using liver slices. Nonetheless, inclusion of other liver stromal cells (i.e. sinusoidal endothelial cells, Kupffer macrophages, hepatic stellate cells) to fully recapitulate the liver microenvironment is a worthwhile endeavor. These stromal cells may give further insights into disease states such as fibrosis, hepatitis, and inflammation that could impact idiosyncratic drug toxicity.[67]

After 1 day of treatment with troglitazone or rosiglitazone, 12 genes were differentially expressed (|fold change| > 2.0 and |difference in expression| > 100 relative to DMSO). Of these, the transcript upregulated by both drugs was *FABP4* (fatty acid binding protein 4), a target gene of PPARγ[207], the nuclear receptor to which both drugs can bind. Rosiglitazone exclusively modulated 1 non-protein-coding transcript, while troglitazone exclusively modulated 10 transcripts involved in retinol metabolism, drug metabolism, linoleic acid metabolism, and steroid hormone biosynthesis. In contrast to 1 day, 7 days of treatment led to 261 transcripts being exclusively modulated by troglitazone in biosynthetic (primary bile acids and steroid hormone) and metabolic (i.e. amino acid, arachidonic acid, drug, fatty acid, and retinol metabolism) pathways. The troglitazone-mediated modulation of bile acid biosynthesis, fatty acid metabolism,

and drug metabolism, in particular, are potentially indicative of a stress on bile acid homeostasis in PHHs, mitochondrial dysfunction, and oxidative stress caused by the generation of reactive metabolites, respectively, all suspected mechanisms of troglitazone-induced hepatotoxicity.[194,208] Additionally, select troglitazone-modulated transcripts clustered into the 'wound healing' GO process (i.e. *CD36* or cluster of differentiation 36, *BMP2* or bone morphogenetic protein 2, *CXCL2* or chemokine (C-X-C motif) ligand 2). Rosiglitazone exclusively modulated 2 transcripts (hypothetical proteins), while PPAR signaling was identified with both drugs.

After 14 days of treatment, both troglitazone and rosiglitazone modulated 127 transcripts in biosynthetic and metabolic pathways, but troglitazone modulated 93% of these transcripts with higher fold changes than rosiglitazone. For instance, troglitazone caused a 38.6-fold and 29.1-fold upregulation in *CYP2C8* and *CYP3A4*, respectively, as compared to 11.6-fold and 3.6-fold by rosiglitazone. Reactive metabolites of troglitazone formed by CYP2C8 and CYP3A4 are implicated in hepatotoxicity.[209,210] Furthermore, troglitazone exclusively modulated 483 transcripts as opposed to 18 transcripts exclusively modulated by rosiglitazone. For instance, troglitazone exclusively modulated an additional 15 transcripts involved in drug metabolism (i.e. *CYP2C19*, *FMO3* or flavin-containing monooxygenase 3). FMOs have been shown to produce endogenous hydrogen peroxide[211], which may be responsible for oxidative stress. Lastly, troglitazone exclusively modulated an additional 18 transcripts in the 'complement and coagulation cascades' pathway (i.e. *C2*, *C3*, and *C8B* or complement component 2, 3, and 8B were each upregulated). Complement proteins/coagulation factors may be a repair mechanism in response to hepatic damage.[212] In humans treated with troglitazone, C3 protein is elevated[213] and may be indicative of an injury response to oxidative stress or related cellular damage, similar to the implicated role of complement activation in acetaminophen-induced hepatotoxicity.[214]

When MPCCs were treated with troglitazone or rosiglitazone for 7 days at 2.82 µg/mL (C_{max} of troglitazone), 88 transcripts were modulated by both drugs as compared to 6 transcripts modulated by the drugs at their respective C_{max}. The corresponding pathways identified for both drugs at 2.82 µg/mL were primarily in steroid hormone biosynthesis and metabolism (drug, linoleic acid, and retinol). However, over half of the total identified transcripts were still flagged with troglitazone exclusively (i.e. *ARG1* or arginase 1, *C8A*, *FMO3*, *GSTM1* or glutathione S-transferase mu 1, and *SULT1A1* or sulfotransferase family 1A member 1). *C3* was not flagged as differentially expressed at the elevated dose of rosiglitazone, but it was flagged when cultures were dosed with troglitazone. Therefore, troglitazone's effect on PHH transcripts is partly due to its inherent properties as opposed to a higher C_{max} than rosiglitazone.

We verified using qPCR in another PHH donor select transcripts that were identified via microarray analysis as upregulated following a 7-day treatment with troglitazone. Furthermore, select genes not flagged as differentially expressed in the microarray analysis were also selected for qPCR validation. Expression of these eight genes in the second PHH donor correlated well with the first PHH donor. Ultimately, profiling gene expression in hundreds and even thousands of induced pluripotent stem cell-derived human hepatocyte (iPSC-HH) donors may be useful to investigate the mechanisms underlying inter-individual susceptibilities to DILI (see Chapter 2).

To determine if results obtained with troglitazone/rosiglitazone extended to other drug pairs, we incubated MPCCs created with another PHH donor (given limitations in the availability of the previous donor) for 7 days with hepatotoxic/non-liver-toxic drug pairs: nefazodone/buspirone, ibufenac/ibuprofen, and tolcapone/entacapone. However, in contrast to the 269 differentially expressed genes identified with troglitazone/rosiglitazone, the other drugs caused 17-24 genes to be differentially expressed using the same filtering criteria (|fold change| >

2.0 and |difference in expression| > 100). Therefore, we made the filtering criteria less conservative (|fold change| > 1.5 and |difference in expression| > 50) to obtain the number of differentially expressed genes by the additional drug pairs on the same magnitude as for troglitazone/rosiglitazone. Nonetheless, both filtering criteria showed that the hepatotoxins exclusively modulated a greater number of transcripts than their non-liver-toxic analogs. In particular, nefazodone, ibufenac, and tolcapone exclusively modulated 59% (out of 149), 76% (out of 225), and 59% (out of 148) of the total number of differentially expressed genes in MPCCs relative to DMSO, respectively. On the other hand, buspirone, ibuprofen, and entacapone exclusively modulated 18%, 8%, and 12% of the transcripts, respectively. Interestingly, ibufenac modulated transcripts in pathways that were also modulated by troglitazone (i.e. retinol metabolism, fatty acid metabolism, and steroid hormone biosynthesis). The aforementioned difference in filtering criteria needed for troglitazone/rosiglitazone versus the other drug pairs is potentially due to the differential sensitivities of PHH donors to the effects of drugs (as in the clinic), which merits future investigation using additional donors.

In conclusion, chronic treatment of MPCCs for up to 14 days at pharmacologically-relevant doses of troglitazone and rosiglitazone revealed gene expression signatures that were specific to each drug. Troglitazone modulated a greater number and fold changes of transcripts in pathways/processes such as drug metabolism and wound healing as compared to rosiglitazone, which may provide clues as to how troglitazone stresses the hepatocytes in ways that can lead to overt liver injury in susceptible patients. Similar trends were also observed with three other toxin/non-toxin pairs. Complementing gene expression profiling with proteomics and metabolomics could enable further insights into DILI pathogenesis at multiple levels. Ultimately, an 'omics'-based approach utilizing MPCCs dosed chronically with drugs could allow

188

investigation of a drug's mode of action across multiple drug classes, which has the potential for mitigating DILI risk to humans.

CHAPTER 6 - Co-Culture of Hepatocytes and Endothelia[6]

Liver sinusoidal endothelial cells (LSECs) comprise the majority of the non-parenchymal cell population in the human liver and play a significant role in biochemical secretion, blood filtration, and liver regeneration. Modeling interactions between hepatocytes and LSECs can aid in understanding liver physiology and mechanisms of drug toxicity. However, most previous studies focus on bovine, rat, or murine endothelia, which may not accurately represent human physiology and disease mechanisms due to species-specific differences. Towards that end, we established co-cultures of micropatterned primary human hepatocytes (PHHs) and either primary human LSECs or human umbilical vein endothelial cells (HUVECs), and found a rapid loss of hepatic morphology and function in these cultures. Alternatively, we created tri-cultures of micropatterned PHHs, 3T3-J2 murine embryonic fibroblasts, and either primary LSECs or HUVECs, since 3T3-J2 fibroblasts have previously been shown to stabilize PHH functions for 4-6 weeks. These cultures maintained a high level of hepatic functions (i.e. albumin secretions, CYP450 activities) and morphology for multiple weeks *in vitro*. We then characterized the tri-cultures for multiple endothelial-specific markers (i.e. CD31, CD54, von Willebrand factor, factor VIII) over time, the uptake of acetylated low-density lipoproteins, and the presence of fenestrations on LSECs via electron microscopy. Lastly, we demonstrate an exacerbation of toxicity upon exposing cultures to compounds known to cause damage to endothelia *in vivo* (i.e. azathioprine, monocrotaline). In conclusion, tri-cultures offer a stable platform for inquires of the interactions

---

[6] Portions of this chapter appear in the following:
Ware, B.R., Durham, M.J., Monckton, C.P., & Khetani, S.R. A cell culture platform to maintain long-term phenotype of primary human hepatocytes and endothelial cells. *Cellular and Molecular Gastroenterology and Hepatology.* 2018. 5(3): 187-207, under the Creative Commons Attribution 4.0 license.

between hepatocytes and endothelia that could provide insights into drug toxicity and endothelia phenotype.

6.1 Introduction and Background

On the microscale, the human liver consists of complex interactions between hepatocytes, extracellular matrix proteins, soluble factors, and several types of non-parenchymal cells, all in a precisely defined architecture. The liver sinusoidal endothelial cell (LSEC) is the most predominant type of non-parenchymal cell, comprising ~70% of the non-parenchymal cells in the liver and ~16% of the total liver cell mass.[6] LSECs, along with the extracellular matrix-based space of Disse, act as a barrier between hepatocytes and blood flowing through the liver sinusoid. As a major component of the liver sinusoid, LSECs are responsible for filtering nutrients from the blood, secreting various biochemicals, maintaining hepatic stellate cell quiescence, and contributing to regeneration after liver injury via increased production of the cytokine HGF.[8,215] LSECs also clear waste molecules (including viruses) entering portal venous blood; are important for induction of CD8$^+$ T cell tolerance; synthesize the critical coagulation co-factor, Factor VIII; and can become insulin resistant and de-fenestrated in non-alcoholic fatty liver disease.[6,216–218] Clinically, LSECs are associated with key pathophysiologic conditions, including liver fibrosis, drug toxicity, and hepatitis. In the early stages of hepatic fibrosis (an imbalance between the production and degradation of extracellular matrix proteins), LSECs secrete the cytokine IL-33, which activates hepatic stellate cells and further promotes fibrosis and may lead to cirrhosis and hepatocellular carcinoma.[219] Some drugs, including azathioprine[220], dacarbazine[221], and monocrotaline[220], are known to cause toxicity specific to LSECs rather than hepatocytes. Lastly, *in vitro* cultures containing LSECs have been shown to readily uptake hepatitis C-like virus particles, whereas cultures lacking LSECs did not.[222]

Significant species-specific differences in drug metabolism and other liver pathways[44,58,145] necessitate the supplementation of animal data with human-relevant *in vitro* assays for drug development.[142] Given their physiological relevance, isolated primary human hepatocytes (PHHs) are widely considered to be ideal for building human liver models. However, when cultured in the presence of ECM proteins (i.e. collagen) alone, PHHs rapidly (hours to days) decline in critical phenotypic functions, such as cytochrome P450 (CYP450) enzyme activities[54], insulin responsiveness[62], and expression of the master liver transcription factor, hepatocyte nuclear factor 4α[223]. Similarly, when cultured alone, LSECs lose their characteristic fenestrations and undergo apoptosis within a few days.[224] In contrast with hepatocyte mono-cultures, co-culture with both liver- and non-liver-derived NPC types can enhance hepatocyte functions in culture.[127] Endothelial cells have been previously explored towards transiently enhancing hepatocyte functions in co-cultures relative to declining hepatocyte mono-cultures. However, many such hepatocyte-endothelial co-culture studies utilize rodent cells[85,225–229] that do not completely suffice for modeling human liver biology as discussed above. Furthermore, the use of abnormal cancerous cell lines[87,230,231] and/or non-liver endothelial cells[85,225,227,232] may provide a first approximation of hepatocyte-endothelial interactions but needs to be complemented with the use of primary cells from human liver tissue to determine similarities and differences in observed cell responses. Indeed, the Yarmush group has created *in vitro* co-cultures of PHHs and primary human LSECs, which showed high level of low-density lipoprotein uptake in PHHs in the presence of LSECs[222], and increased (~1.3 fold) hepatic CYP1A activity in serum-free co-culture with endothelial cells under high (95%) oxygen levels.[143] However, it is not clear from these short-term (≤ 24 hours) data sets whether LSECs can induce high levels of phenotypic functions in PHHs over long-term

(weeks) culture as compared to PHH mono-cultures. Additionally, the differential effects of LSECs on PHH functions relative to non-liver vascular endothelial cells remain to be elucidated.

To address the limitations with the above-mentioned hepatocyte-endothelial co-culture studies, here we sought to first elucidate the effects of primary human LSECs on the long-term functions of PHHs with comparisons to non-liver endothelial cells (human umbilical vein endothelial cells or HUVECs) and PHH mono-cultures. We benchmarked the effects of endothelial cells on PHHs to the effects of 3T3-J2 murine embryonic fibroblasts, a cell type that expresses hepatocyte-supporting molecules present in the liver[158] and is known to induce high levels of functions in PHHs for 4-6 weeks *in vitro*.[54] To maintain consistent homotypic PHH contacts/interactions across the various co-culture configurations towards isolating the effects of the heterotypic interactions between PHHs and NPCs, we utilized a previously developed semiconductor-driven micropatterning technique to create so-called micropatterned co-cultures (MPCCs) in which PHHs are first clustered onto circular collagen-coated domains of precise/reproducible diameters and subsequently surrounded by an NPC layer containing one or more cell types.[154] Lastly, we determined PHH/fibroblast/endothelial tri-culture configurations, including those in which the LSECs were separated from PHHs via an ECM protein gel as in the space of Disse *in vivo*, which promoted stable PHH and LSEC phenotype over several weeks towards developing a model system that has utility in drug development and to better understand PHH and LSEC interactions in liver physiology and disease.

6.2 Materials and Methods

6.2.1 Endothelial Culture

Primary human LSECs[233] and TMNK immortalized liver endothelial cells[234] were a gift from Dr. Hugo Rosen of the University of Colorado-Denver School of Medicine. A second donor

of LSECs was purchased from ScienCell (Carlsbad, CA) and used to verify the trends observed with the first LSEC donor. Pooled-donor HUVECs were purchased from Lonza (Williamsport, PA). Primary endothelial cells were cultured at 37°C, 10% CO_2 in EGM™-2 BulletKit™ medium (Lonza) on tissue culture polystyrene coated with 2 µg/cm² fibronectin (Corning Life Sciences, Manassas, VA). TMNK cells were cultured at 37°C, 10% CO_2 in a high-glucose Dulbecco's Modified Eagle Medium base (DMEM, Corning) supplemented with 10% (v/v) bovine serum and 1% (v/v) penicillin-streptomycin. Primary endothelial cell types were passaged no more than six times; prior to co-culture with PHHs as described below, the endothelial cells were treated with 0.05% (m/v) trypsin for 5 minutes to release cells into suspension, centrifuged, and resuspended in fresh culture medium.

6.2.2 Fibroblast Culture

Murine embryonic 3T3-J2 fibroblasts were a gift from Howard Green of Harvard Medical School.[129] Cells were cultured at 37°C, 10% CO_2 in Dulbecco's Modified Eagle's Medium (DMEM, Corning Life Sciences) with high glucose, 10% (v/v) bovine calf serum (Life Technologies), and 1% (v/v) penicillin-streptomycin. Fibroblasts were passaged up to 12 times prior to use in culture with PHHs.

6.2.3 Micropatterned Co- and Tri-Culture Fabrication

Cryopreserved PHHs were commercially obtained from Triangle Research Labs (Durham, NC); donors included HUM4011 (26-year-old Caucasian male who died of cardiac arrest) and HUM4055A (54-year-old Caucasian female who died of stroke). PHHs were thawed, counted and viability was assessed as previously described.[111] PHHs were subsequently micropatterned on collagen-coated domains as previously described.[154] Briefly, adsorbed rat tail collagen-I (Corning) was lithographically patterned in each well of a 24-well to create 500 µm diameter circular

domains spaced 1200 μm apart, center-to-center. PHHs selectively attached to the collagen

domains leaving ~30K attached PHHs on ~90 collagen-coated islands within each well of a 24-

well plate. The next day after adherent PHHs had spread to fill in the collagen domains, the

cultures were incubated with fibronectin (2 μg/cm^2) to coat the remaining surface area with ECM

protein to enable attachment of NPC types, which included either 3T3-J2 murine embryonic

fibroblasts or endothelial cells at ~90K per well; the endothelial cells included were either

HUVECs or primary human LSECs.

To create co-planar micropatterned tri-cultures, ~6K endothelial cells (HUVECs or

LSECs) were mixed into a suspension of ~84K 3T3-J2 fibroblasts, and then this mixture was

seeded onto micropatterned PHH colonies (~30K total PHHs) in each well of 24-well plate. The

1:5 endothelial:PHH ratio corresponds to the approximate ratio in the liver.[18] To create layered

micropatterned tri-cultures, MPCCs containing PHH colonies surrounded by the fibroblasts were

first overlaid with a thin gel (250 μg/mL) of Matrigel™ (Corning) and then ~6K endothelial cells

were seeded on top of the Matrigel™ the following day. Culture medium containing 40 ng/mL

recombinant vascular endothelial growth factor[224] (VEGF; Thermo Fisher Scientific, Waltham,

MA) in a high-glucose DMEM base (Corning) was replaced on co-cultures and tri-cultures every

other days (300 μL/well). Other culture medium components were described previously.[111]

 6.2.4 Gene Expression Analysis

Total RNA was isolated, purified, and reverse transcribed into complementary DNA

(cDNA) as previously described.[111] Briefly, RNA was extracted from the cultures with the RNeasy

kit (Qiagen, Germantown, MD) and homogenized via centrifugation through homogenizing

columns (Omega Bio-Tek, Norcross, GA). Genomic DNA was removed with a 1-hour treatment

with DNAse I (New England Biolabs, Ipswich, MA), and cDNA was synthesized with the High-

Capacity cDNA Reverse Transcription Kit (Applied Biosystems, Foster City, CA). Then, 250 ng of cDNA was added to each quantitative polymerase chain (qPCR) reaction along with the Taqman™ master mix (Thermo Fisher Scientific) and pre-designed Taqman human-specific primer/probe sets per manufacturer's protocols; primer/probe sets were selected for endothelial genes including cluster of differentiation 31 (*CD31*), cluster of differentiation 54 (*CD54*), factor VIII (*F8*), and von Willebrand factor (*vWF*). The primer/probe sets were selected to be human-specific without cross-reactivity to 3T3-J2 mouse DNA; however, Taqman primer/probe sequences are proprietary to the manufacturer. Gene expression was normalized to glyceraldehyde 3-phosphate dehydrogenase (*GAPDH*).

6.2.5 Drug Dosing Studies

After ~1 week of stabilization, cultures were dosed with compounds believed to cause endothelial-specific toxicity in serum-free culture medium (i.e. little to no binding of drug to protein) for 6 days (3 doses that corresponded to standard media changes). Doses up to $100 \times C_{max}$ (the maximum plasma concentration) were applied to cultures to parallel doses used in previous studies.[58,161] The C_{max} values of azathioprine (3.61 µM), dacarbazine (43.91 µM), and monocrotaline (10 µM) were each established in previous literature.[38,58,235] The dimethyl sulfoxide (DMSO) concentration that MPCCs were exposed to was kept at 0.1% (v/v) relative to culture medium for all conditions. Vehicle-only controls were maintained at 0.1% (v/v) DMSO to serve as a baseline for comparison. Azathioprine and monocrotaline were purchased from Cayman Chemical (Ann Arbor, MI), while dacarbazine was purchased from Sigma-Aldrich.

6.2.6 Cell Morphological and Health Assessments

Cell morphology was monitored using an EVOS®FL microscope (Thermo Fisher Scientific) with standard 4×, 10×, and 20× phase contrast objectives. PHH projected area from

phase contrast pictures was quantified using ImageJ software.[236] Concentrations of human albumin and urea in collected cell culture supernatants were assayed using previously published protocols.[111] Briefly, albumin secretions were assessed using a competitive enzyme-linked immunosorbent assay (ELISA), while urea production was measured via a colorimetric reaction with diacetyl monoxime, acid, and heat (Stanbio Labs, Boerne, TX). CYP450 enzyme activities were measured by first incubating cultures in substrates for 1 hour at 37°C and then detecting either the luminescence or fluorescence of metabolites using previously described protocols.[111] CYP2A6 activity was measured by the modification of coumarin to fluorescent 7-hydroxycoumarin (Sigma-Aldrich, St. Louis, MO), and CYP3A4 activity was measured by cleavage of luciferin-IPA into luminescent luciferin (Promega, Madison, WI). Live cultures containing PHHs were incubated with 2 μg/mL 5 (and 6)-carboxy-2',7'-dichlorofluorescein diacetate for 10 minutes in serum-free and phenol-free culture medium at 37°C, washed three times in serum-free and phenol-free culture medium, and imaged using the GFP (green fluorescent protein; 470 nm excitation, 510 nm emission) light cube on the microscope to visualize functional bile canaliculi. Endothelia were observed by the uptake of acetylated LDL (acLDL). Cultures were washed with phenol red-free media, incubated with 20 μg/mL Alexa Fluor®-conjugated acLDL (Life Technologies) for 3 hours at 37°C, and washed five more times before imaging with fluorescence microscopy (GFP).

6.2.7 Scanning Electron Microscopy

Cultures were fixed in glutaraldehyde (Sigma-Aldrich) diluted to 2.5% (v/v) in phosphate buffered saline (1× PBS, Corning) solution for 20 minutes at room temperature, and fixed cell cultures were washed 3 times with 1× PBS. Then, fixed samples were dehydrated through a series of washes using molecular grade ethanol (Fisher Scientific, Pittsburgh, PA) to dry the samples

thoroughly without damaging the cellular structures; washes were performed for 10 minutes each at 35%, 50%, 75%, 85%, 95%, 100%, and 100% (v/v) ethanol. Following the final ethanol wash, cultures were dried chemically with hexamethyldisilizane (Alfa Aesar) for 10 minutes, excess hexamethyldisilizane was removed, and samples were air dried for 10 minutes at room temperature. Prepared samples were secured to a specimen mount using carbon adhesive tabs. An SEM Coating unit E5100 Series II (Polaron Instruments, London, England) was used to sputter coat samples with a 4.125 nm thick gold/palladium layer, and samples were then imaged using a Hitachi S-3000 variable pressure scanning electron microscope (Research Resources Center, University of Illinois at Chicago).

6.2.8 Data Analysis

Each experiment was carried out in triplicate wells for each condition. Studies were repeated in two PHH and two LSEC donors to confirm trends. Data processing and visualization were performed using Microsoft Excel and GraphPad Prism (La Jolla, CA). Gene expression data was calculated as fold changes with respect to pure LSECs using the $\Delta\Delta C_T$ method with *GAPDH* as the housekeeping gene. Statistical significance was determined with a one- or two-way ANOVA followed by a Bonferroni pair-wise post-hoc test ($p < 0.05$).

6.3 Results

6.3.1 Comparison of PHH/Endothelial and PHH/Fibroblast Co-Cultures

Primary human LSECs and HUVECs displayed prototypical endothelial morphology for up to 6 passages *in vitro* (Figure 6.1) and could be subsequently used for co-cultivation with PHHs. Micropatterned co-cultures of PHHs and endothelial cells (either LSECs or HUVECs) were compared with co-cultures of PHHs and 3T3-J2 fibroblasts (Figure 6.2A); in such co-cultures, 30K PHHs were surrounded by 90K NPCs. Both PHH/LSEC and PHH/HUVEC co-cultures displayed

a loss of prototypical hepatic morphology (i.e. polygonal shape, multi-nucleation, and visible bile canaliculi) over 2 weeks (Figure 6.2B). In contrast, PHH/fibroblast co-cultures maintained hepatic morphology over at least 2 weeks. Micropatterned PHH mono-cultures spread out (de-differentiated) as expected from a previous study.[54]

At the functional level, PHH/fibroblast co-cultures outperformed PHH/endothelial cell co-cultures. Albumin (Figure 6.3A) and urea secretions (Figure 6.3B), CYP3A4 activity (Figure 6.3C), and CYP2A6 activity (Figure 6.3D) in PHH/endothelial cell co-cultures had steady-state values that were ~5-20% of the values in PHH/fibroblast co-cultures. The PHH/fibroblast co-cultures maintained stable levels of all measured functions over 3 weeks, whereas most functions in PHH/endothelial cell co-cultures declined over time. Modulating the PHH:endothelial ratio to 5:1 (physiologic[18]) or 1:4 in co-cultures did not rescue the PHH phenotype (data not shown). Furthermore, co-cultures created using a second donor of LSECs followed similar trends in albumin secretions, urea secretions, CYP3A4 activity, and morphology (Figure 6.4). Nonetheless, PHH/LSEC co-cultures had statistically higher albumin secretions than PHH/HUVEC co-cultures (i.e. ~3.7 fold on day 7 and ~10 fold on day 11) and PHH mono-cultures (undetectable levels) until 11 days in culture, whereas urea secretion and CYP450 enzyme activities were statistically similar (Figure 6.3). Finally, immortalized human liver endothelial cells (TMNK line)—previously used for co-culture with PHHs[237]—were also not able to stabilize PHH morphology or functions (Figure 6.5).

The effects of endothelial cells on PHH functions in co-cultures were observed irrespective of the culture medium formulation since subjecting the PHH/endothelial co-cultures to endothelial culture medium (as that used for expanding pure endothelial cells) or hepatocyte culture medium or a 1:1 mixture of the two types of media did not enable long-term rescue of the PHH phenotype

(data not shown); thus, supplementing the hepatocyte medium with VEGF, a previously developed hepatocyte-endothelial culture medium[224], was used for the remainder of the studies. Therefore, LSECs, but not HUVECs, can induce transient and statistically significant albumin secretion in PHHs for ~11 days; however, neither endothelial cell type can induce functions to the same magnitude and stability as the 3T3-J2 fibroblasts irrespective of PHH-to-endothelial ratio and medium formulation.
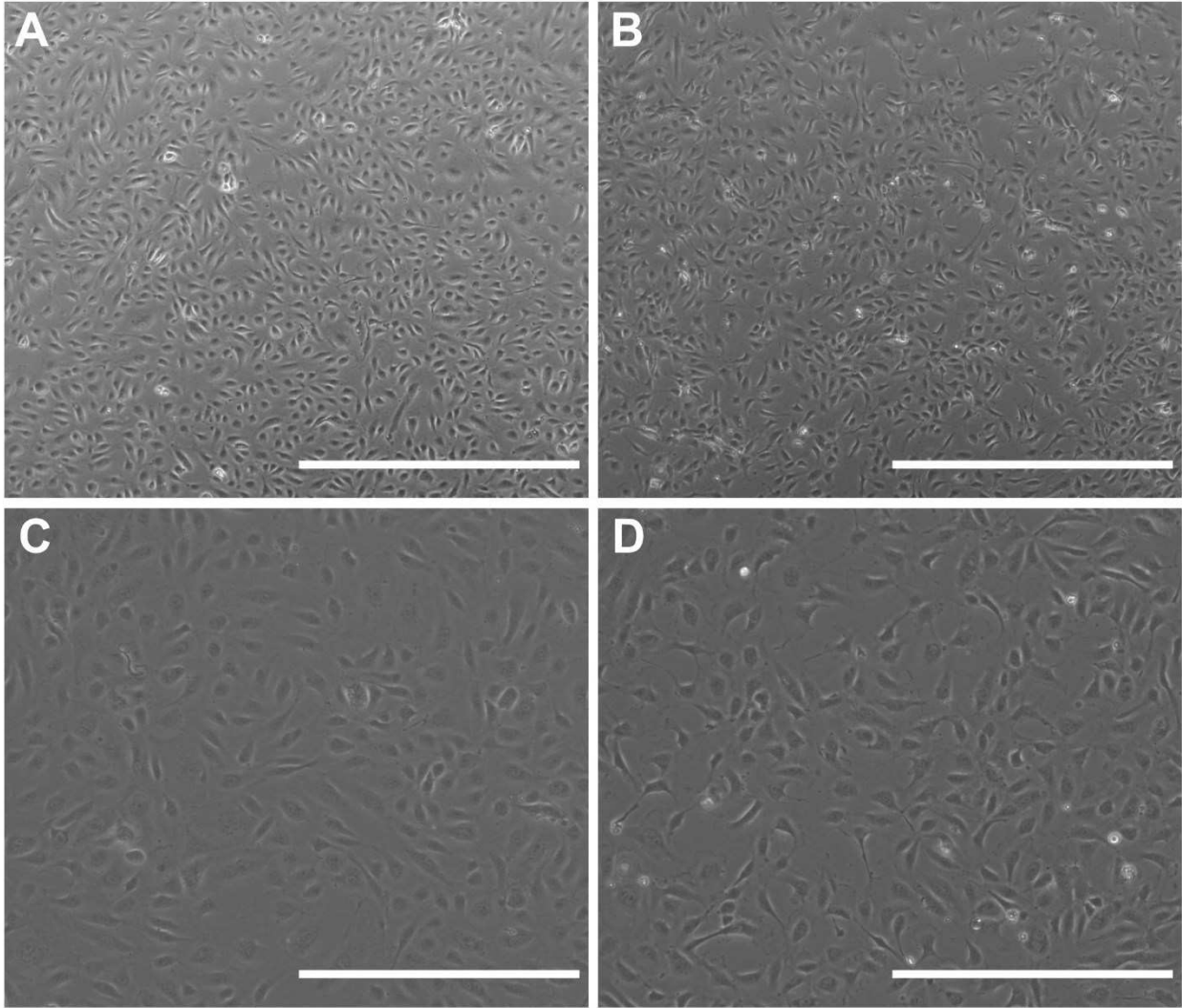
Figure 6.1: Morphology of pure endothelial cells during expansion. Prior to co-culture with PHHs, endothelial cells were expanded in tissue culture flasks as pure cultures up to 6 passages. Both **(A, C)** primary human LSECs and **(B, D)** HUVECs displayed similar morphological characteristics. **(A-B)** Scale bars = 1000 µm; **(C-D)** Scale bars = 400 µm.
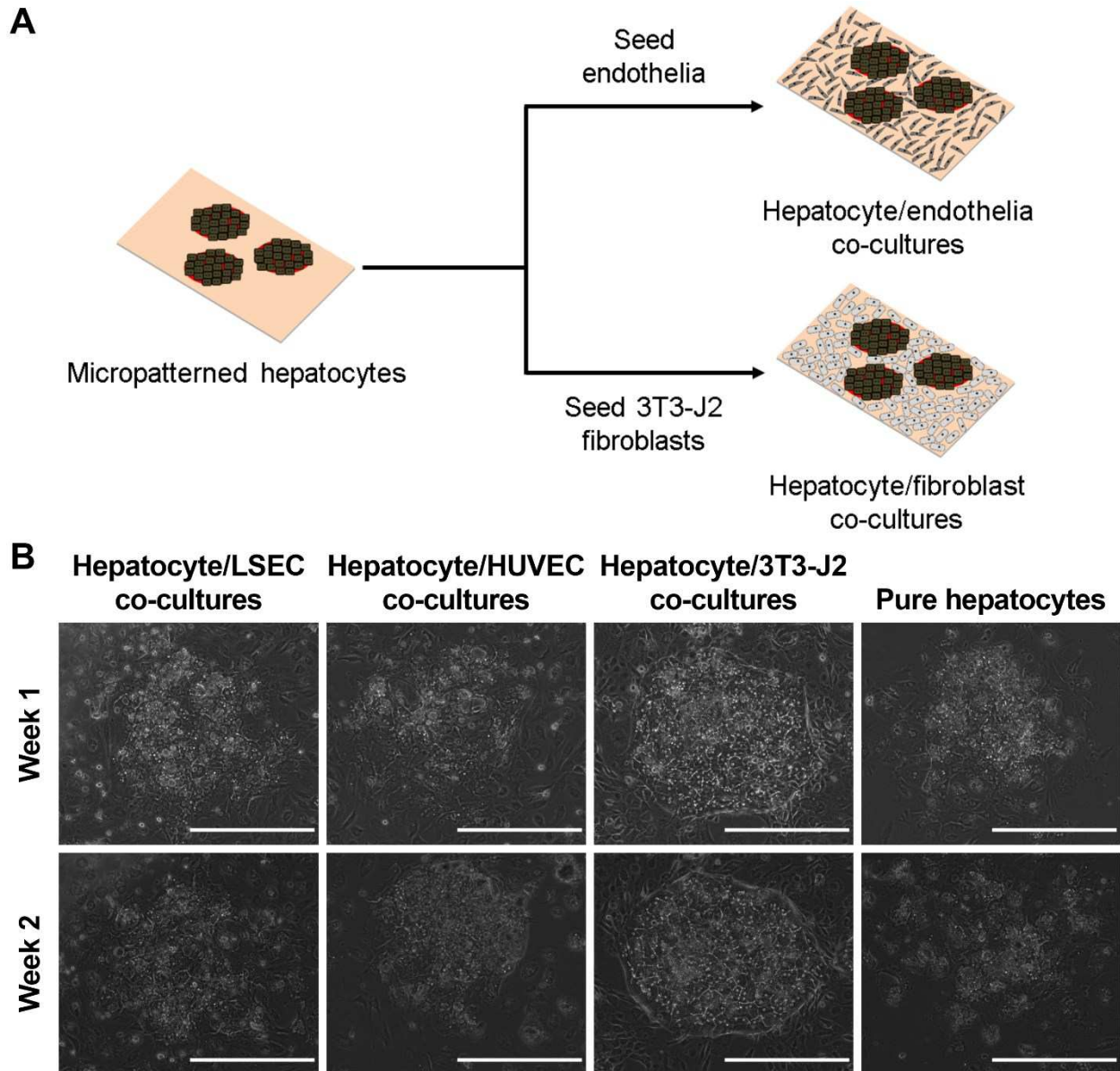
Figure 6.2: Morphology of PHH/endothelial cell and PHH/3T3-J2 fibroblast co-cultures relative to PHH mono-cultures. (A) Schematic depicting the creation of the co-culture models. PHHs were micropatterned using soft-lithography to control for homotypic interactions and then surrounded by NPCs as described previously.[66] **(B)** Morphology of different co-culture models over the course of two weeks in comparison to the pure PHH mono-cultures (right). Note the prototypical PHH morphology (i.e. polygonal shape, multi-nucleation, and presence of visible bile canaliculi) in the PHH/fibroblast co-cultures and spread-out (de-differentiated) morphology in the PHH mono-cultures. All scale bars = 400 μm.
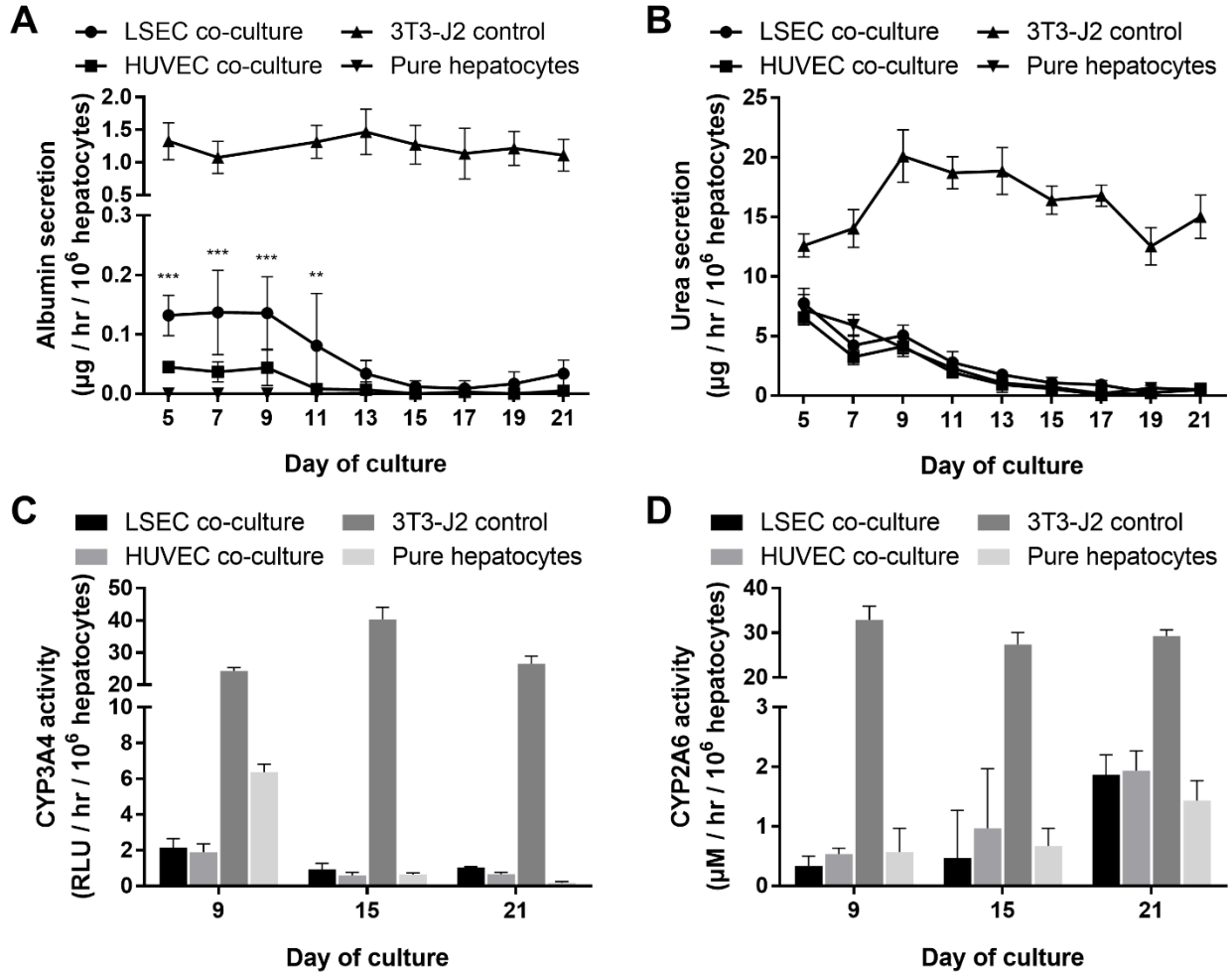
Figure 6.3: Hepatic functions in PHH/endothelial cell and PHH/3T3-J2 fibroblast co-cultures relative to PHH mono-cultures. Co-cultures and PHH mono-cultures were created as depicted in Figure 6.2A (all culture models shown contained micropatterned PHHs) followed by an assessment of hepatic functions over time, including **(A)** albumin secretion, **(B)** urea secretion, **(C)** CYP3A4 enzyme activity, and **(D)** CYP2A6 enzyme activity. Error bars represent standard deviations (n = 3 wells). $**p < 0.01$ and $***p < 0.001$ between the PHH/LSEC co-cultures and PHH/HUVEC co-cultures or PHH mono-cultures.
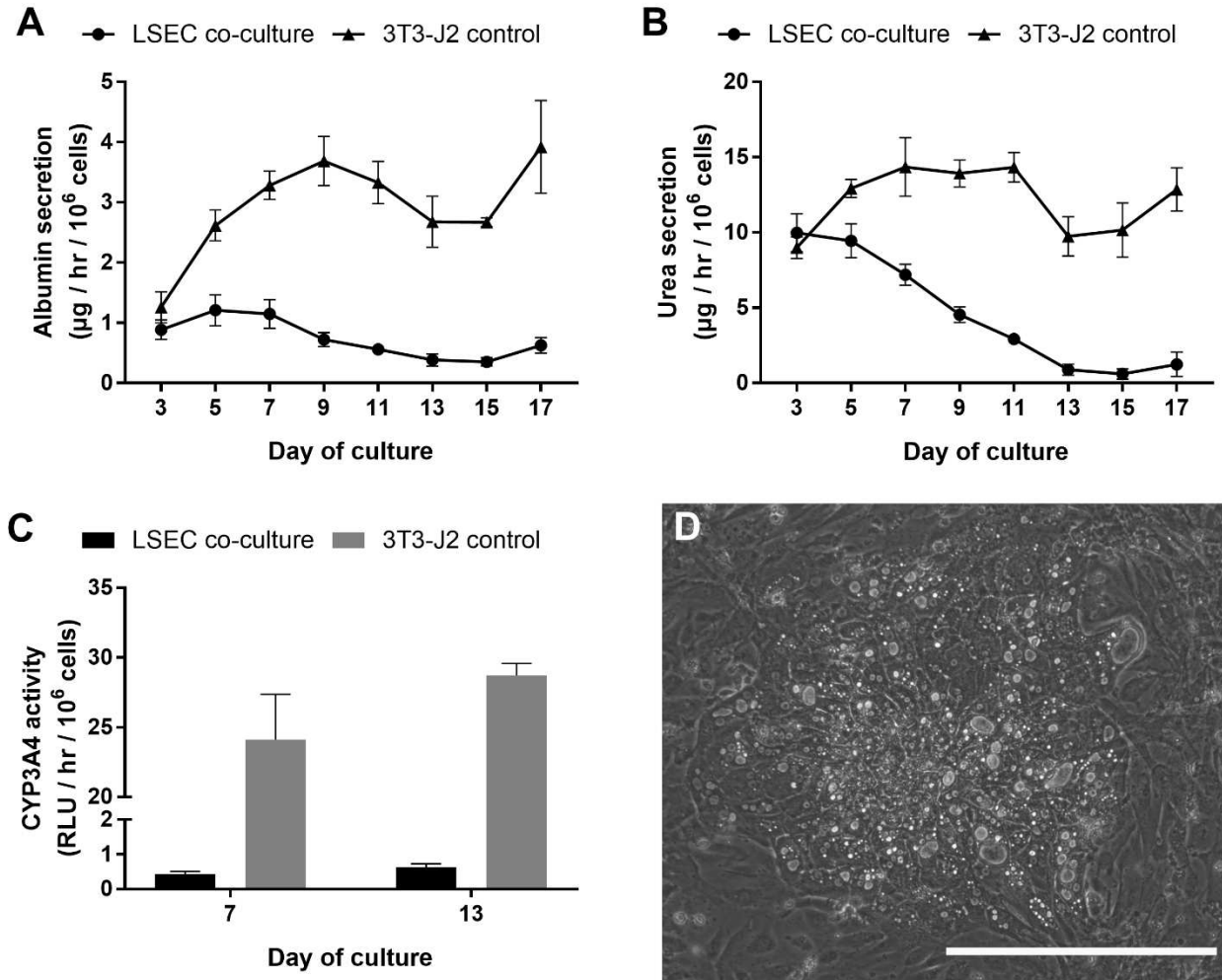
Figure 6.4: PHH/endothelial cell co-cultures creating using a second primary human LSEC donor relative to PHH/fibroblast control co-cultures. Co-cultures were created as depicted in Figure 6.2A (all culture models shown contained micropatterned PHHs) followed by an assessment of hepatic functions over time, including **(A)** albumin secretion, **(B)** urea secretion, and **(C)** CYP3A4 enzyme activity. Error bars represent standard deviations (n = 3 wells). **(D)** PHH morphology in PHH/LSEC co-cultures after 1 week, while PHH morphology in PHH/fibroblast co-cultures is shown in Figure 6.2B. Scale bar = 400 μm.
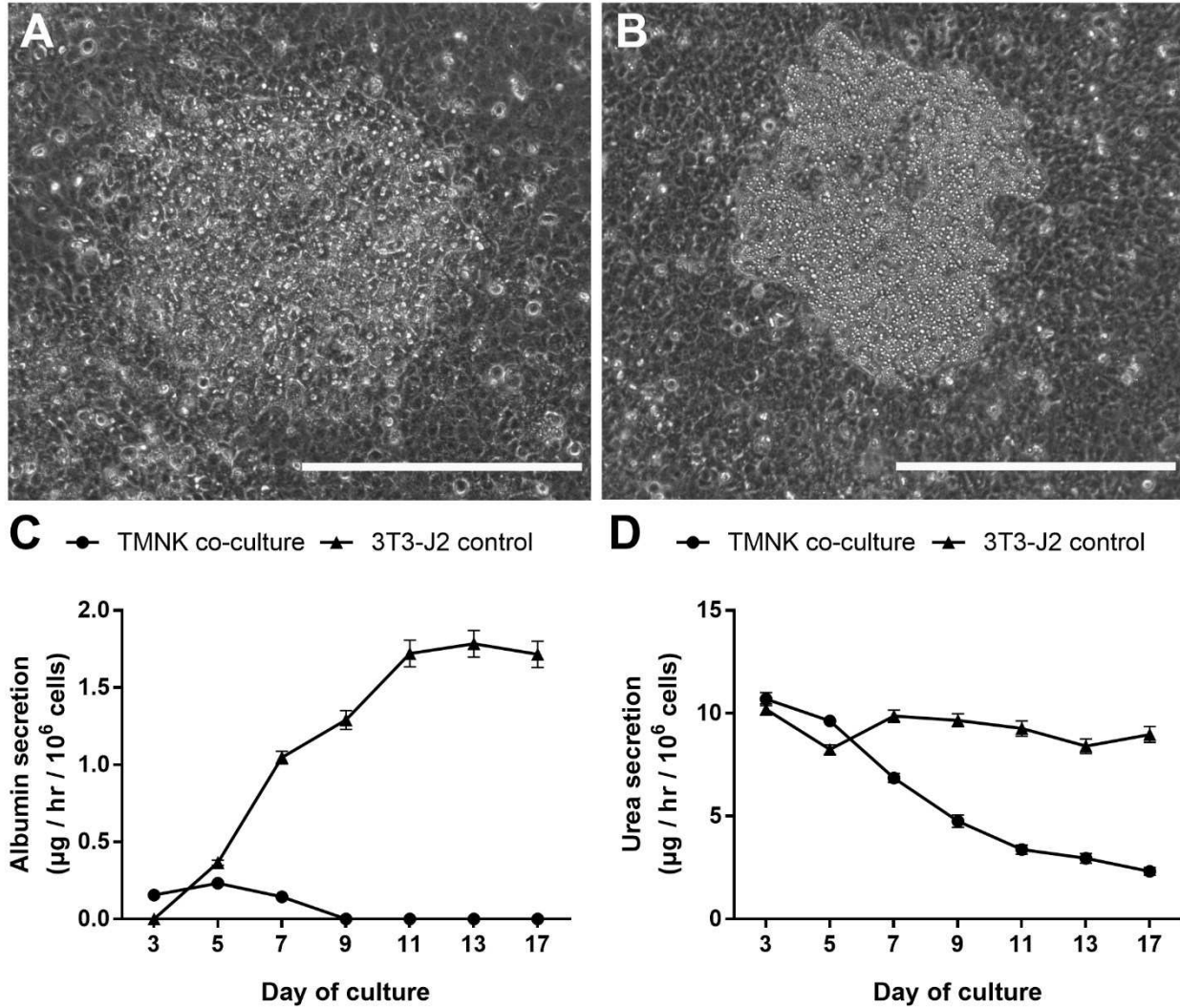
Figure 6.5: PHH/endothelial cell co-cultures created using the immortalized human liver endothelial cell line (TMNK) relative to PHH/fibroblast control co-cultures. Co-cultures were created as depicted in Figure 6.2A (all culture models shown contained micropatterned PHHs) followed by an assessment of PHH morphology in PHH/TMNK co-cultures after **(A)** 1 week and **(B)** 2 weeks. PHH morphology in PHH/fibroblast co-cultures is shown in Figure 2B. Scale bar = 400 μm. **(C)** Albumin and **(D)** urea secretions were also measured from the PHH/TMNK and PHH/fibroblast co-cultures over time. Error bars represent standard deviations (n = 3 wells).

6.3.2 Hepatic Phenotype in Co-Planar PHH/Fibroblast/Endothelial Tri-Cultures

As opposed to PHH/endothelial co-cultures, PHH/fibroblast/endothelial tri-cultures were seeded as shown in Figure 6.6A. Briefly, after PHHs attached and spread on micropatterned collagen-coated domains, a mixture of endothelial cells (LSECs or HUVECs) and 3T3-J2 fibroblasts was seeded and filled the remaining area around the PHH colonies. A PHH:endothelial cell ratio of 5:1 was selected to match that observed *in vivo*. Over the course of 3 weeks, PHH/fibroblast/LSEC and PHH/fibroblast/HUVEC tri-cultures displayed a hepatic morphology comparable to that observed in PHH/fibroblast co-cultures with respect to multi-nucleation, polygonal shape, and the presence of visible bile canaliculi between hepatocytes (Figure 6.6B).

At the functional level, when treated with the bile canaliculi stain, 5 (and 6)-carboxy-2',7'-dichlorofluorescein diacetate (substrate for multidrug resistant-like proteins 2/3 transporters[155]), adjacent PHHs in the tri-cultures displayed functional bile canaliculi as in the PHH/fibroblast co-cultures, whereas PHH mono-cultures displayed little to no functional bile canaliculi (Figure 6.7). Furthermore, PHH/fibroblast/endothelial cell tri-cultures secreted albumin (Figure 6.8A) and urea (Figure 6.8B) at steady-state levels of ~1.4 μg/hr/10^6 cells and ~12 μg/hr/10^6 cells, respectively, for 3 weeks; these secretion levels were statistically similar to the levels measured in PHH/fibroblast co-cultures. Similarly, CYP3A4 (Figure 6.8C) and CYP2A6 (Figure 6.8D) enzyme activities were statistically similar across the tri-cultures and PHH/fibroblast co-cultures. On the other hand, PHH mono-cultures displayed a severe decline in functions (Figure 6.8). Furthermore, the above-mentioned morphological and functional trends in tri-cultures relative to co-cultures were also observed with a second primary LSEC donor (Figure 6.9). However, in contrast to primary human LSECs and primary HUVECs, the use of the immortalized TMNK line

in tri-cultures with fibroblasts did not lead to stable PHH morphology or functions (Figure 6.10),

likely due to over-growth of the TMNK cells.
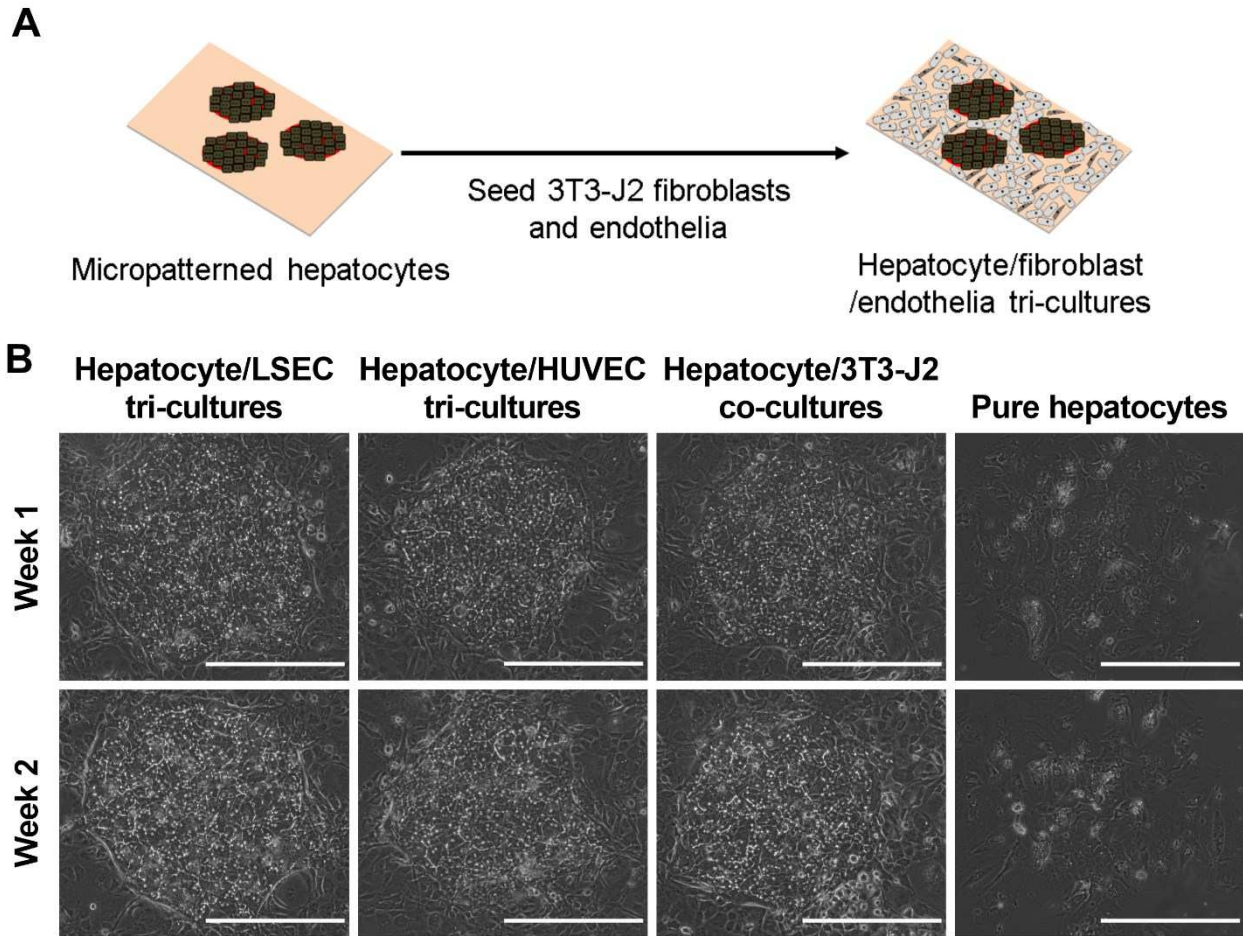
Figure 6.6: Morphology of PHH/fibroblast/endothelial cell tri-cultures (containing either LSECs or HUVECs) relative to PHH/3T3-J2 fibroblast control co-cultures and PHH mono-cultures. (A) Schematic depicting the creation of the tri-cultures, while co-cultures were created as depicted in Figure 6.2A. **(B)** Morphology of tri-cultures models over the course of two weeks in comparison to the PHH/fibroblast co-cultures and pure PHH mono-cultures. Note the prototypical PHH morphology (i.e. polygonal shape, multi-nucleation, and presence of visible bile canaliculi) in the tri-cultures/co-cultures and spread-out (de-differentiated) morphology in the PHH mono-cultures. All scale bars = 400 μm.
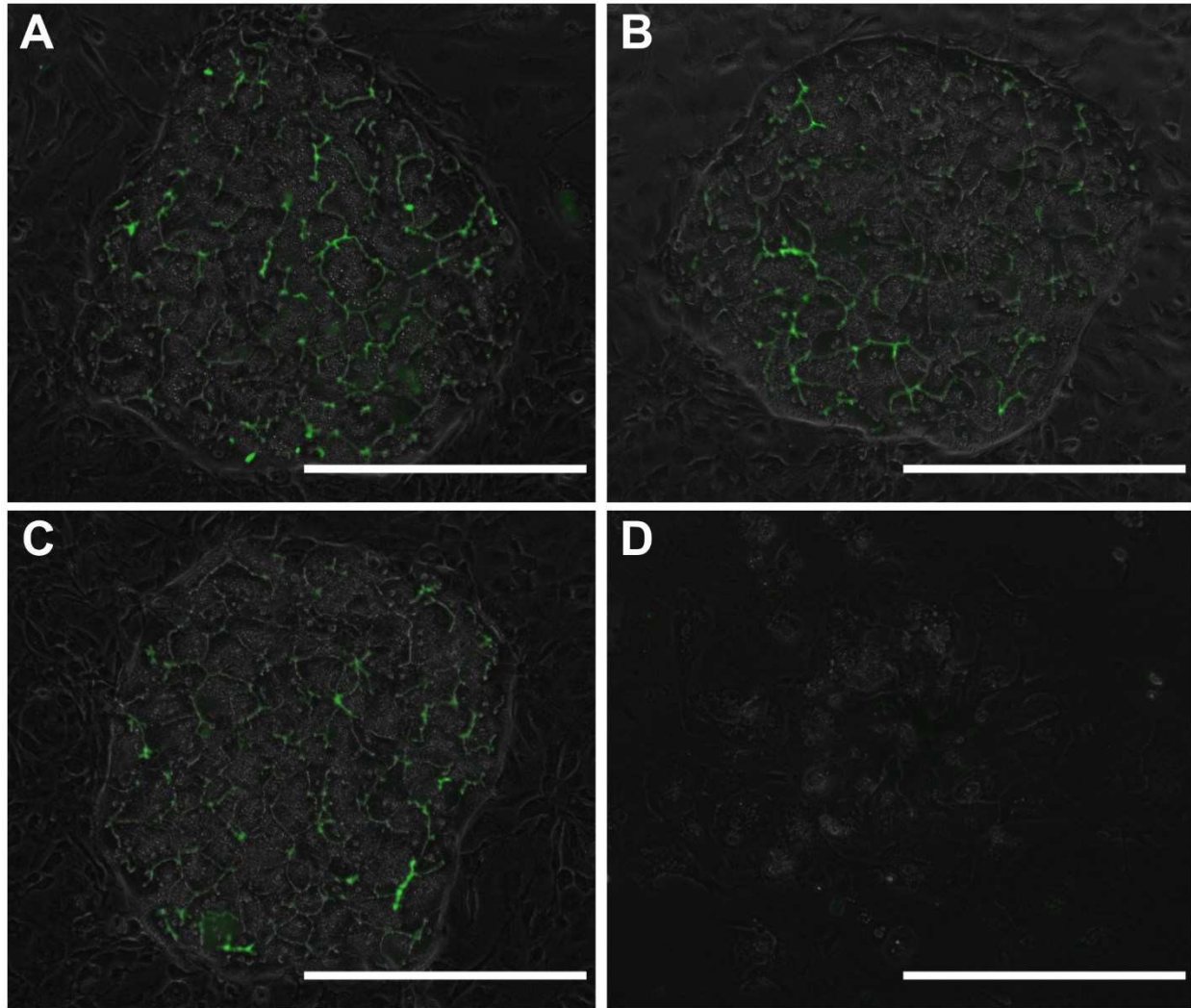
Figure 6.7: Bile canaliculi staining in PHH/fibroblast/endothelial cell tri-cultures (containing either LSECs or HUVECs) relative to PHH/3T3-J2 fibroblast control co-cultures and PHH mono-cultures. Co-cultures and tri-cultures were created as depicted in Figures 6.2A and 6.6A (all culture models shown contained micropatterned PHHs), respectively, followed by an assessment of functional bile canaliculi (green stain) after 2 weeks as described in methods. Both **(A)** PHH/fibroblast/LSEC tri-cultures and **(B)** PHH/fibroblast/HUVEC tri-cultures contained active bile canaliculi as in **(C)** PHH/fibroblast co-cultures. **(D)** On the other hand, pure PHH mono-cultures showed no noticeable bile canaliculi. The bile canaliculi stain is overlaid on phase contrast image for each culture model. All scale bars = 400 μm.
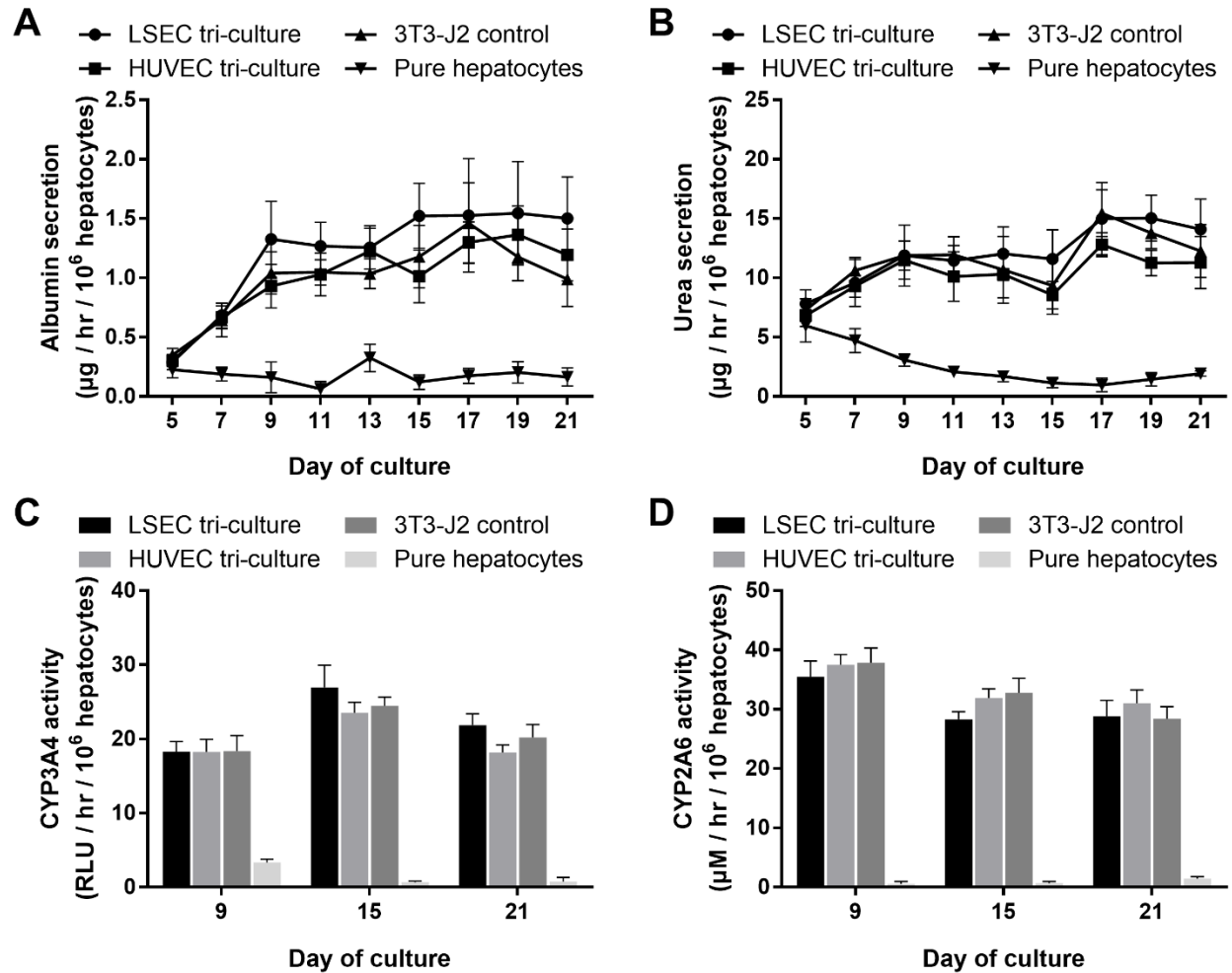
Figure 6.8: Hepatic functions in PHH/fibroblast/endothelial cell tri-cultures (containing either LSECs or HUVECs) relative to PHH/3T3-J2 fibroblast control co-cultures and PHH mono-cultures. Co-cultures and tri-cultures were created as depicted in Figures 6.2A and 6.6A (all culture models shown contained micropatterned PHHs), respectively, followed by an assessment of hepatic functions over time, including **(A)** albumin secretion, **(B)** urea secretion, **(C)** CYP3A4 enzyme activity, and **(D)** CYP2A6 enzyme activity. Error bars represent standard deviations (n = 3 wells).
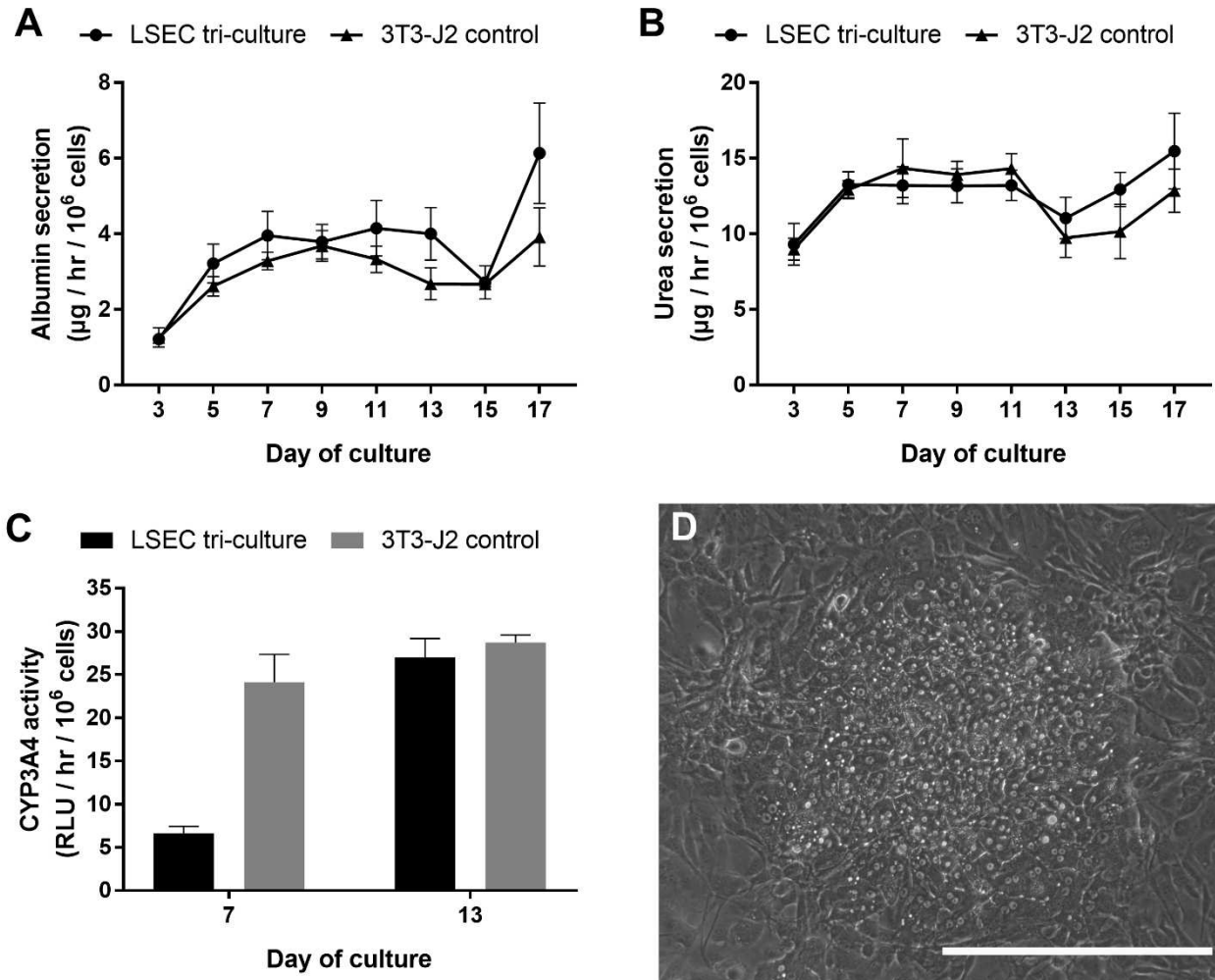
Figure 6.9: PHH/fibroblast/endothelial cell tri-cultures creating using a second primary human LSEC donor relative to PHH/fibroblast control co-cultures. Co-cultures and tri-cultures were created as depicted in Figures 6.2A and 6.6A, respectively, followed by an assessment of hepatic functions over time, including **(A)** albumin secretion, **(B)** urea secretion, and **(C)** CYP3A4 enzyme activity. Error bars represent standard deviations (n = 3 wells). **(D)** PHH morphology in PHH/fibroblast/LSEC tri-cultures after 1 week, while PHH morphology in PHH/fibroblast co-cultures is shown in Figure 6.2B. Scale bar = 400 μm.
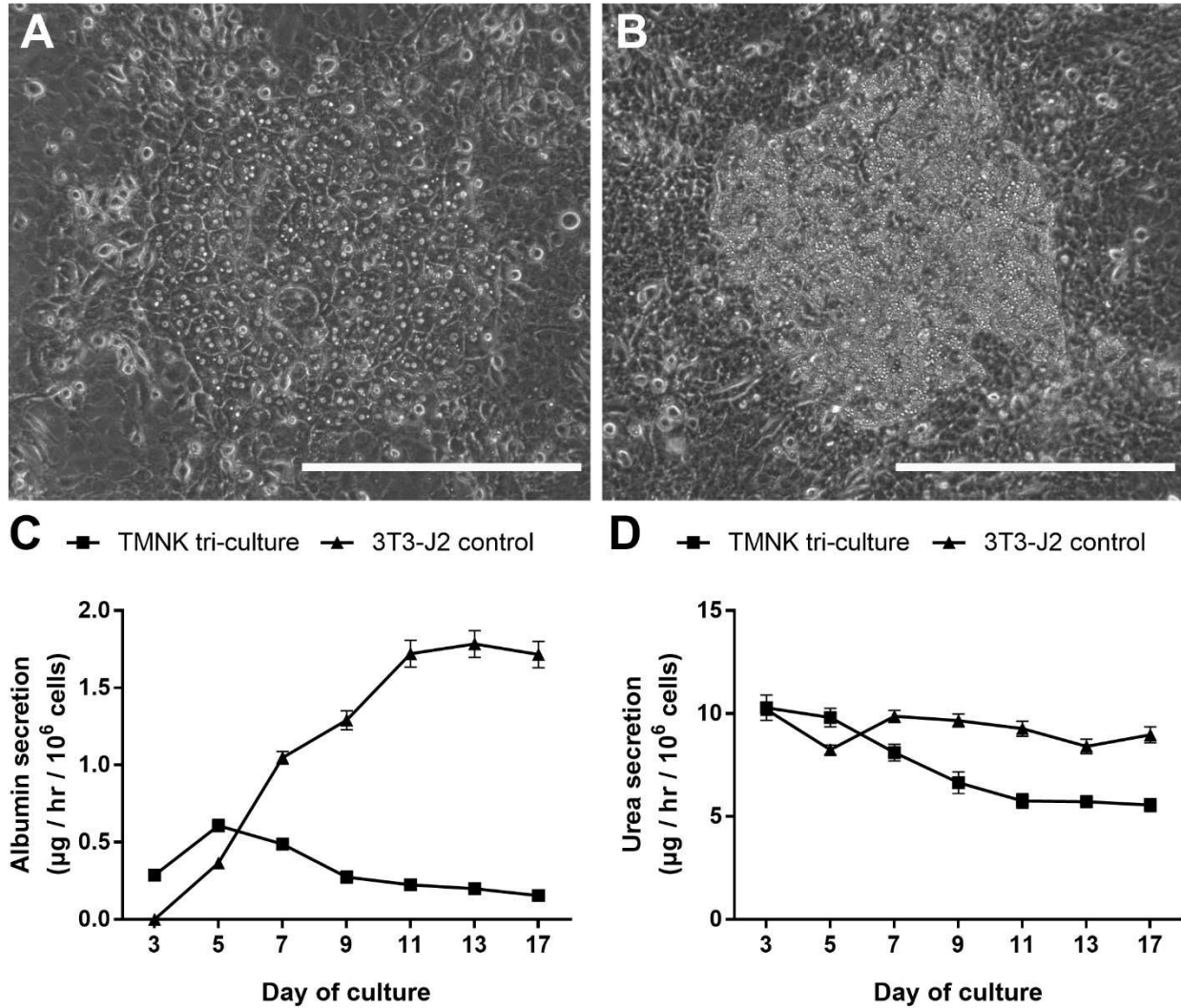
Figure 6.10: PHH/fibroblast/endothelial cell tri-cultures created using the immortalized human liver endothelial cell line (TMNK) relative to PHH/fibroblast control co-cultures. Co-cultures and tri-cultures were created as depicted in Figures 6.2A and 6.6A, respectively, followed by an assessment of PHH morphology in PHH/fibroblast/TMNK tri-cultures after **(A)** 1 week and **(B)** 2 weeks. PHH morphology in PHH/fibroblast co-cultures is shown in Figure 2B. Scale bar = 400 μm. **(C)** Albumin and **(D)** urea secretions were also measured from the PHH/fibroblast/TMNK and PHH/fibroblast control co-cultures over time. Error bars represent standard deviations (n = 3 wells).

6.3.3 Endothelial Phenotype in Co-Planar PHH/Fibroblast/Endothelial Tri-Cultures

The presence of endothelial cells in tri-cultures over time was confirmed via gene expression analysis. Specifically, *CD31* (Figure 6.11A) and *CD54* (Figure 6.11B) gene expression levels increased in PHH/fibroblast/endothelial cell tri-cultures, while *F8* (Figure 6.11C) and *vWF* (Figure 6.11D) expression levels were relatively stable in tri-cultures over the course of 3 weeks. In PHH/endothelial cell co-cultures, all the above-mentioned gene expression markers were detected over 3 weeks; however, similarities and differences with the tri-cultures were observed. *CD31* gene expression in PHH/endothelial cell co-cultures was generally lower than tri-cultures over 3 weeks; *CD54* gene expression in co-cultures was higher than tri-cultures; *F8* gene expression in PHH/LSEC co-cultures was lower than PHH/fibroblast/LSEC tri-cultures but similar between PHH/HUVEC co-cultures and PHH/fibroblast/HUVEC tri-cultures; and *vWF* expression in co-cultures was higher than tri-cultures. We also verified using SEM the presence of fenestrations on LSECs in pure cultures (Figure 6.12A), when co-cultured with 3T3-J2 fibroblasts but without PHHs (Figure 6.12B), in PHH/LSEC co-cultures (Figure 6.12C), and in PHH/fibroblast/LSEC tri-cultures (Figure 6.12D). LSECs displayed noticeable fenestrations regardless of the culture format. We further characterized the cultures for the uptake of acLDL (Figure 6.13) and found that the fluorescence in hepatocyte/fibroblast/endothelia tri-cultures was more widespread than in hepatocyte/fibroblast co-cultures and micropatterned pure hepatocytes, although acLDL is also taken up by 3T3-J2 fibroblasts to a small extent. The above-mentioned endothelial characterization results show that both LSECs and HUVECs display prototypical markers over several weeks in both co-cultures and tri-culture configurations; however, the PHH phenotype is enhanced only in the presence of the fibroblasts in co-cultures and tri-cultures.
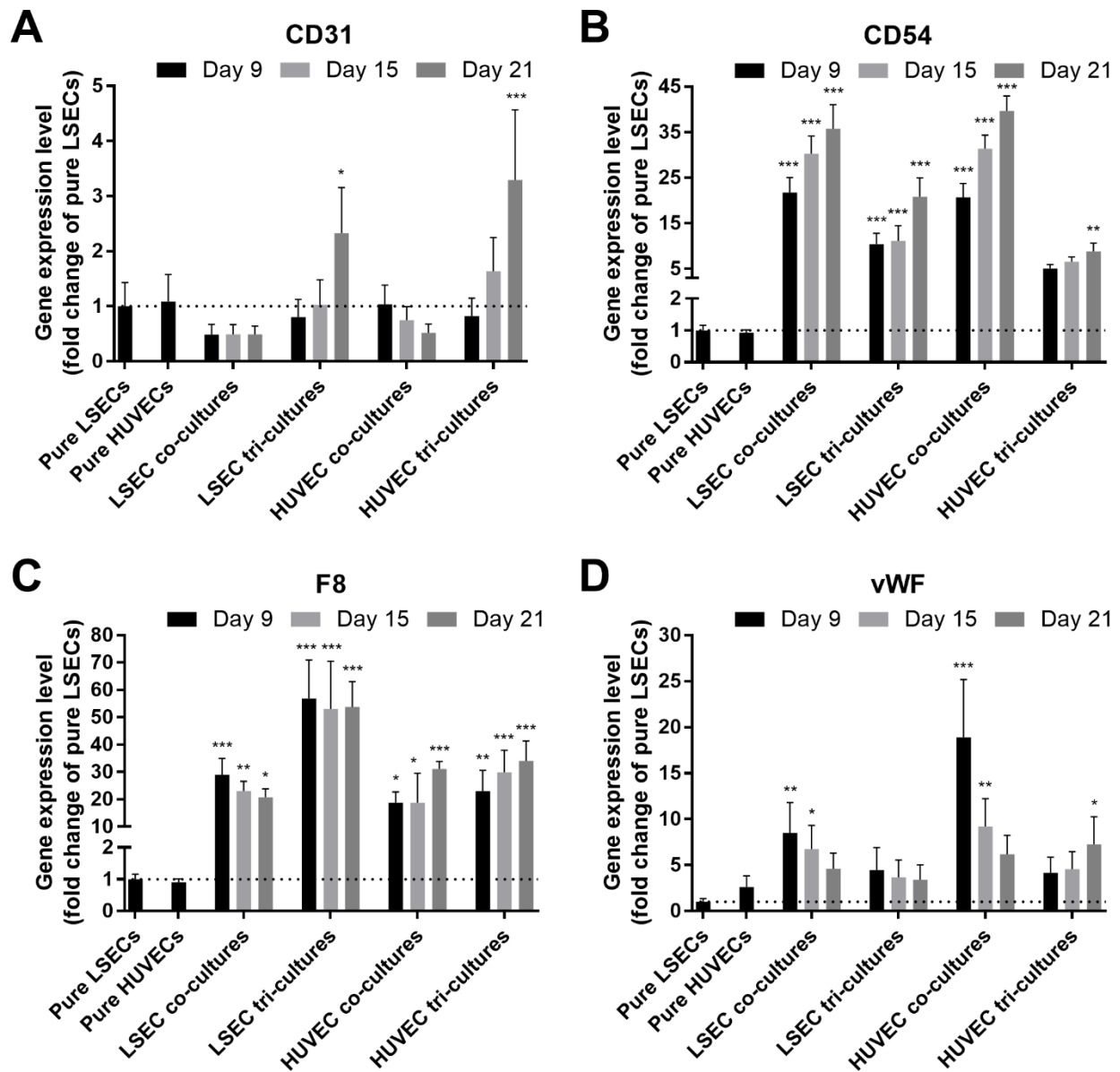
Figure 6.11: Endothelial gene expression patterns in different culture models. PHH/endothelial cell co-cultures and PHH/fibroblast/endothelial cell tri-cultures were created as depicted in Figures 6.2A and 6.6A, respectively, followed by evaluation of endothelial (HUVECs or LSECs) gene expression patterns over time using RT-qPCR, including **(A)** *CD31*, **(B)** *CD54*, **(C)** *F8*, and **(D)** *vWF*. Data plotted are fold changes with respect to pure LSECs calculated with the $\Delta\Delta C_T$ method using *GAPDH* as the housekeeping gene. Error bars represent standard deviations (n = 3 wells). *$p < 0.05$, **$p < 0.01$, and ***$p < 0.001$ between the co-culture or tri-culture condition relative to pure LSECs.
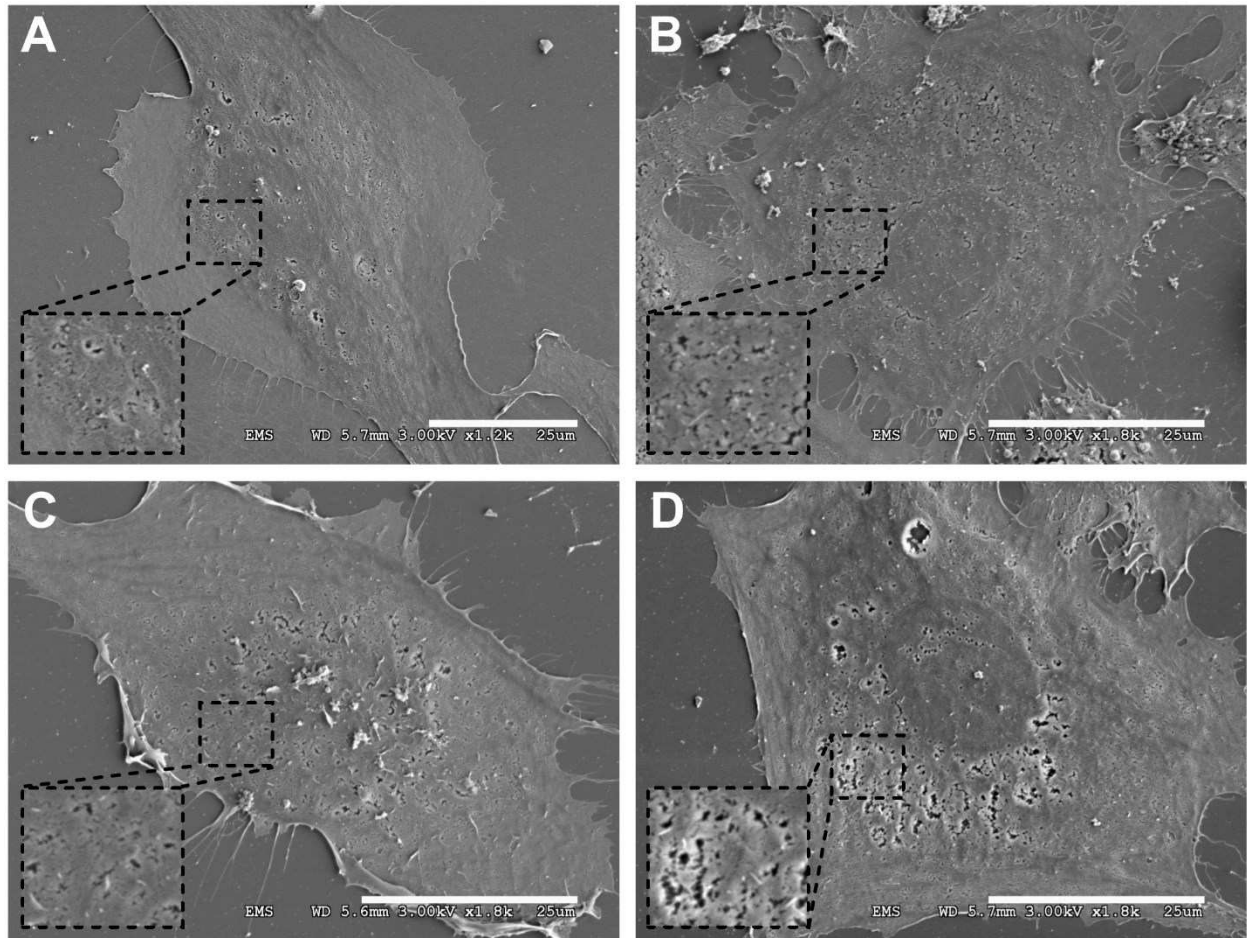
Figure 6.12: Visualization of fenestration via SEM in primary human LSECs in different culture models. **(A)** Pure LSEC cultures, **(B)** LSECs co-cultured with 3T3-J2 fibroblasts, **(C)** PHH/LSEC co-cultures, and **(D)** PHH/fibroblast/LSEC tri-cultures each display noticeable fenestrations. All scale bars = 25 μm.
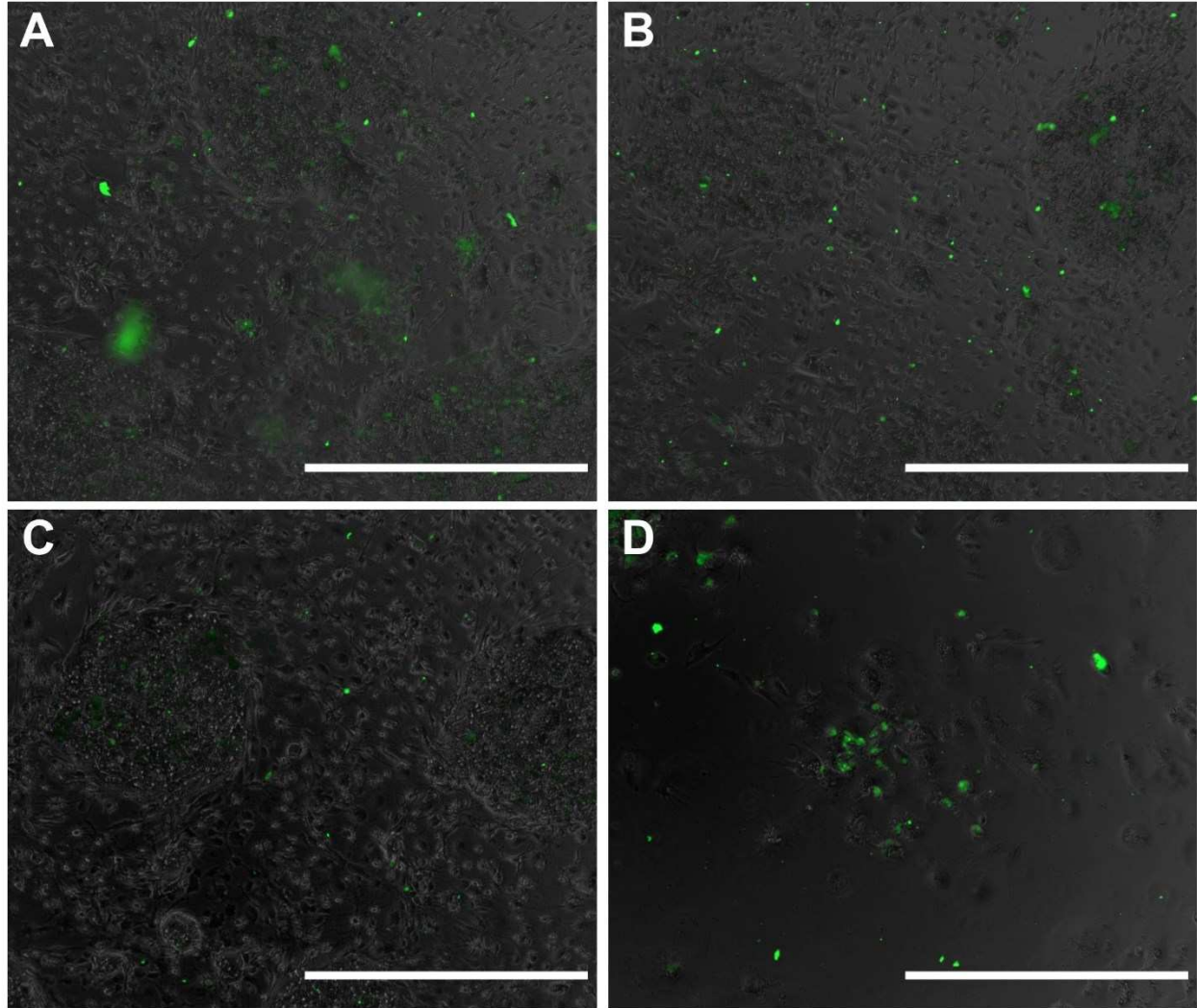
Figure 6.13: Uptake of acetylated LDL. After 3 weeks in culture, cultures were incubated with fluorescently labeled acetylated LDL (acLDL) and imaged with fluorescence microscopy. Both **(A)** hepatocyte/fibroblast/LSEC tri-cultures and **(B)** hepatocyte/fibroblast/HUVEC tri-cultures show more acLDL uptake than **(C)** hepatocyte/fibroblast co-cultures. Contrarily, **(D)** pure hepatocytes show sporadic acLDL uptake. All scale bars = 1000 μm.

6.3.4 Characterization of Layered PHH/Fibroblast/Endothelial Tri-Cultures

To mimic the space of Disse, we created a layered version of the tri-culture model by overlaying a PHH/fibroblast co-culture with a thin layer (250 μg/mL) of Matrigel™ and subsequently seeding endothelial cells (LSECs or HUVECs) on top of the gel (Figure 6.14A). As in the PHH/fibroblast/endothelial cell co-planar tri-culture model, PHHs in the layered configuration maintained prototypical hepatocyte morphology with polygonal shape, multi-nucleation, and visible bile canaliculi between adjacent PHHs (Figure 6.14B). On the other hand, micropatterned PHHs overlaid with Matrigel™ but without any NPC types deteriorated in morphology.

At the functional level, PHH/fibroblast/endothelial cell layered tri-cultures secreted albumin (Figure 6.15A) and urea (Figure 6.15B) at steady-state levels of ~1.4 μg/hr/10^6 cells and ~12 μg/hr/10^6 cells, respectively, for 3 weeks; these secretion levels were statistically similar to the levels measured in control PHH/fibroblast co-cultures with a Matrigel™ overlay. Similarly, CYP3A4 (Figure 6.15C) and CYP2A6 (Figure 6.15D) enzyme activities were ~20 RLU/hr/10^6 cells and ~32 μM 7-hydroxycoumarin/hr/10^6 cells for both PHH/fibroblast/endothelial cell layered tri-cultures and PHH/fibroblast co-cultures with Matrigel™ overlay. Overall, the layered tri-cultures were highly similar in hepatic morphology and functional levels over several weeks as the co-planar tri-cultures, suggesting that separating the endothelial cells from PHHs did not lead to higher induction of hepatic phenotype (compare Figure 6.6 and Figure 6.8 to Figure 6.14 and Figure 6.15).
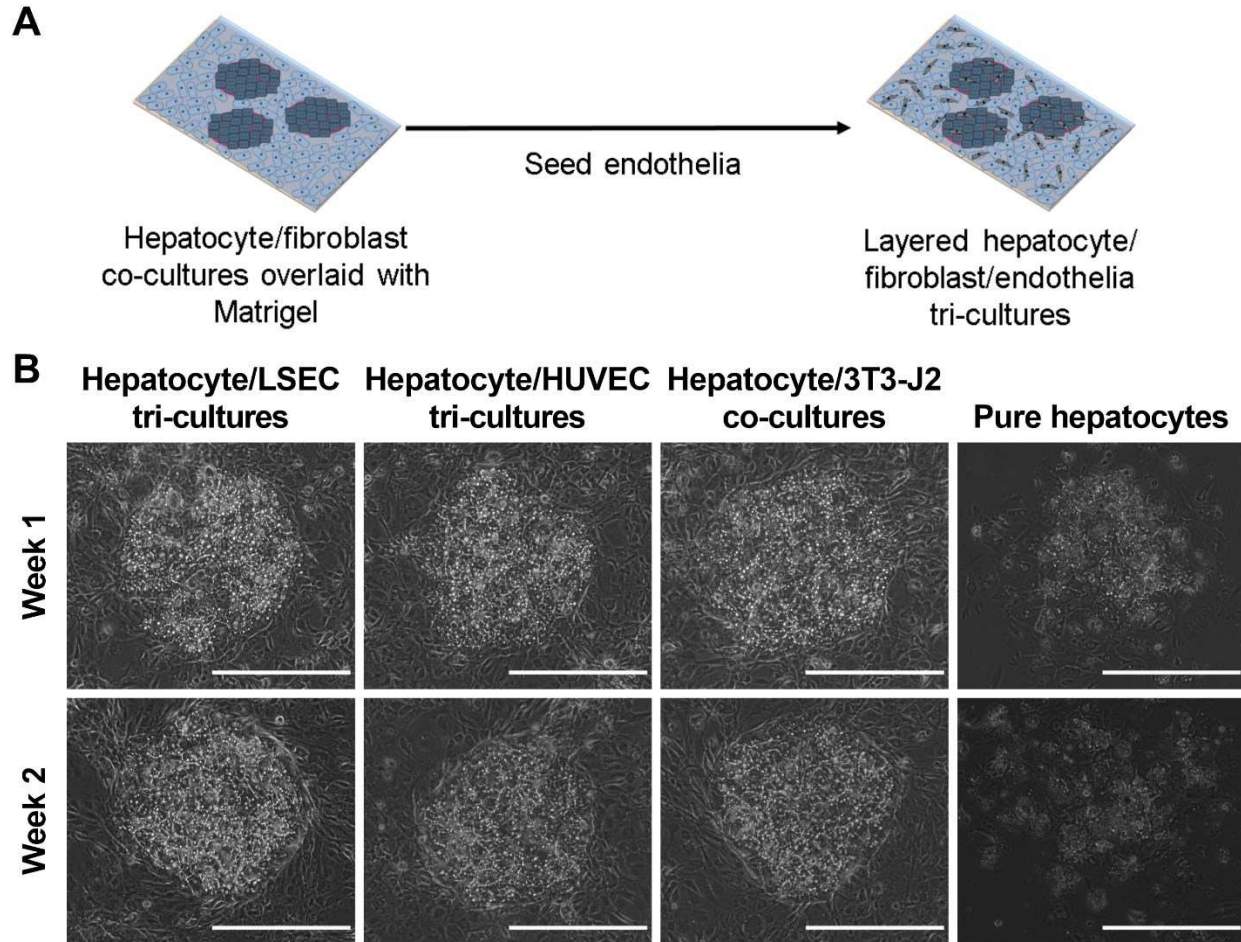
Figure 6.14: Morphology of layered PHH/fibroblast/endothelial cell tri-cultures (containing either LSECs or HUVECs) relative to PHH/3T3-J2 fibroblast control co-cultures and PHH mono-cultures. **(A)** Schematic depicting the creation of the layered tri-cultures; PHH/fibroblast control co-cultures and PHH mono-cultures were created as depicted in Figure 6.2A and subsequently overlaid with Matrigel™ to account for the effects of the protein gel on PHH functions. **(B)** Morphology of layered tri-cultures models over the course of two weeks in comparison to the Matrigel™-coated PHH/fibroblast co-cultures and Matrigel™-coated pure PHH mono-cultures. Note the prototypical PHH morphology (i.e. polygonal shape, multi-nucleation, and presence of visible bile canaliculi) in the tri-cultures/co-cultures and spread-out (de-differentiated) morphology in the PHH mono-cultures. All scale bars = 400 µm.
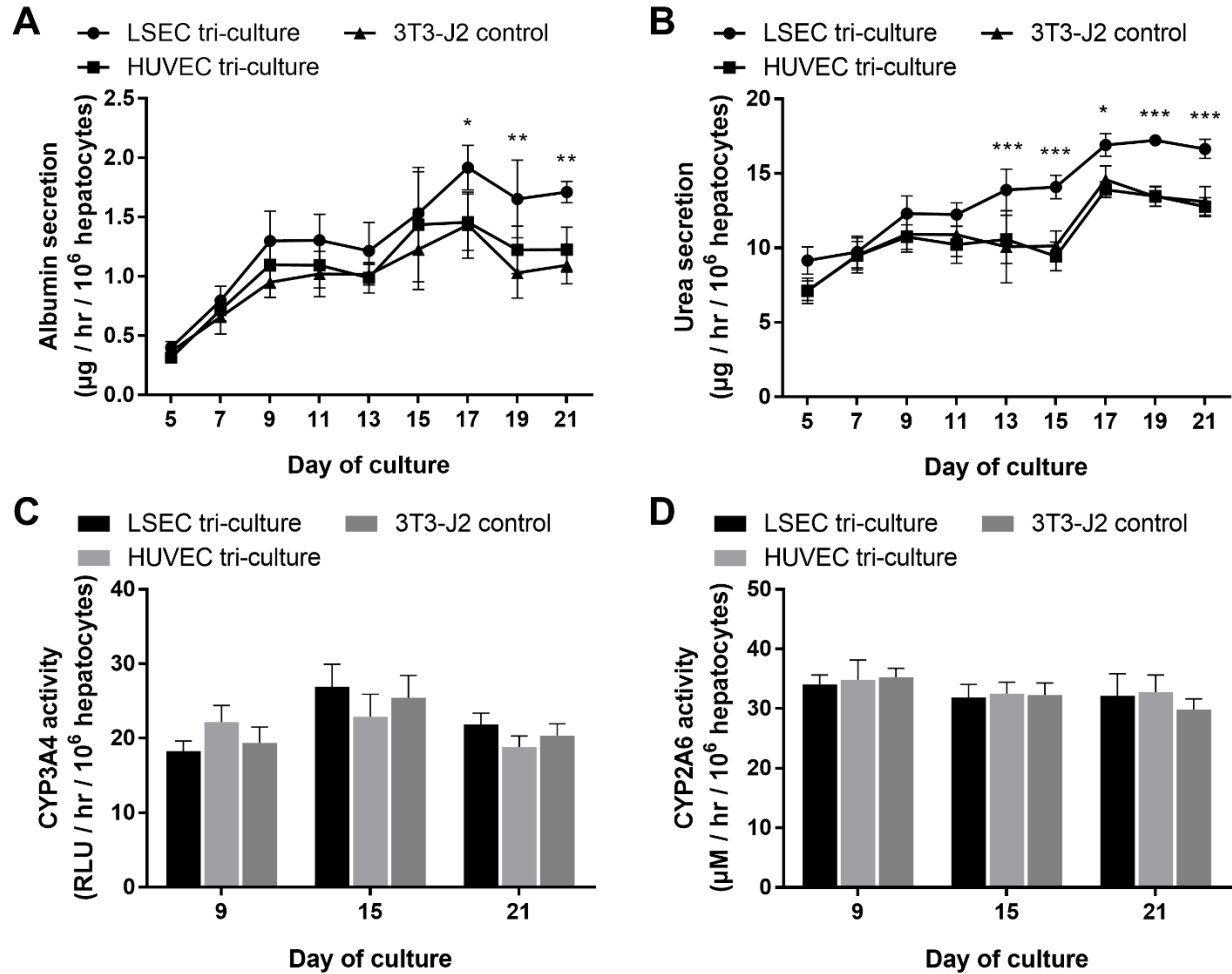
Figure 6.15: Hepatic functions in layered PHH/fibroblast/endothelial cell tri-cultures (containing either LSECs or HUVECs) relative to PHH/3T3-J2 fibroblast control co-cultures and PHH mono-cultures. Matrigel™-coated tri-cultures and co-cultures were created as described in Figure 6.14, followed by an assessment of hepatic functions over time, including **(A)** albumin secretion, **(B)** urea secretion, **(C)** CYP3A4 enzyme activity, and **(D)** CYP2A6 enzyme activity. Error bars represent standard deviations (n = 3 wells). $*p < 0.05$, $**p < 0.01$, and $***p < 0.001$ between the PHH/fibroblast/LSEC tri-cultures and PHH/fibroblast co-cultures.

6.3.5 Comparison of PHH Projected Surface Area in Various Culture Formats

To confirm qualitative observations of PHH spreading out or lack thereof in various culture formats, we quantified the projected surface area of PHHs cultured in all models developed here (Figure 6.16). PHHs in mono-cultures or in PHH/endothelial co-cultures tended to spread out and occupy more projected surface area. On the other hand, PHHs in cultures containing 3T3-J2 fibroblasts (PHH/fibroblast co-cultures, PHH/fibroblast/endothelial co-planar tri-cultures, or PHH/fibroblast/endothelial layered tri-cultures) maintained their polygonal shape and occupied less projected surface area.
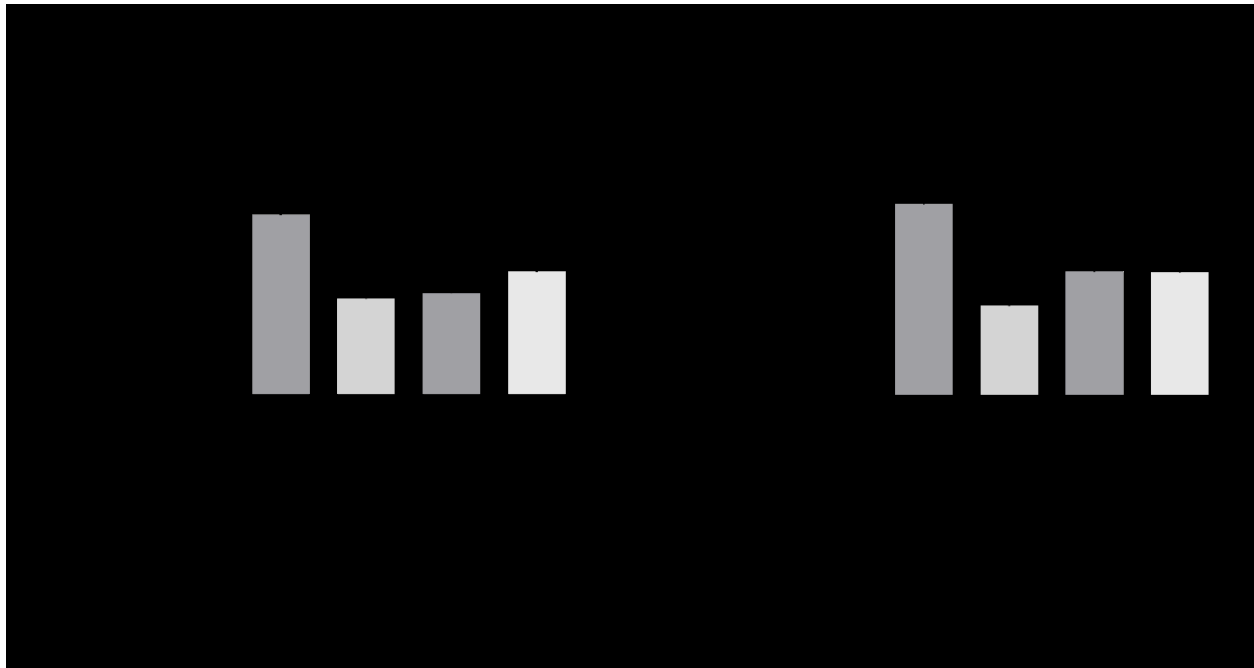
Figure 6.16: Quantification of projected PHH surface area in various culture formats. Co-cultures, tri-cultures, and layered tri-cultures were created as illustrated in Figures 6.2A, 6.6A, and 6.14A, respectively. After a week of culture, three PHHs from each of three independent islands of each condition were quantified for their projected cellular area. Cultures with **(A)** LSECs and **(B)** HUVECs both maintained smaller hepatocyte area when cultured in PHH/fibroblast/endothelia tri-cultures (with or without a Matrigel™ overlay) as compared to PHH/endothelia co-cultures. Error bars represent standard deviations (n = 9 hepatocytes per condition). *******p* < 0.01 and ***p < 0.001 between the indicated culture formats.

6.3.6 Drug Toxicity Studies

Upon exposure to $100 \times C_{max}$ azathioprine, both hepatocyte/fibroblast/LSEC and hepatocyte/fibroblast/HUVEC tri-cultures showed significantly reduced albumin secretions compared to hepatocyte/fibroblast co-culture controls (Figure 6.17A). Reducing the dose to $50 \times C_{max}$ azathioprine lessened the reduction of albumin secretions from hepatocyte/fibroblast/LSEC and hepatocyte/fibroblast/HUVEC tri-cultures. Interestingly, hepatocyte/fibroblast co-cultures showed little dose dependency with respect to albumin secretions between $50 \times C_{max}$ and $100 \times C_{max}$ azathioprine. Exposing hepatocyte/fibroblast/LSEC and hepatocyte/fibroblast/HUVEC tri-cultures to $100 \times C_{max}$ dacarbazine showed a minimal reduction in albumin secretions compared with hepatocyte/fibroblast co-cultures (Figure 6.17B). Lastly, treatment of both hepatocyte/fibroblast/LSEC and hepatocyte/fibroblast/HUVEC tri-cultures with $100 \times C_{max}$ monocrotaline showed a significant decrease in albumin secretions compared with hepatocyte/fibroblast co-cultures (Figure 6.17C).
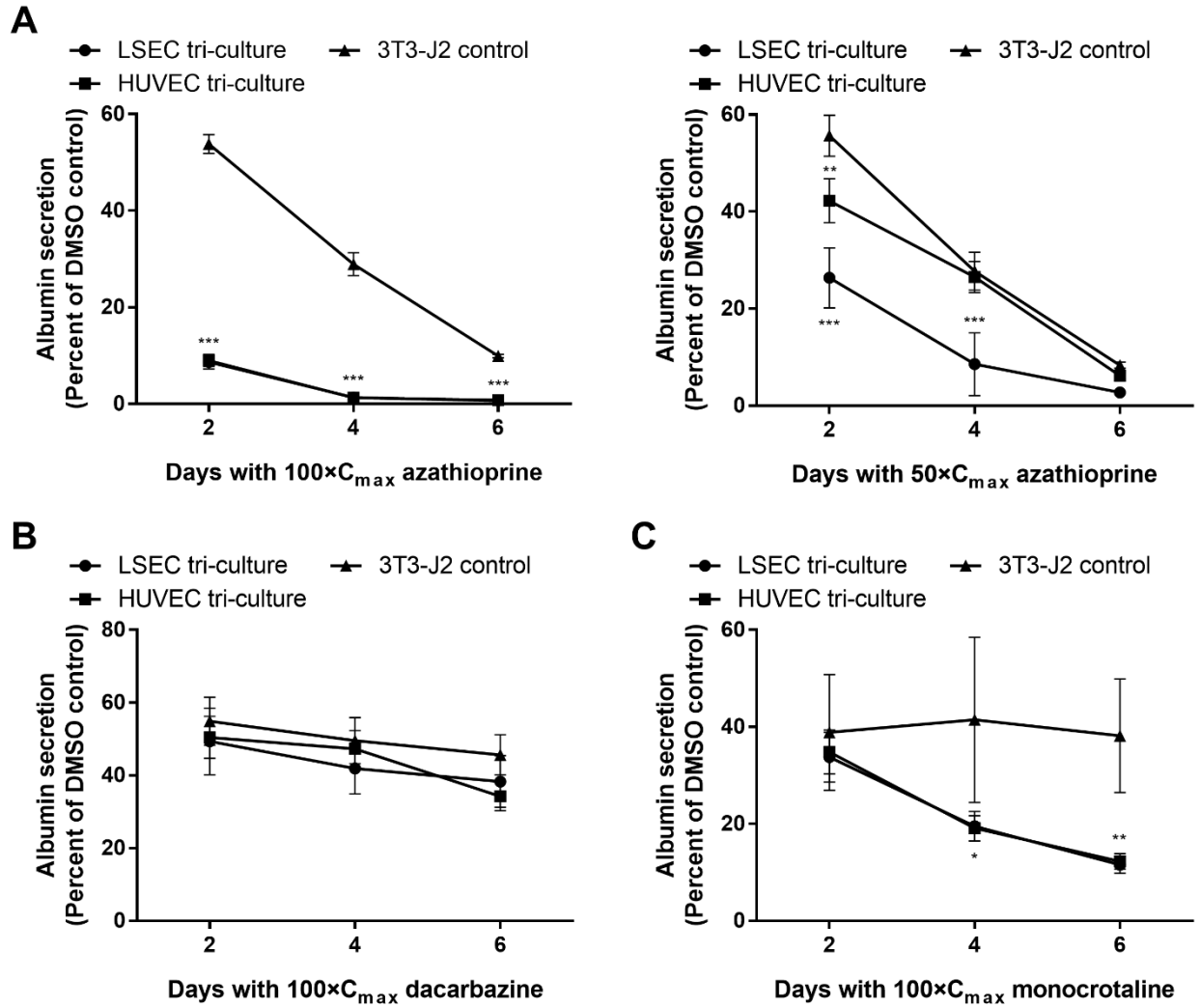
Figure 6.17: Drug toxicity screens in hepatocyte/fibroblast/endothelia tri-cultures. Albumin secretions were compared in tri-cultures of hepatocytes with 3T3-J2 fibroblasts and either LSECs or HUVECs dosed with **(A)** azathioprine at $100 \times C_{max}$ and at $50 \times C_{max}$, **(B)** dacarbazine at $100 \times C_{max}$, and **(C)** monocrotaline at $100 \times C_{max}$ for 6 days in serum-free media. Co-cultures of hepatocytes with 3T3-J2 fibroblasts are included for comparison. All data have been normalized to the respective DMSO-only controls. Error bars represent standard deviations (n = 3 wells). *p < 0.05, **p < 0.01, and ***p < 0.001 between tri-culture condition and 3T3-J2 control.

6.4 Discussion

In this study, we developed the first-of-its-kind cell culture platform that induces high and stable levels of phenotypic functions in both PHHs and primary human LSECs over the course of several weeks. We initially created co-cultures of PHHs and LSECs, while using HUVECs as the non-liver-endothelial cell control; micropatterning was used to control PHH homotypic interactions towards isolating the effects of PHH/NPC interactions.[154] Fibronectin was used here for enabling endothelial cell attachment since this ECM protein has been shown previously to facilitate the attachment of LSECs.[224] However, fibronectin is not amenable to the plasma ablation micropatterning technique utilized here (data not shown). Therefore, we used adsorbed collagen-I for creating micropatterned PHH colonies as in previous studies[56,154]; the use of collagen-I for PHH attachment is also widespread in the field of PHH culture.[142] Hepatic albumin secretion was statistically higher in PHH/LSECs co-cultures for ~11 days than in PHH/HUVEC co-cultures and PHH mono-cultures. However, the effects of both endothelial cell types on PHH phenotype were transient and functions declined over time irrespective of PHH-to-endothelial ratios and medium formulations tested.

Our observations with PHH/endothelial co-cultures are not entirely consistent with previously published data in co-cultures of rat hepatocytes and endothelial cells, which showed relatively stable functions for several weeks. For instance, the Noh group has shown that primary rat hepatocytes displayed relatively stable urea secretion for ~30 days when co-cultivated with immortalized bovine aortic endothelial cells.[85,225] In contrast, our use of an immortalized human liver endothelial cell line (TMNK) did not lead to induction of high and stable PHH functions; we suspect that species-specific differences may be important in the discrepancies observed across the two studies, though we cannot entirely rule out the differences between the use of endothelial cells

from different organ systems. In a more directly comparable study utilizing primary rat hepatocyte and primary rat LSEC co-cultures, Bale *et al.* showed relatively stable albumin and urea secretions, and CYP1A activity over 4 weeks.[226] Some key differences with our study include the use of high concentration (~1 mg/mL) collagen-I gels by Bale *et al.* to sandwich hepatocytes and LSECs in various layers as well as species-specific differences in hepatocyte-LSEC interactions. Here, we did not use high concentration collagen-I gels since they are (a) difficult to miniaturize into 24-well and smaller plate formats (i.e. tend to be inconsistent in gelation height throughout the well and tend to peel off over a few days due to cell contraction), (b) can bind drugs when being used for screening assays, and (c) may represent a more fibrotic state of the liver in which the diverse collagens in the liver get replaced with high levels of collagen-I.[238,239] Thus, due to such limitations, collagen-I gel-based liver models are not routinely used in pharmaceutical practice.[5,240] Ultimately, our approach/model is human-specific and is more amenable to high-throughput applications in the drug development pipeline.

In contrast to declining functions in PHH/endothelial co-cultures, all the PHH functions measured (albumins and urea secretions, and CYP2A6 and CYP3A4 enzyme activities) were significantly higher and stable over 3 weeks in co-cultures of PHHs and 3T3-J2 murine embryonic fibroblasts. This mouse fibroblast cell line can induce functions in PHHs at levels closer to those observed in freshly isolated PHHs from the same donors.[66] More broadly, co-culture with both liver- and non-liver-derived NPC types, including those of 3T3 mouse fibroblast origin[158,241–247], has been long known to induce functions in primary hepatocytes from multiple species, including humans, which suggests that the molecular mediators underlying the "co-culture effect" are relatively well-conserved across species.[127,128] While the complete mechanism underlying the effects of 3T3-J2 fibroblasts on PHHs remains to be elucidated, 3T3-J2 fibroblasts express various

molecules found in the liver, such as decorin[158], VEGF-D[158], and T-cadherin[182], which have been implicated in the ability of these fibroblasts to induce functions in hepatocytes from multiple species.[5] Furthermore, 3T3-J2 fibroblasts have a lack of detectable liver functions, display contact inhibition that avoids over-growth, and are propagated easily before inclusion in co-culture.[54,127,152,158] More importantly, the use of 3T3-J2 fibroblasts in co-culture with PHHs does not prevent the effective use of the stabilized PHHs for many applications in drug development, such as drug clearance prediction[56,180], drug metabolite identification[55], drug-transporter interactions[248], drug hepatotoxicity[58], hepatitis B/C viral infections[59,60], malaria infection[61,249], and steatosis and insulin resistance caused by hyperglycemia as in diabetes[62,111].

We utilized the above-mentioned "co-culture effect" here to create a tri-culture model in which (a) 3T3-J2 fibroblasts were used to stabilize PHHs to functional levels closer to physiological outcomes than possible with endothelial cells (LSECs or HUVECs), and (b) endothelial cells were introduced within the fibroblast monolayer at a physiologic ratio (1 endothelial cell:5 PHHs) to allow PHH/endothelial interactions as *in vivo*. Tri-cultures were created in both co-planar (i.e. all three cell types could interact via paracrine and contact signaling) and layered (separation of PHHs and LSECs via a gelled Matrigel™ layer to mimic the space of Disse) configurations. Matrigel™ is widely used to overlay PHHs with an ECM gel because it has diverse components, many of which are present in the liver (i.e. different collagen types instead of collagen-I alone and laminins).[142,250–252] The projected surface area, functions (albumin and urea secretions, and CYP3A4/2A6 enzyme activities), and active bile canaliculi of PHHs in both tri-culture configurations were remarkably similar to those observed in PHH/fibroblast co-cultures, suggesting that the ability of the fibroblasts to induce and stabilize functions in PHHs is not compromised by inclusion of endothelial cells; such an approach enables a well-differentiated

PHH phenotype independently (via the 3T3-J2 fibroblast support) of the PHHs' ability to interact with endothelial cells. Both the co-planar and layered tri-cultures were statistically similar with respect to PHH functions, suggesting that the *in vivo*-like separation between endothelial cells and PHHs does not induce greater levels of functions than when the cell types can interact via both paracrine and contact signaling. We selected the co-planar tri-culture configuration for all other studies since the lack of protein gels is preferred for drug development applications as described above. Nonetheless, the layered configuration can be highly useful when subjecting the tri-cultures to microfluidic perfusion in "liver-on-a-chip" platforms since it exposes the endothelial cells to shear stress while protecting the PHHs from shear stress as *in vivo*.

While we are the first group to our knowledge to create a human-relevant tri-culture platform utilizing PHHs, fibroblasts, and primary human endothelial cells (LSECs and HUVECs), our findings are consistent with tri-culture data obtained in rat liver platforms. For instance, March *et al.* combined primary rat hepatocytes and primary rat LSECs with 3T3 fibroblasts on a mechanically-actuated dynamic substrate[224]; this tri-culture model better preserved the phenotype of hepatocytes and fenestrations of LSECs relative to cultures without fibroblasts. In another study, Liu *et al.* found that their tri-culture system containing primary rat hepatocytes with 3T3 fibroblasts and HUVECs functionally outperformed the hepatocyte/endothelial co-culture control.[253] These findings suggest that 3T3 fibroblasts can stabilize hepatocyte and endothelial functions across both rodent and human species, which bodes well for utilization of hepatocyte/fibroblast/endothelial cell tri-cultures for elucidating species-specific mechanisms underlying physiological and pathophysiological phenomena. However, for drug development applications, well-documented differences in drug metabolism and toxicity pathways between

227

rodents and humans[44,58,145] necessitate the use of human-relevant liver models; our platform now provides the avenue for predicting the effects of drugs that act on PHHs and/or LSECs.

The sourcing of endothelial cells is a major consideration for building *in vitro* models of the human liver. Ideally, freshly isolated LSECs from human liver tissue would be used in all applications since they are the closest representation of human liver physiology; however, the routine use of this 'gold standard' cell type is not practical for drug screening applications that necessitates creation of on-demand cultures from the same donors via the use of cryopreserved cells towards mitigating donor-to-donor variability when testing a large number of compounds longitudinally.[56,254] Due to such limitations with freshly isolated primary human LSECs, most other groups rely on either immortalized human endothelial cells[87] or endothelial cells from other species and/or organ systems[85] when developing culture platforms for drug development. Several studies have co-cultivated hepatocytes with the TMNK immortalized human liver endothelial cells due to their ease of propagation[255–257]; however, here we show that in contrast to primary endothelial cells, TMNK cells cause a severe decline in PHH morphology and functions with or without fibroblasts, likely due to over-growth. On the other hand, we could passage primary human LSECs from multiple donors at least 6 times and use them subsequently in co-culture and tri-culture studies. Nonetheless, since it is not trivial to commercially source primary human LSECs from more than a few donors, we also evaluated the effects of HUVECs, which are readily available from many donors and have a precedence for use in co-cultures with primary hepatocytes and stem cell-derived hepatocyte-like cells.[69,230,258–260] Our results here indicate that PHH/fibroblast/endothelial cell tri-cultures containing HUVECs display similar levels and longevity of PHH functions over 3 weeks, and thus such tri-cultures can serve as a 'first approximation' when modeling PHH/endothelial interactions, whereas primary human LSECs can

be used in select studies to elucidate similarities and differences with reciprocal interactions between PHHs and non-liver-endothelial cells.

To determine endothelial phenotype in tri-cultures, we first evaluated gene expression of *CD31*, *CD54*, *F8*, and *vWF*, since these markers have been shown to be consistently expressed in human liver slices and isolated LSECs.[261–264] CD31 is a member of the immunoglobulin superfamily known to be expressed in many types of endothelial cells, but specifically in the cytoplasm of LSECs.[8,265] CD54 is a member of the immunoglobulin superfamily expressed on the surface of endothelial cells and implicated in various signaling pathways, including some immune pathways.[266,267] vWF is a multimeric glycoprotein that mediates platelet adhesion and thrombus formation during vascular injury[268], while F8 is a coagulation factor that is carried by vWF in circulating blood that leads to normal arrest of bleeding and thrombus formation.[268,269] All of the above-mentioned gene expression markers were detected in both PHH/endothelial co-cultures and PHH/fibroblast/endothelial tri-cultures for 3 weeks.

The widely accepted hallmark of LSEC phenotype is the presence of fenestrations on the cellular surface, which are responsible for the exchange of soluble and particulate material between the sinusoidal blood and the space of Disse.[10,11] The pattern of fenestration has been extensively studied in rat and mouse LSECs[11,224,270–272], but has been shown to be similar in human LSECs.[273] The distribution of fenestrations is highly dynamic, both with respect to location in the liver and grouping with adjacent fenestrations.[11,274] Furthermore, the number and diameter of fenestrations have been shown to correlate strongly with liver conditions (i.e. fatty liver, hepatitis, and hepatectomy) and exposure to xenobiotic and environmental agents (i.e. ethanol and nicotine).[11] It has also been suggested that the diameter of fenestrations affects the uptake and transport of lipoproteins in the sinusoid, which may greatly impact the pathogenesis of atherosclerosis.[11] In

this study, we detected the presence of fenestrations on LSECs via SEM in pure cultures, PHH/LSECs cell co-cultures, and PHH/fibroblast/LSEC tri-cultures; however, we were not able to elucidate quantitative differences across the culture configurations using SEM analysis. Nonetheless, coupled with gene expression analysis, the presence of fenestrations suggests that both co-cultures and tri-cultures can maintain the survival of endothelial cells irrespective of functional levels in PHHs. However, in contrast to PHH/endothelial co-cultures that display declining PHH functions, tri-cultures are better suited to evaluate reciprocal interactions between stable endothelial cells and PHHs in physiologic and pathophysiologic conditions. For instance, our tri-cultures could be used to model *in vivo*-like paracrine signaling between hepatitis C virus-infected PHHs and LSECs, as infected LSECs are known to release exosomes and inhibit viral replication in infected hepatocytes, albeit from a cancerous origin.[233] Furthermore, some drugs are known to cause toxicity to LSECs[220,221], which can lead to downstream effects in PHHs due to the release of apoptotic factors from the LSECs; our tri-cultures can serve to elucidate such crosstalk following drug exposure.

Our goal in this study was to determine how primary human endothelial cells (LSECs and HUVECs) affect long-term PHH functions relative to 3T3-J2 murine embryonic fibroblasts and then construct a tri-culture platform that can enables stable phenotypes of both PHHs and endothelial cells for several weeks. However, other NPC types in the liver such as hepatic stellate cells and Kupffer macrophages also interact with PHHs and LSECs *in vivo*. The use of the 3T3-J2 fibroblasts to stabilize PHH functions allows us to introduce specific liver NPC types within and around the fibroblast monolayer to study interactions with PHHs, while the use of PHH micropatterning allows us to control for PHH homotypic contacts that are critical for establishment of hepatocyte polarity, such as the formation of cell junctions (i.e. cadherins) and bile canaliculi.

Indeed, Nguyen *et al.* showed that primary human Kupffer macrophages can be cultured atop pre-established micropatterned co-cultures containing PHHs and fibroblasts to study the effects of Kupffer macrophage activation on hepatic CYP450s.[67] Similarly, Davidson *et al.* showed that primary human activated (fibrogenic) hepatic stellate cells can be cultured within the fibroblast monolayer surrounding the PHH micropatterned colonies to model an early non-alcoholic steatohepatitis-like phenotype in the PHHs, which could be alleviated with clinically-relevant drugs.[13] Thus, PHH/fibroblast/liver NPC tri-culture configurations offer robust *in vitro* tools to elucidate reciprocal interactions between PHHs and liver NPCs in physiological/disease contexts and for drug screening.

In conclusion, we showed here that neither primary human LSECs nor non-liver HUVECs can stabilize the PHH phenotype over several weeks, which necessitated the use of 3T3-J2 fibroblasts in a PHH/fibroblast/endothelial cell tri-culture configuration that subsequently led to high levels of prototypical hepatic functions and endothelial phenotype for at least 3 weeks *in vitro*. Separating the endothelial cells from the PHHs via a thin protein gel (Matrigel™) to mimic the space of Disse as *in vivo* did not lead to better PHH functions than the co-planar tri-cultures, though both configurations can have utility for addressing specific liver-specific hypotheses as detailed above. Ultimately, coupling PHH/fibroblast/liver NPC tri-cultures with cultures created from other tissues on a microfluidic chip (i.e. "body-on-a-chip") will allow a systems level exploration of disease progression and the effects of drugs on multiple interacting organ systems.

CHAPTER 7 - Microfluidic Hepatocyte Co-Cultures[7]

The liver is a highly perfused organ which receives about 25% of the total cardiac output. On the microscale, this blood supply is provided to the liver sinusoid, whereby flowing blood is separated from hepatocytes with endothelial cells and the space of Disse. Static *in vitro* platforms fail to recapitulate the resultant shear stress and waste removal, and traditional microfluidic devices often rely on hepatocarcinoma cell lines that do not properly reflect hepatic functionality. In this study, we have developed a novel device that provides fluid flow to a micropatterned co-culture (MPCC) of primary human hepatocytes and 3T3-J2 fibroblasts, as static MPCCs have been shown to support the hepatocytes' phenotype for multiple weeks in culture. Briefly, constructs of polydimethylsiloxane (PDMS) were irreversibly bound to tissue culture plastic, hepatocytes and fibroblasts were seeded in the device, and cultures were exposed to perfusion via a syringe pump or peristaltic pump. Fluid dynamics software modeled the system to verify that a physiologic level of shear stress was applied to the culture surface. This "MPCC-on-a-chip" was then shown to have a remarkably higher level of hepatic functions (albumin and urea secretions, CYP450 activity) for multiple weeks than conventional cultures maintained in the same manner. Interestingly, the addition of liver sinusoidal endothelial cells slightly improved hepatic functions while the exclusion of an extracellular matrix overlay attenuated functionality. In conclusion, "MPCCs-on-a-chip" can provide a stable, perfused hepatic model for studying the effects of shear stress and organ-organ interactions in a "body-on-a-chip" platform.

---

[7] Portions of this chapter are to appear in the following:
Ware, B.R., & Khetani, S.R. Engineered microfluidic co-cultures of primary human hepatocytes and stromal cells. (in preparation for *Lab on a Chip*)

7.1 Introduction and Background

Due to its role in metabolism, the human liver receives about 25% of the total cardiac output via the hepatic artery and portal vein.[19] These vessels divide into smaller branches until they split into the sinusoid, the smallest and most prevalent type of vasculature in the liver.[21] Flowing blood is separated from hepatocytes by liver sinusoidal endothelial cells and the extracellular matrix (ECM)-based space of Disse.[10] While *in vitro* cultures are useful in many aspects of liver physiology, many traditional models cannot be used to study flow-dependent phenomena or the interactions of the liver with other organs. In comparison with static models, perfused systems offer continuous nutrient exchange, removal of waste products, and physiologic shear stress.

Towards that end, several groups have developed "liver-on-a-chip" platforms for mimicking the physiology of the sinusoid.[164] The Yarmush group developed a platform in which primary human hepatocytes (PHHs) are configured in a monolayer an elbow-shaped biochip, and evaluated the hepatic clearance of multiple compounds.[80] Novik *et al.* expounded on this work with the inclusion of non-parenchymal cells.[81] A similar biochip was engineered by the Leclerc group for the culture of HepG2/C3a cells[79,275], primary rat hepatocytes[74,75], and PHHs[76,77]. The Griffith group created a bioreactor of hepatic aggregates attached to collagen-coated wells perfused via microchannels[70], which was later modified for rat hepatocytes and endothelia.[71] Lastly, Yu *et al.* have reported a perfusion-incubator-liver-chip with vacuum sealing for rat hepatocyte spheroids.[276]

One major advantage of perfused liver systems is their integration into "body-on-a-chip" platforms for better understanding the interactions between organs. For instance, Esch *et al.* modeled enterohepatic recirculation of nanoparticles between a liver model (HepG2/C3A cells)

and an intestinal model (Caco-2 and HT29-MTX cells).[84] Drug toxicity between organs was demonstrated by ifosfamide applied in a microfluidic biochip consisting of a liver model (HepaRG cells) and kidney model (Madin-Darby canine kidney cells).[102] Ifosfamide was metabolized by the liver compartment into a metabolite toxic to the kidney compartment. Liver-cancer models can also demonstrate the role of organ-organ interactions in drug metabolism, such as the liver's metabolism of the cancer prodrug tegafur to the bioactive compound 5-fluorouracil in a liver-tumor-marrow perfused model.[108] Other groups have designed biochips for modeling liver-skin interactions such as that observed in troglitazone-induced toxicity[105] and topical substance exposure[106].

Most of the aforementioned perfused models rely on hepatocarcinoma cell lines, which often display an abnormal morphology and levels of liver functions.[47] However, conventional cultures of PHHs or co-cultures of PHHs and endothelial cells rapidly decline in hepatospecific functions[179,277], which precludes long-term drug toxicity screens. On the other hand, micropatterned co-cultures (MPCCs) of PHHs and 3T3-J2 murine embryonic fibroblasts are known to stabilize the phenotype of PHHs for multiple weeks *in vitro* as assessed by major liver functions and gene expression.[54] Briefly, PHHs are seeded onto micropatterned collagen islands of empirically-optimized dimensions and surrounded with 3T3-J2 fibroblasts. As a non-liver cell line, 3T3-J2 fibroblasts can stabilize the hepatic phenotype of PHHs independently of liver stromal cells, thereby allowing studies of perfusion on a stable PHH background. Specifically, this platform is optimized to maintain the homotypic (hepatocyte-hepatocyte) and heterotypic (hepatocyte-stromal) interactions, which is believed to maintain the culture longevity. These cultures have been extensively characterized for their utility in predicting clinically-relevant drug clearance[56,180], drug metabolites[55], drug toxicity[58], and infection with hepatitis B/C viruses[59,60].

Kane *et al.* first reported a microfluidic array utilizing the MPCC platform[278], whereby rat hepatocytes were seeded into open-channel devices that were subsequently sealed with compression and perfused. Perfused cultures had albumin secretions and urea production ~60% of static controls through 32 days of culture. However, static controls were not maintained in the same manner as perfused cultures, and there was no justification of the flow rate. Furthermore, due to species-specific differences in liver metabolism[44,145], rat hepatocytes are not fully representative of human physiology.

Here, we developed an "MPCC-on-a-chip" platform that combines the longevity and high-level functions of a static MPCC with the utility of microfluidics in a human-relevant platform. We designed two methods for providing fluid flow to the cultures with either a syringe pump or peristaltic pump. Using these strategies, we show that perfused "MPCCs-on-a-chip" are superior to conventional cultures of hepatocytes on collagen-coated substrates. We then demonstrated that addition of endothelial cells also improves the hepatic functionality.

7.2 Materials and Methods

7.2.1 Construction of Devices

Devices used in this study were constructed from tissue culture polystyrene (TCPS) OmniTrays (ThermoFisher Scientific, Waltham, MA) and Sylgard-184 polydimethylsiloxane (PDMS; Dow Corning, Midland, MI). TCPS surfaces were treated with a 1% (v/v) aqueous solution of 3-aminopropyltriethoxysilane (3-APTES; Sigma-Aldrich, St. Louis, MO) for 20 minutes to introduce silicon atoms on the TCPS surface and facilitate the bonding of PDMS.[279,280] Areas of TCPS intended for cell culture were protected from the silane with adhesive tape to improve cellular attachment. PDMS slabs with pre-cut openings (10 mm wide by 20 mm long by 5 mm high) were activated with oxygen plasma and bonded to the silane-treated TCPS surface.

Cell culture areas were then uniformly coated with 50 µg/mL rat tail collagen-I (Corning Life Sciences, Tewksbury, MA) for 2 hours and rinsed twice with sterile water. PDMS mask-based soft lithography was then used to pattern the collagen into islands (500 µm diameter, 1200 µm center-to-center spacing).[66] A pre-cut PDMS top was then used to seal the device permanently. After cultures were seeded as described below and allowed to stabilize, each device was connected to flow via Tygon tubing.

7.2.2 Processing and Seeding of Primary Human Hepatocytes

Cryopreserved primary human hepatocytes (PHHs) were obtained from commercial vendors permitted to sell products derived from human organs procured in the United States by federally designated Organ Procurement Organizations. The HUM4145 (20-month-old Caucasian male who died of anoxia secondary to drowning) and HUM4055A (54-year-old Caucasian female who died of stroke) donors from Triangle Research Labs, now part of Lonza (Durham, NC) were the PHH donors used in this study. After thawing, PHHs were suspended in seeding medium (William's E base (Sigma-Aldrich) with 1.5% (v/v) HEPES buffer (Corning Life Sciences, Tewksbury, MA), 1% (v/v) ITS+ Premix (Corning Life Sciences), 1% (v/v) penicillin/streptomycin (Corning Life Sciences), 100 nM dexamethasone (Sigma-Aldrich), and 7 ng/mL glucagon (Sigma-Aldrich)). Cells were centrifuged at $47 \times g$ for 10 minutes, resuspended in fresh seeding medium, and counted.

7.2.3 Fibroblast Culture and Seeding

Murine embryonic 3T3-J2 fibroblasts were a gift from Howard Green of Harvard Medical School.[129] Cells were cultured at 37ºC, 10% CO_2 in Dulbecco's Modified Eagle's Medium (DMEM, Corning Life Sciences) with high glucose, 10% (v/v) bovine calf serum (Life Technologies), and 1% (v/v) penicillin-streptomycin. Before seeding in microfluidic devices,

fibroblasts were growth-arrested with 1 µg/mL mitomycin C (Sigma-Aldrich) for 4 hours. Cells were then passaged with 0.25% (m/v) trypsin-EDTA (Corning Life Sciences), brought to a density of 3.6 x 10^5 cells/mL, and seeded into the device (250 µL/well). Fibroblasts were passaged up to 12 times prior to use in MPCCs.

7.2.4 Endothelial Cell Culture

Primary liver sinusoidal endothelial cells (LSECs) were a gift from Dr. Hugo Rosen of the University of Colorado-Denver Medical School. Cells were cultured at 37ºC, 10% CO_2 in EGM™-2 BulletKit™ medium (Lonza, Williamsport, PA) on fibronectin-coated (2 µg/cm^2) tissue culture polystyrene. LSECs were passaged up to six times before use in co-culture.

7.2.5 Establishment of Micropatterned Co-Cultures (MPCCs)

Devices were constructed as described above including coating with rat tail collagen-I and micropatterning the collagen into islands. After processing as described above, cryopreserved PHHs were seeded at a density of 8 x 10^5 cells/mL into collagen micropatterned devices (250 µL/well). After allowing hepatocytes to attach and spread onto collagen-coated islands, devices were washed 3× in Dulbecco's Modified Eagle's Medium (DMEM) to remove unattached cells, leaving ~25,000 attached hepatocytes on ~90 islands in each device. 3T3-J2 fibroblasts were subsequently seeded at 3.6 x 10^5 cells/mL (250 µL/well) and allowed to fill the remaining area surrounding the PHH islands. The space of Disse was mimicked with an overlay of 500 µg/mL Matrigel™ (Corning Life Sciences) to separate hepatocytes from flowing medium. Devices designated to be 'tri-cultures' were then seeded the following day with 6 x 10^3 endothelial cells per device to approximate the physiologic ratio of 5 hepatocytes to 1 endothelium. The next day, devices were connected to medium perfusion from either a syringe pump or peristaltic pump via Tygon tubing.

7.2.6 Establishment of Conventional Cultures

Devices used for conventional cultures were constructed in the same manner as "MPCCs-on-a-chip", except that the cell culture surface was coated for 2 hours with 50 µg/mL rat tail collagen-I (Corning Life Sciences), rinsed twice with sterile water, and not subjected to micropatterning. Cryopreserved PHHs after processing were seeded at a density of 2×10^6 cells/mL into these devices (250 µL/well). After allowing cellular attachment and spreading onto the collagen-coated surface, unattached cells were rinsed out, and cultures were overlaid with 500 µg/mL Matrigel™. Devices were then connected to perfusion in the same manner as MPCC-based devices.

7.2.7 Syringe Pump Configuration

To duplicate the same media exchange rate as a static tissue culture plate, we used a syringe pump (NE-4000, New Era Pump Systems, Farmingdale, NY) to drive media flow. For each device, a syringe was filled with culture medium and affixed into the syringe pump. Tygon tubing (Saint-Gobain, Malvern, PA) was then linked between the syringe pump and device. Effluent media was collected for later biochemical analyses. As static cultures receive 300 µL of fresh medium every 48 hours, we chose a flow rate of 6.25 µL/hr to provide the same rate of nutrient replenishment as static cultures.

7.2.8 Peristaltic Pump Configuration

To impose a physiologic level of shear stress on the cultures, we used a peristaltic pump (Precision Micro Peristaltic Pump, Cole-Parmer, Vernon Hills, IL) with a media reservoir to cycle the medium from the reservoir to the device and back via Tygon and peristaltic pump tubing. The media reservoir was a 4 mL glass vial with a PTFE/silicone septum lid (ThermoFisher Scientific) pierced with a 20 gauge needle to feed the media flow.

Flow in the devices was assumed to be laminar with Reynold's number less than 2000, to be well-developed with a parabolic profile, and to have no-slip boundary conditions at the walls. As such, the shear stress can be calculated as:[281,282]

$$\tau = \frac{6Q\mu}{wh^2}$$

where τ is the shear stress at the cell surface (0.01 Pa)[283,284], Q is the volumetric flow rate of media, $\mu = \rho\nu$ is the media viscosity (1007 kg/m^3·0.77x10^{-4} m^2/s = 0.0775 kg/(m·s))[285,286], w is the channel width (1x10^{-2} m), and h is the channel height (5x10^{-3} m). Calculating the media flow rate yields 5 µL/s.

To verify this calculation, COMSOL Multiphysics® 5.0 (Burlington, MA) was used to simulate the device geometry and flow rate. After specifying the device geometry, culture medium properties, and inlet/outlet conditions, the laminar flow module with regular meshing was used to model the fluid velocity through the device. Assumptions used with the model included incompressible flow with constant viscosity and no-slip conditions at the walls.

7.2.9 Hepatic Morphological, Functionality, and Health Assessments

Culture morphology was monitored using an EVOS®FL cell imaging system (Life Technologies) with standard 4×, 10×, and 20× phase contrast objectives. Albumin secretions in collected media were assessed with an enzyme-linked immunosorbent assay (ELISA) with horseradish peroxidase detection and 3,3',5,5'-tetramethylbenzidine as the substrate.[54] Urea production was measured via a colorimetric endpoint analysis with diacetyl monoxime, acid, and heat (Stanbio Labs, Boerne, TX). CYP3A4 activity in cultures was measured using the luminescence-based luciferin-IPA assay from Promega (Madison, WI) per manufacturer's instructions.

7.2.10 Data Analysis

Data processing and visualization were performed using Microsoft Excel and GraphPad Prism (La Jolla, CA). All biochemical data is presented as mean and standard deviation values from duplicate devices of the same condition (n = 3 assay wells).

7.3 Results

7.3.1 Construction of Devices

As illustrated in Figure 7.1, "MPCC-on-a-chip" devices were constructed from TCPS coated with 3-APTES and PDMS. After the main PDMS structure was bonded irreversibly to the TCPS, the cell culture surfaces were coated with collagen and micropatterned in the same manner as traditional cell culture plates. The device was then sealed with a pre-cut PDMS top to the PDMS base. Following the seeding of cultures (with PHHs, 3T3-J2 fibroblasts, and LSECs depending on the cultures of interest), Tygon tubing was attached to the cultures to facilitate fluid flow.

Contingent on the desired fluidic arrangement, "MPCC-on-a-chip" devices were attached to either a syringe pump (Figure 7.2) or a peristaltic pump (Figure 7.3) before beginning fluid flow.
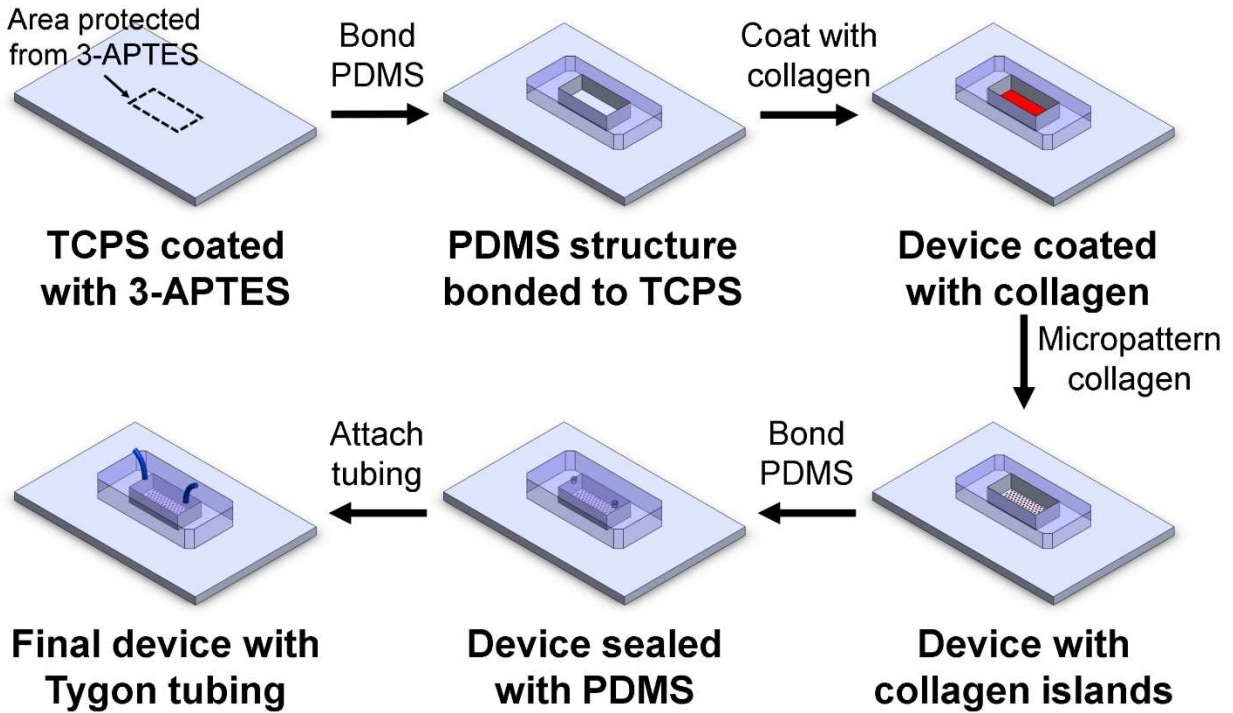
Figure 7.1: Construction of "MPCC-on-a-chip" devices. TCPS surfaces are coated with 3-APTES to introduce silicon atoms onto the surface. Areas for cell culture are protected from 3-APTES to facilitate collagen adsorption and cellular attachment. After activation with oxygen plasma, the main PDMS structure is irreversibly bonded to the TCPS surface. The cell culture area is uniformly coated with rat tail collagen-I and then subjected to soft lithography techniques to micropattern islands 500 μm in diameter with 1200 μm center-to-center spacing. Devices are completed with the irreversible bonding of the PDMS top to the PDMS base. After MPCCs are seeded (hepatocytes followed by 3T3-J2 fibroblasts and LSECs, if desired), Tygon tubing is connected to the device and perfused with either a syringe pump or peristaltic pump.
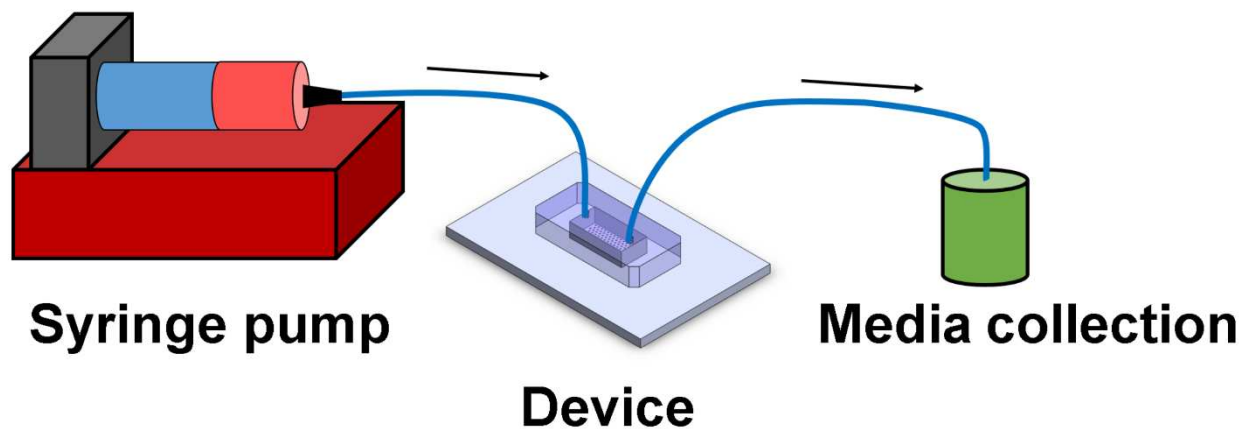
Figure 7.2: Syringe pump configuration of fluid flow. After cultures were established in the "MPCC-on-a-chip" devices, one syringe per device was filled with culture medium and attached to a syringe pump. Culture medium flows from the syringe to the device to a collection tube in a single pass via Tygon tubing. The flow rate was chosen to be 6.25 µL/hr to match the media exchange rate of static culture plates.
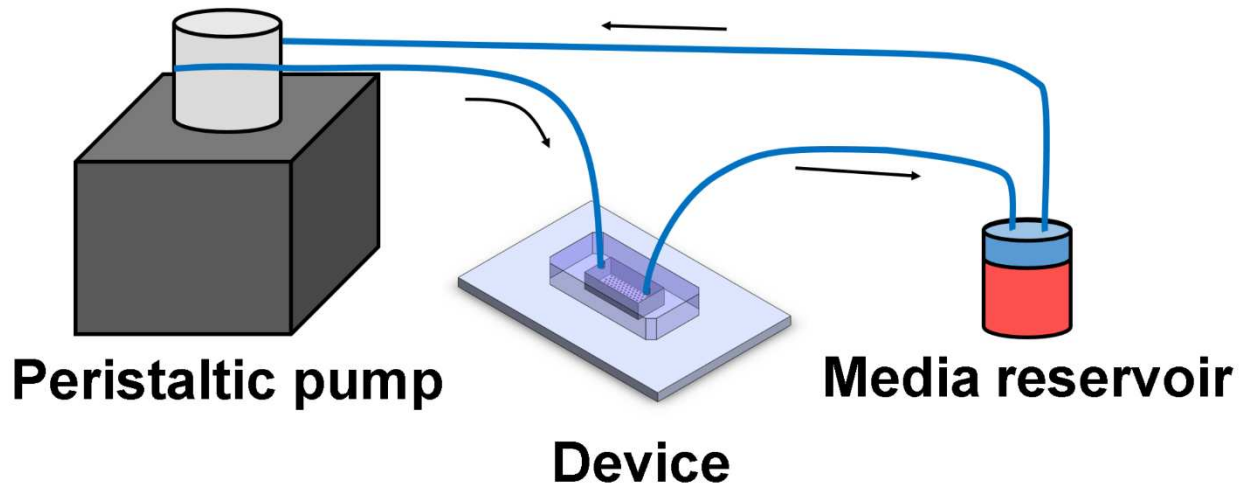
Figure 7.3: Peristaltic pump configuration of fluid flow. After cultures were established in the "MPCC-on-a-chip" devices, one glass reservoir per device was filled with culture medium and attached to the flow circuit driven by the pressure generated from the peristaltic pump. Culture medium flows from the reservoir to the device and back in a recirculating manner via Tygon and peristaltic pump tubing. The flow rate was chosen to be 5 µL/s to provide a physiologic level of shear stress to the cultures.

7.3.2 COMSOL Modeling of Fluid Shear Stress

Using the device geometry, culture medium properties, and inlet velocity calculated above, COMSOL Multiphysics® 5.0 software was used to model the device geometry *in silico* before applying the included laminar flow module. As shown in Figure 7.4, the fluid velocity in the inlet and outlet was approximately an order of magnitude higher (red color) than the velocity in the main cell culture chamber (dark blue color). Sample velocity measurements taken from the COMSOL model were used to validate the shear stress calculations for applying a physiologic level of shear stress to the cultures. Indeed, the calculated velocity correlated well with the computational model.
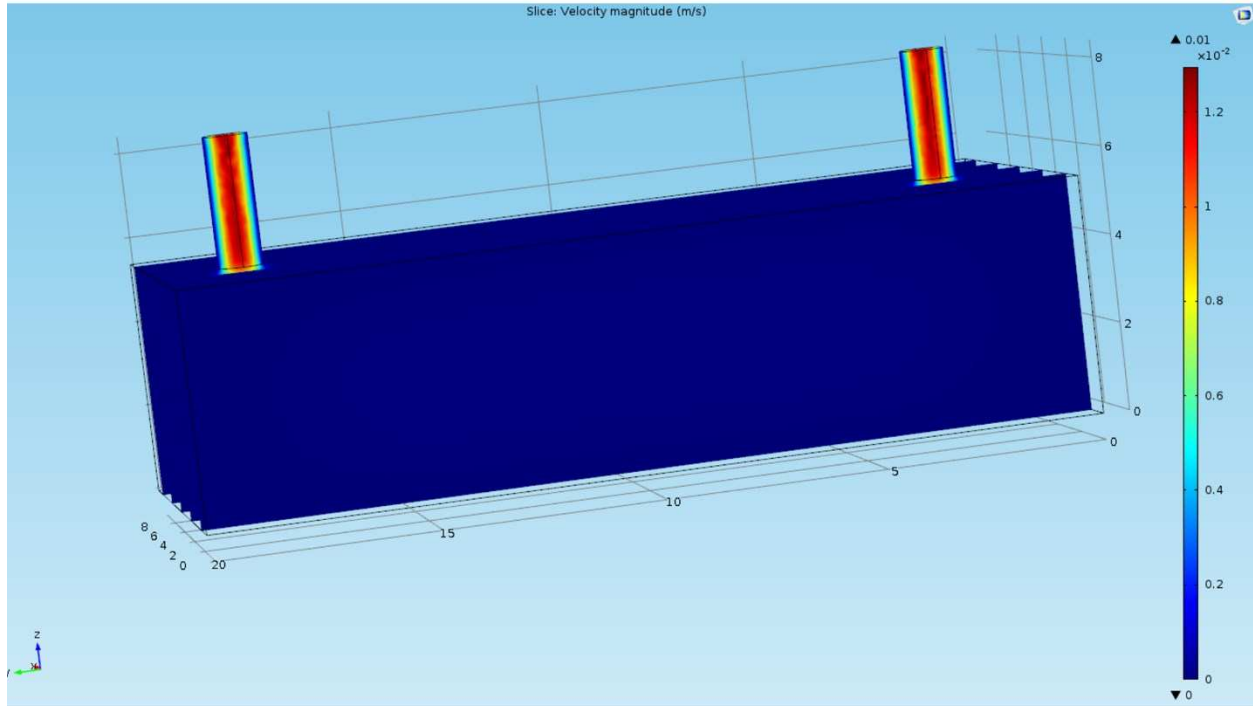
Figure 7.4: COMSOL modeling of fluid flow. COMSOL Multiphysics® 5.0 software was used to model the device geometry *in silico* before applying the included laminar flow module. Fluid velocity in the inlet and outlet was about an order of magnitude higher (red color) than the velocity in the main cell culture chamber (dark blue color). Sample velocity measurements taken from the COMSOL model were used to validate the shear stress calculations for applying a physiologic level of shear stress to the cultures.

7.3.3 Cultures Perfused with a Syringe Pump

After seeding MPCCs of PHHs and 3T3-J2 fibroblasts in the PDMS-based devices, we exposed some cultures to a flow rate of 6.25 µL/hr and kept others in static conditions with traditional media changes every other day. Albumin secretions from static cultures tended to spike after 12 days of culture before reaching steady-state levels of ~1 µg/hr/10^6 cells through 32 days of culture (Figure 7.5A). On the other hand, perfused cultures reached and maintained a similar steady-state level after 12 days of culture. Urea production from both static and perfused cultures reached steady-state levels of ~10 µg/hr/10^6 cells after two weeks in culture and sustained these levels through 32 days of culture (Figure 7.5B).
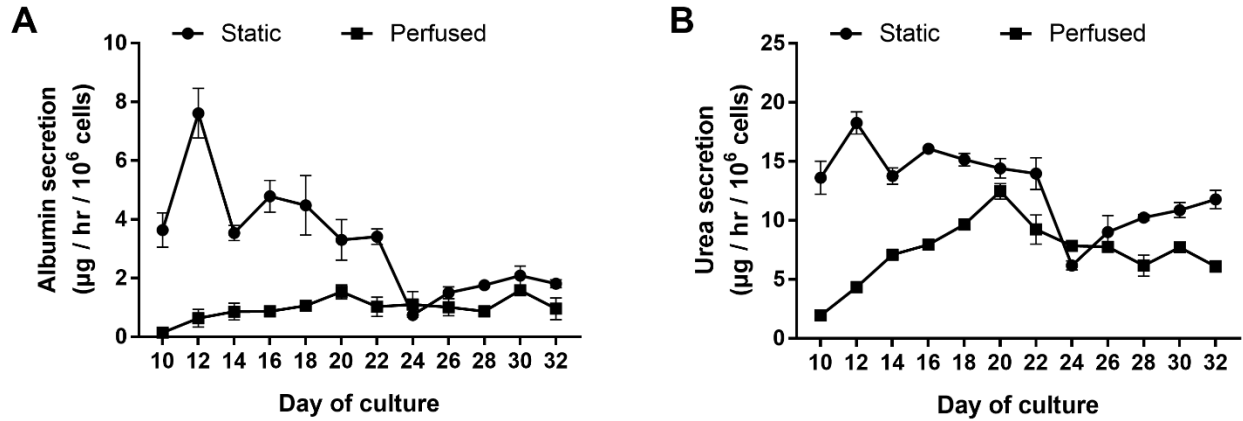
Figure 7.5: Functionality of cultures with syringe pump. MPCCs comprised of PHHs and 3T3-J2 fibroblasts were established in the PDMS- and TCPS-based devices and either exposed to flow at 6.25 µL/hr or media changes every other day. Effluent culture medium was assayed for **(A)** albumin secretions and **(B)** urea production from devices for 32 days of culture. Error bars represent standard deviations (n = 3).

7.3.4 Cultures Perfused with a Peristaltic Pump

To impose a physiologic level of shear stress on the cultures, we subjected both MPCCs (PHHs and 3T3-J2 fibroblasts) and conventional cultures (only PHHs) under a flow rate of 5 µL/s via a peristaltic pump. Like the syringe pump study described above, other cultures were maintained in a static format that received traditional media changes every other day. Steady-state albumin secretions from static cultures ($\sim$1.8 µg/hr/10^6 cells) were approximately 50% higher than perfused cultures ($\sim$1.2 µg/hr/10^6 cells) (Figure 7.6A). Urea production followed similar trends and had steady-state values of $\sim$28 µg/hr/10^6 cells and $\sim$12 µg/hr/10^6 cells for static and perfused cultures, respectively (Figure 7.6B). On the other hand, CYP3A4 activity was $\sim$2-fold higher in perfused cultures relative to static cultures (Figure 7.6C), with levels being $\sim$100,000 RLU/hr/10^6 cells and $\sim$50,000 RLU/hr/10^6 cells, respectively. For each of these three markers, conventional cultures showed less than 10% of the functional levels of their MPCC counterparts, regardless of being perfused or being maintained under static media conditions.

In a second study, we further studied the role of the Matrigel™ overlay and addition of LSECs in a 'tri-culture' platform. Like the previous studies, we ran static controls alongside the perfused cultures to determine the effects of flow. Tri-cultures with LSECs tended to show a higher level of albumin secretion and urea production than co-cultures without LSECs, although this difference was not statistically significant (Figure 7.7A-B). Perfused tri-cultures with LSECs also showed better stability through day 25 than perfused co-cultures without LSECs, potentially indicating that the interaction of flow and LSECs is beneficial to the hepatic phenotype. Interestingly, perfused cultures without a Matrigel™ overlay tended to decline more quickly than those with the overlay, suggesting that a space of Disse mimetic is useful in reconstructing hepatic physiology.

248
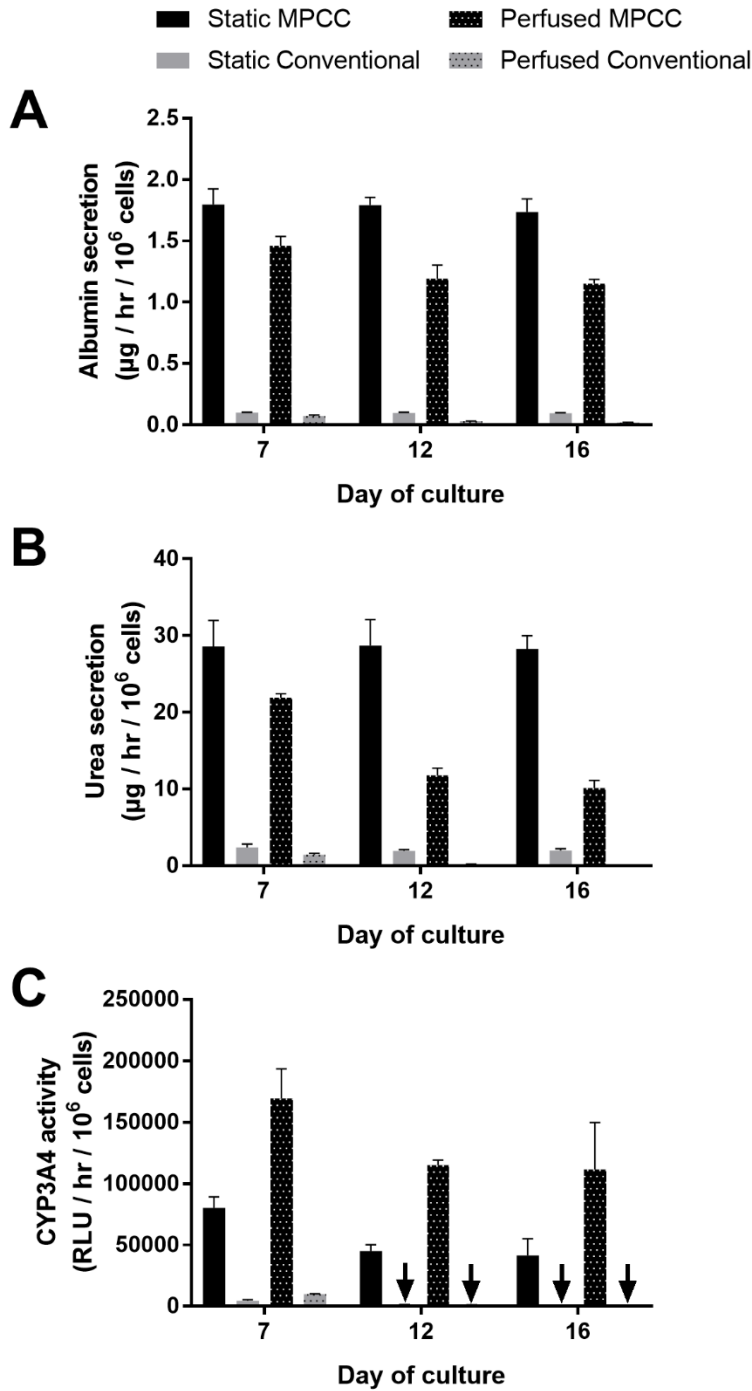
Figure 7.6: Functionality of cultures with peristaltic pump. MPCCs comprised of PHHs and 3T3-J2 fibroblasts were compared against conventional cultures solely of PHHs in the PDMS- and TCPS-based devices. Cultures were either exposed to flow at 5 µL/s or media changes every other day. Collected medium samples were later assayed for **(A)** albumin secretions, **(B)** urea production, and **(C)** CYP3A4 activity for 16 days in culture. Arrows indicate a detectable, albeit very low, level of CYP3A4 activity. Error bars represent standard deviations (n = 3).
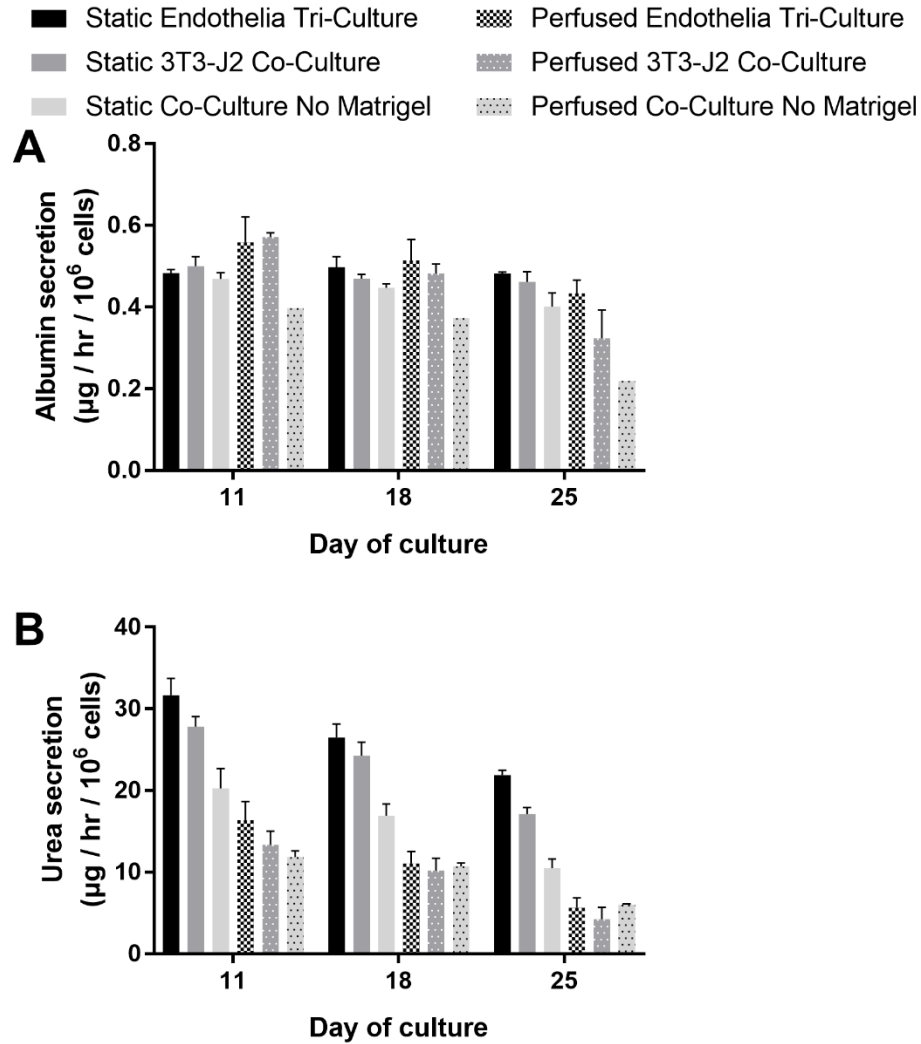
Figure 7.7: Functionality of cultures with peristaltic pump. MPCCs were established in devices as in previous studies. Some cultures also included LSECs to generate a 'tri-culture' while other cultures did not receive a Matrigel™ overlay. Using the collected media samples, **(A)** albumin secretions and **(B)** urea production for 25 days in culture were quantified. Error bars represent standard deviations (n = 3).

7.4 Discussion

To mimic the fluid flow observed in the human liver, many groups have established microfluidic "liver-on-a-chip" platforms towards simulating normal hepatic physiology.[287] The scale of microfluidic devices is small enough to accommodate most cells yet large enough to avoid the continuity problems seen in nanochannels.[288] Many of these platforms require both high cell densities and pressures (~10 psi) to load hepatocytes into the microfluidic chamber. In contrast with traditional, passive seeding methods used for static cultures, these densities and pressures could lead to inaccuracies in cell counts and excessive cellular stress. Furthermore, most of these platforms are based on conventional cultures of hepatocytes or co-cultures of hepatocytes and endothelial cells, which have been shown to lose hepatic functions rapidly.[179,277]

Many previously reported devices rely on artificial constructs to simulate key aspects of the sinusoidal physiology. Multiple groups have replaced endothelial cells with artificial barrier slits.[72,89,90] While this permits the soluble exchange of nutrients and separation of hepatocytes and direct shear stress, the slits do not recapitulate hepatocyte-endothelia crosstalk, which is important in liver diseases.[91] Furthermore, some models implement a porous membrane of polyethylene or polyethylene terephthalate.[289,290] This technique simplifies the process and reproducibility of seeding cultures by not having to rely on layered gels; however, the cell-material interactions do not properly mimic the cell-ECM interactions observed *in vivo* with the space of Disse as the polymeric membranes do not have the protein components the native space of Disse has. As we have demonstrated, the space of Disse mimetic provided for by the Matrigel™ overlay improved hepatic functionality, especially with long-term culture functions. This is consistent with previous reports showing hepatocytes being sheared from the lining of microfluidic devices.[291]

We chose to adapt the MPCC platform into a perfused system to combine the longevity of the static MPCC platform with the additional functionality of fluid flow. While the platform relies on the 3T3-J2 murine embryonic fibroblast, a non-liver stromal cell, to stabilize the hepatic phenotype, no other liver non-parenchymal cell type on its own, including the Kupffer macrophage, hepatic stellate cell, and liver sinusoidal endothelial cell has been shown to yield the same level of hepatic functions.[13,67,158,179] Furthermore, 3T3-J2 fibroblasts are easily propagated, grow under contact inhibition, and have an undetectable level of liver functions. The expression of various molecules observed in the liver which include decorin[158], vascular endothelial growth factor D[158], and T-cadherin[182], could all contribute to the fibroblasts' ability to induce functions in hepatocytes from multiple species.[5] The controlled presentation of homotypic and heterotypic interactions between hepatocytes and fibroblasts provide for the highest functional levels reported to date.[54]

The seeding process of MPCCs is generally passive and requires physical agitation to distribute cells evenly across the micropatterned surface. This in turn requires the height of the microfluidic device to be 5 mm, much higher than most traditional microfluidic devices (typically 100-150 μm). As the relationship between flow rate and channel height is quadratic for a given shear stress, this height requires a high flow rate (5 μL/s) to deliver a physiologic level of shear stress on the cultures. The high flow rate would deplete 432 mL of culture medium per day if run in a single-pass manner; thus, we chose a re-circulating configuration for such a high flow rate. Future iterations of the design could implement a sealing mechanism whereby the cultures are seeded in an open well format, sealed with a magnetic locking mechanism, and perfused. This would allow for proper seeding of cultures and a functional device height comparable to those seen in traditional microfluidic devices, which would greatly diminish the required flow rate.

Introducing fluid flow control greatly increases the complexity of cell culture and reduces throughput, although a new generation of micro-dispensers and micro-pumps are being developed to reduce this complexity.[141] Depending on the application under consideration, flow might not be desirable because of the requisite equipment, reduced throughput, and culturing intricacies. In the drug development pipeline, many early studies with large compound libraries would be run on a high throughput platform to provide preliminary data on efficacy and safety in a rapid manner.[164] Subsequent studies, however, would give more in-depth characterization on a novel compound's mechanism of action, distribution, and metabolite profile, and thus would benefit from perfused cultures. As has been shown previously, organ-organ interactions are a novel application for microfluidic liver models coupled with organ systems. However, while hepatocarcinoma cells used in those studies are readily available to researchers and have been shown to be amenable to microfluidic culture, their metabolic activity does not accurately portray that of PHHs.[37,47] This discrepancy could lead to an inaccurate set of metabolites in the effluent from the liver compartment, which could greatly impact the downstream responses in other organ systems. Instead, similar to the static MPCC platform, we anticipate "MPCCs-on-a-chip" being amenable to all types of hepatocytes depending on the hypothesis in question.

The choice of materials is a crucial component in constructing microfluidic devices. Tissue culture polystyrene (TCPS) was used as the base of the devices to compare against legacy data generated with industry-standard TCPS plates used in standard cultures. Nevertheless, this process is amenable to other substrates including glass. We chose PDMS for the remainder of the microfluidic devices due to its optical clarity, biocompatibility, permeability to oxygen, and ease of fabrication.[292,293] However, PDMS is known to absorb some small molecules, which could artificially reduce the concentration of drugs and metabolites.[294] Future designs could implement

alternative polymers such as thiol-enes, which have been recently developed to minimize the absorption of small molecules.[295] Oxygen plasma treatment is frequently used to bond PDMS to either PDMS or glass due to the formation of Si-O-Si bonds. The aminosilane 3-APTES was used to introduce silicon atoms on the TCPS surface and facilitate the bonding of PDMS.[279,280] We have found that the 3-APTES coating limits the attachment of cells to the TCPS surface relative to untreated TCPS; thus, we protected areas of TCPS intended for cell culture from the silane to improve cellular attachment and spreading.

We chose to use two different fluidic platforms because of the two different flow rates desired. To yield the same media exchange rate as static cultures, we chose a perfusion rate of 6.25 µL/hr. This could easily be provided by the syringe pump in a single-pass manner with medium samples collected from the culture effluent. On the other hand, providing a physiologic level of shear stress necessitated a 2880-fold higher flow rate, 5 µL/s. Instead of using such a large volume with a single-pass system, we chose to recirculate the media via a peristaltic pump and sample the reservoir medium for biochemical assays. Such single-pass[278,296] and recirculation[297,298] systems have each been reported in the literature, and each has its own set of advantages and drawbacks. While the single-pass format allows for easy collection of medium for a given time point, it does not permit the accumulation of metabolites and waste products that might be seen *in vivo*. Recirculating medium does permit the recycling of nutrients and by-products, although the medium collection is more difficult. In either case, the specific hypothesis will dictate the type of flow system used.

We have designed the "MPCC-on-a-chip" to be modular in that various cell sources (i.e. PHHs, hepatic cell lines, iPSC-derived hepatocytes) can be interfaced with ECM proteins, stromal cells, and soluble factors to elucidate aspects of liver physiology that are flow-dependent and not

easily reproduced in static platforms. Future studies can inquire about flow-dependent phenomena and the role of shear stress, especially because endothelial cells have been shown to respond properly to shear stress.[281,299] Furthermore, as "MPCCs-on-a-chip" are a monolayer platform, the platform is amenable to various types of microscopy and high content imaging.[53] This enables on-chip, real-time measurements of biochemical signals as have already been demonstrated with glucose[92], oxygen[93], reactive oxygen species[87], and transforming growth factor β1[94]. Such measurements can give further insights into liver physiology, pathophysiology, and mechanisms of drug toxicity.

In conclusion, we have developed an "MPCC-on-a-chip" that demonstrates a level of hepatic functions on the same order of magnitude as static controls. This model is versatile in the cellular composition, medium formulation, and protein overlays. Future improvements to "MPCCs-on-a-chip" can further improve the ease of seeding cultures and executing perfusion studies. For instance, laser cut plastics can improve the precision of the devices and avoid molecule binding issues observed with PDMS. Similarly, the inclusion of multiple stromal cell types (i.e. Kupffer macrophages, hepatic stellate cells) in an *in vivo*-like environment can enable evaluation of tissue crosstalk. With future improvements to the "MPCC-on-a-chip" and integration with other organ systems, we anticipate that such "body-on-a-chip" platforms will improve our understanding of liver-based diseases and drug toxicity pathways.

8.1 Review of Research Objectives

8.1.1 Use iPSC-Derived Hepatocytes for Toxicity Studies

We screened a set of 47 drugs on the so-called iMPCC platform to compare binary toxicity predictions in iMPCCs, conventional cultures of iPSC-derived hepatocytes, and PHH-based MPCCs. Furthermore, we compared the responses of iMPCCs challenged with known hepatotoxins and their non-toxic structural analogs.

8.1.2 Culture Mouse Hepatocytes In Vitro

As an alternative to time- and resource-consuming whole animal studies, we sought to incorporate mouse hepatocytes into a platform amenable to long-term culture. These cultures would then be characterized for their hepatospecific functions, response to acetaminophen, and bioactivation pathways.

8.1.3 Use HepaRG Cells for Toxicity Studies

As an alternative to primary hepatocytes, we used the cancerous cell line HepaRG in co-culture with 3T3-J2 fibroblasts to maintain high levels of liver-specific functions for multiple weeks and to screen the same 47 drugs used with iMPCCs in Chapter 2.

8.1.4 Run Toxicogenomic Analyses

In contrast with using high drug doses and overt toxicity markers, we investigated changes in the global gene expression of hepatic cultures treated with drugs at pharmacologically-relevant doses. Specifically, we inquired about four pairs of hepatotoxins and their non-toxic structural drug analogs to determine the differentially expressed genes and specific pathways to which those genes belong.

8.1.5 Co-Culture Hepatocytes and Endothelia

We set out to create stable cultures of both hepatocytes and endothelial cells before characterizing their hepatic markers (albumin secretions, urea secretions, CYP3A4 activity, CYP2A6 activity) and endothelial-specific markers (gene expression markers, presence of fenestrations, acLDL uptake).

8.1.6 Establish a Microfluidic Hepatocyte-Fibroblast Co-Culture Model

As an alternative to static cultures, we wanted to construct a device capable of maintaining high levels of liver functions for multiple weeks *in vitro*. This device was characterized *in silico* for shear stress delivered to the culture and compared *in vitro* under static and perfused conditions.

8.2 Summary of Results

8.2.1 Use iPSC-Derived Hepatocytes for Toxicity Studies

We found that iPSC-derived hepatocytes in the iMPCC platform yielded a sensitivity and specificity of 65% and 100%, respectively, which were remarkably similar to PHH-based MPCCs (70% sensitivity and 100% specificity). On the other hand, conventional cultures missed several hepatotoxins. The toxin/non-toxin pairs tolcapone/entacapone and troglitazone/rosiglitazone were correctly differentiated, and bioactivation mechanism pathways of acetaminophen correlated well with known *in vivo* mechanisms.

8.2.2 Culture Mouse Hepatocytes In Vitro

We found that freshly isolated hepatocytes from the C57Bl/6J, NOD/ShiLtJ, and CD-1 mouse strains could be successfully incorporated into a so-called mMPCC platform and maintain a high level of multiple hepatic functions for ~1 month. C57Bl/6J cultures were also responsive when exposed to acetaminophen and showed exacerbated toxicity when co-treated with the CYP450 inducer dexamethasone.

8.2.3 Use HepaRG Cells for Toxicity Studies

We found that HepaRG cells could be successfully be incorporated into a HepaRG-MPCC platform, displayed a high level of hepatospecific functions, and also expressed the biliary marker cytokeratin 19. The sensitivity and specificity were 54% and 100%, respectively, for the 47 compounds screened for toxicity in HepaRG-MPCCs.

8.2.4 Run Toxicogenomic Analyses

We found that the known hepatotoxin troglitazone caused a differential expression of significantly more genes than the structural drug analog rosiglitazone. The total number of differentially expressed genes increased with an increased exposure time, and increasing the dose of rosiglitazone had only a marginal effect on the number of differentially expressed genes. Similar trends were observed with the toxic/non-toxic pairs nefazodone/buspirone, ibufenac/ibuprofen, and tolcapone/entacapone.

8.2.5 Co-Culture Hepatocytes and Endothelia

Despite a hepatic origin, we found that co-cultures solely of hepatocytes and LSECs failed to maintain the hepatic phenotype for extended culture periods. Tri-cultures of hepatocytes, LSECs, and 3T3-J2 fibroblasts, on the other hand, maintained a high level of functions, expressed endothelial-specific markers, and showed a differential response to compounds known to cause toxicity specific to endothelia. These tri-cultures could be arranged in a co-planar format or layered with Matrigel™ to mimic the space of Disse.

8.2.6 Establish a Microfluidic Hepatocyte-Fibroblast Co-Culture Model

We successfully established a perfused co-culture platform in a device composed of PDMS and TCPS before modeling the system in COMSOL. Two different platforms—one with a syringe

pump and one with a peristaltic pump—drove fluid flow at two different flow rates. Both flow

rates yielded high levels of culture functions for multiple weeks *in vitro*.

CHAPTER 9 - Recommendations for Future Research

Despite the work done on the project to date, the human liver is an extremely complex organ that impacts many components of physiology. Thus, these areas still need further work:

1. Expansion of donor pool for iPSC-HHs and mouse hepatocytes. As genetics have been shown to be a contributor to drug toxicity, the larger span of genetic backgrounds possible with iPSC-HHs and mouse hepatocytes can further explore the role of genetics in toxic events.

2. Expound of hepatocyte-endothelial crosstalk. We have shown that inclusion of endothelia into co-cultures can be useful in improving the sensitivity of compounds with endothelial-specific toxicity. This mechanism needs to be further elucidated via microarray analysis, cytokine analysis, or paracrine signal analysis to gain a more thorough understanding of how toxicity is propagated throughout the liver.

3. Combination of hepatic stromal cell types. While liver sinusoidal endothelial cells (LSECs) were investigated in this dissertation, other stromal cell types such as the Kupffer macrophage and hepatic stellate cell also play key roles in physiology and can be better studied *in vitro*.

4. Analysis of hepatic zonation. A combination of oxygen, hormones, ECMs, and stromal cells all play a major role in the heterogeneity of hepatic functions along the liver sinusoid. Furthermore, the Biological Microsystems Laboratory is currently exploring new devices for imposing oxygen concentrations on cultures.[300,293,301,302]

5. Improvement of microfluidic design. While we have successfully built and tested the first generation "MPCC-on-a-chip", we believe that future designs will improve its functionality and ease of use. For instance, a sealed design similar to that of the Agarwal group[303] will

enable the seeding of cultures in an open-well format and closing the device before starting perfusion. This will reduce the final device height and the requisite flow rates.

6. Incorporate other organ systems with liver platforms. As drugs can cause toxicity in a variety of mechanisms, it is crucial to screen for multi-organ toxicity before implementing critical trials. For example, the antineoplastic drug ifosfamide is metabolized into the reactive metabolite chloroacetaldehyde, which can cause downstream kidney damage.[304] Furthermore, dysfunction of the liver can also impact other tissues similar to how α1-antitrypsin deficiency can contribute to the development of emphysema in the lungs.[305]

REFERENCES

1. Tsung, A. & Geller, D. A. in *Molecular Pathology of Liver Diseases* (ed. Monga, S. P. S.) 3–6 (Springer, 2011).

2. Bismuth, H. Revisiting liver anatomy and terminology of hepatectomies. *Ann. Surg.* **257,** 383–386 (2013).

3. Fausto, N. Liver regeneration. *J. Hepatol.* **32,** 19–31 (2000).

4. Chu, X. *et al.* Intracellular drug concentrations and transporters: Measurement, modeling, and implications for the liver. *Clin. Pharmacol. Ther.* **94,** 126–141 (2013).

5. Khetani, S. R. *et al.* Microengineered liver tissues for drug testing. *J. Lab. Autom.* **20,** 216–250 (2015).

6. Smedsrød, B., Pertoft, H., Gustafson, S. & Laurent, T. C. Scavenger functions of the liver endothelial cell. *Biochem. J.* **266,** 313–327 (1990).

7. Damania, A., Jain, E. & Kumar, A. Advancements in *in vitro* hepatic models: Application for drug screening and therapeutics. *Hepatol. Int.* **8,** 23–38 (2013).

8. DeLeve, L. D. Liver sinusoidal endothelial cells and liver regeneration. *J. Clin. Invest.* **123,** 1861–1866 (2013).

9. Voyta, J. C., Via, D. P., Butterfield, C. E. & Zetter, B. R. Identification and isolation of endothelial cells based on their increased uptake of acetylated-low density lipoprotein. *J. Cell Biol.* **99,** 2034–2040 (1984).

10. Wisse, E., De Zanger, R. B., Chareis, K., Van Der Smizzen, P. & McCuskey, R. S. The liver sieve: Considerations concerning the structure and function of endothelial fenestrae, the sinusoidal wall, and the space of Disse. *Hepatology* **5,** 683–692 (1985).

11. Braet, F. & Wisse, E. Structural and functional aspects of liver sinusoidal endothelial cell fenestrae: A review. *Comp. Hepatol.* **1,** 1–17 (2002).

12. Smedsrød, B. *et al.* Cell biology of liver endothelial and Kupffer cells. *Gut* **35,** 1509–1516 (1994).

13. Davidson, M. D., Kukla, D. A. & Khetani, S. R. Microengineered cultures containing human hepatic stellate cells and hepatocytes for drug development. *Integr. Biol.* **9,** 662–677 (2017).

14. Puche, J. E. *et al.* A novel murine model to deplete hepatic stellate cells uncovers their role in amplifying liver damage in mice. *Hepatology* **57,** 339–350 (2013).

15. Friedman, S. L. Hepatic stellate cells: Protean, multifunctional, and enigmatic cells of the liver. *Physiol. Rev.* **88,** 125–172 (2008).

16. Tabibian, J. H., Masyuk, A. I., Masyuk, T. V, O'Hara, S. P. & LaRusso, N. F. Physiology of cholangiocytes. *Compr. Physiol.* **3,** 541–565 (2013).

17. Yoo, K.-S., Lim, W. T. & Choi, H. S. Biology of cholangiocytes: From bench to bedside. *Gut Liver* **10,** 687–698 (2016).

18. LeCluyse, E. L., Witek, R. P., Andersen, M. E. & Powers, M. J. Organotypic liver culture models: Meeting current challenges in toxicity testing. *Crit. Rev. Toxicol.* **42,** 501–548 (2012).

19. Abdel-Misih, S. R. Z. & Bloomston, M. Liver anatomy. *Surg. Clin. North Am.* **90,** 643–653 (2010).

20. Aird, W. C. Phenotypic heterogeneity of the endothelium. *Circ. Res.* **100,** 174–190 (2007).

21. van der Plaats, A. *et al.* Numerical simulation of the hepatic circulation. *Int. J. Artif. Organs* **27,** 222–230 (2004).

22. McCuskey, R. S. Morphological mechanisms for regulating blood flow through hepatic sinusoids. *Liver* **20,** 3–7 (2000).

23. Lalor, P. F., Lai, W. K., Curbishley, S. M., Shetty, S. & Adams, D. H. Human hepatic sinusoidal endothelial cells can be distinguished by expression of phenotypic markers

related to their specialised functions *in vivo*. *World J. Gastroenterol.* **12,** 5429–5439 (2006).

24. Allen, J. W. & Bhatia, S. N. Formation of steady-state oxygen gradients *in vitro*: Application to liver zonation. *Biotechnol. Bioeng.* **82,** 253–262 (2003).

25. Colnot, S. & Perret, C. in *Molecular Pathology of Liver Diseases* (ed. Monga, S. P. S.) 7–16 (Springer, 2011).

26. Frevert, U. *et al.* Intravital observation of *Plasmodium berghei* sporozoite infection of the liver. *PLoS Biol.* **3,** e192 (2005).

27. Kietzmann, T. Metabolic zonation of the liver: The oxygen gradient revisited. *Redox Biol.* **11,** 622–630 (2017).

28. Corsini, A. & Bortolini, M. Drug-induced liver injury: The role of drug metabolism and transport. *J. Clin. Pharmacol.* **53,** 463–474 (2013).

29. Liu, Z.-X. & Kaplowitz, N. Role of innate immunity in acetaminophen-induced hepatotoxicity. *Expert Opin. Drug Metab. Toxicol.* **2,** 493–503 (2006).

30. Leung, L., Kalgutkar, A. S. & Obach, R. S. Metabolic activation in drug-induced liver injury. *Drug Metab. Rev.* **44,** 18–33 (2012).

31. Kaplowitz, N. Idiosyncratic drug hepatotoxicity. *Nat. Rev. Drug Discov.* **4,** 489–499 (2005).

32. Kaplowitz, N. Biochemical and cellular mechanisms of toxic liver injury. *Semin. Liver Dis.* **22,** 137–144 (2002).

33. Grattagliano, I. *et al.* Biochemical mechanisms in drug-induced liver injury: Certainties and doubts. *World J. Gastroenterol.* **15,** 4865–4876 (2009).

34. Yuan, L. & Kaplowitz, N. Mechanisms of drug-induced liver injury. *Clin. Liver Dis.* **17,** 507–518, vii (2013).

35.   Ray, A. Beyond debacle and debate: Developing solutions in drug safety. *Nat. Rev. Drug Discov.* **8,** 775–779 (2009).

36.   Zhang, M., Chen, M. & Tong, W. Is toxicogenomics a more reliable and sensitive biomarker than conventional indicators from rats to predict drug-induced liver injury in humans? *Chem. Res. Toxicol.* **25,** 122–129 (2012).

37.   Gerets, H. H. *et al.* Characterization of primary human hepatocytes, HepG2 cells, and HepaRG cells at the mRNA level and CYP activity in response to inducers and their predictivity for the detection of human hepatotoxins. *Cell Biol. Toxicol.* **28,** 69–87 (2012).

38.   Xu, J. J. *et al.* Cellular imaging predictions of clinical drug-induced liver injury. *Toxicol. Sci.* **105,** 97–105 (2008).

39.   Maertens, C., Droogmans, G., Chakraborty, P. & Nilius, B. Inhibition of volume-regulated anion channels in cultured endothelial cells by the anti-oestrogens clomiphene and nafoxidine. *Br. J. Pharmacol.* **132,** 135–142 (2001).

40.   Park, B. K., Kitteringham, N. R., Pirmohamed, M. & Tucker, G. T. Relevance of induction of human drug-metabolizing enzymes: Pharmacological and toxicological implications. *Br. J. Clin. Pharmacol.* **41,** 477–491 (1996).

41.   Kaitin, K. I. Deconstructing the drug development process: The new face of innovation. *Clin. Pharmacol. Ther.* **87,** 356–361 (2010).

42.   Mullard, A. The phenotypic screening pendulum swings. *Nat. Rev. Drug Discov.* **14,** 807–809 (2015).

43.   Kola, I. & Landis, J. Can the pharmaceutical industry reduce attrition rates? *Nat. Rev. Drug Discov.* **3,** 711–715 (2004).

44.   Olson, H. *et al.* Concordance of the toxicity of pharmaceuticals in humans and in animals. *Regul. Toxicol. Pharmacol.* **32,** 56–67 (2000).

45.   Lin, C., Ballinger, K. R. & Khetani, S. R. The application of engineered liver tissues for

novel drug discovery. *Expert Opin. Drug Discov.* **10,** 519–540 (2015).

46.   Huh, D., Hamilton, G. A. & Ingber, D. E. From 3D cell culture to organs-on-chips. *Trends Cell Biol.* **21,** 745–754 (2011).

47.   Wilkening, S., Stahl, F. & Bader, A. Comparison of primary human hepatocytes and hepatoma cell line HepG2 with regard to their biotransformation properties. *Drug Metab. Dispos.* **31,** 1035–1042 (2003).

48.   Kwon, S. J. *et al.* High-throughput and combinatorial gene expression on a chip for metabolism-induced toxicology screening. *Nat. Commun.* **5,** 3739 (2014).

49.   Lee, D. W. *et al.* Application of the DataChip/MetaChip technology for the evaluation of ajoene toxicity *in vitro*. *Arch. Toxicol.* **88,** 283–290 (2014).

50.   Messner, S., Agarkova, I., Moritz, W. & Kelm, J. M. Multi-cell type human liver microtissues for hepatotoxicity testing. *Arch. Toxicol.* **87,** 209–213 (2013).

51.   Miyamoto, Y., Ikeuchi, M., Noguchi, H., Yagi, T. & Hayashi, S. Spheroid formation and evaluation of hepatic cells in a three-dimensional culture device. *Cell Med.* **8,** 47–56 (2015).

52.   Fukuda, J. & Nakazawa, K. Hepatocyte spheroid arrays inside microwells connected with microchannels. *Biomicrofluidics* **5,** 22205 (2011).

53.   Trask, O. J., Moore, A. & LeCluyse, E. L. A micropatterned hepatocyte coculture model for assessment of liver toxicity using high-content imaging analysis. *Assay Drug Dev. Technol.* **12,** 16–27 (2014).

54.   Khetani, S. R. & Bhatia, S. N. Microscale culture of human liver cells for drug development. *Nat. Biotechnol.* **26,** 120–126 (2008).

55.   Wang, W. W., Khetani, S. R., Krzyzewski, S., Duignan, D. B. & Obach, R. S. Assessment of a micropatterned hepatocyte coculture system to generate major human excretory and circulating drug metabolites. *Drug Metab. Dispos.* **38,** 1900–1905 (2010).

266

56.   Lin, C., Shi, J., Moore, A. & Khetani, S. R. Prediction of drug clearance and drug-drug interactions in microscale cultures of human hepatocytes. *Drug Metab. Dispos.* **44,** 127–136 (2016).

57.   Prueksaritanont, T. *et al.* Drug-drug interaction studies: Regulatory guidance and an industry perspective. *AAPS J.* **15,** 629–645 (2013).

58.   Khetani, S. R. *et al.* Use of micropatterned cocultures to detect compounds that cause drug-induced liver injury in humans. *Toxicol. Sci.* **132,** 107–117 (2013).

59.   Shlomai, A. *et al.* Modeling host interactions with hepatitis B virus using primary and induced pluripotent stem cell-derived hepatocellular systems. *Proc. Natl. Acad. Sci. U. S. A.* **111,** 12193–12198 (2014).

60.   Ploss, A. *et al.* Persistent hepatitis C virus infection in microscale primary human hepatocyte cultures. *Proc. Natl. Acad. Sci. U. S. A.* **107,** 3141–3145 (2010).

61.   March, S. *et al.* A microscale human liver platform that supports the hepatic stages of *Plasmodium falciparum* and *vivax*. *Cell Host Microbe* **14,** 104–115 (2013).

62.   Davidson, M. D., Lehrer, M. & Khetani, S. R. Hormone and drug-mediated modulation of glucose metabolism in a microscale model of the human liver. *Tissue Eng. Part C Methods* **21,** 716–725 (2015).

63.   Schwartz, R. E., Fleming, H. E., Khetani, S. R. & Bhatia, S. N. Pluripotent stem cell-derived hepatocyte-like cells. *Biotechnol. Adv.* **32,** 504–513 (2014).

64.   Davidson, M. D., Ware, B. R. & Khetani, S. R. Stem cell-derived liver cells for drug testing and disease modeling. *Discov. Med.* **19,** 349–358 (2015).

65.   Takayama, K. *et al.* 3D spheroid culture of hESC/hiPSC-derived hepatocyte-like cells for drug toxicity testing. *Biomaterials* **34,** 1781–1789 (2013).

66.   Berger, D. R., Ware, B. R., Davidson, M. D., Allsup, S. R. & Khetani, S. R. Enhancing the functional maturity of iPSC-derived human hepatocytes via controlled presentation of

cell-cell interactions *in vitro*. *Hepatology* **61,** 1370–1381 (2015).

67. Nguyen, T. V *et al.* Establishment of a hepatocyte-Kupffer cell coculture model for assessment of proinflammatory cytokine effects on metabolizing enzymes and drug transporters. *Drug Metab. Dispos.* **43,** 744–785 (2015).

68. Kostadinova, R. *et al.* A long-term three dimensional liver co-culture system for improved prediction of clinically relevant drug-induced hepatotoxicity. *Toxicol. Appl. Pharmacol.* **268,** 1–16 (2013).

69. Ma, X. *et al.* Deterministically patterned biomimetic human iPSC-derived hepatic model via rapid 3D bioprinting. *Proc. Natl. Acad. Sci. U. S. A.* **113,** 2206–2211 (2016).

70. Sivaraman, A. *et al.* A microscale *in vitro* physiological model of the liver: Predictive screens for drug metabolism and enzyme induction. *Curr. Drug Metab.* **6,** 569–591 (2005).

71. Domansky, K. *et al.* Perfused multiwell plate for 3D liver tissue engineering. *Lab Chip* **10,** 51–58 (2010).

72. Toh, Y.-C. *et al.* A microfluidic 3D hepatocyte chip for drug toxicity testing. *Lab Chip* **9,** 2026–2035 (2009).

73. Shih, M.-C., Tseng, S.-H., Weng, Y.-S., Chu, I.-M. & Liu, C.-H. A microfluidic device mimicking acinar concentration gradients across the liver acinus. *Biomed. Microdevices* **15,** 767–780 (2013).

74. Legendre, A. *et al.* Metabolic characterization of primary rat hepatocytes cultivated in parallel microfluidic biochips. *J. Pharm. Sci.* **102,** 3264–3276 (2013).

75. Baudoin, R. *et al.* Evaluation of a liver microfluidic biochip to predict *in vivo* clearances of seven drugs in rats. *J. Pharm. Sci.* **103,** 706–718 (2014).

76. Prot, J. M. *et al.* A cocktail of metabolic probes demonstrates the relevance of primary human hepatocyte cultures in a microfluidic biochip for pharmaceutical drug screening.

Int. J. Pharm. **408,** 67–75 (2011).

77.   Baudoin, R. *et al.* Evaluation of seven drug metabolisms and clearances by cryopreserved human primary hepatocytes cultivated in microfluidic biochips. *Xenobiotica* **43,** 140–152 (2013).

78.   Leclerc, E., Hamon, J., Legendre, A. & Bois, F. Integration of pharmacokinetic and NRF2 system biology models to describe reactive oxygen species production and subsequent glutathione depletion in liver microfluidic biochips after flutamide exposure. *Toxicol. Vitr.* **28,** 1230–1241 (2014).

79.   Choucha-Snouber, L. *et al.* Metabolomics-on-a-chip of hepatotoxicity induced by anticancer drug flutamide and its active metabolite hydroxyflutamide using HepG2/C3a microfluidic biochips. *Toxicol. Sci.* **132,** 8–20 (2013).

80.   Chao, P., Maguire, T. J., Novik, E. I., Cheng, K.-C. & Yarmush, M. L. Evaluation of a microfluidic based cell culture platform with primary human hepatocytes for the prediction of hepatic clearance in human. *Biochem. Pharmacol.* **78,** 625–632 (2009).

81.   Novik, E. I., Maguire, T. J., Chao, P., Cheng, K.-C. & Yarmush, M. L. A microfluidic hepatic coculture platform for cell-based drug metabolism studies. *Biochem. Pharmacol.* **79,** 1036–1044 (2010).

82.   Kim, J.-Y., Fluri, D. A., Kelm, J. M., Hierlemann, A. & Frey, O. 96-well format-based microfluidic platform for parallel interconnection of multiple multicellular spheroids. *J. Lab. Autom.* **20,** 274–282 (2015).

83.   Frey, O., Misun, P. M., Fluri, D. A., Hengstler, J. G. & Hierlemann, A. Reconfigurable microfluidic hanging drop network for multi-tissue interaction and analysis. *Nat. Commun.* **5,** 4250 (2014).

84.   Esch, M. B., Mahler, G. J., Stokol, T. & Shuler, M. L. Body-on-a-chip simulation with gastrointestinal tract and liver tissues suggests that ingested nanoparticles have the potential to cause liver injury. *Lab Chip* **14,** 3081–3092 (2014).

85. Kang, Y. B. A. *et al.* Liver sinusoid on a chip: Long-term layered co-culture of primary rat hepatocytes and endothelial cells in microfluidic platforms. *Biotechnol. Bioeng.* **112,** 2571–2582 (2015).

86. Kasuya, J., Sudo, R., Mitaka, T., Ikeda, M. & Tanishita, K. Spatio-temporal control of hepatic stellate cell-endothelial cell interactions for reconstruction of liver sinusoids *in vitro. Tissue Eng. Part A* **18,** 1045–1056 (2012).

87. Vernetti, L. A. *et al.* A human liver microphysiology platform for investigating physiology, drug safety, and disease models. *Exp. Biol. Med.* **241,** 101–114 (2016).

88. Prodanov, L. *et al.* Long-term maintenance of a microfluidic 3D human liver sinusoid. *Biotechnol. Bioeng.* **113,** 241–246 (2016).

89. Lee, P. J., Hung, P. J. & Lee, L. P. An artificial liver sinusoid with a microfluidic endothelial-like barrier for primary hepatocyte culture. *Biotechnol. Bioeng.* **97,** 1340–1346 (2007).

90. Nakao, Y., Kimura, H., Sakai, Y. & Fujii, T. Bile canaliculi formation by aligning rat primary hepatocytes in a microfluidic device. *Biomicrofluidics* **5,** 22212 (2011).

91. Kmieć, Z. Cooperation of liver cells in health and disease. *Adv. Anat. Embryol. Cell Biol.* **161,** 1–151 (2001).

92. Bavli, D. *et al.* Real-time monitoring of metabolic function in liver-on-chip microdevices tracks the dynamics of mitochondrial dysfunction. *Proc. Natl. Acad. Sci. U. S. A.* **113,** E2231–E2240 (2016).

93. Rennert, K. *et al.* A microfluidically perfused three dimensional human liver model. *Biomaterials* **71,** 119–131 (2015).

94. Matharu, Z. *et al.* Detecting transforming growth factor-β release from liver cells using an aptasensor integrated with microfluidics. *Anal. Chem.* **86,** 8865–8872 (2014).

95. Zhou, Q. *et al.* Liver injury-on-a-chip: Microfluidic co-cultures with integrated biosensors

for monitoring liver cell signaling during injury. *Lab Chip* **15,** 4467–4478 (2015).

96. Anundi, I., Lähteenmäki, T., Rundgren, M., Moldeus, P. & Lindros, K. O. Zonation of acetaminophen metabolism and cytochrome P450 2E1-mediated toxicity studied in isolated periportal and perivenous hepatocytes. *Biochem. Pharmacol.* **45,** 1251–1259 (1993).

97. Allen, J. W., Khetani, S. R. & Bhatia, S. N. *In vitro* zonation and toxicity in a hepatocyte bioreactor. *Toxicol. Sci.* **84,** 110–119 (2005).

98. Sato, A., Kadokura, K., Uchida, H. & Tsukada, K. An *in vitro* hepatic zonation model with a continuous oxygen gradient in a microdevice. *Biochem. Biophys. Res. Commun.* **453,** 767–771 (2014).

99. Peng, C.-C., Liao, W.-H., Chen, Y.-H., Wu, C.-Y. & Tung, Y.-C. A microfluidic cell culture array with various oxygen tensions. *Lab Chip* **13,** 3239–3245 (2013).

100. Viravaidya, K., Sin, A. & Shuler, M. L. Development of a microscale cell culture analog to probe naphthalene toxicity. *Biotechnol. Prog.* **20,** 316–323 (2004).

101. Bricks, T. *et al.* Development of a new microfluidic platform integrating co-cultures of intestinal and liver cell lines. *Toxicol. Vitr.* **28,** 885–895 (2014).

102. Choucha-Snouber, L. *et al.* Investigation of ifosfamide nephrotoxicity induced in a liver-kidney co-culture biochip. *Biotechnol. Bioeng.* **110,** 597–608 (2013).

103. Materne, E.-M. *et al.* A multi-organ chip co-culture of neurospheres and liver equivalents for long-term substance testing. *J. Biotechnol.* **205,** 36–46 (2015).

104. Zervantonakis, I. K. *et al.* Three-dimensional microfluidic model for tumor cell intravasation and endothelial barrier function. *Proc. Natl. Acad. Sci. U. S. A.* **109,** 13515–13520 (2012).

105. Wagner, I. *et al.* A dynamic multi-organ-chip for long-term cultivation and substance testing proven by 3D human liver and skin tissue co-culture. *Lab Chip* **13,** 3538–3547

(2013).

106. Materne, E.-M. *et al.* The multi-organ chip - A microfluidic platform for long-term multi-tissue coculture. *J. Vis. Exp.* **98,** e52526 (2015).

107. Kimura, H., Ikeda, T., Nakayama, H., Sakai, Y. & Fujii, T. An on-chip small intestine-liver model for pharmacokinetic studies. *J. Lab. Autom.* **20,** 265–273 (2015).

108. Sung, J. H., Kam, C. & Shuler, M. L. A microfluidic device for a pharmacokinetic-pharmacodynamic (PK-PD) model on a chip. *Lab Chip* **10,** 446–55 (2010).

109. Maschmeyer, I. *et al.* A four-organ-chip for interconnected long-term co-culture of human intestine, liver, skin, and kidney equivalents. *Lab Chip* **15,** 2688–2699 (2015).

110. Oleaga, C. *et al.* Multi-organ toxicity demonstration in a functional human *in vitro* system composed of four organs. *Sci. Rep.* **6,** 20030 (2016).

111. Davidson, M. D., Ballinger, K. R. & Khetani, S. R. Long-term exposure to abnormal glucose levels alters drug metabolism pathways and insulin sensitivity in primary human hepatocytes. *Sci. Rep.* **6,** 28178 (2016).

112. Takahashi, K. & Yamanaka, S. Induction of pluripotent stem cells from mouse embryonic and adult fibroblast cultures by defined factors. *Cell* **126,** 663–676 (2006).

113. Takahashi, K. *et al.* Induction of pluripotent stem cells from adult human fibroblasts by defined factors. *Cell* **131,** 861–872 (2007).

114. Yu, J. *et al.* Induced pluripotent stem cell lines derived from human somatic cells. *Science* **318,** 1917–1920 (2007).

115. Hannan, N. R. F., Segeritz, C.-P., Touboul, T. & Vallier, L. Production of hepatocyte like cells from human pluripotent stem cells. *Nat. Protoc.* **8,** 430–437 (2013).

116. Gerbal-Chaloin, S. *et al.* Human induced pluripotent stem cells in hepatology: Beyond the proof of concept. *Am. J. Pathol.* **184,** 332–347 (2014).

117. Si-Tayeb, K. *et al.* Highly efficient generation of human hepatocyte-like cells from induced pluripotent stem cells. *Hepatology* **51,** 297–305 (2010).

118. Ma, X. *et al.* Highly efficient differentiation of functional hepatocytes from human induced pluripotent stem cells. *Stem Cells Transl. Med.* **2,** 409–419 (2013).

119. Zhu, S. *et al.* Mouse liver repopulation with hepatocytes generated from human fibroblasts. *Nature* **508,** 93–97 (2014).

120. Touboul, T. *et al.* Generation of functional hepatocytes from human embryonic stem cells under chemically defined conditions that recapitulate liver development. *Hepatology* **51,** 1754–1765 (2010).

121. Du, Y. *et al.* Human hepatocytes with drug metabolic function induced from fibroblasts by lineage reprogramming. *Cell Stem Cell* **14,** 394–403 (2014).

122. Song, Z. *et al.* Efficient generation of hepatocyte-like cells from human induced pluripotent stem cells. *Cell Res.* **19,** 1233–1242 (2009).

123. Chen, Y.-F. *et al.* Rapid generation of mature hepatocyte-like cells from human induced pluripotent stem cells by an efficient three-step protocol. *Hepatology* **55,** 1193–1203 (2012).

124. Huang, P. *et al.* Direct reprogramming of human fibroblasts to functional and expandable hepatocytes. *Cell Stem Cell* **14,** 370–384 (2014).

125. Scott, C. W., Peters, M. F. & Dragan, Y. P. Human induced pluripotent stem cells and their use in drug discovery for toxicity testing. *Toxicol. Lett.* **219,** 49–58 (2013).

126. Medine, C. N. *et al.* Developing high-fidelity hepatotoxicity models from pluripotent stem cells. *Stem Cells Transl. Med.* **2,** 505–509 (2013).

127. Bhatia, S. N., Balis, U. J., Yarmush, M. L. & Toner, M. Effect of cell-cell interactions in preservation of cellular phenotype: Cocultivation of hepatocytes and nonparenchymal cells. *FASEB J.* **13,** 1883–1900 (1999).

128. Guillouzo, A. Liver cell models in *in vitro* toxicology. *Environ. Health Perspect.* **106,** 511–532 (1998).

129. Rheinwald, J. G. & Green, H. Serial cultivation of strains of human epidermal keratinocytes: The formation of keratinizing colonies from single cells. *Cell* **6,** 331–343 (1975).

130. Ukairo, O. *et al.* Bioactivation and toxicity of acetaminophen in a rat hepatocyte micropatterned coculture system. *J. Biochem. Mol. Toxicol.* **27,** 471–478 (2013).

131. Cahan, P. *et al.* CellNet: Network biology applied to stem cell engineering. *Cell* **158,** 903–915 (2014).

132. Easterbrook, J., Lu, C., Sakai, Y. & Li, A. P. Effects of organic solvents on the activities of cytochrome P450 isoforms, UDP-dependent glucuronyl transferase, and phenol sulfotransferase in human hepatocytes. *Drug Metab. Dispos.* **29,** 141–144 (2001).

133. Chen, M. *et al.* The liver toxicity knowledge base: A systems approach to a complex end point. *Clin. Pharmacol. Ther.* **93,** 409–412 (2013).

134. David Josephy, P. The molecular toxicology of acetaminophen. *Drug Metab. Rev.* **37,** 581–594 (2005).

135. O'Brien, P. J. *et al.* High concordance of drug-induced human hepatotoxicity with *in vitro* cytotoxicity measured in a novel cell-based model using high content screening. *Arch. Toxicol.* **80,** 580–604 (2006).

136. Tolosa, L. *et al.* Development of a multiparametric cell-based protocol to screen and classify the hepatotoxicity potential of drugs. *Toxicol. Sci.* **127,** 187–198 (2012).

137. Chen, M. *et al.* Toward predictive models for drug-induced liver injury in humans: Are we there yet? *Biomark. Med.* **8,** 201–213 (2014).

138. Nagamoto, Y. *et al.* The promotion of hepatic maturation of human pluripotent stem cells in 3D co-culture using type I collagen and Swiss 3T3 cell sheets. *Biomaterials* **33,** 4526–

4534 (2012).

139. Ogawa, S. *et al.* Three-dimensional culture and cAMP signaling promote the maturation of human pluripotent stem cell-derived hepatocytes. *Development* **140,** 3285–3296 (2013).

140. Takebe, T. *et al.* Generation of a vascularized and functional human liver from an iPSC-derived organ bud transplant. *Nat. Protoc.* **9,** 396–409 (2014).

141. Yum, K., Hong, S. G., Healy, K. E. & Lee, L. P. Physiologically relevant organs on chips. *Biotechnol. J.* **9,** 16–27 (2014).

142. Godoy, P. *et al.* Recent advances in 2D and 3D *in vitro* systems using primary hepatocytes, alternative hepatocyte sources and non-parenchymal liver cells and their use in investigating mechanisms of hepatotoxicity, cell signaling and ADME. *Arch. Toxicol.* **87,** 1315–1530 (2013).

143. Kidambi, S. *et al.* Oxygen-mediated enhancement of primary hepatocyte metabolism, functional polarization, gene expression, and drug clearance. *Proc. Natl. Acad. Sci. U. S. A.* **106,** 15714–15719 (2009).

144. Sirenko, O., Hesley, J., Rusyn, I. & Cromwell, E. F. High-content assays for hepatotoxicity using induced pluripotent stem cell-derived cells. *Assay Drug Dev. Technol.* **12,** 43–54 (2014).

145. Shih, H., Pickwell, G. V, Guenette, D. K., Bilir, B. & Quattrochi, L. C. Species differences in hepatocyte induction of CYP1A1 and CYP1A2 by omeprazole. *Hum. Exp. Toxicol.* **18,** 95–105 (1999).

146. Threadgill, D. W., Miller, D. R., Churchill, G. A. & de Villena, F. P.-M. The Collaborative Cross: A recombinant inbred mouse population for the systems genetic era. *ILAR J.* **52,** 24–31 (2011).

147. Bogaards, J. J. P. *et al.* Determining the best animal model for human cytochrome P450 activities: A comparison of mouse, rat, rabbit, dog, micropig, monkey, and man. *Xenobiotica* **30,** 1131–1152 (2000).

148. Martinez, S. M. *et al.* Evaluation of an *in vitro* toxicogenetic mouse model for hepatotoxicity. *Toxicol. Appl. Pharmacol.* **249,** 208–216 (2010).

149. Choi, H. J. & Choi, D. Successful mouse hepatocyte culture with sandwich collagen gel formation. *J. Korean Surg. Soc.* **84,** 202–208 (2013).

150. Meng, Q. *et al.* A hybrid substratum for primary hepatocyte culture that enhances hepatic functionality with low serum dependency. *Int. J. Nanomedicine* **10,** 2313–2323 (2015).

151. Desai, S. S. *et al.* Physiological ranges of matrix rigidity modulate primary mouse hepatocyte function in part through hepatocyte nuclear factor 4 alpha. *Hepatology* **64,** 261–275 (2016).

152. Ukairo, O. *et al.* Long-term stability of primary rat hepatocytes in micropatterned cocultures. *J. Biochem. Mol. Toxicol.* **27,** 204–212 (2013).

153. Smith, C. M. *et al.* A comprehensive evaluation of metabolic activity and intrinsic clearance in suspensions and monolayer cultures of cryopreserved primary human hepatocytes. *J. Pharm. Sci.* **101,** 3989–4002 (2012).

154. March, S. *et al.* Micropatterned coculture of primary human hepatocytes and supportive cells for the study of hepatotropic pathogens. *Nat. Protoc.* **10,** 2027–2053 (2015).

155. Zamek-Gliszczynski, M. J. *et al.* Pharmacokinetics of 5 (and 6)-carboxy-2',7'-dichlorofluorescein and its diacetate promoiety in the liver. *J. Pharmacol. Exp. Ther.* **304,** 801–809 (2003).

156. Harrill, A. H. *et al.* Mouse population-guided resequencing reveals that variants in CD44 contribute to acetaminophen-induced liver injury in humans. *Genome Res.* **19,** 1507–1515 (2009).

157. Harrill, A. H. *et al.* A mouse diversity panel approach reveals the potential for clinical kidney injury due to DB289 not predicted by classical rodent models. *Toxicol. Sci.* **130,** 416–426 (2012).

158. Khetani, S. R., Szulgit, G., Del Rio, J. A., Barlow, C. & Bhatia, S. N. Exploring interactions between rat hepatocytes and nonparenchymal cells using gene expression profiling. *Hepatology* **40,** 545–554 (2004).

159. Gonzalez, F. J., Fang, Z.-Z. & Ma, X. Transgenic mice and metabolomics for study of hepatic xenobiotic metabolism and toxicity. *Expert Opin. Drug Metab. Toxicol.* **11,** 869–881 (2015).

160. Raucy, J. L., Lasker, J. M., Lieber, C. S. & Black, M. Acetaminophen activation by human liver cytochromes P450IIE1 and P450IA2. *Arch. Biochem. Biophys.* **271,** 270–283 (1989).

161. Ware, B. R., Berger, D. R. & Khetani, S. R. Prediction of drug-induced liver injury in micropatterned co-cultures containing iPSC-derived human hepatocytes. *Toxicol. Sci.* **145,** 252–262 (2015).

162. Madhu, C., Maziasz, T. & Klaassen, C. D. Effect of pregnenolone-16 alpha-carbonitrile and dexamethasone on acetaminophen-induced hepatotoxicity in mice. *Toxicol. Appl. Pharmacol.* **115,** 191–198 (1992).

163. Teo, Y. L. *et al.* Effect of CYP3A4 inducer dexamethasone on hepatotoxicity of lapatinib: Clinical and *in vitro* evidence. *Breast Cancer Res. Treat.* **133,** 703–711 (2012).

164. Ware, B. R. & Khetani, S. R. Engineered liver platforms for different phases of drug development. *Trends Biotechnol.* **35,** 172–183 (2017).

165. Gripon, P. *et al.* Infection of a human hepatoma cell line by hepatitis B virus. *Proc. Natl. Acad. Sci. U. S. A.* **99,** 15655–15660 (2002).

166. Andersson, T. B., Kanebratt, K. P. & Kenna, J. G. The HepaRG cell line: A unique *in vitro* tool for understanding drug metabolism and toxicology in human. *Expert Opin. Drug Metab. Toxicol.* **8,** 909–920 (2012).

167. Kanebratt, K. P. & Andersson, T. B. Evaluation of HepaRG cells as an *in vitro* model for human drug metabolism studies. *Drug Metab. Dispos.* **36,** 1444–1452 (2008).

168. Le Vee, M. *et al.* Functional expression of sinusoidal and canalicular hepatic drug transporters in the differentiated human hepatoma HepaRG cell line. *Eur. J. Pharm. Sci.* **28,** 109–117 (2006).

169. Le Vee, M., Noel, G., Jouan, E., Stieger, B. & Fardel, O. Polarized expression of drug transporters in differentiated human hepatoma HepaRG cells. *Toxicol. Vitr.* **27,** 1979–1986 (2013).

170. Mueller, D., Krämer, L., Hoffmann, E., Klein, S. & Noor, F. 3D organotypic HepaRG cultures as *in vitro* model for acute and repeated dose toxicity studies. *Toxicol. Vitr.* **28,** 104–112 (2014).

171. Lübberstedt, M. *et al.* HepaRG human hepatic cell line utility as a surrogate for primary human hepatocytes in drug metabolism assessment *in vitro*. *J. Pharmacol. Toxicol. Methods* **63,** 59–68 (2011).

172. Guillouzo, A. *et al.* The human hepatoma HepaRG cells: A highly differentiated model for studies of liver metabolism and toxicity of xenobiotics. *Chem. Biol. Interact.* **168,** 66–73 (2007).

173. Tomida, T., Okamura, H., Satsukawa, M., Yokoi, T. & Konno, Y. Multiparametric assay using HepaRG cells for predicting drug-induced liver injury. *Toxicol. Lett.* **236,** 16–24 (2015).

174. Wu, Y. *et al.* The HepaRG cell line, a superior *in vitro* model to L-02, HepG2, and hiHeps cell lines for assessing drug-induced liver injury. *Cell Biol. Toxicol.* **32,** 37–59 (2016).

175. Ferreira, A., Rodrigues, M., Silvestre, S., Falcão, A. & Alves, G. HepaRG cell line as an *in vitro* model for screening drug-drug interactions mediated by metabolic induction: Amiodarone used as a model substance. *Toxicol. Vitr.* **28,** 1531–1535 (2014).

176. Jackson, J. P., Li, L., Chamberlain, E. D., Wang, H. & Ferguson, S. S. Contextualizing hepatocyte functionality of cryopreserved HepaRG cell cultures. *Drug Metab. Dispos.* **44,** 1463–1479 (2016).

177. Ramaiahgari, S. C. *et al.* Three-dimensional (3D) HepaRG spheroid model with physiologically relevant xenobiotic metabolism competence and hepatocyte functionality for liver toxicity screening. *Toxicol. Sci.* **159,** 124-136 (2017).

178. Wang, Z. *et al.* HepaRG culture in tethered spheroids as an *in vitro* three-dimensional model for drug safety screening. *J. Appl. Toxicol.* **35,** 909–917 (2015).

179. Ware, B. R., Durham, M. J., Monckton, C. P. & Khetani, S. R. A cell culture platform to maintain long-term phenotype of primary human hepatocytes and endothelial cells. *Cell. Mol. Gastroenterol. Hepatol.* **5,** 187-207 (2018).

180. Chan, T. S., Yu, H., Moore, A., Khetani, S. R. & Tweedie, D. J. Meeting the challenge of predicting hepatic clearance of compounds slowly metabolized by cytochrome P450 using a novel hepatocyte model, HepatoPac. *Drug Metab. Dispos.* **41,** 2024–2032 (2013).

181. Ware, B. R. & Khetani, S. R. in *Stem Cell-Derived Models in Toxicology* (eds. Clements, M. & Roquemore, L.) 311–334 (Humana Press, 2017). doi:10.1007/978-1-4939-6659-2

182. Khetani, S. R., Chen, A. A., Ranscht, B. & Bhatia, S. N. T-cadherin modulates hepatocyte functions *in vitro*. *FASEB J.* **22,** 3768–3775 (2008).

183. Szabo, M., Veres, Z., Baranyai, Z., Jakab, F. & Jemnitz, K. Comparison of human hepatoma HepaRG cells with human and rat hepatocytes in uptake transport assays in order to predict a risk of drug induced hepatotoxicity. *PLoS One* **8,** e59432 (2013).

184. Qiu, X. *et al.* Disruption of BSEP function in HepaRG cells alters bile acid disposition and is a susceptive factor to drug-induced cholestatic injury. *Mol. Pharm.* **13,** 1206–1216 (2016).

185. Sharanek, A. *et al.* Cellular accumulation and toxic effects of bile acids in cyclosporine A-treated HepaRG hepatocytes. *Toxicol. Sci.* **147,** 573–587 (2015).

186. Susukida, T. *et al.* Establishment of a drug-induced, bile acid-dependent hepatotoxicity model using HepaRG cells. *J. Pharm. Sci.* **105,** 1550–1560 (2016).

187. Higuchi, Y. *et al.* Functional polymer-dependent 3D culture accelerates the differentiation of HepaRG cells into mature hepatocytes. *Hepatol. Res.* **46,** 1045–1057 (2016).

188. Novotna, A. & Dvorak, Z. Omeprazole and lansoprazole enantiomers induce CYP3A4 in human hepatocytes and cell lines via glucocorticoid receptor and pregnane X receptor axis. *PLoS One* **9,** e105580 (2014).

189. Prestigiacomo, V., Weston, A., Messner, S., Lampart, F. & Suter-Dick, L. Pro-fibrotic compounds induce stellate cell activation, ECM-remodeling, and Nrf2 activation in a human 3D-multicellular model of liver fibrosis. *PLoS One* **12,** e0179995 (2017).

190. Leite, S. B. *et al.* Novel human hepatic organoid model enables testing of drug-induced liver fibrosis *in vitro*. *Biomaterials* **78,** 1–10 (2016).

191. Lin, C. & Khetani, S. R. Advances in engineered liver models for investigating drug-induced liver injury. *Biomed Res. Int.* (2016).

192. Isley, W. L. Hepatotoxicity of thiazolidinediones. *Expert Opin. Drug Saf.* **2,** 581–586 (2003).

193. Hu, D. *et al.* Characterizing the mechanism of thiazolidinedione-induced hepatotoxicity: An *in vitro* model in mitochondria. *Toxicol. Appl. Pharmacol.* **284,** 134–141 (2015).

194. Jaeschke, H. Troglitazone hepatotoxicity: Are we getting closer to understanding idiosyncratic liver injury? *Toxicol. Sci.* **97,** 1–3 (2007).

195. Barros, S. A. & Martin, R. B. in *Methods in Molecular Biology* 89–112 (Humana Press, 2008).

196. Kienhuis, A. S. *et al.* A toxicogenomics-based parallelogram approach to evaluate the relevance of coumarin-induced responses in primary human hepatocytes *in vitro* for humans *in vivo*. *Toxicol. Vitr.* **23,** 1163–1169 (2009).

197. Harris, A. J., Dial, S. L. & Casciano, D. A. Comparison of basal gene expression profiles and effects of hepatocarcinogens on gene expression in cultured primary human

hepatocytes and HepG2 cells. *Mutat. Res.* **549,** 79–99 (2004).

198. Kier, L. D. *et al.* Applications of microarrays with toxicologically relevant genes (tox genes) for the evaluation of chemical toxicants in Sprague Dawley rats *in vivo* and human hepatocytes *in vitro*. *Mutat. Res.* **549,** 101–113 (2004).

199. Uehara, T. *et al.* Species-specific differences in coumarin-induced hepatotoxicity as an example toxicogenomics-based approach to assessing risk of toxicity to humans. *Hum. Exp. Toxicol.* **27,** 25–35 (2008).

200. Dewland, P. M., Reader, S. & Berry, P. Bioavailability of ibuprofen following oral administration of standard ibuprofen, sodium ibuprofen, or ibuprofen acid incorporating poloxamer in healthy volunteers. *BMC Clin. Pharmacol.* **9,** (2009).

201. Li, C. & Wong, W. H. Model-based analysis of oligonucleotide arrays: Expression index computation and outlier detection. *Proc. Natl. Acad. Sci. U. S. A.* **98,** 31–36 (2001).

202. Huang, D. W., Sherman, B. T. & Lempicki, R. A. Systematic and integrative analysis of large gene lists using DAVID bioinformatics resources. *Nat. Protoc.* **4,** 44–57 (2009).

203. Sahi, J. *et al.* Comparative effects of thiazolidinediones on *in vitro* P450 enzyme induction and inhibition. *Drug Metab. Dispos.* **31,** 439–446 (2003).

204. Doshi, U. & Li, A. P. Luciferin IPA-based higher throughput human hepatocyte screening assays for CYP3A4 inhibition and induction. *J. Biomol. Screen.* **16,** 903–909 (2011).

205. Zhang, F., Xue, J., Shao, J. & Jia, L. Compilation of 222 drugs' plasma protein binding data and guidance for study designs. *Drug Discov. Today* **17,** 475–485 (2012).

206. Tweedie, D. J. *et al.* Transporter studies in drug development: Experience to date and follow-up on decision trees from the International Transporter Consortium. *Clin. Pharmacol. Ther.* **94,** 113–125 (2013).

207. Boss, M., Kemmerer, M., Brüne, B. & Namgaladze, D. FABP4 inhibition suppresses PPARγ activity and VLDL-induced foam cell formation in IL-4-polarized human

281

macrophages. *Atherosclerosis* **240,** 424–430 (2015).

208. Yang, K., Woodhead, J. L., Watkins, P. B., Howell, B. A. & Brouwer, K. L. R. Systems pharmacology modeling predicts delayed presentation and species differences in bile acid-mediated troglitazone hepatotoxicity. *Clin. Pharmacol. Ther.* **96,** 589–598 (2014).

209. Kassahun, K. *et al.* Studies on the metabolism of troglitazone to reactive intermediates *in vitro* and *in vivo*: Evidence for novel biotransformation pathways involving quinone methide formation and thiazolidinedione ring scission. *Chem. Res. Toxicol.* **14,** 62–70 (2001).

210. Usui, T., Hashizume, T., Katsumata, T., Yokoi, T. & Komuro, S. *In vitro* investigation of the glutathione transferase M1 and T1 null genotypes as risk factors for troglitazone-induced liver injury. *Drug Metab. Dispos.* **39,** 1303–1310 (2011).

211. Siddens, L. K., Krueger, S. K., Henderson, M. C. & Williams, D. E. Mammalian flavin-containing monooxygenase (FMO) as a source of hydrogen peroxide. *Biochem. Pharmacol.* **89,** 141–147 (2014).

212. Qin, X. & Gao, B. The complement system in liver diseases. *Cell. Mol. Immunol.* **3,** 333–340 (2006).

213. Ebeling, P. *et al.* Troglitazone reduces hyperglycaemia and selectively acute-phase serum proteins in patients with Type II diabetes. *Diabetologia* **42,** 1433–1438 (1999).

214. Singhal, R., Ganey, P. E. & Roth, R. A. Complement activation in acetaminophen-induced liver injury in mice. *J. Pharmacol. Exp. Ther.* **341,** 377–385 (2012).

215. Poisson, J. *et al.* Liver sinusoidal endothelial cells: Physiology and role in liver diseases. *J. Hepatol.* **66,** 212–227 (2017).

216. Limmer, A. *et al.* Efficient presentation of exogenous antigen by liver endothelial cells to CD8+ T cells results in antigen-specific T-cell tolerance. *Nat. Med.* **6,** 1348–1354 (2000).

217. Do, H., Healey, J. F., Waller, E. K. & Lollar, P. Expression of factor VIII by murine liver

sinusoidal endothelial cells. *J. Biol. Chem.* **274,** 19587–19592 (1999).

218. Maslak, E., Gregorius, A. & Chlopicki, S. Liver sinusoidal endothelial cells (LSECs) function and NAFLD; NO-based therapy targeted to the liver. *Pharmacol. Reports* **67,** 689–694 (2015).

219. Marvie, P. *et al.* Interleukin-33 overexpression is associated with liver fibrosis in mice and humans. *J. Cell. Mol. Med.* **14,** 1726–1739 (2010).

220. DeLeve, L. D., Wang, X., Kuhlenkamp, J. F. & Kaplowitz, N. Toxicity of azathioprine and monocrotaline in murine sinusoidal endothelial cells and hepatocytes: The role of glutathione and relevance to hepatic venoocclusive disease. *Hepatology* **23,** 589–599 (1996).

221. DeLeve, L. D. Dacarbazine toxicity in murine liver cells: A model of hepatic endothelial injury and glutathione defense. *J. Pharmacol. Exp. Ther.* **268,** 1261–1270 (1994).

222. Nahmias, Y., Casali, M., Barbe, L., Berthiaume, F. & Yarmush, M. L. Liver endothelial cells promote LDL-R expression and the uptake of HCV-like particles in primary rat and human hepatocytes. *Hepatology* **43,** 257–265 (2006).

223. Godoy, P. *et al.* Gene network activity in cultivated primary hepatocytes is highly similar to diseased mammalian liver tissue. *Arch. Toxicol.* **90,** 2513–2529 (2016).

224. March, S., Hui, E. E., Underhill, G. H., Khetani, S. R. & Bhatia, S. N. Microenvironmental regulation of the sinusoidal endothelial cell phenotype *in vitro*. *Hepatology* **50,** 920–928 (2009).

225. Kang, Y. B. A., Rawat, S., Cirillo, J., Bouchard, M. J. & Noh, H. M. Layered long-term co-culture of hepatocytes and endothelial cells on a transwell membrane: Toward engineering the liver sinusoid. *Biofabrication* **5,** 45008 (2013).

226. Bale, S. S. *et al.* Long term co-culture strategies for primary hepatocytes and liver sinusoidal endothelial cells. *Tissue Eng. Part C Methods* **21,** 413–422 (2015).

227. Kim, K., Ohashi, K., Utoh, R., Kano, K. & Okano, T. Preserved liver-specific functions of hepatocytes in 3D co-culture with endothelial cell sheets. *Biomaterials* **33,** 1406–1413 (2012).

228. Kim, Y. & Rajagopalan, P. 3D hepatic cultures simultaneously maintain primary hepatocyte and liver sinusoidal endothelial cell phenotypes. *PLoS One* **5,** e15456 (2010).

229. Harimoto, M. *et al.* Novel approach for achieving double-layered cell sheets co-culture: Overlaying endothelial cell sheets onto monolayer hepatocytes utilizing temperature-responsive culture dishes. *J. Biomed. Mater. Res.* **62,** 464–470 (2002).

230. Ho, C.-T. *et al.* Liver-cell patterning Lab Chip: Mimicking the morphology of liver lobule tissue. *Lab Chip* **13,** 3578–3587 (2013).

231. Ohno, M., Motojima, K., Okano, T. & Taniguchi, A. Induction of drug-metabolizing enzymes by phenobarbital in layered co-culture of a human liver cell line and endothelial cells. *Biol. Pharm. Bull.* **32,** 813–817 (2009).

232. Jindal, R., Patel, S. J. & Yarmush, M. L. Tissue-engineered model for real-time monitoring of liver inflammation. *Tissue Eng. Part C Methods* **17,** 113–122 (2011).

233. Giugliano, S. *et al.* Hepatitis C virus infection induces autocrine interferon signaling by human liver endothelial cells and release of exosomes, which inhibits viral replication. *Gastroenterology* **148,** 392–402 (2015).

234. Matsumura, T. *et al.* Establishment of an immortalized human-liver endothelial cell line with SV40T and hTERT. *Transplantation* **77,** 1357–1365 (2004).

235. Estep, J. E. *et al.* [14C]monocrotaline kinetics and metabolism in the rat. *Drug Metab. Dispos.* **19,** 135–139 (1991).

236. Collins, T. J. ImageJ for microscopy. *Biotechniques* **43,** S25–S30 (2007).

237. Chen, A. A. *et al.* Humanized mice with ectopic artificial liver tissues. *Proc. Natl. Acad. Sci. U. S. A.* **108,** 11842–11847 (2011).

238. Norona, L. M., Nguyen, D. G., Gerber, D. A., Presnell, S. C. & LeCluyse, E. L. Modeling compound-induced fibrogenesis *in vitro* using three-dimensional bioprinted human liver tissues. *Toxicol. Sci.* **154,** 354–367 (2016).

239. Perepelyuk, M. *et al.* Hepatic stellate cells and portal fibroblasts are the major cellular sources of collagens and lysyl oxidases in normal liver and early after injury. *Am. J. Physiol. Gastrointest. Liver Physiol.* **304,** G605–G614 (2013).

240. Proctor, W. R. *et al.* Utility of spherical human liver microtissues for prediction of clinical drug-induced liver injury. *Arch. Toxicol.* **91,** 2849–2863 (2017).

241. Cho, C. H. *et al.* Oxygen uptake rates and liver-specific functions of hepatocyte and 3T3 fibroblast co-cultures. *Biotechnol. Bioeng.* **97,** 188–199 (2007).

242. Chia, S.-M., Lin, P.-C. & Yu, H. TGF-beta1 regulation in hepatocyte-NIH3T3 co-culture is important for the enhanced hepatocyte function in 3D microenvironment. *Biotechnol. Bioeng.* **89,** 565–573 (2005).

243. De La Vega, F. M. & Mendoza-Figueroa, T. Dimethyl sulfoxide enhances lipid synthesis and secretion by long-term cultures of adult rat hepatocytes. *Biochimie* **73,** 621–624 (1991).

244. Donato, M. T., Gómez-Lechón, M. J. & Castell, J. V. Drug metabolizing enzymes in rat hepatocytes co-cultured with cell lines. *Vitr. Cell. Dev. Biol.* **26,** 1057–1062 (1990).

245. Kuri-Harcuch, W. & Mendoza-Figueroa, T. Cultivation of adult rat hepatocytes on 3T3 cells: Expression of various liver differentiated functions. *Differentiation* **41,** 148–157 (1989).

246. Goulet, F., Normand, C. & Morin, O. Cellular interactions promote tissue-specific function, biomatrix deposition and junctional communication of primary cultured hepatocytes. *Hepatology* **8,** 1010–1018 (1988).

247. Shimaoka, S., Nakamura, T. & Ichihara, A. Stimulation of growth of primary cultured adult rat hepatocytes without growth factors by coculture with nonparenchymal liver cells.

Exp. Cell Res. **172,** 228–242 (1987).

248. Ramsden, D., Tweedie, D. J., Chan, T. S. & Tracy, T. S. Altered CYP2C9 activity following modulation of CYP3A4 levels in human hepatocytes: An example of protein-protein interactions. *Drug Metab. Dispos.* **42,** 1940–1946 (2014).

249. Ng, S. *et al.* Hypoxia promotes liver-stage malaria infection in primary human hepatocytes *in vitro*. *Dis. Model. Mech.* **7,** 215–224 (2014).

250. Schug, M. *et al.* Primary rat hepatocytes as *in vitro* system for gene expression studies: Comparison of sandwich, Matrigel, and 2D cultures. *Arch. Toxicol.* **82,** 923–931 (2008).

251. Bi, Y., Kazolias, D. & Duignan, D. B. Use of cryopreserved human hepatocytes in sandwich culture to measure hepatobiliary transport. *Drug Metab. Dispos.* **34,** 1658–1665 (2006).

252. Govindarajan, R. *et al.* Expression and hepatobiliary transport characteristics of the concentrative and equilibrative nucleoside transporters in sandwich-cultured human hepatocytes. *Am. J. Physiol. Gastrointest. Liver Physiol.* **295,** G570–G580 (2008).

253. Liu, Y., Li, H., Yan, S., Wei, J. & Li, X. Hepatocyte cocultures with endothelial cells and fibroblasts on micropatterned fibrous mats to promote liver-specific functions and capillary formation capabilities. *Biomacromolecules* **15,** 1044–1054 (2014).

254. Li, A. P. *et al.* Cryopreserved human hepatocytes: Characterization of drug-metabolizing enzyme activities and applications in higher throughput screening assays for hepatotoxicity, metabolic stability, and drug-drug interaction potential. *Chem. Biol. Interact.* **121,** 17–35 (1999).

255. Xiao, W., Perry, G. & Sakai, Y. New physiologically-relevant liver tissue model based on hierarchically cocultured primary rat hepatocytes with liver endothelial cells. *Integr. Biol.* **7,** 1412–1422 (2015).

256. Kawasaki, T. *et al.* Activation of human liver sinusoidal endothelial cell by human platelets induces hepatocyte proliferation. *J. Hepatol.* **53,** 648–654 (2010).

257. Taylor, D. P., Clark, A. M., Wheeler, S. E. & Wells, A. Hepatic nonparenchymal cells drive metastatic breast cancer outgrowth and partial epithelial to mesenchymal transition. *Breast Cancer Res. Treat.* **144,** 551–560 (2014).

258. Nelson, L. J. *et al.* Acetaminophen cytotoxicity is ameliorated in a human liver organotypic co-culture model. *Sci. Rep.* **5,** 17455 (2015).

259. Takayama, G., Taniguchi, A. & Okano, T. Identification of differentially expressed genes in hepatocyte/endothelial cell co-culture system. *Tissue Eng.* **13,** 159–166 (2007).

260. Guzzardi, M. A., Vozzi, F. & Ahluwalia, A. D. Study of the crosstalk between hepatocytes and endothelial cells using a novel multicompartmental bioreactor: A comparison between connected cultures and cocultures. *Tissue Eng. Part A* **15,** 3635–3644 (2009).

261. Scoazec, J.-Y. & Feldmann, G. The cell adhesion molecules of hepatic sinusoidal endothelial cells. *J. Hepatol.* **20,** 296–300 (1994).

262. Scoazec, J.-Y. & Feldmann, G. In situ immunophenotyping study of endothelial cells of the human hepatic sinusoid: Results and functional implications. *Hepatology* **14,** 789–797 (1991).

263. Karrar, A., Broomé, U., Uzunel, M., Qureshi, A. R. & Sumitran-Holgersson, S. Human liver sinusoidal endothelial cells induce apoptosis in activated T cells: A role in tolerance induction. *Gut* **56,** 243–252 (2007).

264. van der Kwast, T. H., Stel, H. V, Cristen, E., Bertina, R. M. & Veerman, E. C. I. Localization of factor VIII-procoagulant antigen: An immunohistological survey of the human body using monoclonal antibodies. *Blood* **67,** 222–227 (1986).

265. Neubauer, K., Wilfling, T., Ritzel, A. & Ramadori, G. Platelet-endothelial cell adhesion molecule-1 gene expression in liver sinusoidal endothelial cells during liver injury and repair. *J. Hepatol.* **32,** 921–932 (2000).

266. Wolf, S. I., Howat, S., Abraham, D. J., Pearson, J. D. & Lawson, C. Agonistic anti-ICAM-

1 antibodies in scleroderma: Activation of endothelial pro-inflammatory cascades. *Vascul. Pharmacol.* **59,** 19–26 (2013).

267. Zhu, X.-W. & Gong, J.-P. Expression and role of ICAM-1 in the occurrence and development of hepatocellular carcinoma. *Asian Pacific J. Cancer Prev.* **14,** 1579–1583 (2013).

268. Ruggeri, Z. M. & Ware, J. Von Willebrand factor. *FASEB J.* **7,** 308–316 (1993).

269. Shahani, T. *et al.* Human liver sinusoidal endothelial cells but not hepatocytes contain factor VIII. *J. Thromb. Haemost.* **12,** 36–42 (2014).

270. DeLeve, L. D., Wang, X. & Guo, Y. Sinusoidal endothelial cells prevent rat stellate cell activation and promote reversion to quiescence. *Hepatology* **48,** 920–930 (2008).

271. Fraser, R., Clark, S. A., Day, W. A. & Murray, F. E. Nicotine decreases the porosity of the rat liver sieve: A possible mechanism for hypercholesterolaemia. *Br. J. Exp. Pathol.* **69,** 345–350 (1988).

272. Carpenter, B. *et al.* VEGF is crucial for the hepatic vascular development required for lipoprotein uptake. *Development* **132,** 3293–3303 (2005).

273. Horn, T., Christoffersen, P. & Henriksen, J. H. Alcoholic liver injury: Defenestration in noncirrhotic livers-A scanning electron microscopic study. *Hepatology* **7,** 77–82 (1987).

274. Yokomori, H., Oda, M., Yoshimura, K. & Hibi, T. Recent advances in liver sinusoidal endothelial ultrastructure and fine structure immunocytochemistry. *Micron* **43,** 129–134 (2012).

275. Prot, J. M. *et al.* Improvement of HepG2/C3a cell functions in a microfluidic biochip. *Biotechnol. Bioeng.* **108,** 1704–1715 (2011).

276. Yu, F. *et al.* A perfusion incubator liver chip for 3D cell culture with application on chronic hepatotoxicity testing. *Sci. Rep.* **7,** 14528 (2017).

277. Guillouzo, A. & Guguen-Guillouzo, C. Evolving concepts in liver tissue modeling and

implications for *in vitro* toxicology. *Expert Opin. Drug Metab. Toxicol.* **4,** 1279–1294 (2008).

278. Kane, B. J., Zinner, M. J., Yarmush, M. L. & Toner, M. Liver-specific functional studies in a microfluidic array of primary mammalian hepatocytes. *Anal. Chem.* **78,** 4291–4298 (2006).

279. Sunkara, V. *et al.* Simple room temperature bonding of thermoplastics and poly(dimethylsiloxane). *Lab Chip* **11,** 962–965 (2011).

280. Sunkara, V. & Cho, Y.-K. Investigation on the mechanism of aminosilane-mediated bonding of thermoplastics and poly(dimethylsiloxane). *ACS Appl. Mater. Interfaces* **4,** 6537–6544 (2012).

281. van der Meer, A. D., Vermeul, K., Poot, A. A., Feijen, J. & Vermes, I. Flow cytometric analysis of the uptake of low-density lipoprotein by endothelial cells in microfluidic channels. *Cytom. Part A* **77,** 971–975 (2010).

282. Shah, V. H. *et al.* Liver sinusoidal endothelial cells are responsible for nitric oxide modulation of resistance in the hepatic sinusoids. *J. Clin. Invest.* **100,** 2923–2930 (1997).

283. Lalor, P. F. & Adams, D. H. Adhesion of lymphocytes to hepatic endothelium. *Mol. Pathol.* **52,** 214–219 (1999).

284. Rashidi, H., Alhaque, S., Szkolnicka, D., Flint, O. & Hay, D. C. Fluid shear stress modulation of hepatocyte-like cell function. *Arch. Toxicol.* **90,** 1757–1761 (2016).

285. Hinderliter, P. M. *et al.* ISDD: A computational model of particle sedimentation, diffusion and target cell dosimetry for *in vitro* toxicity studies. *Part. Fibre Toxicol.* **7,** 36 (2010).

286. Coleman, S. E. The development of an *in vitro* flow simulation device to study the effects of arterial shear stress profiles on endothelial cells. (Georgia Institute of Technology and Emory University, 2009).

287. Bhatia, S. N. & Ingber, D. E. Microfluidic organs-on-chips. *Nat. Biotechnol.* **32,** 760–772

(2014).

288. Hamblin, M. N. *et al.* Capillary flow in sacrificially etched nanochannels. *Biomicrofluidics* **5,** 21103 (2011).

289. Hegde, M. *et al.* Dynamic interplay of flow and collagen stabilizes primary hepatocytes culture in a microfluidic platform. *Lab Chip* **14,** 2033–2039 (2014).

290. Du, Y. *et al.* Mimicking liver sinusoidal structures and functions using a 3D-configured microfluidic chip. *Lab Chip* **17,** 782–794 (2017).

291. Goral, V. N. & Yuen, P. K. Microfluidic platforms for hepatocyte cell culture: New technologies and applications. *Ann. Biomed. Eng.* **40,** 1244–1254 (2012).

292. Meyvantsson, I. & Beebe, D. J. Cell culture models in microfluidic systems. *Annu. Rev. Anal. Chem.* **1,** 423–449 (2008).

293. Oppegard, S. C. & Eddington, D. T. A microfabricated platform for establishing oxygen gradients in 3-D constructs. *Biomed. Microdevices* **15,** 407–414 (2013).

294. Sollier, E., Murray, C., Maoddi, P. & Di Carlo, D. Rapid prototyping polymers for microfluidic devices and high pressure injections. *Lab Chip* **11,** 3752–3765 (2011).

295. Lowe, A. B. Thiol-ene 'click' reactions and recent applications in polymer and materials synthesis: A first update. *Polym. Chem.* **5,** 4820 (2014).

296. Kim, M. S., Yeon, J. H. & Park, J.-K. A microfluidic platform for 3-dimensional cell culture and cell-based assays. *Biomed. Microdevices* **9,** 25–34 (2007).

297. Tilles, A. W., Baskaran, H., Roy, P., Yarmush, M. L. & Toner, M. Effects of oxygenation and flow on the viability and function of rat hepatocytes cocultured in a microchannel flat-plate bioreactor. *Biotechnol. Bioeng.* **73,** 379–389 (2001).

298. Leclerc, E., Sakai, Y. & Fujii, T. Perfusion culture of fetal human hepatocytes in microfluidic environments. *Biochem. Eng. J.* **20,** 143–148 (2004).

299. Shetty, S., Weston, C. J., Adams, D. H. & Lalor, P. F. A flow adhesion assay to study leucocyte recruitment to human hepatic sinusoidal endothelium under conditions of shear stress. *J. Vis. Exp.* **85,** 1–7 (2014).

300. Lo, J. F., Sinkala, E. & Eddington, D. T. Oxygen gradients for open well cellular cultures via microfluidic substrates. *Lab Chip* **10,** 2394–2401 (2010).

301. Rexius-Hall, M. L., Mauleon, G., Malik, A. B., Rehman, J. & Eddington, D. T. Microfluidic platform generates oxygen landscapes for localized hypoxic activation. *Lab Chip* **14,** 4688–4695 (2014).

302. Brennan, M. D., Rexius-Hall, M. L. & Eddington, D. T. A 3D-printed oxygen control insert for a 24-well plate. *PLoS One* **10,** e0137631 (2015).

303. Lenguito, G. *et al.* Resealable, optically accessible, PDMS-free fluidic platform for ex vivo interrogation of pancreatic islets. *Lab Chip* **17,** 772–781 (2017).

304. Benesic, A. *et al.* The nephrotoxic ifosfamide-metabolite chloroacetaldehyde interferes with renal extracellular matrix homeostasis. *Cell. Physiol. Biochem.* **33,** 1106–1116 (2014).

305. Ehlers, M. R. Immune-modulating effects of alpha-1 antitrypsin. *Biol. Chem.* **395,** 1187–1193 (2014).

LIST OF ABBREVIATIONS

3-APTES – 3-aminopropyltriethoxysilane

ABT – 1-aminobenzotriazole

acLDL – acetylated low-density lipoprotein

ADME/Tox – absorption, distribution, metabolism, excretion, and toxicity

ALT – alanine aminotransferase

APAP – *N*-acetyl-*p*-aminophenol (acetaminophen)

ATP – adenosine triphosphate

BSA – bovine serum albumin

BSO – L-buthionine (S,R)-sulfoximine

CD – cluster of differentiation

CDF – 5 (and 6)-carboxy-2',7'-dichlorofluorescein

cDNA – complimentary deoxyribonucleic acid

C_{max} – maximum drug concentration in human plasma

C_T – cycle threshold

CYP450 – cytochrome P450 enzyme

DAPI – 4',6-diamidino-2-phenylindole

DAVID – Database for Annotation, Visualization, and Integrated Discovery

DEX – dexamethasone

DILI – drug-induced liver injury

DMEM – Dulbecco's modified Eagle's medium

DMSO – dimethyl sulfoxide

DNA – deoxyribonucleic acid

EA.hy926 – transformed endothelial cell line

EDTA – ethylene diamine tetraacetic acid

EGTA – ethylene glycol-bis(β-aminoethyl ether)-*N,N,N',N'*-tetraacetic acid

ELISA – enzyme-linked immunosorbent assay

F8 – factor VIII

FBS – fetal bovine serum

FDA – United States Food and Drug Administration

FGF – fibroblast growth factor

FN – false negative

FP – false positive

GAPDH – glyceraldehyde-3-phosphate dehydrogenase

GFP – green fluorescent protein

GI – gastrointestinal

GO – Gene Ontology

GSH – glutathione

HCS – high content screening

HEPES – 4-(2-hydroxyethyl)-1-piperazineethanesulfonic acid

HIAT – hepatocyte imaging assay technology

HRP – horseradish peroxidase

HSC – hepatic stellate cell

HUVEC – human umbilical vein endothelial cell

IC$_{50}$ – 50% inhibitory concentration

IL – interleukin

iMPCC – micropatterned co-culture of iPSC-HHs

iMPH – micropatterned pure iPSC-HHs

IPA – isopropyl alcohol

iPSC-HH – induced pluripotent stem cell-derived human hepatocyte

ITS+ – insulin, transferrin, and selenous acid with BSA and linoleic acid

KEGG – Kyoto Encyclopedia of Genes and Genomes

KM – Kupffer macrophage

LPS – lipopolysaccharide

LSEC – liver sinusoidal endothelial cell

LX-2 – transformed stellate cell line

MDCK – Madin-Darby canine kidney cells

HGF – hepatocyte growth factor

mSCH – sandwich culture of mouse hepatocytes

mMPCC – micropatterned co-culture of mouse hepatocytes

mMPH – micropatterned pure mouse hepatocytes

MOA – mechanism of action

MPCC – micropatterned co-culture

MPH – micropatterned pure hepatocytes

NAPQI – N-acetyl-p-benzoquinone imine

NASH – non-alcoholic steatohepatitis

NPC – non-parenchymal cell

OsM – oncostatin M

PBPK – physiologically-based pharmacokinetics

PBS – phosphate buffered saline

PDMS – polydimethylsiloxane

PHH – primary human hepatocyte

PPAR – peroxisome proliferator-activated receptor

qPCR – quantitative polymerase chain reaction

RFP – red fluorescent protein

RNA – ribonucleic acid

ROS – reactive oxygen species

SAR – structure-activity relationships

SEM – scanning electron microscopy

SULT – sulfotransferase

TC_{50} – drug concentration that reduces a biochemical signal by 50%

TCPS – tissue culture polystyrene

TGF – transforming growth factor

TGx – toxicogenomics

TMB – 3,3',5,5'-tetramethylbenzidine

TMNK – immortalized endothelial cell line

TN – true negative

TNF – tumor necrosis factor

TP – true positive

VEGF – vascular endothelial growth factor

vWF – von Willebrand factor